U.PORTO

3º CICLO

DOUTORAMENTO EM BIOLOGIA MOLECULAR E CELULAR

Sensory neurons have an axon initial segment that initiates spontaneous activity in neuropathic pain

Ana Isabel Nascimento

D

2022

Ana Isabel Nascimento. Sensory neurons have an axon initial segment that initiates spontaneous activity in neuropathic pain

D.ICBAS **2022**

Sensory neurons have an axon initial segment that initiates spontaneous activity in neuropathic pain

Ana Isabel Nascimento

SEDE ADMINISTRATIVA

INSTITUTO DE CIÊNCIAS BIOMÉDICAS ABEL SALAZAR
FACULDADE DE CIÊNCIAS

Ana Isabel Delgado Cravo Lopes Nascimento

SENSORY NEURONS HAVE AN AXON INITIAL SEGMENT THAT INITIATES SPONTANEOUS ACTIVITY IN NEUROPATHIC PAIN

Tese de Candidatura ao grau de Doutor em
Biologia Molecular e Celular;
Programa Doutoral da Universidade do Porto
(Instituto de Ciências Biomédicas de Abel
Salazar e Faculdade de Ciências)

Orientador – Doutora Mónica Mendes Sousa
Categoria – Investigadora Coordenadora
Afiliação – Instituto de Biologia Molecular e
Celular (IBMC), Instituto de Investigação e
Inovação em Saúde (i3S), Universidade do Porto

Co-orientador – Doutor Boris Safronov
Categoria – Investigador Principal
Afiliação – Instituto de Biologia Molecular e
Celular (IBMC), Instituto de Investigação e
Inovação em Saúde (i3S), Universidade do Porto

This work was funded by FEDER through NORTE 2020, Portugal 2020 and Fundação para a Ciência e Tecnologia (FCT)/Ministério da Ciência, Tecnologia e Ensino Superior (PTDC/MED-NEU/28623/2017 and SFRH/BD/130014/2017), Santa Casa da Misericórdia de Lisboa (MC-39-2019), and Fundação Grunenthal, Bolsa de Jovens Investigadores em Dor 2016.

"*O caminho faz-se caminhando*"

António Machado

(Ensinado pela minha Mãe)

This Thesis is associated with the following literature review:

Nascimento, A.I., F.M. Mar, and M.M. Sousa. (2018). The intriguing nature of dorsal root ganglion neurons: Linking structure with polarity and function. *Progress in Neurobiology*, 168, 86-103. doi: 10.1016/j.pneurobio.2018.05.002.

This Thesis includes the scientific data presented in the following manuscript:

Nascimento, A.I., Da Silva, T.F., Fernandes, E.C., Luz, L.L, Mar, F.M., Safronov, B.V., & Sousa, M.M. (2022). Sensory neurons have an axon initial segment that initiates spontaneous activity in neuropathic pain. *Brain*, In Press. doi: 10.1093/brain/awac078.

Contents

ACKNOWLEDGMENTS/AGRADECIMENTOS

À Mónica, por me proporcionar todas as condições para desenvolver este trabalho, pelo apoio e confiança durante todo o tempo em que trabalhei no laboratório, e por ser um exemplo de otimismo e coragem a explorar novos caminhos em ciência.

Ao Boris, pelo precioso conhecimento que me transmitiu ao longo dos anos e pela ajuda prestada em várias fases deste projeto.

Aos meus colegas e amigos do(s) laboratório(s), e aos bons momentos que proporcionaram ao longo destes anos, tão importantes para conferir mais leveza ao quotidiano. Em particular, agradeço à Rita Costa, Joana, Tiago, Sara, Rita Leitão e Catarina, pela doce amizade e companheirismo que guardarei sempre comigo, e pelas peculariedades que fazem deles pessoas tão especiais. Aos restantes membros do laboratório, em particular a Márcia, a Marina, o Luís e a Bárbara, que vão deixar saudades. Ao Zé e ao Steeve, pela garantia de bons momentos e gargalhadas. À Elisabete e à Liliana, pelo carinho com que sempre me receberam.

Ao núcleo forte da minha vida, a quem dedico esta Tese: a minha Mãe, Pai, João e Tiago, sempre presentes, sempre prontos a acarinhar, a ajudar e a ouvir. Ao Tiago pelo amor incondicional e tão terno, por ser uma autêntica luz na minha vida.

Um especial agradecimento à minha mãe, ao Tiago, à Dra. Fernanda, e à Helena, pela dedicação e compromisso, por me darem a chance de viver melhor.

A todos os Familiares e Amigos de longa data que não menciono aqui e que me ajudaram a ultrapassar falhanços e a saborear vitórias, dando significado a todos os momentos.

SUMMARY

The axon initial segment (AIS) is a specialized compartment of the proximal axon of central nervous system neurons where action potentials are initiated. However, it remains unknown whether this domain is assembled in sensory dorsal root ganglion neurons, in which spikes are initiated in the peripheral terminals. Here we investigate whether sensory neurons have an AIS and if it contributes to spontaneous activity in neuropathic pain. Our results demonstrate that myelinated dorsal root ganglion neurons assemble an AIS in the proximal region of their stem axon, enriched in the voltage-gated sodium channels $Na_v1.1$ and $Na_v1.7$. Using correlative immunofluorescence and calcium imaging, we demonstrate that the $Na_v1.7$ channels at the AIS are associated with spontaneous activity. Computer simulations further indicate that the AIS plays a key role in the initiation of spontaneous discharges by lowering their voltage threshold. Finally, using a Cre-based mouse model for time-controlled AIS disassembly, we demonstrate that this compartment is a major source of spontaneous discharges causing mechanical allodynia in neuropathic pain. Thus, an AIS domain is present in sensory neurons and facilitates their spontaneous activity. This study provides a new insight in the cellular mechanisms that cause pathological pain and identifies a new potential target for chronic pain management.

SUMÁRIO

O segmento inicial do axónio (SIA) é um compartimento especializado do axónio proximal dos neurónios do sistema nervoso central onde os potenciais de ação são iniciados. No entanto, ainda não se sabe se este domínio existe no neurónios sensoriais dos gânglios da raíz dorsal, em que os potenciais de ação são iniciados nos terminais periféricos. Neste trabalho, investiga-se se os neurónios sensoriais possuem um SIA na região proximal do seu axónio, e se este compartimento contribui para a atividade espontânea observada em dor neuropática. Os nossos resultados demonstram que os neurónios dos gânglios da raíz dorsal mielinizados possuem um SIA na região proximal do seu axónio, enriquecido nos canais de sódio dependentes de voltagem $Na_v1.1$ e $Na_v1.7$. Usando imunofluorescência correlativa e imagiologia de cálcio, demonstramos que os canais $Na_v1.7$ do SIA estão associados a atividade espontânea. Para além disso, simulações computacionais indicam que o SIA tem um papel importante na iniciação de atividade espontânea através da diminuição do limiar de voltagem. Finalmente, usando um modelo de murganho genético baseado no sistema Cre para destruição temporalmente controlada do SIA, demonstramos que este compartimento é uma fonte crucial de atividade espontânea causadora de alodinia mecânica em dor neuropática. Assim, o SIA é um compartimento que está presente nos neurónios sensoriais e que facilita a sua atividade espontânea. Este estudo apresenta uma nova descoberta sobre os mecanismos celulares que causam dor patológica e identifica um potencial novo alvo terapêutico para o tratamento da dor crónica.

ABBREVIATIONS LIST

AP	Action potential
AnkG	Ankyrin-G
CAM	Cell adhesion molecule
CNS	Central nervous system
CCD	Chronic compression of the DRG
CCI	Chronic constriction injury
DAPs	Depolarizing afterpotentials
DPI	Days post-injury
DRG	Dorsal root ganglion
Ndel1	Dynein regulator nuclear distribution element-like 1
EB	End-binding protein
ICWs	Intercellular calcium waves
isi	Interspike interval
MAP	Microtubule-associated protein
NF186	Neurofascin-186
NP	Neuropathic pain
TRIM	Tripartite motif containing protein
PNS	Peripheral nervous system
PSD-93	Postsynaptic density-93 protein
SMPO	Subthreshold membrane oscillation
SGCs	Satellite glial cells
SNI	Spared nerve injury
SNL	Spinal nerve ligation
SNT	Spinal nerve transection
SA	Spontaneous activity
WPT	Weeks after tamoxifen injection
TTX	Tetrodotoxin
Ca_v	Voltage-gated calcium
K_v	Voltage-gated potassium
Na_v	Voltage-gated sodium

INTRODUCTION

The axon initial segment (AIS)

The axon initial segment (AIS) is a unique and specialized ~20–60-µm-long axonal structure that is intrinsically assembled by neurons [1]. The AIS was first described more than 50 years ago [2], and its functions, molecular composition, and organization have since been elucidated [3, 4]. Although the AIS is typically described as being positioned just after the axon hillock (fig. 1), it is now recognized that its position varies substantially between neuronal cell types [3]. In fact, in some neurons it is located far from the cell body, either because it has a more distal axonal position or because the axon emerges from a dendrite, or even due to a combination of both situations [5].

The AIS plays crucial physiological roles, as it is the site of action potential (AP) initiation, it undergoes alterations in response to changes in activity likely to modulate intrinsic excitability, and functions as a gatekeeper which maintains axonal identity. In agreement with its physiological importance, the AIS has emerged as a therapeutic target, since genetic mutations in AIS proteins have been associated with a diverse group neurological disorders, including epilepsy, cognitive disability and psychiatric diseases [3, 4].

Molecular organization of the AIS

It is consensual in the field that the defining molecular component of the AIS is the submembranous scaffold protein Ankyrin G (AnkG) (fig. 1B-C) [4]. This protein is encoded by the *Ank3* gene and is present in the AIS and nodes of Ranvier as two isoforms, the 480 and 270kDa variants. Both AnkG isoforms contain a membrane-binding domain which anchors AIS-specific membrane proteins, as well as a spectrin-binding domain which connects AnkG to the spectrin/actin submembranous scaffold. In addition, the 480kDa isoform contains a tail domain that interacts with microtubule-associated proteins [3].

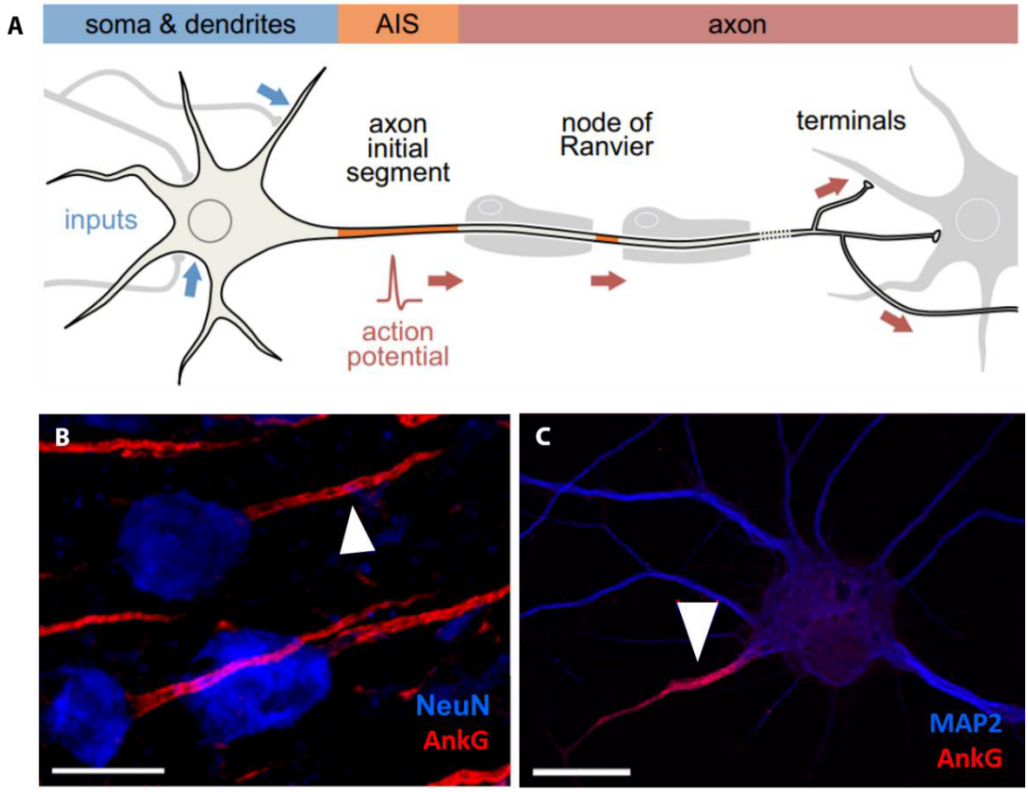

Fig. 1. The axon initial segment (AIS). (A) Schematic drawing showing the localization of the AIS at the proximal axon (orange). The AIS integrates inputs coming from the somatodendritic compartment and initiates action potentials (APs) that propagate along the axon toward presynaptic terminals contacting downstream neurons. In the case of myelinated neurons, APs are regenerated at nodes of Ranvier between myelin sheets. (B) Brain cortical neurons from an adult rat (labeled with NeuN, blue) with AISs labeled with Ankyrin G (AnkG, red, arrowhead). Adapted from [6]. (C) Embryonic rat hippocampal neuron after 14 days in culture, labeled for the somatodendritic marker MAP2 (blue) and AnkG (red, arrowhead). Adapted from [7]. Scale bars, 10 µm.

The events leading to AnkG clustering at the nascent AIS have only recently started to be unraveled. After axon specification, AnkG begins to cluster at the proximal axon, which occurs *in vivo* during embryonic development and up to the first postnatal days depending on the neuronal type [8-10]. Overall, the assembly of the AIS is cell intrinsic and contrasts with the formation of nodes of Ranvier, which despite also being enriched in AnkG and sharing some aspects of molecular organization, require axonal–glial interactions for their formation [1]. It is known that early loss of AnkG prevents the formation of the AIS, probably because AnkG recruits and clusters several AIS proteins in this structure [11]. In particular, the 480kDa variant of AnkG is the isoform necessary for AIS assembly [12]. However, AnkG recruitment alone does not explain how the accumulation of the different AIS proteins is achieved in the nascent AIS, when the levels of AnkG are still low. A detailed model was proposed in which, during AIS formation, endocytosis of AIS proteins is inhibited at this region, increasing the time window to allow interactions between AIS components until a high density of proteins is achieved [13]. In the mature AIS, the importance of AnkG is demonstrated by the fact that abolishment of its expression leads to AIS disassembly [14]. In spite of this, the stability of this structure is affected by depletion of other molecules, so there seems to be an interdependence between AIS components [15].

AIS cytoskeleton

Some years ago, super-resolution microscopy studies revealed that the axon contains a periodically organized actin/spectrin submembrane complex, composed of actin rings spaced by ~190 nm and connected by tetramers of spectrin (fig. 2) [16]. Throughout the axon, this periodic scaffold contains α2/β2-spectrin and anchors ankyrin B, while in the AIS, tetramers of α2/β4-spectrins are connected to AnkG. AnkG binds to the center of spectrin tetramers, thus positioning its associated AIS proteins midway between actin rings [16]. It was demonstrated that the periodic actin/spectrin scaffold appears before the assembly of the AIS, but it remains elusive how AnkG is incorporated in this periodic lattice in the proximal axon [17]. A model was suggested in which AnkG clusters in the nascent AIS by exclusion and not by recruitment. The distal actin subcortical cytoskeleton of the axon is progressively filled with Ankyrin B from its distal end towards the cell body, and leaves the remaining proximal axon free for AnkG assembly [10]. Nevertheless, the events leading to the reproducible clustering of AnkG at the proximal axon are poorly understood.

While the aminoterminal side of 480kDa AnkG connects to the actin/spectrin submembrane complex, its carboxyterminal side extends ~35 nm toward the cytoplasm [3]. Here, the tail domain of AnkG interacts with end-binding (EB) proteins 1 and 3, which are

positioned along microtubules in the AIS (fig. 2). This interaction is necessary for both the formation and maintenance of the AIS [18]. The microtubule network at the AIS has specific properties compared to the rest of the neuron, which are due to the presence of several microtubule-associated proteins (MAPs). For instance, electron microscopy studies show that, in the AIS, microtubules are arranged in fascicles consisting of 3–6 closely apposed microtubules connected by electron-dense cross bridges [2]. This feature is due to the MAP TRIM46, which is a member of the tripartite motif containing (TRIM) protein family that is specifically localized to the proximal axon before AIS assembly and, at later stages, is located in the proximal AIS [19]. TRIM46 forms closely spaced microtubule bundles oriented with their plus-end out, which have been recently shown to be actively recruited by AnkG to the vicinity of the plasma membrane in the AIS [20]. Another MAP involved in the stabilization of microtubule bundles at the AIS is the microtubule cross-linking factor 1 [21]. Besides being organized in bundles, AIS microtubules have other peculiarities. They exhibit specific post-translational modifications, and a high density of non-hydrolysed GTP-tubulin clusters termed GTP islands, which might help recruit EBs to the AIS [3].

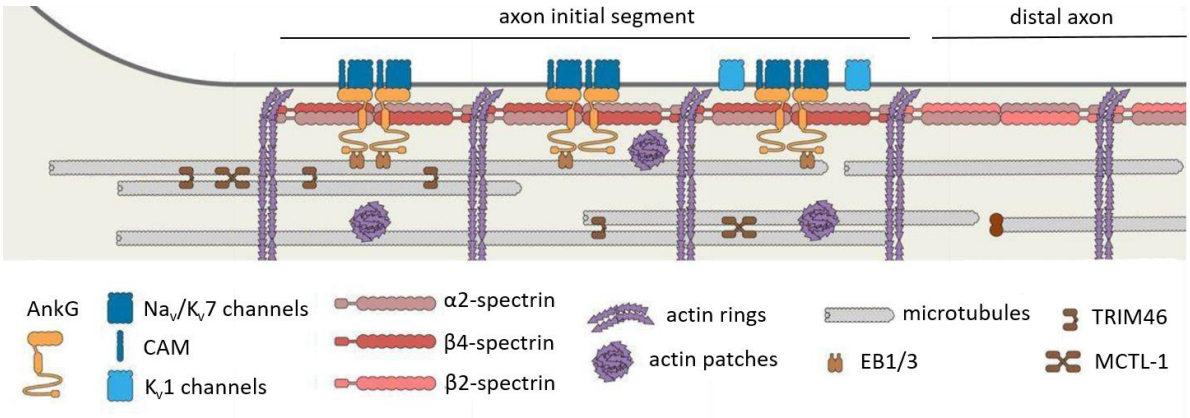

Fig. 2. Molecular organization of the AIS. Throughout the entire axon, spectrin tetramers (pink) lie horizontally under the plasma membrane, connecting actin rings (purple) with a distance of ~190 nm. In the AIS, Ankyrin G (AnkG, orange) is bound to β4-spectrin in the middle of the spectrin tetramers and anchors AIS membrane proteins, such as cell adhesion molecules (CAMs) and ion channels (Na$_v$ and K$_v$7 channels, dark blue). K$_v$1 channels (light blue) are present along the distal AIS. AnkG also binds to microtubules (grey) via EB1 and EB3 (brown). AIS microtubules are grouped in fascicles crosslinked by TRIM46 and stabilized by microtubule cross-linking factor 1 (MTCL1, brown). Actin patches (purple) are also present along the AIS. Adapted from [3].

Cell adhesion molecules (CAMs)

Several CAMs are specifically present at the AIS, playing many different roles. Among these, Neurofascin-186 (NF186) seems to be important for the stabilization of the AIS, both during its assembly and maintenance [13, 22]. In addition, NF186 is necessary for the formation of a specialized brevican-containing extracellular matrix that surrounds the AIS [11]. This CAM was also shown to play a role in the organization of GABAergic synapses at the AIS of hippocampal granule cells, which is innervated by chandelier cells [23]. Similarly, another CAM, the L1CAM, was recently demonstrated to be necessary for innervation of the AIS of pyramidal neurons by chandelier cells [24]. Besides, L1CAM deletion leads to an impairment of AP initiation, probably by causing a delocalization of voltage-gated sodium (Na_v) channels [25]. Other CAMs have an interdependent distribution at the AIS and are part of the Kv1 complex, such as transient axonal glycoprotein-1 (TAG-1), contactin-associated protein-like 2 (Caspr2), postsynaptic density-93 (PSD-93), leucine-rich glioma-inactivated 1 (LGI1) and ADAM proteins [26, 27].

Voltage-gated ion channels

A defining feature of the AIS is the high density of voltage-gated ion channels, including Na_v, potassium (K_v) and calcium (Ca_v) channels. Their distribution inside this structure is precisely determined to shape the neuronal firing behavior, but the molecular mechanisms for such subcompartmentalization within the AIS are unknown [4]. Overall, the mechanisms for targeting of channels to the mature AIS have been the subject of debate. A “diffusion trapping” hypothesis was put forward in which channels are transported to the plasma membrane and diffuse to the AIS where they are immobilized by AnkG. As an alternative, a “direct insertion” model has been proposed in which AnkG and its membrane partners are co-transported to the AIS, where they are immediately anchored. There is evidence that once channels are immobilized at the AIS, their diffusion and turnover are limited [15].

Nav channels

Na_v channels are accumulated in the AIS approximately 50 times higher than in dendrites [28]. Structurally, these channels are transmembrane proteins that enable the influx of sodium with a voltage-dependent activation. These channels consist of a pore-forming α-subunit (of ~260 kDa) and auxiliary smaller β-subunits (30–40 kDa). The α-

subunit is arranged in four domains connected by intracellular loops, and each domain consists of six transmembrane segments (fig. 3A) [29].

There are nine distinct sodium channel α-subunits which are voltage-gated ($Na_v1.1$-1.9), all containing the AnkG-binding motif [30]. Of these, the major isoforms located at the AIS are the $Na_v1.1$, $Na_v1.2$ and $Na_v1.6$. The specific α-subunits present in the AIS vary according to the developmental stage and neuronal type [4]. In addition, the densities of Na_v channels may vary along the AIS. In most mature neurons, the $Na_v1.1$ or $Na_v1.2$ channels are the predominant channels in the proximal AIS region, whereas the distal AIS contains mainly the $Na_v1.6$ channel [31-33].

Na_v channels are thought to be anchored in the AIS by binding to AnkG, which occurs via an interaction motif in the intracellular loop between the second and third channel domains (fig. 3A) [30, 34]. This interaction is regulated by the protein kinase CK2, which is concentrated in the AIS and phosphorylates residues of the AnkG-binding motif [35]. It has been claimed that this motif alone does not confer the preferential enrichment of Na_v channels to the AIS, and other mechanisms may play a role, for instance involving NF186 [22]. However, such mechanisms are still not well understood [3].

Potassium (K^+) channels

The K^+ channel family is one of the largest and most complex and diverse families of ion channels, with more than 80 genes encoding α-subunits in humans [36]. K^+ channels are classified into four distinct large groups, based on structural and functional characteristics: voltage-gated K^+ (K_v) channels, two-pore domain background K^+ (K_{2P}) channels, Ca^{2+}-activated K^+ (K_{Ca}) channels, and inwardly rectifying K^+ (K_{ir}) channels. Based on channel conductance, these families are further divided into subfamilies [36, 37]. Despite their diversity, all K^+ channels have a pore-forming domain and a regulatory domain. While the structure of the pore-forming domain is similar in all types of K^+ channels, the structure of the regulatory domain differs among the families. Moreover, these channels usually have three states: resting, activated and inactivated [38]. Upon activation, K^+ channels allow rapid transmembrane K^+ efflux that can repolarize or even hyperpolarize the cell membrane, thus controlling AP generation, waveform and frequency. In other words, K^+ channels oppose the depolarization of the membrane by excitatory channels [36, 37].

Over the years, it has been discovered that K^+ channels belonging to the group of K_v channels are enriched at the AIS. Among these, the $K_v7.2$ and $K_v7.3$ channels (KCNQ2 and KCNQ3) are localized to the distal part of the AIS [39]. These channels act as attenuators of excitability and determine the inherent spontaneous firing of hippocampal

pyramidal neurons [40]. Localization of KCNQ2/3 channels to the AIS has been proposed to follow the model of Na_v channels, as they contain a similar AnkG-binding motif located at the distal end of their intracellular C terminus [41] (fig. 3B). Since Na_v and KCNQ2/3 channels bind preferentially to an overlapped region on AnkG, it was suggested that the relative strength of binding to AnkG provides a basis for Na_v:KCNQ channel ratio regulation at the AIS [42]. However, additional modes of regulation have been suggested due to the discovery of other determinants for AIS localization outside of the AnkG-binding motif [43].

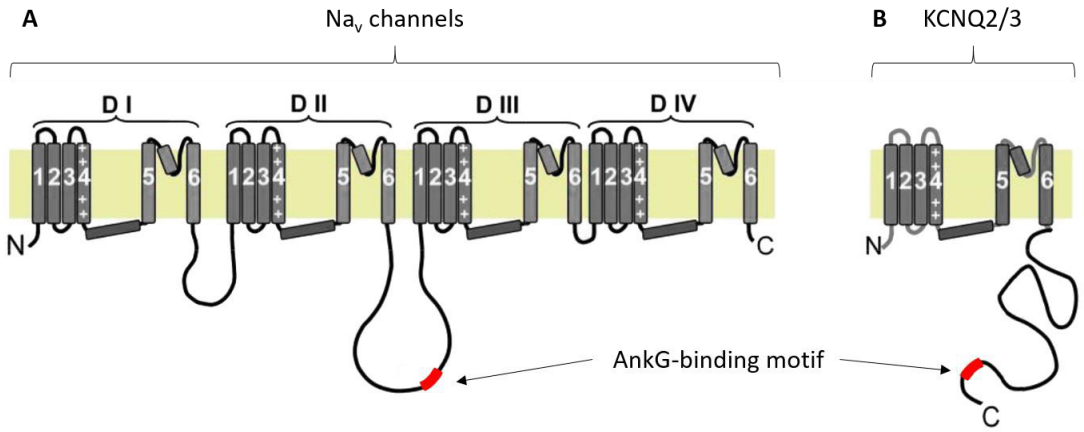

Fig. 3. Domain structures of Na_v channels and KCNQ2/3. (A) Nav channels possess four domains (I-IV) containing six transmembrane segments each. The AnkG binding motif is located in the intracellular loop between the second and third domains. (B) In contrast, K_v7.2 and K_v7.3 channels (KCNQ2/3) possess six transmembrane segments and an unusually long intracellular C terminus which contains the AnkG-binding motif. Adapted from [44].

K_v1.1 and K_v1.2 channels are also found at the AIS, where they form a macromolecular protein complex together with the CAMs [1]. These channels are involved in synaptic efficacy, as well as in determining the axonal AP waveform [45]. In contrast to KCNQ2/3, these two K_v channels do not bind to AnkG and instead are recruited to the AIS by a still unknown mechanism which *in vitro* is dependent on PSD-93 [3].

K_v2.1 channels are also found in the AIS, but they are clustered in noncanonical AnkG-deficient microdomains, near cisternal organelles and GABAergic synapses [46]. It was shown that the fraction of K_v2.1 channels destined for the AIS is targeted by a nonconventional trafficking pathway which bypasses the Golgi apparatus. In addition, K_v2.1 channels possess an AIS-trafficking motif in the C terminus. Nevertheless, the precise mechanism of recruitment of Kv2.1 channels to the AIS remains unknown [47].

Recently, clusters of K^+ channels belonging to the K_{Ca} family, predominantly the $K_{Ca}2.3$ channel subtype, have also been observed at the AIS of cultured pyramidal neurons. Although $K_{Ca}2$ channels have a widely accepted role in afterhyperpolarization, additional studies are needed to elucidate their specific role in the AIS [48].

Ca_v channels

Ca_v channels constitute the predominant pathway allowing the influx of calcium ions in response to membrane depolarization [49]. In the nervous system of vertebrates, there are nine distinct types of Ca_v channels which can be classified according to their voltage-dependence of activation into low voltage-activated (LVA) and high voltage-activated (HVA). While LVA calcium channels are constituted by a single subunit capable of generating calcium influx (α_1 subunit), HVA are heteromultimeric complexes formed through the assembly of the α_1 subunit with auxiliary subunits. Alternatively, Ca_v channels can be classified into three major families according to the α_1 subunit expressed: Ca_v1, Ca_v2 and Ca_v3. Overall, functional diversity of Ca_v channels is greatly increased not only by alternate splicing of the α_1 subunit, but also by interactions with different types of auxiliary subunits [49, 50].

Electrophysiological findings suggest that calcium currents from $Ca_v2.3$ and Ca_v3 channels are prevalent in the AIS, where they facilitate AP initiation [51]. In addition, $Ca_v2.1$ and $Ca_v2.2$ are enriched in the AIS, where they contribute to AP repolarization and decrease neuronal excitability [52]. Despite these findings, it is still unknown how Ca_v channels are localized specifically to the AIS.

The AIS as the gatekeeper which maintains neuronal polarity

The AIS has a remarkable role as a gatekeeper which maintains axonal identity, despite not contributing to axon specification. It is widely accepted that the AIS is the domain precluding the entrance of somatodendritic molecules into the axon, while permitting axonal molecules to enter. Therefore, there has been a great effort to understand the mechanisms for excluding specifically somatodendritic proteins from the axon [4]. Apparently, such mechanisms depend on AnkG, since loss of this protein causes the redistribution of somatodendritic molecules to the former axon of cultured neurons, as well as the formation of spines enriched in postsynaptic molecules along the axon both *in vitro* and *in vivo* [14, 53].

One of the mechanisms the AIS uses to maintain neuronal polarity and axonal identity is by restricting membrane diffusion [3, 4]. This hypothesis is supported by single particle tracking experiments showing that membrane proteins and lipids are less mobile at the AIS than in the cell body or in the rest of the axon [54, 55]. A model was proposed where a subset of immobilized AIS membrane proteins, likely ion channels and CAMs, functions as 'pickets' that slow the diffusion of membrane proteins and lipids [54]. However, a super resolution study showed that actin rings, rather than the AnkG-associated complex, seem to restrict lateral diffusion [55]. Given that actin rings exist throughout the entire axon, additional experiments are needed to clarify how membrane diffusion is restricted specifically in the AIS [4].

It has been suggested that, besides limiting membrane diffusion, the AIS also limits the diffusion of large soluble molecules through the axoplasm. It was proposed that an actin-based cytoplasmic sieve located at the AIS functions as a passive physical barrier impeding the transit of cytoplasmic macromolecules [56]. Contradicting this view, a variety of imaging techniques reveal that, in the AIS, actin exists as rings underlying the plasma membrane or as actin patches, and no actin structures are observed that could provide such diffusion physical barrier [3]. Moreover, an actin-based filter that functions solely based on size is difficult to reconcile with the fact that axonal large molecules diffuse through the AIS without impediment [4]. Altogether, the mechanisms regulating soluble molecule diffusion at the AIS are still unclear.

Intracellular trafficking implies active vesicular transport of membranous organelles and vesicles. The latter is driven by motor proteins, which can either move along actin (which is the case of myosins) or microtubules (kinesins and dynein) [57]. Active sorting of vesicles to their correct compartments seems to occur in the AIS, given that live-imaging of

vesicles harboring dendritic cargoes shows them halting or even reversing direction in this domain (fig. 4) [58]. It has been proposed that vesicles carrying somatodendritic cargoes are immobilized in actin patches along the AIS by recruitment of the actin-based molecular motor Myosin V [59]. However, besides this mechanism of immobilization, an additional process is required to return the mislocalized cargoes to the cell body. Fortunately, recent studies have shed light on how vesicles may be reversed at the AIS. The dynein regulator nuclear distribution element-like 1 (Ndel1), which was shown to localize to the AIS via an interaction with AnkG, can activate dynein-mediated transport of somatodendritic cargoes at the AIS [60]. This transport leads to the return of these cargoes to the cell body, because axonal microtubules have a uniform orientation with their plus-ends toward the axon tip, and dynein moves along microtubules towards minus-ends [57, 60]. Nevertheless, it remains unknown how Ndel1 recognizes somatodendritic cargoes. In contrast, axonal vesicles are preferentially trafficked into the axon by some kinesins, which move along microtubules toward plus-ends [61]. It is thought that kinesins play a role in this selective transport by preferentially interacting with microtubules from axons, but the biochemical cues these motor proteins recognize to distinguish axonal from dendritic microtubules are still unknown [61].

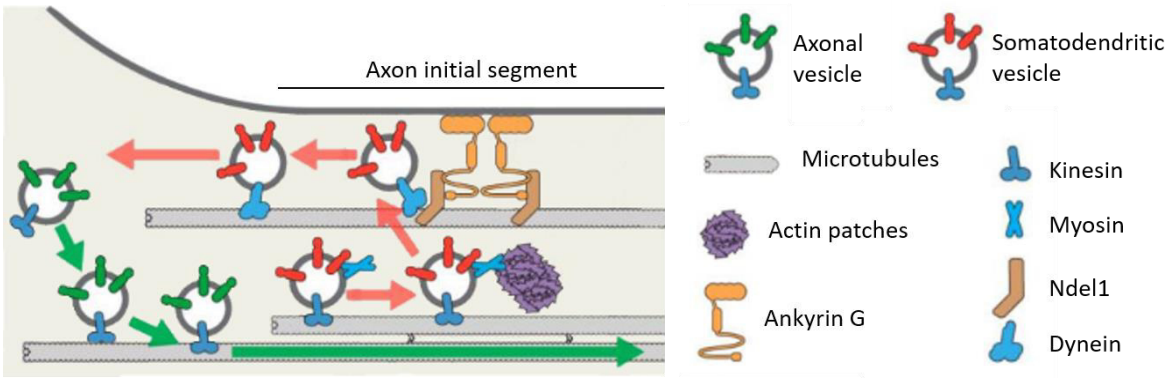

Fig. 4. Sorting of vesicles at the AIS. Vesicles containing axonal cargoes (green) are associated with kinesins that may recognize cues on axonal microtubules, which may promote their preferential transport to this domain. In contrast, mistargeted somatodendritic vesicles (red) which enter into the AIS are stopped by myosin-dependent immobilization at actin patches. These immobilized vesicles are then returned to the cell body by Ndel1-mediated dynein transport. Adapted from [3].

Despite the evidence provided in a number of studies, it is not completely consensual that the AIS is the structure which maintains cellular polarity. Some authors claim that sorting of cargoes does not occur at the AIS but instead within the axon hillock at a region termed “pre-axonal exclusion zone” [62]. Moreover, in the particular case of dorsal root ganglion (DRG) neurons, which have been claimed to virtually not have an AIS, it is suggested that cargo sorting is regulated by MAP2 via coordination of the activities of molecular motors [63]. However, this mechanism of trafficking regulation may apply specifically to DRG neurons given their peculiar pseudo-unipolar morphology and alleged absence of an AIS.

The AIS is the site of initiation of action potentials

Studies using electrophysiology recordings and voltage-sensitive dye imaging demonstrated that in many central nervous system (CNS) neurons, APs initiate in the AIS [64, 65]. The AIS has been shown to have the lowest threshold for AP initiation, up to 15 mV lower than that at the soma [66]. This is widely accepted to be the result of a higher concentration of Na_v channels in the AIS comparing to the soma [28]. Of note, some authors attribute the lower threshold for AP initiation in the AIS to the specific biophysical properties of AIS Na_v channels, such as higher propensity to generate persistent sodium current [67] or faster activation [68].

Within the AIS, APs are initiated first in the most distal part, a region which has been termed “AP trigger zone” [64, 65]. The mechanisms that determine the preferential AP initiation in the distal AIS have been the subject of debate. One hypothesis is that Na_v channels located specifically in the distal AIS, namely $Na_v1.6$ channels, have specialized biophysical properties which place the AP initiation site in this portion [32]. However, evidence from a study using $Na_v1.6$ channel knockout mice shows that deletion of this channel is not critical and results in relatively subtle differences in excitable properties [69]. Another hypothesis is that the distal AIS is the preferential AP initiation site due to its relative electrical isolation from the adjacent somatodendritic compartment [70]. Supporting this view, modeling studies demonstrate that, even if the AIS has a single sodium conductance of uniform gating properties, the preferential site for AP initiation is the distal portion, provided the AIS is a highly excitable domain [71, 72]. This hypothesis is based on the theory of resistive coupling, which applies when an AP initiation site is located in a thin axon electrotonically close to a much larger somatodendritic compartment [73, 74]. In this theory, the sodium current generated in the AIS flows primarily towards the cell body, where it will exist as capacitive current through the somatodendritic membrane. Therefore, the somatodendritic compartment acts as a current sink. Since the intracellular medium is resistive, there is an axial coupling resistance between the AIS and the soma that is proportional to the distance between them [74]. As so, the distal AIS is the region that is the most electrically isolated from somatodendritic capacitive loads and where the amount of sodium current needed for a given depolarization is lower comparing to more proximal AIS regions [70].

AIS plasticity as a mechanism of fine-tuning neuronal excitability

Given that the AIS is the site of initiation of APs, it is not surprising that alterations in its channels or morphology has an impact on neuronal electrical properties. In fact, a large number of studies provide evidence that AIS-specific parameters are dynamically regulated in order to fine-tune neuronal intrinsic excitability [75].

AIS morphology varies with activity, pathology and development

Two hallmark papers published in 2010 were the first to report forms of structural plasticity at the AIS [76, 77]. Since then, several studies have showed that AIS length and/or location undergoes alterations in response to changes in activity, likely to modulate neuronal excitability [4]. It is thought that structural AIS alterations may counterbalance the excess or insufficient activity in neural circuits and therefore they may work as a negative-feedback mechanism which maintains homeostasis [75]. This type of plasticity occurs on time scales ranging from hours to days [78, 79].

Alterations in AIS location were first observed in cultured hippocampal neurons chronically depolarized (for 2 days) via photo-stimulation or high extracellular potassium [76]. This increase in activity led to a distal repositioning of the AIS, which reversed when neurons were returned to non-depolarized conditions. In this study, patch clamp recordings showed that the AIS start position correlated with the threshold current density for firing an AP, and neurons with more proximal AISs fired more spikes in response to current pulses comparing to neurons with distal AISs [76]. Similarly, chronic depolarization of rat hippocampal organotypic slices resulted in a distal shift of the AIS of chandelier cells [80]. Importantly, alterations in AIS location were observed in several *in vivo* rodent disease models, in some cases associated with changes in neuronal excitability (table 1).

Alterations in AIS length were first reported in avian brainstem auditory neurons, some days after the removal of the cochlea of chickens after birth [77]. Deprivation from auditory input resulted in elongation of the AIS by 1.7 times, without changes in Na_v channel density but with the partial replacement of $K_v1.1$ channels for $K_v7.2$ channels [77, 81]. These alterations were accompanied by augmented whole-cell sodium current, membrane excitability and spontaneous firing. The authors suggested that AIS elongation and the switch of the dominant AIS K_v channels worked cooperatively as a homeostatic response to lack of activity in auditory circuits, allowing neurons to compensate for hearing loss [77, 81]. Besides elongation, the AIS can also undergo shortening. This type of plasticity is

observed in cultured hippocampal dentate granule cells, in which the AIS shortens within 3 hours of elevated activity, which is accompanied by de-phosphorylation of AIS Na_v channels [78]. Pharmacological separation of these two alterations revealed that they are antagonistic, since shortening reduced excitability in multiple spike firing, whereas the de-phosphorylation of Na_v channels increased excitability. Nevertheless, the physiological significance of this interaction is unknown [78]. Importantly, similarly to AIS repositioning, changes in the length of the AIS have been observed in pathological conditions *in vivo* (table 1).

AIS morphological plasticity is characterized by changes in the spatial distribution of several AIS components. As so, not only AnkG and Na_v channels [76, 78, 80], but also NF186 [76, 80] and βIV-spectrin [76], among other AIS molecules, undergo alterations in their distribution in the proximal axon. Notably, plasticity may not occur simultaneously for all components. In cultured hippocampal pyramidal neurons in which AIS plasticity is triggered by M-current inhibition, Na_v and K_v7 channels relocate away from the soma a few hours after inhibition, but AnkG only relocates 2 days later [79]. This is a curious observation, since AnkG seems to recruit these channels to the AIS, as described in a previous section.

Structural changes in the AIS occur not only in pathological conditions but also during embryonic and postnatal development [9, 82, 83] and with ageing [84, 85], suggesting its involvement in the refinement of neural circuits throughout life. Moreover, AIS plasticity seems to be cell-type-specific. For instance, in response to *in vitro* chronic depolarization, the AIS of inhibitory dopaminergic neurons from the olfactory bulb undergoes elongation and a proximal shift, while the AIS of hippocampal neurons and non-GABAergic neurons from olfactory bulb shortens and is located more distally [80].

Molecular mechanisms leading to AIS structural plasticity

The mechanisms that cause structural AIS alterations are still elusive. Overall, it seems that plasticity starts with the disassembly of the entire AIS complex, since the density of many AIS components decreases as early as 15-30 min after induction of chronic depolarization *in vitro* [86]. This depolarization-induced AIS disassembly is dependent on calcium signaling and is in accompanied by accumulation of AIS proteins in the distal axon, suggesting that they can be reassembled in a new AIS spatial distribution [86].

Table 1. Rodent models of disease with AIS structural plasticity

Disease model	Neuron type	AIS plasticity	Effect of AIS alterations on excitability
Type 2 diabetes [87]	Cortical and hippocampal neurons	16% shortening	Not assessed
Acquired epilepsy [88]	Newborn neurons in the dentate gyrus	13-14% shortening and 1 µm proximal relocation	Not assessed
Angelman syndrome [89]	CA1 and CA3 pyramidal neurons	- CA1: 13% elongation - CA3: 18% elongation	Not assessed
Focal cortical stroke [90]		- 3.7 µm of shortening	Not assessed
Acute and chronic demyelinatio n [91]	L5 pyramidal neurons	Demyelination types: - acute: 2 µm of proximal relocation and 9% shortening - chronic: 2 µm of proximal relocation	IR and CM: AIS start position positively correlates with AP amplitude, suggesting that AIS relocation reduced the capacity of Na_v channels to generate inward current for AP rising phase
Genetic and acquired epilepsy [92]	L5 pyramidal neurons	- genetic: 0.2µm of distal relocation - acquired: 0.6µm of proximal relocation	CM: proximal AIS relocation lowers the AP current threshold
Traumatic brain injury [93]	CA1 hippocampal pyramidal neurons and cortical neurons	- 2% shortening	CM: AIS shortening increases the AP current threshold and the interspike interval in repetitively firing neurons
ALS before symptom onset [94]	Alpha and gamma motor neurons	- Alpha neurons: 7% shorter and 7-10% wider - Gamma neurons: 12% shorter or 10% thinner proximally	IR: no consequence on individual APs or on the ability to initiate repetitive firing.
ALS after symptom onset [95]	Alpha motor neurons	- 13% longer and 6% thinner proximally	IR: faster maximum rate of AP rise, suggesting that AIS elongation represents an increase in AIS Na_v channels

* ALS: amyotrophic lateral sclerosis; IR: intracellular recordings; CM: computational modeling

Calcium signaling seems to be vital not only for AIS disassembly, but also for the spatial redistribution of its components, which results in AIS structural alterations. However, the specific mechanisms governing AIS plasticity seem to vary with the specific type of structural change (elongation *vs.* shortening, proximal *vs.* distal relocation), and also with cell type. In excitatory hippocampal neurons, distal AIS relocation and shortening are mediated by activation of L-type Ca_v1 channels, and the subsequent downstream events require calcineurin [78, 96]. In contrast, in hippocampal neurons subjected to M-current inhibition, the distal shift of the AIS is insensitive to L-type Ca_v1 channel activity but is dependent on protein kinase CK2 [79]. In inhibitory olfactory bulb dopaminergic cells, the elongation and proximal AIS shift is also dependent on L-type Ca_v1 calcium channels, but not on the activity of calcineurin [80]. AIS plasticity seems to be opposed in part by cyclin-dependent kinase 5, since its blockade causes AIS shortening and, in the case of inhibitory interneurons, a proximal AIS shift [78, 80].

Despite these findings concerning upstream pathways, much less is known about downstream mechanisms regulating AIS plasticity. Myosin II contractility seems to play a key role in this context, presumably by being involved in the cytoskeletal arrangements that produce structural alterations. This idea is supported by the fact that AIS shortening and relocation are completely blocked by blebbistatin, which is a selective myosin II inhibitor [97]. Accordingly, phosphorylated myosin light chain, which is an activator of contractile myosin II, is highly enriched at the AIS and is disassembled from this structure when sustained firing begins [86]. A model was proposed in which loss of phosphorylated myosin light chain from the AIS disrupts myosin II filaments and destabilizes the actin rings, leading to AIS disassembly and enabling this structure to be reassembled in the axon in a different position [86]. There is evidence that AIS structural plasticity may also require changes to the microtubule network, which may be dependent on tau phosphorylation [98]. Overall, the molecular mechanisms underlying the structural plasticity of the AIS remain unknown and require further investigation.

Electrical significance of changes in AIS morphology

The impact of structural AIS changes on neuronal excitability has been hotly debated since it was initially proposed. It has been questioned whether AIS morphological plasticity is the cause of the altered neuronal excitability observed across many studies, since correlation between AIS position/length and electrical properties does not imply causality [74]. However, it is quite challenging to conclusively determine the effect of AIS

position/length on neuronal excitability, since other cellular properties may play an important role, such as axon diameter and phosphorylation or inactivation state of Na_v and K_v channels [74, 99]. In fact, some studies describe AIS morphological changes that are not theoretically predicted to produce the reported alterations in excitability [99].

Theoretical studies have been demonstrating that the electrical impact of variations in AIS location and length depends on the relative sizes of the somatodendritic compartment and axon [100, 101]. Model simulations show that neurons with smaller somatodendritic compartments are more excitable when the AIS has an intermediate length and proximal position, whereas neurons with a larger somatodendritic compartment are more excitable when the AIS is longer and has a more distal position [100]. The explanation for this is based on the fact that, in neurons with a relatively large somatodendritic compartment, the latter acts as a current sink. It follows that if the AIS undergoes a distal shift, the axial resistance and the electrotonic isolation between the two compartments increases. As a result, less sodium current generated at the AIS is transmitted to the soma and more current is used to produce a local AIS depolarization. Therefore, neurons with a large somatodendritic compartment become more excitable when the AIS is positioned more distally [73, 99]. In contrast, neurons that have an axon and a somatodendritic compartment with comparable sizes become more excitable with a proximal AIS relocation [73, 99]. In these cells, the somatodendritic compartment no longer acts as a current sink. Instead, in more proximal axon positions, the local input resistance is higher, which means that local depolarizations are more easily produced in response to sodium current [99, 100]. Of note, neurons with large somatodendritic compartments can also become more excitable with more proximal AIS locations, if a strong hyperpolarizing conductance is present at this domain [79, 99].

Overall, changes in AIS morphology, especially AIS position, are predicted to have only a modest impact on intrinsic excitability [70, 99, 100]. Nevertheless, AIS plasticity may have an important role in modulating the frequency of repetitively firing neurons. A study combining *in vivo* extracellular recordings with morphological analysis and computational modeling demonstrated that the length of the AIS is the major determinant of tonic firing rate of dopaminergic neurons in the substantia nigra [102]. However, this conclusion was not corroborated in a subsequent study analyzing the same neuronal population [103].

Conclusively demonstrating the impact of structural AIS alterations on intrinsic excitability has proven to be quite challenging, since this phenomenon cannot be experimentally isolated from other factors that affect the neuronal electrical properties. The combination of anatomical analysis, functional recordings and computational modeling will

ultimately allow the discovery of the functional significance of AIS plasticity. However, this still awaits the development of new methodologies to selectively manipulate AIS properties.

Fast AIS plasticity

It has been recently proposed that neuronal excitability can be modulated by fast alterations in AIS ion channels. This type of AIS alterations takes place within seconds to minutes after activation of receptors located near or at the AIS [104].

An example of this type of plasticity is observed in cultured hippocampal neurons, in which high extracellular glutamate levels, but not neuronal stimulation, triggers a rapid and irreversible endocytosis of $Na_v1.2$, $K_v7.2$ and $K_v7.3$ channels that occurs within a few minutes. It seems that only AnkG-bound proteins are endocytosed rapidly during excitotoxicity, since this phenomenon was not observed with AIS $GABA_A$ receptors. These alterations required the activation of NMDA receptors, calcium influx, and calpain activation [105].

Regulation of neuronal excitability via rapid modulation of AIS ion channels does not necessarily involve channel internalization., as it may instead implicate alterations in the biophysical properties of the channels [75]. For instance, in hippocampal granule cells there is a negative shift in the activation curve of AIS K_v7 channels which is caused by activation of AIS muscarinic receptors by acetylcholine [106]. In cortical pyramidal neurons, activation of serotonergic receptors causes a positive shift in the activation curve of AIS $Na_v1.2$ channels [107]. There are many examples of this type of biophysical changes, which are cell-type specific and ultimately alter neuronal excitability [75].

Dorsal root ganglion neurons: a neuron type without AIS?

Most vertebrate CNS neurons have a multipolar morphology (i.e. dendrites and axon arising from the cell body) and possess an AIS. In contrast, there is a peripheral nervous system (PNS) neuron type, the DRG neuron, which does not have dendrites and it is still unknown whether it has an AIS. In the following sections, the anatomy and morphology of this peculiar neuron type are described, and the evidence indicating that these neurons might have an AIS is discussed.

Anatomy and Morphology of DRG neurons

In vertebrates, all somatosensory pathways (with the exception of those coming from the head) begin with the activation of DRG neurons. These neurons are responsible for the transmission of sensory information to the CNS, namely: thermoception (sensing temperature), nociception (feeling pain), mechanoreception (sensing pressure) and proprioception (sensing body spatial position). Their cell body is inside DRGs, which are ganglia located alongside the spinal cord (fig. 5A). Interestingly, DRG neurons have a unique morphology, which is termed pseudo-unipolar. They have a single process -the stem axon- which bifurcates within the ganglion into a peripheral and a central axonal branch. Sensory stimuli lead to the generation of APs in the peripheral branch terminals that are then conducted toward the stem axon bifurcation. From this point, APs are conducted along the central axon towards the CNS. The central axon enters the spinal cord via the dorsal root and then bifurcates into an ascending and a descending branch that grow longitudinally along the lateral margin of the spinal cord over several segments. In the case of some neurons, the ascending central branches synapse in the gracile or cuneate nuclei of the brainstem. From the ascending and descending central branches, collaterals are generated in the spinal cord that penetrate the gray matter and synapse in specific laminae of the spinal grey matter [108].

To achieve their final unique morphology, DRG neurons undergo a morphological transformation termed pseudo-unipolarization (fig. 5B). During embryonic development, DRG neurons are spindle-shaped bipolar. Then, the cell body bulges more in a direction, and the two processes approach each other forming an angle of less than 90 degrees (bell-shaped bipolar conformation). Most evidence suggest that subsequently, the stem axon originates from elongation of the cell body between the two processes [109]. Of note, results from *in vitro* studies indicate that pseudo-unipolarization is not cell-autonomous but instead

depends on glial cells [108, 110]. In the case of medium and large DRG neurons, which are myelinated, the stem axon usually forms a structure termed glomerulus of Cajal. This glomerulus consists of the stem axon making a tortuous coiled path and eventually spiraling. When present, myelin starts in the stem axon within this glomerulus or more distally, as shown in fig. 5C [108].

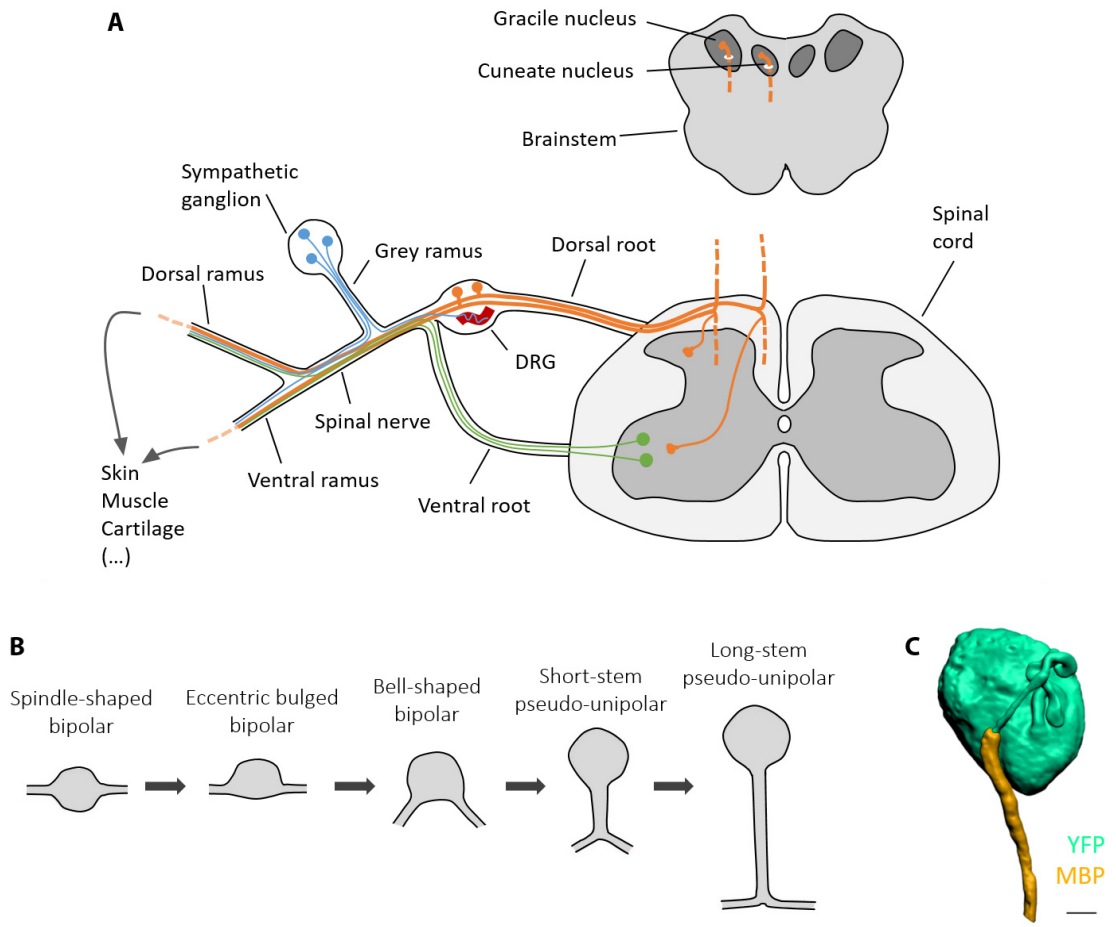

Fig. 5. Anatomy and morphology of DRG neurons. (A) Schematic drawing showing DRG neurons (orange) with an axonal branch going to the periphery, and a central axon bifurcating and synapsing in the spinal cord laminae and in the brainstem nuclei. The spinal nerve contains not only the axons of DRG neurons but also of motor (green) and sympathetic (blue) neurons. Sympathetic fibers are depicted entering in the DRG, where they associate with blood vessels (red). (B) Morphological stages of DRG neurons during pseudo-unipolarization. (C) Segmented confocal z-stack of a myelinated YFP$^+$ DRG neuron from adult Thy1-YFP-16 mice immunostained for myelin basic protein (MBP). Scale bar, 10 µm. Images from [108].

Evidence that DRG neurons may have an AIS

In vitro, embryonic DRG neurons assemble a distinctive region that has a position and molecular composition similar to the AIS [111]. This domain is enriched in AnkG [112], βIV-spectrin [11, 113], Na_v channels [111] and NF186 [111, 112]. In cultured DRG neurons with multiple neurites, this AIS-like structure is located in the initial portion of some of these processes [111], whereas in cultured pseudo-unipolar neurons this domain is located in the proximal stem axon [11, 113]. Given that DRG neurons have this structure even in the absence of glial cells, they seem to have the intrinsic capacity to assemble an AIS [112]. Altogether, these observations suggest that DRG neurons may possess an AIS-like structure *in vivo*. Of note, this domain seems to be absent from cultured adult DRG neurons [63], possibly because adult neurons lose the ability to recapitulate *in vitro* the AIS assembly as embryonic neurons do.

The *in vivo* existence of the AIS in the proximal stem axon of DRG neurons, as defined by the enrichment in AIS-specific components, lacks experimental support. Early findings suggest that the stem axon of DRG neurons has ultrastructural specializations and a Na_v channel density similar to those of Nodes of Ranvier and AISs. Using electron microscopy, Matsumoto and Rosenbluth (1985) showed that the proximal stem axon of frog DRG neurons has patches of a layer of dense material lining the plasma membrane [114], similar to the undercoat that is observed in nodes of Ranvier and in the AIS [2]. Moreover, using freeze-fracture replicas, these authors demonstrate that the concentration of intramembranous particles at the cell body (~300μm^{-2}) is much lower than that at the axon hillock and proximal stem axon (~800-1000μm^{-2}) [114]. The particle concentrations in the latter regions approach that at the nodes of Ranvier in the frog brain (~1200μm^{-2}) [115]. Since these intramembranous particles are believed to partially represent Na_v channels, these observations suggest that the proximal stem axon has a high Na_v channel density [114], which is compatible with the presence of an AIS. In another study, Devor and Obermayer (1984) obtained similar results using the ferric ion-ferrocyanide method, which is believed to label selectively membrane regions with high Na_v channel content [116, 117]. These authors showed that not only a variable portion of the soma, but also the axon hillock and the proximal stem axon are heavily stained with this method [116]. Despite these early evidences, a single immunofluorescence report suggests that the proximal stem axon of adult mouse and rat DRG neurons contains AnkG [118]. However, evidence for this is not presented, since the specific enrichment of AnkG in this region is not clear in the images provided by the authors. More recently, AnkG-enriched stem axon regions compatible with AISs were only detected in less than 2% of adult rat DRG neurons [63].

So far, there is no compelling evidence that the AIS is a ubiquitous feature of DRG neurons *in vivo*, although these cells have the ability to assemble an AIS-like structure *in vitro*. Given that the AIS is of utmost importance for neuronal physiology, it is of considerable importance to definitely determine if DRG neurons, or a subpopulation of DRG neurons, have an AIS *in vivo*.

For more detailed information about DRG neuron ultrastructure and polarity please consult the appendix section, which contains the literature review written in the context of this thesis.

Peripheral neuropathic pain

In physiological conditions, nociceptive pain functions as a protective alarm that signals potentially-damaging stimuli and continues only in the maintained presence of a noxious stimulus. However, a pathological condition termed neuropathic pain (NP) may arise due to a lesion or disease of the somatosensory nervous system. In this maladaptive response, pain is spontaneous and responses to innocuous and noxious stimuli are abnormally amplified [119]. NP is a specific type of chronic pain, which in turn is defined as pain that persists or recurs for more than 3 months [120].

Several lesions or diseases can damage the CNS or PNS and determine the onset of NP. Spinal cord injury, multiple sclerosis and stroke are examples of common causes of central NP. By contrast, peripheral NP, which can have a generalized or focal distribution, is commonly triggered by metabolic, inflammatory and infectious diseases, chemotherapy, trauma and surgery, among other causes [121]. Since NP occurs after neuronal damage of various etiologies, it is a common clinical problem likely affecting between 7 and 10% of the general population [122].

Patients with NP present an abnormal sensory perception, not only with negative symptoms (such as reduced sensation to stimuli), but also with positive ones. The latter can be spontaneous (for instance electrical shock-like pain and tingling or skin crawling

sensations), or stimulus-evoked, such as allodynia (pain from a non-nociceptive stimulus, i. e. light touch) and hyperalgesia (increased pain sensitivity to a nociceptive stimulus) [123]. Furthermore, NP is associated with reduced scores in all domains of quality of life, as well as sleep disturbances, anxiety and depression, even more than in patients with other chronic pain conditions [124].

Despite representing a source of major disability, NP is still very difficult to treat. In most cases the management of the pathological condition causing NP is insufficient to relieve pain, so available treatments focus on attenuating symptoms. Traditionally, management of NP is based on oral (i.e. antidepressants, antiepileptics and opioids) or topical pharmacotherapy (lidocaine and capsaicin) [121, 125]. In patients who are not responsive to standard treatments, interventional approaches may be used, such as injection of drugs and electrical stimulation of targeted areas [121]. Overall, most of the currently available treatments for NP have moderate efficacy and are associated with adverse effects that limit their clinical use. Therefore, a significant effort has been made on the development of novel therapeutic agents targeting new pathological mechanisms [121, 125].

Numerous promising analgesics have derived from molecular findings in experimental animal models [126]. These preclinical models attempt to replicate the many human pain conditions underlying NP [127]. Among these, there are many surgical, as well as chemotherapy- and diabetes-induced rodent models, as shown in table 2. Each model has its own benefits and limitations, regarding for instance reproducibility, underlying molecular mechanisms and the type of pain behaviors elicited, which should be all taken into account when a model is selected [127]. Despite this diversity of pain models, it has been claimed that preclinical pain research needs to change to provide additional translational value, because drugs that have being impressively effective in attenuating pain in animals, have failed once tested in clinical trials [128].

Table 2. Common rodent models of peripheral NP affecting DRG neurons

Type of model	NP model	Type of injury
Surgical	Sciatic Nerve transection	Complete transection of the sciatic nerve at mid-thigh level [127].
	Chronic Constriction Injury (CCI)	In rats, four loose ligatures with 1-mm spacing are placed around the sciatic nerve proximal to the trifurcation [129]. In mice, typically three ligatures are made [130].
	Partial Sciatic Nerve Ligation	Ligation of the dorsal third or half of the sciatic nerve at the upper-thigh level [127].
	Spinal Nerve Transection (SNT)	Removal of 1-3mm of the L5 spinal nerve [127].
	Spinal nerve Ligation (SNL)	One (L5) or two (L5 and L6) spinal nerves are ligated in the rat [131]. In mice, the L4 and L5 are ligated [132].
	Spared Nerve Injury (SNI)	Tight ligation of the common tibial and peroneal nerves, followed by removal of a 2-3mm section of the nerves distally to the ligature [127].
	Chronic Compression of the DRG (CCD)	Implantation of a stainless steel rod into the L4 and/or L5 intervertebral foramen in rats [133], and L3/L4 in mice [134].
Chemotherapy-induced	-	Single or repeated intraperitoneal injection of chemotherapeutics such as paclitaxel, oxaliplatin and vincristine in rodents [135].
Diabetic	Streptozotocin-induced	Single intraperitoneal or intravenous injection of streptozotocin leading to β-cell impairment in pancreas [136].
	Diet/nutrition-induced	Rodents are fed with high fat/energy diet, leading to obesity and type 2 diabetes [136].

Spontaneous activity (SA) in DRG neurons triggers peripheral neuropathic pain

SA generated in DRG neurons is considered to be a key mechanism driving NP. In human patients with different painful neuropathies, microneurography recordings demonstrate the existence of spontaneous ongoing discharges in the affected nerves [137-140], which suggests that this pathological phenomenon may be a hallmark of NP independently of its etiology.

Spontaneous discharges originating in DRG neurons have been reported since at least the 1930s in NP animal models [141]. Of note, in some studies, a residual or small percentage of DRG neurons presents spontaneous discharges before lesion [142], or in control animals [133, 143]. Many of these studies have implicated SA as a causative factor in the development of NP, not only as a raw pain signal but also as a trigger of central sensitization, which amplifies the signal from intact and injured sensory neurons resulting in increased symptoms. This hypothesis is supported by the observation that SA appears in the hours or days following injury, which coincides with the time of onset of pain behaviors [143-145], and its blockade attenuates or eliminates pain symptoms [143]. But while it is consensual that DRG neuron SA is a trigger of central sensitization and pain behaviors, the importance of these discharges to the maintenance of NP has raised some controversy, as experiments analyzing later time-points have yielded contradicting results [143, 145-148]. The hypothesis that SA not only triggers but also maintains NP is supported by many studies in which transiently blocking SA by local application of anesthetics reduces or eliminates pain symptoms only temporarily, both in animals and patients [149-151]. Similarly, it has been demonstrated that blocking the access of SA to the spinal cord by dorsal root transection attenuates pain [148, 149, 152]. Taken together, most observations support the view that once established, central sensitization and pain symptoms are not completely self-perpetuating but instead need to be maintained by peripheral SA [153].

It is likely that SA from each DRG neuron subtype represents a distinct pathophysiological mechanism that contributes to the establishment of specific NP symptoms. Therefore, the identification of the DRG neuron types which are spontaneously firing could be useful in the development of targeted analgesia tailored to each patient [154]. Overall, NP has been associated with spontaneous discharges in injured sensory neurons with conduction velocities distributed across all fiber ranges (Aβ, Aδ and C fibers) [143, 155], although it seems that the predominant axonal population with SA are large myelinated fibres [142, 144, 147, 156].

It is logical that SA from DRG neurons with Aδ- and particularly C-fibers directly provokes pain, since these cells encode noxious stimuli. In fact, SA in primary afferents with C-fibers has been associated with ongoing symptoms including burning-like pain [154]. In contrast, at first sight, Aβ-fiber inputs would not be expected to contribute to pain behaviors, as most of these are non-nociceptive and encode innocuous mechanical sensations such as light touch [153, 157]. Nevertheless, activation of Aβ-fiber neurons for instance by gentle skin brushing provokes pain sensations in patients with NP (a symptom termed mechanical dynamic allodynia). In fact, there is evidence that inputs from injured Aβ-axons cause the development of mechanical allodynia [153, 154]. In particular, SA originated in Aβ neurons seems to contribute to this type of pain behavior in animals [144, 145, 149, 158]. But how could spontaneous discharges in large DRG neurons contribute to pain symptoms in NP? Many studies have presented evidence that could explain this [153, 154]. One of the possible explanations is phenotypic switching, in which upon injury Aβ neurons start to express and release neurotransmitters that are usually restricted to nociceptors, such as substance P and calcitonin gene-related peptide (CGRP) [159, 160]. Aβ-fibers typically terminate in the intermediate and deep spinal laminae of the dorsal horn, while second-order nociceptive neurons, which have receptors for these peptides, are located in the superficial laminae. However, these neurotransmitters may gain access to nociceptive spinal neurons for instance by being released from Aβ axons which have sprouted to more superficial laminae following injury [161], among other possibilities [153]. In this way, phenotypic switching may enable DRG neurons with Aβ-fibers to render noxious stimuli by directly activating second-order nociceptive neurons. Crossover onto central pain pathways may also occur by cross-excitation of nociceptive C- and Aδ-fiber neurons by neighbor spontaneously firing Aβ neurons within the DRG, particularly in NP conditions [162, 163]. Alternatively, SA from Aβ neurons may contribute to mechanical allodynia not only by directly driving pain-signaling pathways, but also by triggering and maintaining central sensitization [153, 154]. There is indirect evidence of this, such as the observation that application of lidocaine in the peripheral nerve reverses the pathological hyperexcitability of spinal nociceptive neurons [146]. Besides mechanical dynamic allodynia, it is also hypothesized that electrical shock-like pain is associated with Aβ-fiber damage, namely focal demyelinations, but this hypothesis awaits further confirmation [154].

Determining the site of origin of SA in DRG neurons

Unraveling the compartment of the DRG neuron which initiates SA could facilitate the development of new therapies.

Early extracellular electrophysiological findings have implicated the neuroma (the injury site containing aborted axon growth) and the ends of regenerating nerves as sites of initiation of SA [164]. Spontaneous discharges likely originate in the swollen endings of non-regenerating axons and in the endings of regenerating sprouts, which have accumulation of Na_v channels [165, 166].

Along the nerve, axonal regions with focal demyelination have also been indicated as potential initiators of SA [167]. In fact, there is evidence associating focal demyelination with NP, namely electrical shock-like symptoms [154]. It has been suggested that SA might initiate in putative large clusters of Na_v channels that form in extended demyelinated gaps, but this is yet to be proven [168].

Besides the neuroma, animal studies have shown for decades that a significant part of SA comes from the DRG [142, 169-171]. This conclusion is supported by the fact that spontaneous discharges recorded from dorsal roots are completely [156, 169] or mostly [133, 142, 144] unaffected by nerve transection, but are eliminated after transection of the dorsal root. Human findings also provide indirect evidence that SA originates within the ganglion. For example, in patients suffering from phantom limb pain, SA and spontaneous pain are not suppressed by application of lidocaine in the neuroma [137], but the application of this analgesic to the DRG by spinal and intraforaminal epidural blocks spontaneous pain [172].

In vitro findings have implicated the cell body of DRG neurons as the neuronal compartment originating SA within the DRG. This hypothesis is supported by the fact that acutely dissociated neurons (isolated cell bodies) from animals with NP have a higher incidence of SA than dissociated neurons from control animals [173-175]. Similarly, patch-clamp recordings in acutely dissociated DRG neurons from NP patients showed the existence of a strong correlation between NP and SA [176]. However, despite facilitating the study of SA, results from dissociated DRG neurons should be taken with a grain of salt, as these cells acquire an injury-like phenotype in culture, with increased excitability and altered gene expression comparing to neurons from intact ganglia [177, 178].

Electrophysiological recordings of DRG neurons in intact ganglia have the potential to shed some light regarding the sites triggering SA within the DRG. In fact, two sharp electrode intracellular studies provide evidence that the soma is not the only cellular compartment capable of initiating discharges inside the ganglion [179, 180]. Three groups

of DRG neurons are observed in these reports, based on the cellular sites originating SA within the ganglion:

- In some neurons, all SA originates in the cell body and/or in the proximal stem axon, since discharges remain after these cells are pulled from the surface of the DRG to break the stem axon at a maximum of 50µm in length [180]. Moreover, this type of activity is quenched when the cell body is hyperpolarized [179].
- In a second group of neurons, SA is completely abolished after the cell body and attached proximal stem axon are pulled from the DRG, showing that discharges are initiated exclusively in the axon [180]. Moreover, in these neurons, the firing rate of discharges is sensitive to somatic resting membrane potential, suggesting that the site of origin of SA is relatively close to cell body. The authors propose that the T-junction is likely the place initiating this ectopic activity due to its structural features [179].
- In a third group of DRG neurons, two coexisting sites generate repetitive firing: the soma and the nearby axonal site. In such cells, hyperpolarization of the cell body eliminates somatic spikes, but invading axonal spikes remain [179, 180]. The results also indicate that spikes initiating in the cell body can be triggered by spikes originating in the axon, giving rise to complex discharge patterns [179].

Taken together, these two studies show that SA can originate in multiple structures in the DRG neuron besides the peripheral axon endings, and spikes generated at multiple sources within the same cell may interact [179, 180].

Overall, technical limitations have precluded the definite identification of the cellular sites of the DRG neuron which originate SA. It is still unclear whether it is the cell body itself and/or the proximal stem axon that initiates discharges, and also other putative axonal sources of SA within the ganglion are not identified. This topic is certainly worth of future investigations.

Electrophysiology of SA

In rodent models of NP, the firing patterns of SA recorded from DRG neurons can be classified into three categories: irregular, tonic and bursting (fig. 6A). Irregular SA has a highly variable interspike interval (isi) and relatively low spike frequency, while tonic firing has high frequency and a fixed isi. Bursting discharges have a fixed isi and high spike frequency within each burst, but a fixed or variable isi between bursts [142, 145, 180-182]. Evidence suggests that both the neuroma and DRG can originate SA with the three

patterns. The proportion of each pattern type originating in each place seems to vary with the animal model used [142, 144] and with time [144, 145, 183].

Studies using intracellular sharp electrode recordings provide evidence that small sinusoidal oscillations of the membrane potential, which are termed subthreshold membrane oscillations (SMPOs), underlie SA in DRG neurons. It has been demonstrated that spontaneous APs emerge from the rising phase of SMPOs, and neurons which do not have these oscillations are not capable of firing repetitively even when strongly depolarized [184, 185]. In addition, the percentage of DRG neurons with SMPOs increases after injury [185, 186]. Intracellular recordings also suggest that SA with irregular pattern is generated when SMPOs occasionally reach threshold, initiating single spikes. Similarly, in bursting SA, the first spike of each burst is thought to be triggered by SMPOs, though the subsequent spikes are seemingly triggered by depolarizing afterpotentials (DAPs), which depolarize the membrane beyond threshold during recovery from the previous AP (fig. 6B left). Similarly to bursts, tonic firing is also thought to be maintained by DAPs [184]. Despite these observations, repetitive firing and particularly SA have been observed in the absence of SMPOs (fig. 6B right). For instance, most spontaneously firing DRG neurons that share the nerve with injured neurons do not have SMPOs [187]. It was proposed that most SA triggered by SMPOs originates in the cell body of DRG neurons, while SA originating in the axon occurs in the absence of SMPOs, being initiated and maintained by distinct electrogenic mechanisms [179, 180]. Overall, several findings have challenged the initial view that SMPOs are a necessary condition for SA.

Besides SMPOs, other electrophysiological properties of DRG neurons have been associated with painful neuropathy. Overall, injured DRG neurons from animals with pain symptoms have increased excitability comparing to uninjured neurons from control animals [181, 188-191]. Nevertheless, the analysis of the entire population of damaged DRG neurons as a whole overlooks the fact that only some neurons are firing spontaneously, while the majority of cells are silent. Unfortunately, few studies discriminate injured spontaneously firing neurons from injured silent ones. In a few existing reports, it is shown that injured neurons with spontaneous discharges are in fact more excitable compared to uninjured and injured silent neurons, with altered properties such as higher resting membrane potential and more hyperpolarized voltage threshold, both *in vivo* [180] and *in vitro* [192]. Overall, there is evidence that spontaneously-active DRG neurons are more excitable than their silent counterparts.

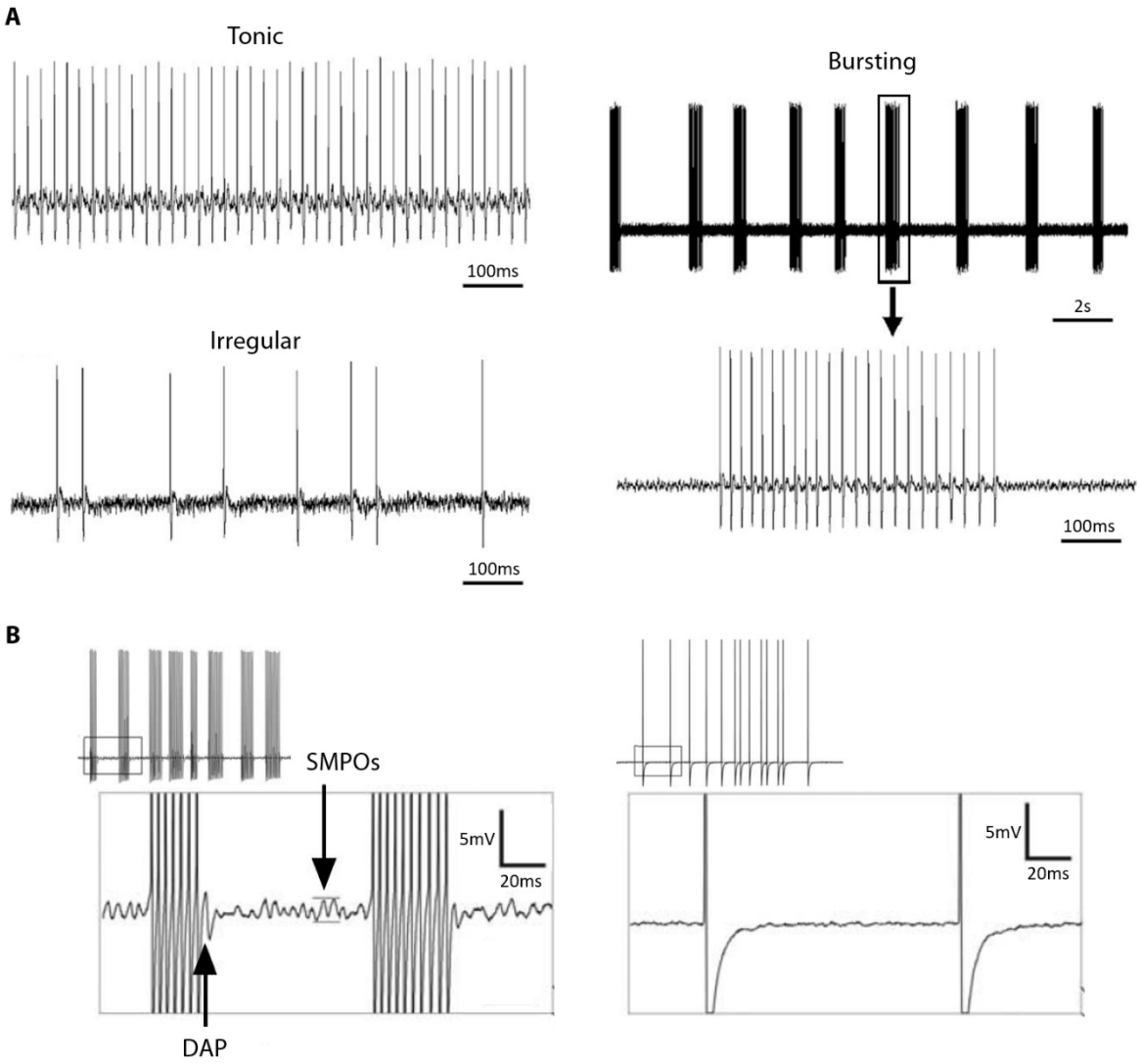

Fig. 6. Electrophysiological features of spontaneous activity (SA) in DRG neurons. (A) Extracellular recordings showing typical examples of firing patterns in neuropathic pain animal models: tonic, irregular and bursting. Adapted from [145]. (B) Intracellular recordings of a neuron with a bursting pattern of SA with SMPOs and DAPs (left), and a neuron with irregular SA and without SMPOs nor DAPs (right). Adapted from [180].

Changes in membrane electrical properties lead to DRG neuron hyperexcitability

It is still not clear if pathological SA in sensory neurons is intrinsically or extrinsically evoked, or results from both types of causes. Several observations suggest that, once established, neuronal SA is independent of external influences, such as the fact that acutely dissociated cell bodies from previously injured DRG neurons initiate repetitive firing spontaneously [180]. In fact, the view that prevails is that hyperexcitability and SA in sensory neurons emerges from alterations in the intrinsic electrical properties of their membrane [193]. It is thought that following injury, pathological changes lead to the formation of pacemaker regions, which are sites capable of generating repetitive firing which in physiological conditions exist exclusively in the peripheral axon endings [193]. Supporting this hypothesis, results from somatic injection of depolarizing currents, either by a slow ramp or step function, show that most healthy DRG neurons do not have this pacemaker capability and respond to this stimulus with a single spike, while a higher proportion of injured neurons respond with rhythmic firing [186].

A bulk of transcriptional studies have shown that after peripheral injury, there are profound alterations in gene expression in DRG neurons [194]. Such changes lead to a remodeling of the cell membrane after lesion, including in voltage-gated ion channels, which are major determinants of excitability. Changes in the density and subcellular distribution of these channels are thought to trigger hyperexcitability [193]. Channel density can be altered not only by dysregulation of the expression of channels themselves, but also by abnormal channel trafficking and anchoring in the cell membrane, caused for instance by posttranslational modifications of channels or enhanced interactions between channels and kinesin molecular motors or CAMs [195]. Moreover, in a pathological context there are new regions permissive to channel insertion such as neuroma endbulbs, sprouts and demyelinated regions, which are new potential pacemaker sites [193]. Even if channel density and distribution remain unchanged after injury, alterations in the intrinsic properties of channels could also affect the ionic current densities, leading to hyperexcitability [193].

Despite most studies tend to focus on the role of a specific voltage- or ligand-gated ion channel in primary afferent excitability and chronic pain states, surveying across these reports reveals that a striking amount of channels is implicated. This includes Na_v channels, K^+ channels, Ca_v channels, transient receptor potential (TRP) channels and hyperpolarization-activated cyclic nucleotide-gated (HCN) channels, among others [196, 197]. The next sections provide an overview of the channels that are particularly important for DRG neuron excitability and are considered major targets for analgesic drug discovery.

Na_v channels

In a simplistic view, Na_v channels can adopt three voltage-dependent conformational states that determine channel conductance: closed, open, and inactive. At hyperpolarized membrane potentials, Na_v channels are closed and do not allow the influx of sodium, but in response to membrane depolarization, the protein domains that are sensitive to voltage rotate, opening the pore within a millisecond. Sodium current is terminated via fast inactivation, by movement of a cytoplasmic loop of the protein that occludes the intracellular side of the pore, impeding the flow of sodium. As an alternative to fast inactivation, which occurs within a millisecond or so, slow inactivation can take place, occurring within tens of seconds. Slow inactivation is still not completely understood, but it is known to occur in response to prolonged depolarizations. When the cell membrane becomes hyperpolarized again, Na_v channels recover from inactivation (repriming) and return to the closed state, being available again for activation [29]. Importantly, Na_v channels undergo inactivation not only from the open state at strongly depolarized membrane potentials (open-state inactivation). Alternatively, closed-state inactivation may occur before Na_v channels open, at hyperpolarized or modestly depolarized membrane potentials [198].

Although the expression of α-subunits is sufficient for functional sodium currents, five β-subunits have been described (β1, its splice variant β1B, β2, β3 and β4), which associate noncovalently or covalently with α-subunits [199]. β-subunits modulate the biophysical properties of Na_v channels, and regulate channel density at the plasma membrane [29, 199]. Moreover, these subunits can have a role in cell adhesion even in the absence of α-subunits, and hence they contribute to multiple physiological and developmental processes. DRG neurons express varying levels of all β-subunits, and there is some data implicating them in chronic pain states [199].

Na_v channels are obvious targets for the development of new treatments for chronic pain, because they play an essential role in neuronal excitability [29, 167, 200]. In fact, the pacemaker capability depends primarily on Na_v channels [193]. Simulation results suggest that in order to behave as a pacemaker, a region requires a certain density of these channels, as otherwise only single spikes can be initiated or propagated. Besides, a higher Na_v channel density leads to a lower threshold for initiating repetitive spiking [201]. This is the rationale behind the peripheral application of low doses of non-selective Na_v channel blockers such as lidocaine to suppress DRG neuron SA and relieve pain, while simultaneously allowing normal axonal impulse propagation [202]. However, some Na_v channels types are also present in the skeletal and cardiac muscles and other neuronal populations besides DRG neurons, so a non-selective approach may elicit unwanted side

effects. Considering this risk, drug developers have struggled to achieve selectivity for subtypes of Na_v channels [203].

Mammalians express nine distinct Na_v channel α-subunits. Among these, $Na_v1.1$, $Na_v1.6$, $Na_v1.7$, $Na_v1.8$ and $Na_v1.9$ channels are robustly expressed in the healthy adult DRG. In contrast, $Na_v1.2$ and $Na_v1.3$ are expressed but at very low levels. $Na_v1.4$ is not found at all in the adult DRG [204], and instead is present in the skeletal muscle [205]. $Na_v1.5$ is found in the cardiac muscle [206], and there is evidence of its expression in the adult DRG, but its role and cellular distribution have not been unraveled [207]. Besides the nine voltage-gated α-subunits, there is a non-voltage-gated channel, the Nax, which is gated by sodium concentration [208] and is also expressed by DRG neurons in adulthood [204]. Of note, during embryonic development the combination of Na_v channel isoforms expressed in DRG neurons is different, with $Na_v1.2$, $Na_v1.3$ and $Na_v1.5$ channels being found during this period [209, 210].

DRG neurons with different sizes and functional properties express distinct combinations of Na_v channels (table 3). Overall, large-diameter DRG neurons express predominantly the α-subunits $Na_v1.1$, $Na_v1.6$, $Na_v1.7$ and, in a subset of these cells, $Na_v1.8$. In contrast, small-diameter neurons express predominantly the $Na_v1.7$, $Na_v1.8$ and $Na_v1.9$ isoforms [211]. These variations in Na_v channel expression result in electrophysiological differences, such as AP waveform and the response to tetrodotoxin (TTX), a toxin that blocks all α-subunits except $Na_v1.5$, $Na_v1.8$ and $Na_v1.9$ isoforms due to a single amino acid substitution in the S5–S6 linker [212].

In the following sections, each Na_v channel subtype is reviewed in respect to its biophysical properties, as well as its role in DRG neuron hyperexcitability and chronic pain, in particular NP. The $Na_v1.2$ and $Na_v1.5$ channels are not discussed, due to lack of evidence of their involvement in NP [200].

$Na_v1.1$ channels

Mutations in the $Na_v1.1$ channel have been associated with migraine, but it is unknown if this is a consequence of alterations in neuronal excitability in the CNS or in the trigeminal ganglia [213]. In fact, until relatively recently there was no association between $Na_v1.1$ channels and nociception [200, 213]. The first study establishing such link is from Osteen *et al*. (2016), who used two tarantula-derived algogenic toxins to selectively activate $Na_v1.1$ channels. These authors demonstrated that activation or sensitization of fibers expressing these channels elicit robust acute pain, as well as mechanical allodynia [214]. Although these findings establish an unexpected role for $Na_v1.1$ channels in regulating the

excitability of DRG neurons that underlies mechanical pain, the role of these channels in the development of chronic pain remains obscure.

Table 3. Sodium channel isoforms expressed in DRG neurons

Na_v channel subtype	Gene name [167]	Sensitivity to TTX? [193]	% of neurons with Na_v^+ mRNA [204]; distribution among DRG neurons	Subcellular localization in healthy and injured adult DRG neurons
1.1	SCN1A	Yes	~30%; predominant in larger neurons [214]	Soma [214]
1.2	SCN2A	Yes	Very low levels [204]	Not detected at all
1.3	SCN3A	Yes	Very low levels/absent [215]	Soma [216] and ends of transected peripheral axons [217].
1.6	SCN8A	Yes	~30%; neurons of all sizes [218]	Soma, along unmyelinated axons [218], peripheral terminals [219, 220], nodes of Ranvier [221], and nodes of Ranvier with altered morphology within the neuroma [222].
1.7	SCN9A	Yes	~85%; expressed by neurons of all sizes [204], but its expression is stronger in unmyelinated and thinly myelinated nociceptive neurons [223, 224].	Soma, along unmyelinated axons, nodes of Ranvier of some Aδ-fibers, peripheral and central terminals [224] and ends of transected peripheral axons [225].
1.8	SCN10A	No	~67%; predominant in small/medium, but also present in large-diameter neurons [226]	Soma [227], along unmyelinated axons [228], free nerve endings and ends of transected peripheral axons [229].
1.9	SCN11A	No	~60%; neurons of all sizes [204]	Soma, along unmyelinated axons, nodes of Ranvier of some Aδ-fibers, free nerve endings and central terminals [230].
NaX	SCN7A	Yes	~70%; predominant in medium/large neurons [231]	Soma [232]

$Na_v1.3$ channels

Despite being expressed in DRG neurons during development and postnatally, the $Na_v1.3$ channel has very low expression levels in the adult DRG [215]. Nevertheless, after peripheral nerve axotomy and in painful diabetic neuropathy, this channel is robustly reexpressed by both small and large-diameter neurons [216, 217, 233]. Due to its fast kinetics, namely fast repriming, $Na_v1.3$ channel could enable higher firing frequency and contribute to the pathological hyperexcitability of DRG neurons [29, 193]. In fact, many observations support a role of $Na_v1.3$ channels in NP. In animal models, injury induces the accumulation of $Na_v1.3$ in neuronal cell bodies and within the ends of transected axons [217]. Similarly, $Na_v1.3$ was detected in human painful neuromas [229]. In addition, the time-course of $Na_v1.3$ upregulation matches well with the development of SA and mechanical allodynia in animals [216]. However, unfortunately, preclinical studies testing the importance of $Na_v1.3$ in the development of NP have yielded contradictory results. Pain-like behaviors developed normally in $Na_v1.3$ knockout mice subjected to SNL [234] and to SNT, but were attenuated in knockout mice subjected to CCI [235]. In another study, intrathecal administration of antisense oligonucleotides after SNI resulted in the reduction of $Na_v1.3$ expression, but it had no effect on mechanical allodynia [236]. In contrast, mechanical allodynia was attenuated by injection of an AAV expressing shRNA for knockdown of $Na_v1.3$ in the SNI and streptozotocin-induced diabetes models [237, 238]. Despite the inconsistent results, these preclinical studies show that $Na_v1.3$ channels are a potential target for analgesics at least in some NP states.

$Na_v1.6$ channels

$Na_v1.6$ channels produce resurgent currents in DRG neurons [239]. Resurgent currents are generated due to transient opening of Na_v channels after the membrane is repolarized, during recovery from inactivation [240]. Due to these currents, selective activation of $Na_v1.6$ channels increases repetitive firing of DRG neurons *in vitro* [241].

Pharmacological activation of $Na_v1.6$ channels enhances the response of DRG neurons to mechanical stimuli *in vivo*, which supports an important role of these channels in the development of painful mechanosensations [241]. However, only recently has human evidence emerged showing a role for $Na_v1.6$ channel in chronic pain. A mutation in this channel was described in a patient with a human painful disorder termed trigeminal neuralgia, and was associated with increased resurgent currents and hyperexcitability in sensory neurons [242]. Accordingly, evidence from animal models has implicated the $Na_v1.6$ channel in NP. Oxaliplatin-induced NP seems to depend specifically on the $Na_v1.6$

channel, since selective inhibitors for this channel attenuate cold allodynia in this model, whereas knockout mice lacking the $Na_v1.3$, $Na_v1.7$, $Na_v1.8$ or $Na_v1.9$ channels develop pain-like behaviors normally [235, 243]. $Na_v1.6$ channels also seem to be important for injury-induced NP. Knockdown of these channels by injection of small inhibitory RNA in the DRG abolished SA and reduced sympathetic sprouting and mechanical allodynia induced by SNL, although cold allodynia was not attenuated [244]. In the CCD model, knockdown of $Na_v1.6$ channels also using small inhibitory RNA reduced both mechanical and cold allodynia and SA [245]. In addition, AAV-mediated knockout of $Na_v1.6$ channel attenuated mechanical allodynia and DRG neuron hyperexcitability after SNI [222]. Although this relatively recent evidence suggests that Nav1.6 channel plays an essential role in the development of NP, the mechanisms by which this channel contributes to DRG neuron hyperexcitability remain unclear. Using the oxaliplatin-induced NP model, Zhang *et al*. (2019) proposed that palmitoylation of δ-catenin promotes kinesin-mediated membrane trafficking of $Na_v1.6$ to the plasma membrane, leading to neuronal hyperexcitability and pain [246].

$Na_v1.7$ channels

The $Na_v1.7$ channel exhibits a slow closed-state inactivation. As a consequence, it can produce a robust ramp current in response to subthreshold, slow depolarizations. Therefore, it has been suggested that $Na_v1.7$ channel has an important role in impulse initiation and pacemaking, by amplifying generator potentials originated from stimulation of sensory nerve endings [29, 247].

The importance of $Na_v1.7$ channels for normal pain sensations is evidenced by the association of human pain threshold levels with single nucleotide polymorphisms in the SCN9A gene, which encodes these channels. In addition, patients with a disease termed congenital insensitivity to pain are unable to feel pain in response to noxious stimuli due to loss-of-function mutations in the SCN9A gene [29]. Accordingly, mice lacking $Na_v1.7$ channel expression also have less sensitivity to noxious stimuli [248, 249]. Many mechanisms have been mentioned to explain how lack of $Na_v1.7$ channel leads to a defect in nociceptive processing, such as compromised AP initiation in peripheral axon terminals, failure to transmit APs, and impaired neurotransmitter release by central axon terminals [29]. However, studies using conditional knockout mice show that not all acute pain sensations are dependent on $Na_v1.7$ channel expression in DRG neurons. Instead, acute pain responses to noxious heat are affected only when this channel is simultaneously abolished in sensory and sympathetic neurons [250]. Conversely, gain-of-function

mutations in the SCN9A gene can lead to disabling chronic pain conditions such as inherited erythromelalgia or paroxysmal extreme pain disorder. These mutations lead to abnormal biophysical channel properties, hyperexcitability and in some cases increased DRG neuron SA [29]. Overall, animal studies and human genetics have demonstrated that the $Na_v1.7$ channel has an important role in acute nociception and sensitization in several chronic pain conditions. Therefore, there has been a huge effort to develop selective $Na_v1.7$ channel blockers for clinical use [203].

Preclinical studies support a pivotal role for the $Na_v1.7$ channel in the development of some types of NP. Mice lacking $Na_v1.7$ channels exhibit attenuated pain-like behaviors after CCI and SNT comparing to their wildtype littermates [235]. However, the specific role of $Na_v1.7$ channel is unclear. In the CCI model, abolishment of $Na_v1.7$ channel expression in DRG neurons is sufficient to eliminate pain-like behaviors, but in contrast, after SNT, pain is only ameliorated when this channel is eliminated from both DRG and sympathetic neurons [250]. These results suggest that $Na_v1.7$ channels contribute to NP through distinct cellular and molecular mechanisms depending on the type of injury. Supporting this view, this channel has been shown to be down- or upregulated following peripheral injury, depending on the animal model used [251, 252].

$Na_v1.7$ channels accumulate in nerve neuromas, both in animals and humans [225, 229, 253]. Evidence indicates that, after peripheral injury, $Na_v1.7$ channels may contribute to SA and pain-like behaviors by being modulated by mitogen-activated protein kinases (MAPKs). In fact, activated (phosphorylated) MAPKs are also abnormally accumulated in human and animal neuromas [225, 229], and are able to phosphorylate $Na_v1.7$ channels and alter their gating properties *in vitro* [254]. $Na_v1.7$ channels may also lead to DRG neuron hyperexcitability by undergoing changes in alternative splicing after injury, since different splice variants have distinct biophysical properties when regulated by protein kinase A [255] or β-subunits [256]. Supporting this hypothesis, the relative proportions of the alternatively SCN9A spliced variants are altered after SNL [257].

$Na_v1.8$ channels

Although the initial prevailing view was that $Na_v1.8$ channel expression is restricted to nociceptive DRG neurons, later reports have shown it has a much wider expression, being present and carrying functional currents at least also in A- and C-fiber low-threshold mechanoreceptors [226].

Due to its biophysical properties, the $Na_v1.8$ channel plays a key role in neuronal excitability and repetitive firing. In nociceptors, it carries the majority of the current during

the rising phase of APs. Moreover, since its fast inactivation is depolarized, it is available to activate even at depolarized resting membrane potentials, when other Na_v channels are inactivated. As so, it is not completely inactivated during the falling phase of APs, contributing significantly to AP duration and to an inflection (hump) in this phase. This channel also contributes to repetitive firing, probably because of its depolarized inactivation and fast repriming [29, 247]. The current originated in $Na_v1.8$ channels can be modulated in a number of ways, such as by association of this channel with β-subunits, or by binding to partners that regulate its density in the cell membrane [29].

Similarly to $Na_v1.7$ channels, $Na_v1.8$ channels seem to be important both for acute nociception and chronic pain states. Evidence from human studies shows that single nucleotide polymorphisms in the SCN10A, the gene which encodes $Na_v1.8$ channels, affect pain threshold levels. Moreover, a number of gain-of-function mutations in the SCN9A gene are associated with small fiber neuropathy, probably by contributing to DRG neuron hyperexcitability and increased repetitive firing [29]. This evidence highlights the potential of $Na_v1.8$ as a therapeutic target for pain relief.

Preclinical studies show that $Na_v1.8$ channels are crucial for inflammatory pain, but their contribution to NP is still not very clear [247]. Inhibition of these channels, either by administration of antisense oligodeoxynucleotides or $Na_v1.8$ channel blockers [258, 259], attenuates pain-like behaviors in rodent NP models. In addition, $Na_v1.8$ channels seem to be required for the generation of spontaneous discharges, since there is virtually no SA initiating in the neuromas of $Na_v1.8$ channel knockout mice, in contrast to wild-type neuromas [260]. Accordingly, the $Na_v1.8$ channel accumulates in human neuromas, where it colocalizes with p38 MAPK [229]. It has been suggested that the interaction between these two molecules in neuromas contributes to DRG neuron hyperexcitability, because p38 MAPK increases the current of $Na_v1.8$ channel and inhibition of this MAPK attenuates pain-like behaviors after CCI [29]. Contradicting the view that $Na_v1.8$ channels are essential for the development of NP, mice lacking this channel develop all or some of the pain-like behaviors analyzed after SNL, SNT and CCI, similarly to their wildtype littermates [250, 261]. However, gene knockout experiments are particularly difficult to interpret, due to potential compensatory changes in ion channel expression [262].

$Na_v1.9$ channels

The $Na_v1.9$ channel has unique gating properties that distinguish it from all the other channels. These channels activate at more hyperpolarized voltages and inactivate with unusually slow kinetics, which results in a persistent current after activation. In addition,

since activation and inactivation of $Na_v1.9$ channels exhibit a large overlap, there is a large window current within the physiological voltage domain which includes the resting membrane potential of DRG neurons. Therefore, it has been suggested that $Na_v1.9$ channels act as threshold channels, by inducing depolarization of resting membrane potential and contributing to boosting weak stimuli [29, 263].

Human studies have validated the role of $Na_v1.9$ channel in pain perception, due to the identification of $Na_v1.9$ mutations in patients with painful and painless channelopathies [29]. In addition, preclinical models demonstrate the importance of $Na_v1.9$ channels to inflammatory chronic pain, but its relevance to NP is not understood due to discrepancies among animal studies [29]. Knockdown of this channel with antisense oligodeoxynucleotides does not attenuate pain-like behaviors after SNL [264], and $Na_v1.9$ channel knockout mice develop mechanical allodynia similarly to their wildtype littermates after partial sciatic nerve ligation, SNI and CCI [235, 265, 266]. Nevertheless, mice lacking $Na_v1.9$ channel exhibit less cold sensitivity after CCI then their littermates [235, 266].

Na_x channels

In contrast to Na_v channels, Na_x channels are not regulated by voltage. Instead, they act as sensors of sodium concentration and are critically involved in body-fluid homeostasis [208]. So far, only one study has associated Na_x channels with chronic pain. Ke *et al*. (2012) demonstrated that these channels are upregulated in a bone cancer pain model in which cancer cells are implanted into the tibia. Knockdown of Na_x channels attenuated pain-like behaviors and reversed DRG neuron hyperexcitability [232]. However, further studies are needed to understand if these effects are triggered directly or indirectly by Na_x channels, as well as investigate if they are also important for injury-induced NP models.

Potassium (K^+) channels

DRG neurons express a panoply of K^+ channels in each subcellular compartment (soma, unmyelinated axon, peripheral and central terminals, nodes of Ranvier, paranodes, and juxtaparanodes), which may vary depending on neuron subtype. Independently of their subcellular location, K^+ channels are seen as endogenous brakes to DRG neuron hyperexcitability [36, 37]. This is shown by application of broad-spectrum K^+ channel inhibitors in peripheral terminals, neuromas and in the ganglion, which induces repetitive firing [179, 267, 268]. Moreover, pharmacological or small interfering RNA inhibition of many

K^+ channel types induces primary afferent hyperexcitability and pain behaviors. Therefore, it is thought that NP is triggered by a reduction in the expression of K^+ channels in DRG neurons [36, 37]. Supporting this view, downregulation of K^+ channels is one of the most common observations in preclinical models of NP (table 4), and often it has a time course that matches the development of SA and pain-like behaviors [36]. Another observation that seems to confirm this hypothesis is that *in vivo* knockdown of these channels in DRG neurons, such as $K_v1.2$, $K_v3.4$, $K_v4.3$, $K_v9.1$ and TRESK, is sufficient to increase pain-like behaviors [269-272]. Conversely, NP symptoms triggered by peripheral injury can be attenuated by K^+ channel openers, or injection of AAVs promoting the expression of specific channels, such as $K_v1.2$, $K_v7.2$ and $K_{ir}2.1$ [272-274]. Due to these observations, K^+ channels are seen as promising targets for the treatment of pain syndromes. However, their exceptional diversity and varied cellular and subcellular distribution have made the discovery of their precise function in chronic pain and primary afferent excitability extremely challenging [36, 37].

Ca_v channels

With the exception of $Ca_v1.4$ and $Ca_v3.1$, DRG neurons express all subtypes of Ca_v channels [275]. Among these, $Ca_v2.2$ and $Ca_v3.2$ channels have emerged has validated targets for analgesia [49]. It has been demonstrated that, in NP models, these channels are upregulated [50], and their pharmacological blockade or knockdown reduce pain-like behaviors [276-280]. It is known that $Ca_v2.2$ channels are located in the soma and in central terminals of primary afferents [281], while $Ca_v3.2$ channels are present not only in these subcellular compartments but also along unmyelinated axons, in nodes of Ranvier and peripheral terminals [282]. However, the mechanisms by which these channels contribute to NP states at the level of the DRG neuron remain unclear. These channels might simply regulate neuron excitability [50, 196]. Other possibilities by which these calcium channels might contribute to pain signaling is by enhancing neurotransmitter release at central terminals, or by playing a direct role in mechanotransduction [50, 196]. Besides these two α_1 subunits, there is evidence demonstrating the relevance of the regulatory subunit $Ca_v\alpha_2\delta$ for NP, presumably by controlling the trafficking of $Ca_v2.2$ channels in DRG neurons, among other possible mechanisms [49, 281].

Table 4. Dysregulation of K^+ channels at the level of the DRG in models of NP (analyzed by RT-PCR, IHC and WB)

NP model	Downregulated K^+ channels	K^+ channels with no changes in expression	Upregulated K^+ channels
SNL	K_v1.1, K_v1.2, K_v1.4 [283], K_v2.2, K_v6.3, K_v6.4, K_v8.1, K_v9.1 [284], K_v3.4, K_v4.3 [269], TWIK1 [285], BK_{Ca} [286]	K_{ir}6.2 [287]	-
SNT	K_v2.1, K_v2.2 [288], K_v9.1 [270]	-	-
CCI	K_v1.1, K_v1.2, K_v1.4, K_v2.2, K_v4.2, K_v4.3 [289], K_v12.1, TREK1, K_{ir}4.1, K_{Ca}3.1 [290]	K_v1.5, K_v1.6, K_v2.1, K_v3.1, K_v3.2, K_v3.5, K_v4.1 [289]	-
SNI	K_v1.2, TWIK, TASK3 [291]	TASK1 [291]	-
Nerve transection	K_v1.1, K_v1.2, K_v1.3, K_v1.4 [292], K_v1.2 [293], K_v7.2 [294], TRESK [271], K_{ir}3.1, K_{ir}3.2 [295]	K_v1.5, K_v1.6 [292] K_v1.4, K_v1.6 [293]	
Oxaliplatin-induced NP	K_v1.1, TREK1, TRAAK (RT-PCR [296])	K_v1.2 [296]	-
Paclitaxel-induced NP	K_{ir}1.1, K_{ir}3.4, TWIK1 [191]	K_v1.5, K_v4.2, K_v7.1, K_v7.3, K_v10.1, K_{ir}1.4, K_{ir}3.4, K_{ir}4.2, SK_{Ca}2 [191]	K_v1.2, K_v11.3, K_{ir}3.1 [191]
Painful diabetic neuropathy	K_v1.4, K_v3.4, K_v4.2, K_v4.3 [297], K_v7.2, K_v7.3, K_v7.5 [298]	K_v1.1, K_v1.2, K_v2.1, K_v2.2 [297]	-

Challenges of developing drugs that target ion channels

Since ion channels are key determinants of neuronal excitability, they are a major target for analgesia in chronic pain. Promising findings using rodent pain models have been reported, and for some channels, preclinical results have been validated by human genetic evidence [29]. But unfortunately, extensive efforts to discover selective and efficacious modulators of ion channels, such as blockers of Na_v1.7, Ca_v2.2 and Ca_v3.2 channels, have resulted in clinical failures [203, 299, 300].

One possible explanation for these clinical failures is that abnormalities observed in established rodent pain models are different from those underlying pain occurring in patients, so the usefulness of these models to predict drug responses in patients may be limited [196].

Another explanation for drug discovery failure is that seemingly similar pain syndromes may differ mechanistically, thus requiring further subdivision of patients according to molecular mechanisms [235]. However, given the uncertainty about mechanisms involved and the lack of biomarkers, such personalized medicine still lies out of reach and polypharmacy is suggested as a solution [235].

The failures in devising novel pain therapies may also be related to the fact that many different ion channel alterations are sufficient to cause neuron hyperexcitability [301, 302]. In fact, some authors have claimed that chronic pain is characterized by degeneracy, a term that is gaining recognition in fields like cancer. Degeneracy consists of multiple different mechanisms producing an equivalent outcome [302, 303]. If multiple pathological alterations, which are individually sufficient to cause hyperexcitability, occur after injury, then none of these changes is individually necessary. This hypothesis has significant implications for clinical practice. It means that increased function of a particular Na_v channel may be sufficient to trigger DRG neuron hyperexcitability, but its abolishment may fail in preventing the development of pain. Moreover, even if targeting a specific ion channel provides a reduction in excitability and pain-like behaviors, this attenuation may only exist for a short period of time, since compensatory changes in other ion channels can occur. Altogether, if the pathological changes associated with chronic pain are degenerate, then targeting one single channel is not likely to produce a lasting pain relief [303].

Cell extrinsic factors that modulate DRG neuron SA

It is widely accepted that in pathological conditions, DRG neurons undergo changes that lead to the intrinsic initiation of spontaneous discharges. Nevertheless, it is also well established that their hyperexcitability is affected by external factors, namely the cross-talk with neighboring DRG neurons, glial cells and with sprouted sympathetic fibers inside the ganglion. These topics are discussed in the following sections.

The influence of communication with satellite glial cells

DRG neurons are supported by two types of glial cells: the satellite glial cells (SGCs) and the Schwann cells, which associate with different neuronal compartments. SGCs are only present inside ganglia, where they envelop each neuron cell body and its initial part of the stem axon. In contrast, the distal part of the stem axon and its two branches are ensheathed by Schwann cells [304, 305]. SGCs and Schwann cells have a similar morphology [306], and it was recently hypothesized that SGCs are a population of cells of the Schwann cell lineage that have their differentiation arrested through contact with the DRG neuronal soma and proximal stem axon [307]. Each DRG neuron cell body is completely wrapped by one or more layers of SGCs, creating a structural unit that is separated from other units by connective tissue (fig. 7). Occasionally, there are two or three neuron cell bodies sharing a common connective envelope [308]. Although SGCs and DRG neurons do not establish synapses, these cells communicate extensively through the release of chemical mediators that diffuse in the extracellular space between them.

As a consequence of damage to sensory neurons, SGCs undergo major changes which seem to contribute to chronic pain states. These changes appear to follow a common pattern across a wide range of animal models, such as augmented expression of glial fibrillary acidic protein (GFAP), which is a marker of astrocyte activation [309]. It has been proposed that following peripheral injury, SGCs are activated by DRG neurons with SA. As a consequence, SGCs release bioactive molecules which further potentiate neuronal excitability, leading to an auto-amplifying loop of neuronal and glial sensitization [310]. As so, despite apparently not being a trigger of SA in DRG neurons, glial cell activation appears to have a major role in pathological pain. Therefore, as an alternative to a classical “neuron-centric” approach, it has been suggested that SGCs and abnormal SGC-neuron interactions in sensory ganglia can serve as therapeutic targets to treat chronic pain conditions, including NP [311].

There is strong evidence that the cross-talk between DRG neurons and SGCs is mediated primarily by ATP release (fig. 7). Both types of cells express a variety of receptors for ATP (purinergic P2 receptors) [312]. In chronic pain states, there are alterations in the expression of some P2 receptors in SGCs and DRG neurons that lead to increased sensitivity to ATP and neuronal depolarization [310, 312]. In addition, there is upregulation of pannexin1, which is a channel that releases ATP and other signaling molecules [313]. A model has been proposed in which, in response to peripheral damage, spontaneously firing DRG neurons release ATP via pannexin1. Extracellular ATP activates the P2 receptors of neurons themselves and on adjacent SGCs, leading to an increase in intracellular calcium, augmented sensitivity to ATP, and enhanced release of ATP and neuronal depolarization, thereby creating a positive feedback loop [314, 315].

Excitatory signals exchanged between each DRG neuron and its neighbor SGCs can spread to adjacent morphological units. The propagation of these signals inside sensory ganglia likely involves intercellular calcium waves (ICWs) generated by SGCs [315]. In the CNS, ICWs are created when the augmented levels of intracellular Ca^{2+} of a stimulated astrocyte spread to neighbor astrocytes [316]. It has been hypothesized that these ICWs also happen in sensory ganglia because SGCs are capable of sustaining ICWs i*n vitro* [317]. It is speculated that the existence of ICWs between different morphological units leads to the spread of excitatory signals and stimulation of neighboring neurons [315]. In fact, ICWs might be one of the mechanisms leading to a phenomenon termed cross-excitation, in which previously silent DRG neurons are excited by neighbors that are firing repetitively [318]. For a long time it has been suggested that this dialog between sensory neurons is chemically mediated [319]. In fact, the purinergic receptor P2Y1, which is expressed in both neurons and SGCs, was recently implicated in cross-excitation [320]. Accordingly, there is evidence that ICWs are propagated by the purinergic system [317].

There is evidence that ICWs generated by SGCs propagate not only by extracellular ATP release, but also by diffusion of second messengers via gap junctions (fig. 7) [317]. Gap junctions are one of the means through which SGCs communicate with each other. In models of peripheral injury and inflammation, there is an increase in the number of gap junctions between SGCs and consequently an augmented coupling of SGCs, which contributes to pain-like behaviors [315]. Given the contribution of gap junctions to ICW propagation, it is not surprising that this increased gap junction-mediated coupling contributes to pathological pain by promoting cross-excitation of DRG neurons [321]. Together, these findings suggest that SGCs mediate the dialog between neurons, in particular cross-excitation, via ICWs propagated by purinergic receptors and gap junctions.

A decrease in the putative K^+ buffering capacity of SGCs has also been indicated as a possible mechanism leading to depolarization of neuronal cell bodies and pain symptoms [309, 312]. It was demonstrated that the principal inwardly rectifying K^+ channel of SGCs, the $K_{ir}4.1$, is downregulated after nerve injury, and pain-like behaviors can be triggered merely by silencing this channel [322]. This channel is implicated in the regulation of extracellular K^+ by astrocytes [323] and so it is presumed that SGCs also have this buffering capacity [309]. It has been hypothesized that, following peripheral injury, downregulation of $K_{ir}4.1$ impairs the K^+ buffering capacity of SGCs, leading to an increase in the extracellular K^+ in the vicinity of active DRG neurons and consequent depolarization and SA (fig. 7) [309]. Accordingly, a modelling study also predicts that cross-depolarization between DRG neurons could result from changes in the K^+ buffering capacity of SGCs [324].

It is possible that changes in GABAergic and glutamatergic transmission inside the DRG might also contribute to the alterations in neuronal activity observed in NP. Regarding glutamate, both SGCs and the cell bodies of DRG neurons possess glutamate receptors and are capable of releasing this transmitter [325, 326]. In addition, an increased distribution of glutamate receptors was observed at the membrane of DRG neuron cell bodies following peripheral injury [327], similarly to what happens to sensitized peripheral terminals upon inflammation [328]. Regarding GABAergic communication, it was shown that the soma of DRG neurons produces and releases GABA in response to depolarizing stimuli, and targeting the somatic/perisomatic GABAergic system in DRG alleviated not only acute pain but also NP [329]. However, so far there is no evidence of GABA release from SGCs [309].

Evidence from several papers suggest that pro-inflammatory molecules modify DRG neuron activity after peripheral damage [330]. Attesting the importance of inflammation, injection of an anti-inflammatory drug near the DRG or an inhibitor of TNF-α synthesis attenuated pain-like behaviors in two studies [330, 331]. Following peripheral injury, macrophages and lymphocytes infiltrate in the ganglia and release pro-inflammatory factors [332, 333], but the inflammatory effect on DRG neurons may also be mediated by SGCs. Supporting this theory, after peripheral injury, activated SGCs start to express or upregulate pro-inflammatory cytokines, such as IL-6 and TNF-α, and their respective receptors [334, 335]. Conversely, DRG neurons express the receptors for these cytokines, in some cases only after injury [334, 335].

Nitric oxide is a gaseous transmitter that is produced and released by sensory neurons [336]. It has been hypothesized that nitric oxide may serve as a mediator for communication between sensory neurons and SGCs, and that this communication may contribute to augmented neuronal activity [337]. However, the link between these nitric oxide-based intercellular communication and DRG neuron activity is still not fully

understood. Nitric oxide synthase is upregulated in DRG neurons after peripheral injury [336]. Moreover, *in vitro* studies have shown that this compound induces cyclic GMP production in SGCs [337, 338], which is a signaling pathway that appears to lead to SGC activation, increase in gap junctions, ICWs and augmented neuronal excitability [337].

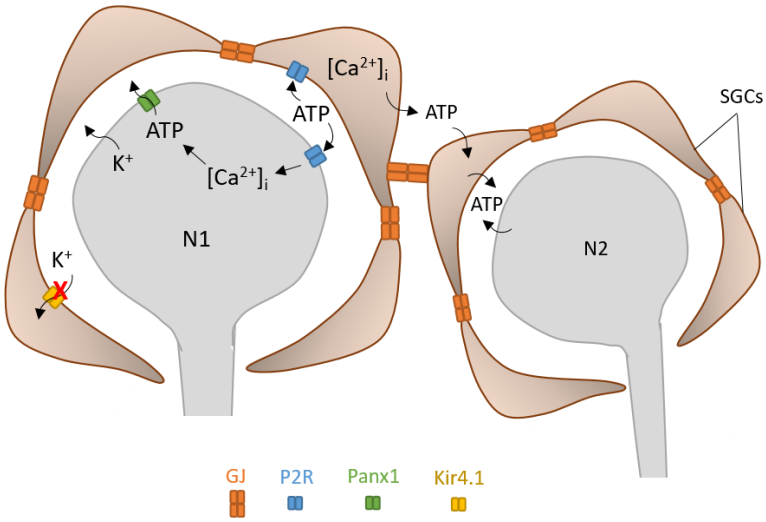

Fig. 7. Hypothesized mechanisms of intercellular communication in the DRG and cross-depolarization. The axon of neuron 1 (N1) had been injured, which leads to increased neuronal activity and, consequently, ATP release by pannexin1 (Panx1) [315]. Elevated extracellular ATP activates purinergic P2 receptors (P2Rs) on surrounding SGCs and on the neuron itself, causing an increase in intracellular calcium levels ($[Ca^{2+}]_i$) in these cells. In turn, higher $[Ca^{2+}]_i$ leads to augmented ATP release. This, together with a greater communication between SGCs by gap junctions (GJs) following injury, causes an augmented spread of Ca^{2+} waves to neighboring neurons (N2) and their surrounding SGCs [309]. On the other hand, following injury, augmented neuronal K^+ release, in combination with decreased $K_{ir}4.1$ expression in SGCs, causes an increase in extracellular K^+, which could lead to depolarization of neighbor SGC-neuron units [324].

The contribution of sympathetic inputs in some neuropathic pain conditions

It is assumed that the pathological hyperexcitability of DRG neurons is not due to synaptic action, especially because in healthy adult DRGs identifiable synapses are exceedingly rare [193, 305, 339]. Still, some evidence challenges this view by suggesting that peripheral injury triggers synaptogenesis inside the DRG. In animal models of

peripheral damage, synapse-like structures have been observed by electron microscopy and immunofluorescence in axons located near DRG neuron cell bodies [340, 341]. The majority of studies attribute these synapse-like structures to fibers of sympathetic neurons which sprouted in response to peripheral injury, and a few reports indicate that these structures also belong to sprouted fibers of nociceptive DRG neurons [341].

Sympathetic sprouting inside the DRG occurs from axons that normally innervate the blood vessels inside sensory ganglia and from axons coming from the spinal nerve [342]. It can lead to the formation of dense plexuses around DRG neuron cell bodies, in particular those that have activated SGCs nearby [341]. These plexuses, which are classically named “Terminal Dogiel’s nests”, have also been reported in healthy animals [343].

The functional consequences of this potential sympathetic-sensory coupling on NP have been controversial, since animal and clinical studies using sympathetic blockade have yielded inconsistent results [343, 344]. In fact, some patients present sympathetically maintained NP, whereas in other patients pain is independent of the sympathetic system [344]. Preclinical studies show that DRG neurons surrounded by sympathetic axons are more likely to have SA [345]. However, sympathetic sprouting does not trigger SA nor NP, since SA arises before sprouting [345] and the onset of pain behaviors is independent of the sympathetic system [346]. Instead, spontaneously-active primary afferents seem to provoke the sprouting of sympathetic fibers and attract them [244]. But although sympathetic fibers do not seem to contribute to the establishment of NP, their inputs may contribute to the maintenance of pain symptoms [346]. In fact, repeated stimulation to sympathetic fibers enhances SA in DRG neurons and increases their excitability, which suggests that there can be functional interactions between sensory neurons and sympathetic sprouts [342]. Some authors propose that these interactions may rely on the release of neurotransmitters, such as norepinephrine and ATP, by sympathetic endings which in turn were stimulated by spontaneously-active DRG neurons and activated SGCs. Therefore, DRG neurons, SGCs and adjacent sympathetic axons might have mutually excitatory interactions that could function has a positive feedback loop influencing DRG neuron SA. This mechanism is yet to be proven, but it could explain why in some cases sympathetic blockade relieves pain [344].

References

1. Ogawa, Y. and M.N. Rasband. (2008). The functional organization and assembly of the axon initial segment. *Current opinion in neurobiology*, 18(3), 307-13.
2. Palay, S.L., et al. (1968). The axon hillock and the initial segment. *The Journal of cell biology*, 38(1), 193-201.
3. Leterrier, C. (2018). The Axon Initial Segment: An Updated Viewpoint. *The Journal of neuroscience : the official journal of the Society for Neuroscience*, 38(9), 2135-2145.
4. Huang, C.Y.-M. and M.N. Rasband. (2018). Axon initial segments: structure, function, and disease. *Annals of the New York Academy of Sciences*, 1420(1), 46-61.
5. Höfflin, F., et al. (2017). Heterogeneity of the Axon Initial Segment in Interneurons and Pyramidal Cells of Rodent Visual Cortex. *Frontiers in cellular neuroscience*, 11, 332.
6. Leterrier, C. (2016). The Axon Initial Segment, 50Years Later: A Nexus for Neuronal Organization and Function. *Current topics in membranes*, 77, 185-233.
7. Hamdan, H., et al. (2020). Mapping axon initial segment structure and function by multiplexed proximity biotinylation. *Nature Communications*, 11(1), 100.
8. Le Bras, B., et al. (2014). In vivo assembly of the axon initial segment in motor neurons. *Brain structure and function*, 219(4), 1433-50.
9. Gutzmann, A., et al. (2014). A period of structural plasticity at the axon initial segment in developing visual cortex. *Frontiers in neuroanatomy*, 8, 11-11.
10. Galiano, M.R., et al. (2012). A distal axonal cytoskeleton forms an intra-axonal boundary that controls axon initial segment assembly. *Cell*, 149(5), 1125-39.
11. Hedstrom, K.L., et al. (2007). Neurofascin assembles a specialized extracellular matrix at the axon initial segment. *The Journal of cell biology*, 178(5), 875-886.
12. Jenkins, P.M., et al. (2015). Giant ankyrin-G: A critical innovation in vertebrate evolution of fast and integrated neuronal signaling. *Proceedings of the National Academy of Sciences*, 112(4), 957-964.
13. Torii , T., et al. (2019). NuMA1 promotes axon initial segment assembly through inhibition of endocytosis. *Journal of Cell Biology*, 219(2).

14. Hedstrom, K.L., Y. Ogawa, and M.N. Rasband. (2008). AnkyrinG is required for maintenance of the axon initial segment and neuronal polarity. *The Journal of cell biology*, 183(4), 635-640.
15. Leterrier, C., et al. (2017). Ankyrin G Membrane Partners Drive the Establishment and Maintenance of the Axon Initial Segment [Original Research]. *Frontiers in Cellular Neuroscience*, 11(6).
16. Xu, K., G. Zhong, and X. Zhuang. (2013). Actin, spectrin, and associated proteins form a periodic cytoskeletal structure in axons. *Science*, 339(6118), 452-6.
17. Zhong, G., et al. (2014). Developmental mechanism of the periodic membrane skeleton in axons. *eLife*, 3, e04581.
18. Leterrier, C., et al. (2011). End-binding proteins EB3 and EB1 link microtubules to ankyrin G in the axon initial segment. *Proceedings of the National Academy of Sciences of the United States of America*, 108(21), 8826-8831.
19. van Beuningen, S.F.B., et al. (2015). TRIM46 Controls Neuronal Polarity and Axon Specification by Driving the Formation of Parallel Microtubule Arrays. *Neuron*, 88(6), 1208-1226.
20. Fréal, A., et al. (2019). Feedback-Driven Assembly of the Axon Initial Segment. *Neuron*, 104(2), 305-321.e8.
21. Satake, T., et al. (2017). MTCL1 plays an essential role in maintaining Purkinje neuron axon initial segment. *The EMBO journal*, 36(9), 1227-1242.
22. Alpizar, S.A., et al. (2019). Loss of Neurofascin-186 Disrupts Alignment of AnkyrinG Relative to Its Binding Partners in the Axon Initial Segment. *Frontiers in cellular neuroscience*, 13, 1-1.
23. Kriebel, M., et al. (2011). The cell adhesion molecule neurofascin stabilizes axo-axonic GABAergic terminals at the axon initial segment. *The Journal of biological chemistry*, 286(27), 24385-24393.
24. Saha, R., et al. (2017). GABAergic Synapses at the Axon Initial Segment of Basolateral Amygdala Projection Neurons Modulate Fear Extinction. *Neuropsychopharmacology : official publication of the American College of Neuropsychopharmacology*, 42(2), 473-484.
25. Valente, P., et al. (2016). Cell adhesion molecule L1 contributes to neuronal excitability regulating the function of voltage-gated Na+ channels. *Journal of cell science*, 129(9), 1878-91.
26. Ogawa, Y., et al. (2008). Postsynaptic density-93 clusters Kv1 channels at axon initial segments independently of Caspr2. *The Journal of neuroscience : the official journal of the Society for Neuroscience*, 28(22), 5731-5739.

27. Hivert, B., et al. (2019). ADAM22 and ADAM23 modulate the targeting of the Kv1 channel-associated protein LGI1 to the axon initial segment. *Journal of Cell Science*, 132(2), jcs219774.
28. Kole, M.H., et al. (2008). Action potential generation requires a high sodium channel density in the axon initial segment. *Nature Neuroscience*, 11(2), 178-86.
29. Bennett, D.L., et al. (2019). The Role of Voltage-Gated Sodium Channels in Pain Signaling. *Physiological reviews*, 99(2), 1079-1151.
30. Lemaillet, G., B. Walker, and S. Lambert. (2003). Identification of a conserved ankyrin-binding motif in the family of sodium channel alpha subunits. *The Journal of biological chemistry*, 278(30), 27333-9.
31. Lorincz, A. and Z. Nusser. (2008). Cell-type-dependent molecular composition of the axon initial segment. *The Journal of neuroscience : the official journal of the Society for Neuroscience*, 28(53), 14329-14340.
32. Hu, W., et al. (2009). Distinct contributions of Na(v)1.6 and Na(v)1.2 in action potential initiation and backpropagation. *Nature Neuroscience*, 12(8), 996-1002.
33. Duflocq, A., et al. (2011). Characterization of the axon initial segment (AIS) of motor neurons and identification of a para-AIS and a juxtapara-AIS, organized by protein 4.1B. *BMC biology*, 9, 66-66.
34. Gasser, A., et al. (2012). An ankyrinG-binding motif is necessary and sufficient for targeting Nav1.6 sodium channels to axon initial segments and nodes of Ranvier. *The Journal of neuroscience : the official journal of the Society for Neuroscience*, 32(21), 7232-7243.
35. Bréchet, A., et al. (2008). Protein kinase CK2 contributes to the organization of sodium channels in axonal membranes by regulating their interactions with ankyrin G. *The Journal of cell biology*, 183(6), 1101-1114.
36. Wood, J.N., et al., *Potassium Channels and Pain*. 2019, Oxford University Press.
37. Tsantoulas, C. and S.B. McMahon. (2014). Opening paths to novel analgesics: the role of potassium channels in chronic pain. *Trends in neurosciences*, 37(3), 146-58.
38. Kuang, Q., P. Purhonen, and H. Hebert. (2015). Structure of potassium channels. *Cellular and molecular life sciences : CMLS*, 72(19), 3677-3693.
39. Kole, M.H. and G.J. Stuart. (2012). Signal processing in the axon initial segment. *Neuron*, 73(2), 235-47.
40. Shah, M.M., et al. (2008). Functional significance of axonal Kv7 channels in hippocampal pyramidal neurons. *Proceedings of the National Academy of Sciences of the United States of America*, 105(22), 7869-7874.

41. Pan, Z., et al. (2006). A common ankyrin-G-based mechanism retains KCNQ and NaV channels at electrically active domains of the axon. *The Journal of neuroscience : the official journal of the Society for Neuroscience*, 26(10), 2599-613.
42. Xu, M. and E.C. Cooper. (2015). An Ankyrin-G N-terminal Gate and Protein Kinase CK2 Dually Regulate Binding of Voltage-gated Sodium and KCNQ2/3 Potassium Channels. *The Journal of biological chemistry*, 290(27), 16619-16632.
43. Hefting, L.L., et al. (2020). Multiple Domains in the Kv7.3 C-Terminus Can Regulate Localization to the Axon Initial Segment [Original Research]. *Frontiers in Cellular Neuroscience*, 14(10).
44. Hill, A.S., et al. (2008). Ion channel clustering at the axon initial segment and node of Ranvier evolved sequentially in early chordates. *PLoS genetics*, 4(12), e1000317-e1000317.
45. Kole, M.H., J.J. Letzkus, and G.J. Stuart. (2007). Axon initial segment Kv1 channels control axonal action potential waveform and synaptic efficacy. *Neuron*, 55(4), 633-47.
46. King, A.N., C.F. Manning, and J.S. Trimmer. (2014). A unique ion channel clustering domain on the axon initial segment of mammalian neurons. *The Journal of comparative neurology*, 522(11), 2594-2608.
47. Jensen, C.S., et al. (2017). Trafficking of Kv2.1 Channels to the Axon Initial Segment by a Novel Nonconventional Secretory Pathway. *The Journal of neuroscience : the official journal of the Society for Neuroscience*, 37(48), 11523-11536.
48. Abiraman, K., A.V. Tzingounis, and G. Lykotrafitis. (2018). K(Ca)2 channel localization and regulation in the axon initial segment. *FASEB journal : official publication of the Federation of American Societies for Experimental Biology*, 32(4), 1794-1805.
49. John, N.W., et al., *Voltage-Gated Calcium Channels: Molecular Targets for Treating Chronic Pain*. 2019, Oxford University Press.
50. Bourinet, E., et al. (2014). Calcium-permeable ion channels in pain signaling. *Physiological reviews*, 94(1), 81-140.
51. Bender, K.J. and L.O. Trussell. (2009). Axon initial segment Ca2+ channels influence action potential generation and timing. *Neuron*, 61(2), 259-271.
52. Yu, Y., et al. (2010). P/Q and N Channels Control Baseline and Spike-Triggered Calcium Levels in Neocortical Axons and Synaptic Boutons. *The Journal of Neuroscience*, 30(35), 11858-11869.

53. Sobotzik, J.-M., et al. (2009). AnkyrinG is required to maintain axo-dendritic polarity in vivo. *Proceedings of the National Academy of Sciences of the United States of America*, 106(41), 17564-17569.
54. Nakada, C., et al. (2003). Accumulation of anchored proteins forms membrane diffusion barriers during neuronal polarization. *Nature cell biology*, 5(7), 626-32.
55. Albrecht, D., et al. (2016). Nanoscopic compartmentalization of membrane protein motion at the axon initial segment. *The Journal of cell biology*, 215(1), 37-46.
56. Song, A.H., et al. (2009). A selective filter for cytoplasmic transport at the axon initial segment. *Cell*, 136(6), 1148-60.
57. Hirokawa, N., S. Niwa, and Y. Tanaka. (2010). Molecular Motors in Neurons: Transport Mechanisms and Roles in Brain Function, Development, and Disease. *Neuron*, 68(4), 610-638.
58. Al-Bassam, S., et al. (2012). Differential trafficking of transport vesicles contributes to the localization of dendritic proteins. *Cell reports*, 2(1), 89-100.
59. Janssen, A.F.J., et al. (2017). Myosin-V Induces Cargo Immobilization and Clustering at the Axon Initial Segment. *Frontiers in cellular neuroscience*, 11, 260-260.
60. Kuijpers, M., et al. (2016). Dynein Regulator NDEL1 Controls Polarized Cargo Transport at the Axon Initial Segment. *Neuron*, 89(3), 461-71.
61. Huang, C.-F. and G. Banker. (2012). The translocation selectivity of the kinesins that mediate neuronal organelle transport. *Traffic (Copenhagen, Denmark)*, 13(4), 549-564.
62. Farías, G.G., et al. (2015). Sorting of Dendritic and Axonal Vesicles at the Pre-axonal Exclusion Zone. *Cell reports*, 13(6), 1221-1232.
63. Gumy, L.F., et al. (2017). MAP2 Defines a Pre-axonal Filtering Zone to Regulate KIF1- versus KIF5-Dependent Cargo Transport in Sensory Neurons. *Neuron*, 94(2), 347-362.e7.
64. Palmer, L.M. and G.J. Stuart. (2006). Site of action potential initiation in layer 5 pyramidal neurons. *The Journal of neuroscience : the official journal of the Society for Neuroscience*, 26(6), 1854-1863.
65. Palmer, L.M., et al. (2010). Initiation of simple and complex spikes in cerebellar Purkinje cells. *The Journal of physiology*, 588(Pt 10), 1709-1717.
66. Kole, M.H. and G.J. Stuart. (2008). Is action potential threshold lowest in the axon? *Nature Neuroscience*, 11(11), 1253-5.

67. Fleidervish, I.A., et al. (2010). Na+ imaging reveals little difference in action potential-evoked Na+ influx between axon and soma. *Nature neuroscience*, 13(7), 852-860.
68. Schmidt-Hieber, C. and J. Bischofberger. (2010). Fast sodium channel gating supports localized and efficient axonal action potential initiation. *The Journal of neuroscience : the official journal of the Society for Neuroscience*, 30(30), 10233-10242.
69. Katz, E., et al. (2018). Role of sodium channel subtype in action potential generation by neocortical pyramidal neurons. *Proceedings of the National Academy of Sciences of the United States of America*, 115(30), E7184-E7192.
70. Baranauskas, G., Y. David, and I.A. Fleidervish. (2013). Spatial mismatch between the Na+ flux and spike initiation in axon initial segment. *Proceedings of the National Academy of Sciences of the United States of America*, 110(10), 4051-4056.
71. Mainen, Z.F., et al. (1995). A model of spike initiation in neocortical pyramidal neurons. *Neuron*, 15(6), 1427-39.
72. Eyal, G., et al. (2014). Dendrites impact the encoding capabilities of the axon. *The Journal of neuroscience : the official journal of the Society for Neuroscience*, 34(24), 8063-8071.
73. Telenczuk, M., B. Fontaine, and R. Brette. (2017). The basis of sharp spike onset in standard biophysical models. *PloS one*, 12(4), e0175362-e0175362.
74. Kole, M.H. and R. Brette. (2018). The electrical significance of axon location diversity. *Current opinion in neurobiology*, 51, 52-59.
75. Yamada, R. and H. Kuba. (2016). Structural and Functional Plasticity at the Axon Initial Segment. *Frontiers in cellular neuroscience*, 10, 250-250.
76. Grubb, M.S. and J. Burrone. (2010). Activity-dependent relocation of the axon initial segment fine-tunes neuronal excitability. *Nature*, 465(7301), 1070-1074.
77. Kuba, H., Y. Oichi, and H. Ohmori. (2010). Presynaptic activity regulates Na+ channel distribution at the axon initial segment. *Nature*, 465(7301), 1075-1078.
78. Evans, M.D., et al. (2015). Rapid Modulation of Axon Initial Segment Length Influences Repetitive Spike Firing. *Cell Reports*, 13(6), 1233-1245.
79. Lezmy, J., et al. (2017). M-current inhibition rapidly induces a unique CK2-dependent plasticity of the axon initial segment. *Proceedings of the National Academy of Sciences of the United States of America*, 114(47), E10234-E10243.
80. Chand, A.N., et al. (2015). A distinct subtype of dopaminergic interneuron displays inverted structural plasticity at the axon initial segment. *The Journal of neuroscience : the official journal of the Society for Neuroscience*, 35(4), 1573-1590.

81. Kuba, H., et al. (2015). Redistribution of Kv1 and Kv7 enhances neuronal excitability during structural axon initial segment plasticity. *Nature communications*, 6, 8815-8815.
82. Cruz, D.A., et al. (2009). Postnatal development of synaptic structure proteins in pyramidal neuron axon initial segments in monkey prefrontal cortex. *The Journal of comparative neurology*, 514(4), 353-367.
83. Kuba, H., R. Adachi, and H. Ohmori. (2014). Activity-dependent and activity-independent development of the axon initial segment. *The Journal of neuroscience : the official journal of the Society for Neuroscience*, 34(9), 3443-3453.
84. Ding, Y., et al. (2018). Axon initial segment plasticity accompanies enhanced excitation of visual cortical neurons in aged rats. *Neuroreport*, 29(18), 1537-1543.
85. Atapour, N. and M.G.P. Rosa. (2017). Age-related plasticity of the axon initial segment of cortical pyramidal cells in marmoset monkeys. *Neurobiology of Aging*, 57, 95-103.
86. Berger, S.L., et al. (2018). Localized Myosin II Activity Regulates Assembly and Plasticity of the Axon Initial Segment. *Neuron*, 97(3), 555-570.e6.
87. Yermakov, L.M., et al. (2018). Type 2 Diabetes Leads to Axon Initial Segment Shortening in db/db Mice. *Frontiers in cellular neuroscience*, 12, 146-146.
88. Liu, T.-T., et al. (2017). Altered axon initial segment in hippocampal newborn neurons, associated with recurrence of temporal lobe epilepsy in rats. *Molecular medicine reports*, 16(3), 3169-3178.
89. Kaphzan, H., et al. (2011). Alterations in intrinsic membrane properties and the axon initial segment in a mouse model of Angelman syndrome. *The Journal of neuroscience : the official journal of the Society for Neuroscience*, 31(48), 17637-17648.
90. Hinman, J.D., M.N. Rasband, and S.T. Carmichael. (2013). Remodeling of the axon initial segment after focal cortical and white matter stroke. *Stroke*, 44(1), 182-189.
91. Hamada, M.S. and M.H.P. Kole. (2015). Myelin loss and axonal ion channel adaptations associated with gray matter neuronal hyperexcitability. *The Journal of neuroscience : the official journal of the Society for Neuroscience*, 35(18), 7272-7286.
92. Harty, R.C., et al. (2013). Axon initial segment structural plasticity in animal models of genetic and acquired epilepsy. *Epilepsy research*, 105(3), 272-9.
93. Baalman, K.L., et al. (2013). Blast wave exposure impairs memory and decreases axon initial segment length. *Journal of neurotrauma*, 30(9), 741-751.

94. Bonnevie, V.S., et al. (2020). Shorter axon initial segments do not cause repetitive firing impairments in the adult presymptomatic G127X SOD-1 Amyotrophic Lateral Sclerosis mouse. *Scientific Reports*, 10(1), 1280.
95. Jørgensen, H.S., et al. (2021). Increased Axon Initial Segment Length Results in Increased Na(+) Currents in Spinal Motoneurones at Symptom Onset in the G127X SOD1 Mouse Model of Amyotrophic Lateral Sclerosis. *Neuroscience*, 468, 247-264.
96. Evans, M.D., et al. (2013). Calcineurin signaling mediates activity-dependent relocation of the axon initial segment. *The Journal of neuroscience : the official journal of the Society for Neuroscience*, 33(16), 6950-6963.
97. Evans, M.D., et al. (2017). Myosin II activity is required for structural plasticity at the axon initial segment. *The European journal of neuroscience*, 46(2), 1751-1757.
98. Hatch, R.J., et al. (2017). Hyperphosphorylated tau causes reduced hippocampal CA1 excitability by relocating the axon initial segment. *Acta neuropathologica*, 133(5), 717-730.
99. Goethals, S. and R. Brette. (2020). Theoretical relation between axon initial segment geometry and excitability. *Elife*, 9.
100. Gulledge, A.T. and J.J. Bravo. (2016). Neuron Morphology Influences Axon Initial Segment Plasticity. *eNeuro*, 3(1), ENEURO.0085-15.2016.
101. Hamada, M.S., et al. (2016). Covariation of axon initial segment location and dendritic tree normalizes the somatic action potential. *Proceedings of the National Academy of Sciences of the United States of America*, 113(51), 14841-14846.
102. Meza, R.C., et al. (2018). Role of the Axon Initial Segment in the Control of Spontaneous Frequency of Nigral Dopaminergic Neurons In Vivo. *The Journal of neuroscience : the official journal of the Society for Neuroscience*, 38(3), 733-744.
103. Moubarak, E., et al. (2019). Robustness to Axon Initial Segment Variation Is Explained by Somatodendritic Excitability in Rat Substantia Nigra Dopaminergic Neurons. *The Journal of neuroscience : the official journal of the Society for Neuroscience*, 39(26), 5044-5063.
104. Petersen, A.V., F. Cotel, and J.F. Perrier. (2017). Plasticity of the Axon Initial Segment: Fast and Slow Processes with Multiple Functional Roles. *Neuroscientist*, 23(4), 364-373.
105. Benned-Jensen, T., et al. (2016). Live Imaging of Kv7.2/7.3 Cell Surface Dynamics at the Axon Initial Segment: High Steady-State Stability and Calpain-Dependent Excitotoxic Downregulation Revealed. *The Journal of neuroscience : the official journal of the Society for Neuroscience*, 36(7), 2261-2266.

106. Martinello, K., et al. (2015). Cholinergic afferent stimulation induces axonal function plasticity in adult hippocampal granule cells. *Neuron*, 85(2), 346-363.
107. Yin, L., et al. (2015). Selective Modulation of Axonal Sodium Channel Subtypes by 5-HT1A Receptor in Cortical Pyramidal Neuron. *Cerebral Cortex*, 27(1), 509-521.
108. Nascimento, A.I., F.M. Mar, and M.M. Sousa. (2018). The intriguing nature of dorsal root ganglion neurons: Linking structure with polarity and function. *Progress in Neurobiology*, 168, 86-103.
109. Matsuda, S., et al. (1998). Morphological transformation of sensory ganglion neurons and satellite cells. *Kaibogaku Zasshi*, 73(6), 603-13.
110. Takahashi, K. and T. Ninomiya. (1987). Morphological changes of dorsal root ganglion cells in the process-forming period. *Progress in Neurobiology*, 29(4), 393-410.
111. Dzhashiashvili, Y., et al. (2007). Nodes of Ranvier and axon initial segments are ankyrin G-dependent domains that assemble by distinct mechanisms. *The Journal of cell biology*, 177(5), 857-870.
112. Zhang, X. and V. Bennett. (1998). Restriction of 480/270-kD ankyrin G to axon proximal segments requires multiple ankyrin G-specific domains. *The Journal of cell biology*, 142(6), 1571-1581.
113. Yang, Y., et al. (2007). betaIV spectrin is recruited to axon initial segments and nodes of Ranvier by ankyrinG. *The Journal of cell biology*, 176(4), 509-519.
114. Matsumoto, E. and J. Rosenbluth. (1985). Plasma membrane structure at the axon hillock, initial segment and cell body of frog dorsal root ganglion cells. *Journal of neurocytology*, 14(5), 731-47.
115. Rosenbluth, J. (1976). Intramembranous particle distribution at the node of Ranvier and adjacent axolemma in myelinated axons of the frog brain. *Journal of neurocytology*, 5(6), 731-45.
116. Devor, M. and M. Obermayer. (1984). Membrane differentiation in rat dorsal root ganglia and possible consequences for back pain. *Neuroscience Letters*, 51(3), 341-346.
117. Quick, D.C. and S.G. Waxman. (1977). Specific staining of the axon membrane at nodes of Ranvier with ferric ion and ferrocyanide. *Journal of the Neurological Sciences*, 31(1), 1-11.
118. Brandao, K.E., M.L. Dell'Acqua, and S.R. Levinson. (2012). A-kinase anchoring protein 150 expression in a specific subset of TRPV1- and CaV 1.2-positive nociceptive rat dorsal root ganglion neurons. *The Journal of comparative neurology*, 520(1), 81-99.

119. Costigan, M., J. Scholz, and C.J. Woolf. (2009). Neuropathic pain: a maladaptive response of the nervous system to damage. *Annual review of neuroscience*, 32, 1-32.
120. Treede, R.D., et al. (2019). Chronic pain as a symptom or a disease: the IASP Classification of Chronic Pain for the International Classification of Diseases (ICD-11). *Pain*, 160(1), 19-27.
121. Colloca, L., et al. (2017). Neuropathic pain. *Nature reviews. Disease primers*, 3, 17002.
122. van Hecke, O., et al. (2014). Neuropathic pain in the general population: a systematic review of epidemiological studies. *Pain*, 155(4), 654-62.
123. Baron, R., A. Binder, and G. Wasner. (2010). Neuropathic pain: diagnosis, pathophysiological mechanisms, and treatment. *The Lancet. Neurology*, 9(8), 807-19.
124. Attal, N., et al. (2011). The specific disease burden of neuropathic pain: results of a French nationwide survey. *Pain*, 152(12), 2836-43.
125. Attal, N. (2019). Pharmacological treatments of neuropathic pain: The latest recommendations. *Revue neurologique*, 175(1-2), 46-50.
126. Finnerup, N.B., et al. (2018). Neuropathic pain clinical trials: factors associated with decreases in estimated drug efficacy. *Pain*, 159(11), 2339-2346.
127. Challa, S.R. (2015). Surgical animal models of neuropathic pain: Pros and Cons. *The International journal of neuroscience*, 125(3), 170-4.
128. Clark, J.D. (2016). Preclinical Pain Research: Can We Do Better? *Anesthesiology*, 125(5), 846-849.
129. Bennett, G.J. and Y.K. Xie. (1988). A peripheral mononeuropathy in rat that produces disorders of pain sensation like those seen in man. *Pain*, 33(1), 87-107.
130. van der Wal, S., et al. (2015). Behavior of neuropathic pain in mice following chronic constriction injury comparing silk and catgut ligatures. *SpringerPlus*, 4, 225-225.
131. Chung, J.M., H.K. Kim, and K. Chung. (2004). Segmental spinal nerve ligation model of neuropathic pain. *Methods in molecular medicine*, 99, 35-45.
132. Ye, G.L., et al. (2015). Ligation of mouse L4 and L5 spinal nerves produces robust allodynia without major motor function deficit. *Behavioural brain research*, 276, 99-110.
133. Song, X.J., et al. (1999). Mechanical and thermal hyperalgesia and ectopic neuronal discharge after chronic compression of dorsal root ganglia. *Journal of neurophysiology*, 82(6), 3347-58.

134. Fan, N., et al. (2011). Increased Na+ and K+ currents in small mouse dorsal root ganglion neurons after ganglion compression. *Journal of neurophysiology*, 106(1), 211-218.
135. Hama, A. and H. Takamatsu. (2016). Chemotherapy-Induced Peripheral Neuropathic Pain and Rodent Models. *CNS and neurological disorders drug targets*, 15(1), 7-19.
136. Gao, F. and Z.M. Zheng. (2014). Animal models of diabetic neuropathic pain. *Experimental and clinical endocrinology and diabetes*, 122(2), 100-6.
137. Nystrom, B. and K.E. Hagbarth. (1981). Microelectrode recordings from transected nerves in amputees with phantom limb pain. *Neuroscience letters*, 27(2), 211-6.
138. Nordin, M., et al. (1984). Ectopic sensory discharges and paresthesiae in patients with disorders of peripheral nerves, dorsal roots and dorsal columns. *Pain*, 20(3), 231-45.
139. Serra, J., et al. (2012). Microneurographic identification of spontaneous activity in C-nociceptors in neuropathic pain states in humans and rats. *Pain*, 153(1), 42-55.
140. Kleggetveit, I.P., et al. (2012). High spontaneous activity of C-nociceptors in painful polyneuropathy. *Pain*, 153(10), 2040-7.
141. North, R.Y., T.T. Lazaro, and P.M. Dougherty. (2018). Ectopic Spontaneous Afferent Activity and Neuropathic Pain. *Neurosurgery*, 65(CN_suppl_1), 49-54.
142. Wall, P.D. and M. Devor. (1983). Sensory afferent impulses originate from dorsal root ganglia as well as from the periphery in normal and nerve injured rats. *Pain*, 17(4), 321-39.
143. Xie, W., et al. (2005). Neuropathic pain: early spontaneous afferent activity is the trigger. *Pain*, 116(3), 243-56.
144. Liu, C.N., et al. (2000). Tactile allodynia in the absence of C-fiber activation: altered firing properties of DRG neurons following spinal nerve injury. *Pain*, 85(3), 503-21.
145. Sun, Q., et al. (2005). Ectopic discharges from injured nerve fibers are highly correlated with tactile allodynia only in early, but not late, stage in rats with spinal nerve ligation. *Experimental neurology*, 191(1), 128-36.
146. Pitcher, G.M. and J.L. Henry. (2008). Governing role of primary afferent drive in increased excitation of spinal nociceptive neurons in a model of sciatic neuropathy. *Experimental neurology*, 214(2), 219-28.
147. Han, H.C., D.H. Lee, and J.M. Chung. (2000). Characteristics of ectopic discharges in a rat neuropathic pain model. *Pain*, 84(2-3), 253-61.
148. Sheen, K. and J.M. Chung. (1993). Signs of neuropathic pain depend on signals from injured nerve fibers in a rat model. *Brain Res*, 610(1), 62-8.

149. Sukhotinsky, I., et al. (2004). Key role of the dorsal root ganglion in neuropathic tactile hypersensibility. *European journal of pain (London, England)*, 8(2), 135-43.
150. Gracely, R.H., S.A. Lynch, and G.J. Bennett. (1992). Painful neuropathy: altered central processing maintained dynamically by peripheral input. *Pain*, 51(2), 175-94.
151. Koltzenburg, M., H.E. Torebjork, and L.K. Wahren. (1994). Nociceptor modulated central sensitization causes mechanical hyperalgesia in acute chemogenic and chronic neuropathic pain. *Brain*, 117 (Pt 3), 579-91.
152. Loeser, J.D. (1972). Dorsal rhizotomy for the relief of chronic pain. *Journal of neurosurgery*, 36(6), 745-50.
153. Devor, M. (2009). Ectopic discharge in Abeta afferents as a source of neuropathic pain. *Experimental brain research*, 196(1), 115-28.
154. Truini, A., L. Garcia-Larrea, and G. Cruccu. (2013). Reappraising neuropathic pain in humans—how symptoms help disclose mechanisms. *Nature Reviews Neurology*, 9(10), 572-582.
155. Khan, G.M., S.R. Chen, and H.L. Pan. (2002). Role of primary afferent nerves in allodynia caused by diabetic neuropathy in rats. *Neuroscience*, 114(2), 291-9.
156. Kajander, K.C., S. Wakisaka, and G.J. Bennett. (1992). Spontaneous discharge originates in the dorsal root ganglion at the onset of a painful peripheral neuropathy in the rat. *Neuroscience letters*, 138(2), 225-8.
157. Djouhri, L. and S.N. Lawson. (2004). Abeta-fiber nociceptive primary afferent neurons: a review of incidence and properties in relation to other afferent A-fiber neurons in mammals. *Brain research. Brain research reviews*, 46(2), 131-45.
158. Liu, C.N., et al. (2001). Hyperexcitability in sensory neurons of rats selected for high versus low neuropathic pain phenotype. *Neuroscience*, 105(1), 265-75.
159. Malcangio, M., et al. (2000). Abnormal substance P release from the spinal cord following injury to primary sensory neurons. *The European journal of neuroscience*, 12(1), 397-9.
160. Miki, K., et al. (1998). Calcitonin gene-related peptide increase in the rat spinal dorsal horn and dorsal column nucleus following peripheral nerve injury: up-regulation in a subpopulation of primary afferent sensory neurons. *Neuroscience*, 82(4), 1243-52.
161. Woolf, C.J., P. Shortland, and R.E. Coggeshall. (1992). Peripheral nerve injury triggers central sprouting of myelinated afferents. *Nature*, 355(6355), 75-8.
162. Amir, R. and M. Devor. (2000). Functional cross-excitation between afferent A- and C-neurons in dorsal root ganglia. *Neuroscience*, 95(1), 189-95.

163. Kim, Y.S., et al. (2016). Coupled Activation of Primary Sensory Neurons Contributes to Chronic Pain. *Neuron*, 91(5), 1085-1096.
164. Chen, Y. and M. Devor. (1998). Ectopic mechanosensitivity in injured sensory axons arises from the site of spontaneous electrogenesis. *European journal of pain (London, England)*, 2(2), 165-178.
165. England, J.D., et al. (1996). Sodium channel accumulation in humans with painful neuromas. *Neurology*, 47(1), 272-6.
166. Devor, M., R. Govrin-Lippmann, and K. Angelides. (1993). Na+ channel immunolocalization in peripheral mammalian axons and changes following nerve injury and neuroma formation. *The Journal of neuroscience : the official journal of the Society for Neuroscience*, 13(5), 1976-92.
167. Levinson, S.R., S. Luo, and M.A. Henry. (2012). The role of sodium channels in chronic pain. *Muscle nerve*, 46(2), 155-165.
168. England, J.D., et al. (1990). Changed distribution of sodium channels along demyelinated axons. *Proceedings of the National Academy of Sciences of the United States of America*, 87(17), 6777-80.
169. Kirk, E.J. (1974). Impulses in dorsal spinal nerve rootlets in cats and rabbits arising from dorsal root ganglia isolated from the periphery. *The Journal of comparative neurology*, 155(2), 165-75.
170. DeSantis, M. and J.W. Duckworth. (1982). Properties of primary afferent neurons from muscle which are spontaneously active after a lesion of their peripheral processes. *Experimental neurology*, 75(2), 261-74.
171. Burchiel, K.J. (1984). Effects of electrical and mechanical stimulation on two foci of spontaneous activity which develop in primary afferent neurons after peripheral axotomy. *Pain*, 18(3), 249-65.
172. Vaso, A., et al. (2014). Peripheral nervous system origin of phantom limb pain. *Pain*, 155(7), 1384-91.
173. Petersen, M., et al. (1996). Abnormal spontaneous activity and responses to norepinephrine in dissociated dorsal root ganglion cells after chronic nerve constriction. *Pain*, 67(2-3), 391-7.
174. Ma, C. and R.H. LaMotte. (2005). Enhanced excitability of dissociated primary sensory neurons after chronic compression of the dorsal root ganglion in the rat. *Pain*, 113(1-2), 106-12.
175. Megat, S., et al. (2019). Nociceptor Translational Profiling Reveals the Ragulator-Rag GTPase Complex as a Critical Generator of Neuropathic Pain. *The Journal of neuroscience : the official journal of the Society for Neuroscience*, 39(3), 393-411.

176. North, R.Y., et al. (2019). Electrophysiological and transcriptomic correlates of neuropathic pain in human dorsal root ganglion neurons. *Brain*, 142(5), 1215-1226.
177. Zheng, J.H., E.T. Walters, and X.J. Song. (2007). Dissociation of dorsal root ganglion neurons induces hyperexcitability that is maintained by increased responsiveness to cAMP and cGMP. *Journal of neurophysiology*, 97(1), 15-25.
178. Wangzhou, A., et al. (2020). Pharmacological target-focused transcriptomic analysis of native versus cultured human and mouse dorsal root ganglia. *Pain*.
179. Amir, R., J.D. Kocsis, and M. Devor. (2005). Multiple interacting sites of ectopic spike electrogenesis in primary sensory neurons. *The Journal of neuroscience : the official journal of the Society for Neuroscience*, 25(10), 2576-85.
180. Ma, C. and R.H. LaMotte. (2007). Multiple sites for generation of ectopic spontaneous activity in neurons of the chronically compressed dorsal root ganglion. *The Journal of neuroscience : the official journal of the Society for Neuroscience*, 27(51), 14059-14068.
181. Ma, C., et al. (2003). Similar electrophysiological changes in axotomized and neighboring intact dorsal root ganglion neurons. *Journal of neurophysiology*, 89(3), 1588-602.
182. Xie, Y., et al. (1995). Functional changes in dorsal root ganglion cells after chronic nerve constriction in the rat. *Journal of neurophysiology*, 73(5), 1811-20.
183. Tal, M. and E. Eliav. (1996). Abnormal discharge originates at the site of nerve injury in experimental constriction neuropathy (CCI) in the rat. *Pain*, 64(3), 511-8.
184. Amir, R., M. Michaelis, and M. Devor. (2002). Burst discharge in primary sensory neurons: triggered by subthreshold oscillations, maintained by depolarizing afterpotentials. *The Journal of neuroscience : the official journal of the Society for Neuroscience*, 22(3), 1187-98.
185. Amir, R., M. Michaelis, and M. Devor. (1999). Membrane potential oscillations in dorsal root ganglion neurons: role in normal electrogenesis and neuropathic pain. *The Journal of neuroscience : the official journal of the Society for Neuroscience*, 19(19), 8589-96.
186. Liu, C.N., et al. (2000). Spinal nerve injury enhances subthreshold membrane potential oscillations in DRG neurons: relation to neuropathic pain. *Journal of neurophysiology*, 84(1), 205-15.
187. Djouhri, L., et al. (2018). Membrane potential oscillations are not essential for spontaneous firing generation in L4 Aβ-afferent neurons after L5 spinal nerve axotomy and are not mediated by HCN channels. *Experimental Physiology*, 103(8), 1145-1156.

188. Kim, Y.I., et al. (1998). Cell type-specific changes of the membrane properties of peripherally-axotomized dorsal root ganglion neurons in a rat model of neuropathic pain. *Neuroscience*, 86(1), 301-9.
189. Song, X.J., et al. (2003). Hyperalgesia and neural excitability following injuries to central and peripheral branches of axons and somata of dorsal root ganglion neurons. *Journal of neurophysiology*, 89(4), 2185-93.
190. Zhu, Y.F. and J.L. Henry. (2012). Excitability of Abeta sensory neurons is altered in an animal model of peripheral neuropathy. *BMC neuroscience*, 13, 15.
191. Zhang, H. and P.M. Dougherty. (2014). Enhanced excitability of primary sensory neurons and altered gene expression of neuronal ion channels in dorsal root ganglion in paclitaxel-induced peripheral neuropathy. *Anesthesiology*, 120(6), 1463-75.
192. Bedi, S.S., et al. (2010). Chronic spontaneous activity generated in the somata of primary nociceptors is associated with pain-related behavior after spinal cord injury. *The Journal of neuroscience : the official journal of the Society for Neuroscience*, 30(44), 14870-82.
193. Devor, M. (2006). Sodium channels and mechanisms of neuropathic pain. *The journal of pain : official journal of the American Pain Society*, 7(1 Suppl 1), 3-12.
194. Hu, G., et al. (2016). Single-cell RNA-seq reveals distinct injury responses in different types of DRG sensory neurons. *Scientific reports*, 6, 31851-31851.
195. Bao, L. (2015). Trafficking regulates the subcellular distribution of voltage-gated sodium channels in primary sensory neurons. *Molecular pain*, 11, 61-61.
196. Waxman, S.G. and G.W. Zamponi. (2014). Regulating excitability of peripheral afferents: emerging ion channel targets. *Nature Neuroscience*, 17(2), 153-63.
197. Ciotu, C.I., et al. (2019). Noncanonical Ion Channel Behaviour in Pain. *International journal of molecular sciences*, 20(18), 4572.
198. Bähring, R. and M. Covarrubias. (2011). Mechanisms of closed-state inactivation in voltage-gated ion channels. *The Journal of physiology*, 589(Pt 3), 461-479.
199. O'Malley, H.A. and L.L. Isom. (2015). Sodium channel β subunits: emerging targets in channelopathies. *Annual review of physiology*, 77, 481-504.
200. Wang, W., et al. (2011). Are voltage-gated sodium channels on the dorsal root ganglion involved in the development of neuropathic pain? *Molecular pain*, 7, 16.
201. Matzner, O. and M. Devor. (1992). Na+ conductance and the threshold for repetitive neuronal firing. *Brain research*, 597(1), 92-8.

202. Yatziv, S.L. and M. Devor. (2019). Suppression of neuropathic pain by selective silencing of dorsal root ganglion ectopia using nonblocking concentrations of lidocaine. *Pain*, 160(9), 2105-2114.
203. Kingwell, K. (2019). Nav1.7 withholds its pain potential. *nature reviews. Drug discovery*.
204. Fukuoka, T., et al. (2008). Comparative study of the distribution of the alpha-subunits of voltage-gated sodium channels in normal and axotomized rat dorsal root ganglion neurons. *The Journal of comparative neurology*, 510(2), 188-206.
205. Trimmer, J.S., et al. (1989). Primary structure and functional expression of a mammalian skeletal muscle sodium channel. *Neuron*, 3(1), 33-49.
206. Rogart, R.B., et al. (1989). Molecular cloning of a putative tetrodotoxin-resistant rat heart Na+ channel isoform. *Proceedings of the National Academy of Sciences of the United States of America*, 86(20), 8170-4.
207. Kerr, N.C.H., et al. (2007). The sodium channel Nav1.5a is the predominant isoform expressed in adult mouse dorsal root ganglia and exhibits distinct inactivation properties from the full-length Nav1.5 channel. *Molecular and cellular neurosciences*, 35(2), 283-291.
208. Noda, M. and T.Y. Hiyama. (2015). The Na(x) Channel: What It Is and What It Does. *Neuroscientist*, 21(4), 399-412.
209. Felts, P.A., et al. (1997). Sodium channel alpha-subunit mRNAs I, II, III, NaG, Na6 and hNE (PN1): different expression patterns in developing rat nervous system. *Brain research. Molecular brain research*, 45(1), 71-82.
210. Renganathan, M., S. Dib-Hajj, and S.G. Waxman. (2002). Na(v)1.5 underlies the 'third TTX-R sodium current' in rat small DRG neurons. *Brain research. Molecular brain research*, 106(1-2), 70-82.
211. Ho, C. and M.E. O'Leary. (2011). Single-cell analysis of sodium channel expression in dorsal root ganglion neurons. *Molecular and cellular neurosciences*, 46(1), 159-166.
212. Laedermann, C.J., H. Abriel, and I. Decosterd. (2015). Post-translational modifications of voltage-gated sodium channels in chronic pain syndromes. *Frontiers in pharmacology*, 6, 263-263.
213. Cummins, T.R., P.L. Sheets, and S.G. Waxman. (2007). The roles of sodium channels in nociception: Implications for mechanisms of pain. *Pain*, 131(3), 243-57.
214. Osteen, J.D., et al. (2016). Selective spider toxins reveal a role for the Nav1.1 channel in mechanical pain. *Nature*, 534(7608), 494-499.

215. Waxman, S.G., J.D. Kocsis, and J.A. Black. (1994). Type III sodium channel mRNA is expressed in embryonic but not adult spinal sensory neurons, and is reexpressed following axotomy. *Journal of neurophysiology*, 72(1), 466-70.
216. Kim, C.H., et al. (2001). The changes in expression of three subtypes of TTX sensitive sodium channels in sensory neurons after spinal nerve ligation. *Brain research. Molecular brain research*, 95(1-2), 153-61.
217. Black, J.A., et al. (1999). Upregulation of a silent sodium channel after peripheral, but not central, nerve injury in DRG neurons. *Journal of neurophysiology*, 82(5), 2776-85.
218. Black, J.A., M. Renganathan, and S.G. Waxman. (2002). Sodium channel Na(v)1.6 is expressed along nonmyelinated axons and it contributes to conduction. *Brain research. Molecular brain research*, 105(1-2), 19-28.
219. Carrasco, D.I., J.A. Vincent, and T.C. Cope. (2017). Distribution of TTX-sensitive voltage-gated sodium channels in primary sensory endings of mammalian muscle spindles. *Journal of neurophysiology*, 117(4), 1690-1701.
220. Persson, A.K., et al. (2010). Sodium-calcium exchanger and multiple sodium channel isoforms in intra-epidermal nerve terminals. *Molecular pain*, 6, 84.
221. Caldwell, J.H., et al. (2000). Sodium channel Na(v)1.6 is localized at nodes of ranvier, dendrites, and synapses. *Proceedings of the National Academy of Sciences of the United States of America*, 97(10), 5616-5620.
222. Chen, L., et al. (2018). Conditional knockout of Na(V)1.6 in adult mice ameliorates neuropathic pain. *Scientific reports*, 8(1), 3845-3845.
223. Djouhri, L., et al. (2003). Sensory and electrophysiological properties of guinea-pig sensory neurones expressing Nav 1.7 (PN1) Na+ channel alpha subunit protein. *The Journal of physiology*, 546(Pt 2), 565-76.
224. Black, J.A., et al. (2012). Expression of Nav1.7 in DRG neurons extends from peripheral terminals in the skin to central preterminal branches and terminals in the dorsal horn. *Molecular pain*, 8, 82-82.
225. Persson, A.K., et al. (2011). Nav1.7 accumulates and co-localizes with phosphorylated ERK1/2 within transected axons in early experimental neuromas. *Experimental neurology*, 230(2), 273-9.
226. Shields, S.D., et al. (2012). Nav1.8 expression is not restricted to nociceptors in mouse peripheral nervous system. *Pain*, 153(10), 2017-30.
227. Djouhri, L., et al. (2003). The TTX-resistant sodium channel Nav1.8 (SNS/PN3): expression and correlation with membrane properties in rat nociceptive primary afferent neurons. *The Journal of physiology*, 550(Pt 3), 739-52.

228. Rush, A.M., et al. (2005). Contactin regulates the current density and axonal expression of tetrodotoxin-resistant but not tetrodotoxin-sensitive sodium channels in DRG neurons. *The European journal of neuroscience*, 22(1), 39-49.
229. Black, J.A., et al. (2008). Multiple sodium channel isoforms and mitogen-activated protein kinases are present in painful human neuromas. *Annals of neurology*, 64(6), 644-53.
230. Fjell, J., et al. (2000). Localization of the tetrodotoxin-resistant sodium channel NaN in nociceptors. *Neuroreport*, 11(1), 199-202.
231. Black, J.A., et al. (1996). Spinal sensory neurons express multiple sodium channel alpha-subunit mRNAs. *Brain research. Molecular brain research*, 43(1-2), 117-31.
232. Ke, C.B., et al. (2012). Enhanced SCN7A/Nax expression contributes to bone cancer pain by increasing excitability of neurons in dorsal root ganglion. *Neuroscience*, 227, 80-9.
233. Craner, M.J., et al. (2002). Changes of sodium channel expression in experimental painful diabetic neuropathy. *Annals of neurology*, 52(6), 786-92.
234. Nassar, M.A., et al. (2006). Nerve injury induces robust allodynia and ectopic discharges in Nav1.3 null mutant mice. *Molecular pain*, 2, 33.
235. Minett, M.S., et al. (2014). Pain without nociceptors? Nav1.7-independent pain mechanisms. *Cell reports*, 6(2), 301-12.
236. Lindia, J.A., et al. (2005). Relationship between sodium channel NaV1.3 expression and neuropathic pain behavior in rats. *Pain*, 117(1-2), 145-53.
237. Samad, O.A., et al. (2013). Virus-mediated shRNA knockdown of Na(v)1.3 in rat dorsal root ganglion attenuates nerve injury-induced neuropathic pain. *Molecular therapy : the journal of the American Society of Gene Therapy*, 21(1), 49-56.
238. Tan, A.M., et al. (2015). Virus-Mediated Knockdown of Nav1.3 in Dorsal Root Ganglia of STZ-Induced Diabetic Rats Alleviates Tactile Allodynia. *Molecular medicine (Cambridge, Mass.)*, 21, 544-52.
239. Cummins, T.R., et al. (2005). Nav1.6 channels generate resurgent sodium currents in spinal sensory neurons. *FEBS letters*, 579(10), 2166-70.
240. Cannon, S.C. and B.P. Bean. (2010). Sodium channels gone wild: resurgent current from neuronal and muscle channelopathies. *The Journal of clinical investigation*, 120(1), 80-83.
241. Israel, M.R., et al. (2019). NaV1.6 regulates excitability of mechanosensitive sensory neurons. *The Journal of Physiology*, 597(14), 3751-3768.
242. Tanaka, B.S., et al. (2016). A gain-of-function mutation in Nav1.6 in a case of trigeminal neuralgia. *Molecular medicine (Cambridge, Mass.)*, 22, 338-348.

243. Deuis, J.R., et al. (2013). An animal model of oxaliplatin-induced cold allodynia reveals a crucial role for Nav1.6 in peripheral pain pathways. *Pain*, 154(9), 1749-57.
244. Xie, W., J.A. Strong, and J.M. Zhang. (2015). Local knockdown of the NaV1.6 sodium channel reduces pain behaviors, sensory neuron excitability, and sympathetic sprouting in rat models of neuropathic pain. *Neuroscience*, 291, 317-330.
245. Xie, W., et al. (2019). Role of Na(V)1.6 and Na(V)β4 Sodium Channel Subunits in a Rat Model of Low Back Pain Induced by Compression of the Dorsal Root Ganglia. *Neuroscience*, 402, 51-65.
246. Zhang, X.-L., et al. (2018). Palmitoylation of δ-catenin promotes kinesin-mediated membrane trafficking of Nav1.6 in sensory neurons to promote neuropathic pain. *Science Signaling*, 11(523), eaar4394.
247. Hameed, S. (2019). Na(v)1.7 and Na(v)1.8: Role in the pathophysiology of pain. *Molecular pain*, 15, 1744806919858801-1744806919858801.
248. Nassar, M.A., et al. (2004). Nociceptor-specific gene deletion reveals a major role for Nav1.7 (PN1) in acute and inflammatory pain. *Proceedings of the National Academy of Sciences of the United States of America*, 101(34), 12706-12711.
249. Gingras, J., et al. (2014). Global Nav1.7 knockout mice recapitulate the phenotype of human congenital indifference to pain. *PLoS One*, 9(9), e105895.
250. Minett, M.S., et al. (2012). Distinct Nav1.7-dependent pain sensations require different sets of sensory and sympathetic neurons. *Nature communications*, 3, 791.
251. Berta, T., et al. (2008). Transcriptional and functional profiles of voltage-gated Na(+) channels in injured and non-injured DRG neurons in the SNI model of neuropathic pain. *Molecular and cellular neurosciences*, 37(2), 196-208.
252. Liu, C., et al. (2012). Nav1.7 protein and mRNA expression in the dorsal root ganglia of rats with chronic neuropathic pain. *Neural regeneration research*, 7(20), 1540-4.
253. Kretschmer, T., et al. (2002). Accumulation of PN1 and PN3 sodium channels in painful human neuroma-evidence from immunocytochemistry. *Acta neurochirurgica*, 144(8), 803-10; discussion 810.
254. Stamboulian, S., et al. (2010). ERK1/2 mitogen-activated protein kinase phosphorylates sodium channel Na(v)1.7 and alters its gating properties. *The Journal of neuroscience : the official journal of the Society for Neuroscience*, 30(5), 1637-1647.
255. Chatelier, A., et al. (2008). Biophysical properties of human Na v1.7 splice variants and their regulation by protein kinase A. *Journal of neurophysiology*, 99(5), 2241-50.

256. Farmer, C., et al. (2012). Splice variants of Na(V)1.7 sodium channels have distinct β subunit-dependent biophysical properties. *PloS one*, 7(7), e41750-e41750.
257. Raymond, C.K., et al. (2004). Expression of alternatively spliced sodium channel alpha-subunit genes. Unique splicing patterns are observed in dorsal root ganglia. *The Journal of biological chemistry*, 279(44), 46234-41.
258. Mert, T. and Y. Gunes. (2012). Antinociceptive activities of lidocaine and the nav1.8 blocker a803467 in diabetic rats. *Journal of the American Association for Laboratory Animal Science : JAALAS*, 51(5), 579-85.
259. Jarvis, M.F., et al. (2007). A-803467, a potent and selective Nav1.8 sodium channel blocker, attenuates neuropathic and inflammatory pain in the rat. *Proceedings of the National Academy of Sciences of the United States of America*, 104(20), 8520-5.
260. Roza, C., et al. (2003). The tetrodotoxin-resistant Na+ channel Nav1.8 is essential for the expression of spontaneous activity in damaged sensory axons of mice. *The Journal of physiology*, 550(Pt 3), 921-926.
261. Nassar, M.A., et al. (2005). Neuropathic pain develops normally in mice lacking both Na(v)1.7 and Na(v)1.8. *Molecular pain*, 1, 24-24.
262. Akopian, A.N., et al. (1999). The tetrodotoxin-resistant sodium channel SNS has a specialized function in pain pathways. *Nature Neuroscience*, 2(6), 541-8.
263. Dib-Hajj, S.D., J.A. Black, and S.G. Waxman. (2015). NaV1.9: a sodium channel linked to human pain. *Nature reviews. Neuroscience*, 16(9), 511-9.
264. Porreca, F., et al. (1999). A comparison of the potential role of the tetrodotoxin-insensitive sodium channels, PN3/SNS and NaN/SNS2, in rat models of chronic pain. *Proceedings of the National Academy of Sciences of the United States of America*, 96(14), 7640-7644.
265. Priest, B.T., et al. (2005). Contribution of the tetrodotoxin-resistant voltage-gated sodium channel NaV1.9 to sensory transmission and nociceptive behavior. *Proceedings of the National Academy of Sciences of the United States of America*, 102(26), 9382-9387.
266. Leo, S., R. D'Hooge, and T. Meert. (2010). Exploring the role of nociceptor-specific sodium channels in pain transmission using Nav1.8 and Nav1.9 knockout mice. *Behavioural brain research*, 208(1), 149-57.
267. Burchiel, K.J. and L.C. Russell. (1985). Effects of potassium channel-blocking agents on spontaneous discharges from neuromas in rats. *Journal of neurosurgery*, 63(2), 246-9.

268. Kirchhoff, C., et al. (1992). Excitation of cutaneous sensory nerve endings in the rat by 4-aminopyridine and tetraethylammonium. *Journal of neurophysiology*, 67(1), 125-31.
269. Chien, L.Y., et al. (2007). Reduced expression of A-type potassium channels in primary sensory neurons induces mechanical hypersensitivity. *The Journal of neuroscience : the official journal of the Society for Neuroscience*, 27(37), 9855-65.
270. Tsantoulas, C., et al. (2012). Sensory neuron downregulation of the Kv9.1 potassium channel subunit mediates neuropathic pain following nerve injury. *The Journal of neuroscience : the official journal of the Society for Neuroscience*, 32(48), 17502-13.
271. Tulleuda, A., et al. (2011). TRESK channel contribution to nociceptive sensory neurons excitability: modulation by nerve injury. *Molecular pain*, 7, 30.
272. Fan, L., et al. (2014). Impaired neuropathic pain and preserved acute pain in rats overexpressing voltage-gated potassium channel subunit Kv1.2 in primary afferent neurons. *Molecular pain*, 10, 8-8.
273. Rose, K., et al. (2011). Transcriptional repression of the M channel subunit Kv7.2 in chronic nerve injury. *Pain*, 152(4), 742-754.
274. Ma, C., et al. (2010). Expression of inwardly rectifying potassium channels by an inducible adenoviral vector reduced the neuronal hyperexcitability and hyperalgesia produced by chronic compression of the spinal ganglion. *Mol Pain*, 6, 65.
275. Yusaf, S.P., et al. (2001). Expression of voltage-gated calcium channel subunits in rat dorsal root ganglion neurons. *Neuroscience letters*, 311(2), 137-41.
276. Scott, D.A., C.E. Wright, and J.A. Angus. (2002). Actions of intrathecal omega-conotoxins CVID, GVIA, MVIIA, and morphine in acute and neuropathic pain in the rat. *European journal of pharmacology*, 451(3), 279-86.
277. Bourinet, E., et al. (2005). Silencing of the Cav3.2 T-type calcium channel gene in sensory neurons demonstrates its major role in nociception. *The EMBO journal*, 24(2), 315-324.
278. Yang, J., et al. (2018). Upregulation of N-type calcium channels in the soma of uninjured dorsal root ganglion neurons contributes to neuropathic pain by increasing neuronal excitability following peripheral nerve injury. *Brain, behavior, and immunity*, 71, 52-65.
279. Wen, X.J., et al. (2006). Intrathecal administration of Cav3.2 and Cav3.3 antisense oligonucleotide reverses tactile allodynia and thermal hyperalgesia in rats following chronic compression of dorsal root of ganglion. *Acta pharmacologica Sinica*, 27(12), 1547-52.

280. Dogrul, A., et al. (2003). Reversal of experimental neuropathic pain by T-type calcium channel blockers. *Pain*, 105(1-2), 159-68.
281. Nieto-Rostro, M., et al. (2018). Ablation of α(2)δ-1 inhibits cell-surface trafficking of endogenous N-type calcium channels in the pain pathway in vivo. *Proceedings of the National Academy of Sciences of the United States of America*, 115(51), E12043-E12052.
282. Francois, A., et al. (2015). The Low-Threshold Calcium Channel Cav3.2 Determines Low-Threshold Mechanoreceptor Function. *Cell Reports*, 10(3), 370-382.
283. Rasband, M.N., et al. (2001). Distinct potassium channels on pain-sensing neurons. *Proceedings of the National Academy of Sciences of the United States of America*, 98(23), 13373-13378.
284. Wu, S., et al. (2016). Dorsal root ganglion transcriptome analysis following peripheral nerve injury in mice. *Molecular pain*, 12, 1744806916629048.
285. Mao, Q., et al. (2017). Role of dorsal root ganglion K2p1.1 in peripheral nerve injury-induced neuropathic pain. *Molecular pain*, 13, 1744806917701135-1744806917701135.
286. Chen, S.-R., Y.-Q. Cai, and H.-L. Pan. (2009). Plasticity and emerging role of BKCa channels in nociceptive control in neuropathic pain. *Journal of neurochemistry*, 110(1), 352-362.
287. Zoga, V., et al. (2010). KATP channel subunits in rat dorsal root ganglia: alterations by painful axotomy. *Molecular pain*, 6, 6-6.
288. Tsantoulas, C., et al. (2014). Kv2 dysfunction after peripheral axotomy enhances sensory neuron responsiveness to sustained input. *Experimental neurology*, 251, 115-26.
289. Kim, D.S., et al. (2002). Downregulation of voltage-gated potassium channel alpha gene expression in dorsal root ganglia following chronic constriction injury of the rat sciatic nerve. *Brain research. Molecular brain research*, 105(1-2), 146-52.
290. Reinhold, A.K., et al. (2015). Differential transcriptional profiling of damaged and intact adjacent dorsal root ganglia neurons in neuropathic pain. *PloS one*, 10(4), e0123342-e0123342.
291. Pollema-Mays, S.L., et al. (2013). Expression of background potassium channels in rat DRG is cell-specific and down-regulated in a neuropathic pain model. *Molecular and cellular neurosciences*, 57, 1-9.
292. Yang, E.K., et al. (2004). Altered expression of potassium channel subunit mRNA and alpha-dendrotoxin sensitivity of potassium currents in rat dorsal root ganglion neurons after axotomy. *Neuroscience*, 123(4), 867-74.

293. Calvo, M., et al. (2016). Altered potassium channel distribution and composition in myelinated axons suppresses hyperexcitability following injury. *eLife*, 5, e12661-e12661.
294. Cisneros, E., et al. (2015). A New Regulatory Mechanism for Kv7.2 Protein During Neuropathy: Enhanced Transport from the Soma to Axonal Terminals of Injured Sensory Neurons. *Frontiers in cellular neuroscience*, 9, 470.
295. Lyu, C., et al. (2015). G protein-gated inwardly rectifying potassium channel subunits 1 and 2 are down-regulated in rat dorsal root ganglion neurons and spinal cord after peripheral axotomy. *Molecular pain*, 11, 44-44.
296. Descoeur, J., et al. (2011). Oxaliplatin-induced cold hypersensitivity is due to remodelling of ion channel expression in nociceptors. *EMBO molecular medicine*, 3(5), 266-278.
297. Cao, X.H., et al. (2010). Reduction in voltage-gated K+ channel activity in primary sensory neurons in painful diabetic neuropathy: role of brain-derived neurotrophic factor. *Journal of neurochemistry*, 114(5), 1460-75.
298. Yu, T., et al. (2018). KCNQ2/3/5 channels in dorsal root ganglion neurons can be therapeutic targets of neuropathic pain in diabetic rats. *Molecular pain*, 14, 1744806918793229.
299. Snutch, T.P. and G.W. Zamponi. (2018). Recent advances in the development of T-type calcium channel blockers for pain intervention. *British journal of pharmacology*, 175(12), 2375-2383.
300. Patel, R., C. Montagut-Bordas, and A.H. Dickenson. (2018). Calcium channel modulation as a target in chronic pain control. *British journal of pharmacology*, 175(12), 2173-2184.
301. Rho, Y.A. and S.A. Prescott. (2012). Identification of molecular pathologies sufficient to cause neuropathic excitability in primary somatosensory afferents using dynamical systems theory. *PLoS computational biology*, 8(5), e1002524.
302. Ratté, S., et al. (2014). Criticality and degeneracy in injury-induced changes in primary afferent excitability and the implications for neuropathic pain. *eLife*, 3, e02370-e02370.
303. Ratte, S. and S.A. Prescott. (2016). Afferent hyperexcitability in neuropathic pain and the inconvenient truth about its degeneracy. *Current opinion in neurobiology*, 36, 31-7.
304. Spencer, P.S., C.S. Raine, and H. WiśNiewski. (1973). Axon diameter and myelin thickness—unusual relationships in dorsal root ganglia. *The Anatomical Record*, 176(2), 225-243.

305. Zenker, W. and E. Hogl. (1976). The prebifurcation section of the axon of the rat spinal ganglion cell. *Cell and tissue research*, 165(3), 345-63.
306. Pannese, E. (1981). The satellite cells of the sensory ganglia. *Advances in anatomy, embryology, and cell biology*, 65, 1-111.
307. George, D., P. Ahrens, and S. Lambert. (2018). Satellite glial cells represent a population of developmentally arrested Schwann cells. *Glia*, 66(7), 1496-1506.
308. Pannese, E. (2010). The structure of the perineuronal sheath of satellite glial cells (SGCs) in sensory ganglia. *Neuron glia biology*, 6(1), 3-10.
309. Hanani, M. and D.C. Spray, *Satellite Glial Cells as a Target for Chronic Pain Therapy*, in *Pathological Potential of Neuroglia: Possible New Targets for Medical Intervention*, V. Parpura and A. Verkhratsky, Editors. 2014, Springer New York: New York, NY. p. 473-492.
310. Villa, G., et al. (2010). Expression and contribution of satellite glial cells purinoceptors to pain transmission in sensory ganglia: an update. *Neuron glia biology*, 6(1), 31-42.
311. Magni, G. and S. Ceruti. (2014). The purinergic system and glial cells: emerging costars in nociception. *BioMed research international*, 2014, 495789.
312. Huang, L.Y., Y. Gu, and Y. Chen. (2013). Communication between neuronal somata and satellite glial cells in sensory ganglia. *Glia*, 61(10), 1571-81.
313. Zhang, Y., et al. (2015). Pannexin-1 Up-regulation in the Dorsal Root Ganglion Contributes to Neuropathic Pain Development. *The Journal of biological chemistry*, 290(23), 14647-55.
314. Hanani, M. (2012). Intercellular communication in sensory ganglia by purinergic receptors and gap junctions: implications for chronic pain. *Brain research*, 1487, 183-91.
315. Spray, D.C. and M. Hanani. (2019). Gap junctions, pannexins and pain. *Neuroscience letters*, 695, 46-52.
316. Scemes, E. and C. Giaume. (2006). Astrocyte calcium waves: what they are and what they do. *Glia*, 54(7), 716-25.
317. Suadicani, S.O., et al. (2010). Bidirectional calcium signaling between satellite glial cells and neurons in cultured mouse trigeminal ganglia. *Neuron Glia Biology*, 6(1), 43-51.
318. Devor, M. and P.D. Wall. (1990). Cross-excitation in dorsal root ganglia of nerve-injured and intact rats. *Journal of neurophysiology*, 64(6), 1733-46.

319. Amir, R. and M. Devor. (1996). Chemically mediated cross-excitation in rat dorsal root ganglia. *The Journal of neuroscience : the official journal of the Society for Neuroscience*, 16(15), 4733-41.
320. Carvalho, G.B., et al. (2019). A Role for The P2Y1 Receptor in Nonsynaptic Cross-depolarization in the Rat Dorsal Root Ganglia. *Neuroscience*, 423, 98-108.
321. Huang, T.Y., V. Belzer, and M. Hanani. (2010). Gap junctions in dorsal root ganglia: possible contribution to visceral pain. *European journal of pain (London, England)*, 14(1), 49.e1-11.
322. Vit, J.P., et al. (2008). Silencing the Kir4.1 potassium channel subunit in satellite glial cells of the rat trigeminal ganglion results in pain-like behavior in the absence of nerve injury. *The Journal of neuroscience : the official journal of the Society for Neuroscience*, 28(16), 4161-71.
323. Neusch, C., et al. (2006). Lack of the Kir4.1 channel subunit abolishes K+ buffering properties of astrocytes in the ventral respiratory group: impact on extracellular K+ regulation. *Journal of neurophysiology*, 95(3), 1843-52.
324. Mandge, D., et al. *Computational Model for Cross-Depolarization in DRG Neurons via Satellite Glial Cells using [K]o: Role of Kir4.1 Channels and Extracellular Leakage*. in *2019 41st Annual International Conference of the IEEE Engineering in Medicine and Biology Society (EMBC)*. 2019.
325. Kung, L.H., et al. (2013). Evidence for glutamate as a neuroglial transmitter within sensory ganglia. *PLoS One*, 8(7), e68312.
326. Wagner, L., et al. (2014). Glutamate release from satellite glial cells of the murine trigeminal ganglion. *Neuroscience letters*, 578, 143-7.
327. Gong, K., et al. (2014). Increased response to glutamate in small diameter dorsal root ganglion neurons after sciatic nerve injury. *PLoS One*, 9(4), e95491.
328. Du, J., S. Zhou, and S.M. Carlton. (2006). Kainate-induced excitation and sensitization of nociceptors in normal and inflamed rat glabrous skin. *Neuroscience*, 137(3), 999-1013.
329. Du, X., et al. (2017). Local GABAergic signaling within sensory ganglia controls peripheral nociceptive transmission. *The Journal of clinical investigation*, 127(5), 1741-1756.
330. Li, J.Y., et al. (2011). Mechanical hypersensitivity, sympathetic sprouting, and glial activation are attenuated by local injection of corticosteroid near the lumbar ganglion in a rat model of neuropathic pain. *Regional anesthesia and pain medicine*, 36(1), 56-62.

331. Xu, J.T., et al. (2006). The role of tumor necrosis factor-alpha in the neuropathic pain induced by Lumbar 5 ventral root transection in rat. *Pain*, 123(3), 306-21.
332. Schmid, A.B., et al. (2013). Local and remote immune-mediated inflammation after mild peripheral nerve compression in rats. *Journal of neuropathology and experimental neurology*, 72(7), 662-80.
333. Hu, P. and E.M. McLachlan. (2002). Macrophage and lymphocyte invasion of dorsal root ganglia after peripheral nerve lesions in the rat. *Neuroscience*, 112(1), 23-38.
334. Ohtori, S., et al. (2004). TNF-alpha and TNF-alpha receptor type 1 upregulation in glia and neurons after peripheral nerve injury: studies in murine DRG and spinal cord. *Spine (Phila Pa 1976)*, 29(10), 1082-8.
335. Dubovy, P., et al. (2010). Satellite glial cells express IL-6 and corresponding signal-transducing receptors in the dorsal root ganglia of rat neuropathic pain model. *Neuron glia biology*, 6(1), 73-83.
336. Fiallos-Estrada, C.E., et al. (1993). Long-lasting increase of nitric oxide synthase immunoreactivity, NADPH-diaphorase reaction and c-JUN co-expression in rat dorsal root ganglion neurons following sciatic nerve transection. *Neuroscience letters*, 150(2), 169-73.
337. Belzer, V. and M. Hanani. (2019). Nitric oxide as a messenger between neurons and satellite glial cells in dorsal root ganglia. *Glia*, 67(7), 1296-1307.
338. Morris, R., et al. (1992). Nitric oxide may act as a messenger between dorsal root ganglion neurones and their satellite cells. *Neuroscience letters*, 137(1), 29-32.
339. Kayahara, T., T. Takimoto, and S. Sakashita. (1981). Synaptic junctions in the cat spinal ganglion. *Brain research*, 216(2), 277-90.
340. Chung, K., Y.W. Yoon, and J.M. Chung. (1997). Sprouting sympathetic fibers form synaptic varicosities in the dorsal root ganglion of the rat with neuropathic injury. *Brain research*, 751(2), 275-80.
341. Cheng, C.F., et al. (2015). Nerve growth factor-induced synapse-like structures in contralateral sensory ganglia contribute to chronic mirror-image pain. *Pain*, 156(11), 2295-309.
342. Xie, W., J.A. Strong, and J.M. Zhang. (2010). Increased excitability and spontaneous activity of rat sensory neurons following in vitro stimulation of sympathetic fiber sprouts in the isolated dorsal root ganglion. *Pain*, 151(2), 447-59.
343. Garcia-Poblete, E., et al. (2003). Sympathetic sprouting in dorsal root ganglia (DRG): a recent histological finding? *Histology and histopathology*, 18(2), 575-86.
344. Chen, S.-S. and J.-M. Zhang. (2015). Progress in Sympathetically Mediated Pathological Pain. *Journal of anesthesia and perioperative medicine*, 2(4), 216-225.

345. Xie, W., et al. (2011). Highly localized interactions between sensory neurons and sprouting sympathetic fibers observed in a transgenic tyrosine hydroxylase reporter mouse. *Molecular pain*, 7, 53.
346. Pertin, M., et al. (2007). Delayed sympathetic dependence in the spared nerve injury (SNI) model of neuropathic pain. *Molecular pain*, 3, 21-21.

RESEARCH AIMS

Research Aims

The ultimate goal of this Thesis was to determine whether DRG neurons possess an AIS *in vivo* and determine its contribution to peripheral neuropathic pain. For that, the following objectives were pursued:

1. Develop a physiologically-relevant *in vitro* model of DRG neurons in which they recapitulate their morphological maturation process – pseudounipolarization - and assemble an AIS;
2. Determine whether DRG neurons have an AIS *in vivo* and characterize its structure and molecular composition using immunofluorescence;
3. Determine the functional contribution of the AIS to DRG neuron spontaneous activity in the context of neuropathic pain, using the mouse chronic constriction injury (CCI) model. For that, the following objectives were established:
    - Implement a technique of calcium imaging and correlative immunofluorescence to compare the AIS of spontaneously-active DRG neurons with the AIS of neurons without detectable spontaneous activity;
    - Build a computational model of a DRG neuron to better understand how the AIS can contribute to spontaneous activity. To implement realistic morphological and intrinsic electrical properties in the model, experimental data were collected from immunofluorescence analysis and patch clamp recordings;
    - Establish and characterize a genetic mouse model of adult DRG neurons without AIS to determine the functional impact of the absence of this compartment in the CCI model, namely its effects on spontaneous activity and pain-like behaviors.

RESULTS

The following section contains the manuscript

Nascimento, A.I., Da Silva, T.F., Fernandes, E.C., Luz, L.L, Mar, F.M., Safronov, B.V., & Sousa, M.M. (2022). Sensory neurons have an axon initial segment that initiates spontaneous activity in neuropathic pain. *Brain*, In Press. doi: 10.1093/brain/awac078

Sensory neurons have an axon initial segment that initiates spontaneous activity in neuropathic pain

Ana I. Nascimento[1,2], Tiago F. Da Silva[1], Elisabete C. Fernandes[3], Liliana L. Luz[3], Fernando M. Mar[1], Boris V. Safronov[3], Monica M. Sousa[1,*]

Author affiliations:

1 Nerve Regeneration Group, Instituto de Biologia Molecular e Celular (IBMC), Instituto de Investigação e Inovação em Saúde (i3S), University of Porto, 4200-135 Porto, Portugal.

2 Graduate Program in Molecular and Cell Biology, Instituto de Ciências Biomédicas Abel Salazar (ICBAS), University of Porto, 4050-313 Porto, Portugal.

3 Neuronal Networks Group, Instituto de Biologia Molecular e Celular (IBMC), Instituto de Investigação e Inovação em Saúde (i3S), University of Porto, 4200-135 Porto, Portugal.

Correspondence to: Monica Mendes Sousa
Instituto de Biologia Molecular e Celular (IBMC), Instituto de Investigação e Inovação em Saúde (i3S), University of Porto, Rua AlfredoAllen nº208, 4200-135 Porto, Portugal.
msousa@ibmc.up.pt

Abbreviations: AIS = axon initial segment; AnkG = AnkyrinG; AP = action potential; CCI = chronic constriction injury; DPI = days post-injury; DRG = dorsal root ganglion; K_v = voltage-gated potassium channels; Na_v = voltage-gated sodium channels; SA = spontaneous activity; WPT = weeks after tamoxifen injection;

Abstract

The axon initial segment (AIS) is a specialized compartment of the proximal axon of CNS neurons where action potentials are initiated. However, it remains unknown whether this domain is assembled in sensory dorsal root ganglion neurons, in which spikes are initiated in the peripheral terminals. Here we investigate whether sensory neurons have an AIS and if it contributes to spontaneous activity in neuropathic pain. Our results demonstrate that myelinated dorsal root ganglion neurons assemble an AIS in the proximal region of their stem axon, enriched in the voltage-gated sodium channels Nav1.1 and Nav1.7. Using correlative immunofluorescence and calcium imaging, we demonstrate that the Nav1.7 channels at the AIS are associated with spontaneous activity. Computer simulations further indicate that the AIS plays a key role in the initiation of spontaneous discharges by lowering their voltage threshold. Finally, using a Cre-based mouse model for time-controlled AIS disassembly, we demonstrate that this compartment is a major source of spontaneous discharges causing mechanical allodynia in neuropathic pain. Thus, an AIS domain is present in sensory neurons and facilitates their spontaneous activity. This study provides a new insight in the cellular mechanisms that cause pathological pain and identifies a new potential target for chronic pain management.

Introduction

Neuropathic pain is an incapacitating condition caused by neuronal damage in the somatosensory system, which arises from a variety of lesions and diseases.[1] A better understanding of its molecular mechanisms is required, so that effective treatments are developed.

Peripheral neuropathic pain is usually associated with spontaneous activity (SA) in sensory dorsal root ganglion (DRG) neurons. Such SA occurs in humans and several rodent models, suggesting that it represents a manifestation of neuropathic pain of diverse origins.[2] There has been an enormous effort to identify in the DRG neuron the specific compartment initiating SA. These studies show that most of the SA associated with peripheral injury originates in the DRG, rather than distal nerve sites such as focal demyelination portions or the injury region.[3-5] The SA originated in the ganglion is transmitted to the dorsal roots,[3-5] contributing to neuropathic pain.[6] Within the DRG, cell bodies were suggested to initiate SA.[2] However, recordings from intact ganglia indicated that SA can originate from another cellular compartment.[7, 8] Thus, the site of SA initiation in DRG neurons remains unknown.

In CNS neurons, the axon initial segment (AIS) is a specialized compartment typically located in the proximal axon.[9] This structure plays crucial roles in action potential (AP) initiation[10] and protein trafficking.[11] The AIS has a specialized scaffold whose central component is ankyrinG (AnkG), which anchors cell adhesion molecules, and voltage-gated sodium (Na_v) and potassium (K_v) channels to the membrane.[9] Although the AIS plays a key role in neuronal excitability, it is still unclear whether it exists in DRG neurons *in vivo*. These neurons have a peculiar pseudounipolar morphology; their single stem axon bifurcates within the ganglion originating a peripheral and central branch.[12] Early studies suggested that the proximal stem axon has an ultrastructure and a high channel density similar to the nodes of Ranvier and AIS of CNS neurons.[13, 14] Nevertheless, no evidence was presented so far that *in vivo* DRG neurons possess an AIS with clustering of AnkG and Na_v channels. In fact, it has been assumed that *in vivo* DRG neurons are devoid of an AIS.[15] Thus, the possibility that DRG neurons might possess an AIS as the site of ectopic AP discharge origin has been overlooked.

In this study we demonstrate that DRG neurons have an AIS which is a source of SA within the DRG leading to mechanical allodynia in neuropathic pain. These findings disclose the AIS as a potential new therapeutic target for analgesic drug development.

Materials and methods

Animals

Experiments were performed in accordance with the European Union Directive 2010/63/EU and national Decree-law nº113-2013 and all protocols were approved by the i3S Ethical Committee and by the Portuguese Veterinarian Board. Ank3-floxed mice (with loxP sites flanking exons 22 and 23 of the Ank3 gene[16]; provided by Prof V. Bennett, Duke University, Durham, NC) were crossed with Advillin-CreERT2 mice (The Jackson Laboratory), and resulting Avil-Ank3$^{fl/fl}$ and Avil-Ank3$^{wt/wt}$ mice were injected with tamoxifen, leading to AnkG ablation[17]. This was expected to lead to AIS disintegration, because of the crucial role of AnkG in Na_v channel clustering.[18] Advillin-CreERT2$^{+/-}$ Ank3$^{fl/wt}$ animals were crossed with Ank3$^{fl/wt}$ mice to generate Advillin-CreERT2$^{+/-}$ Ank3$^{wt/wt}$ (abbreviated as Avil-Ank3$^{wt/wt}$, used as controls) and Advillin-CreERT2$^{+/-}$ Ank3$^{fl/fl}$ animals (abbreviated as Avil-Ank3$^{fl/fl}$). Genotyping was performed by standard PCR using genomic DNA isolated from ear biopsies, and the following primers were used: Advillin1 (forward) 5'CCCTGTTCACTGTGAGTAGG3'; Advillin2 (reverse) 5'AGTATCTGGTAGGTGCTTCCAG3'; Avil-CreERT2 (reverse) 5'GCGATCCCTGAACATGTCCATC3'; AnkG3flox (forward) 5'CTAACCTCTCATGTCATTTCGAG3'; and AnkG3flox (reverse) 5'TGGGATGCTTTGATTCAGG3'. The expected sizes of amplicons were: Advillin-CreERT2, 180 bp; Advillin wild-type, 480 bp; Ank3-floxed, 450 bp; and Ank3 wild-type, 390 bp. Advillin-CreERT2 expression was induced in Avil-Ank3$^{fl/fl}$ animals and control littermates (Avil-Ank3$^{wt/wt}$) via a series of five consecutive daily intraperitoneal injections of tamoxifen dissolved in corn oil (75 mg/kg, Sigma-Aldrich), at 5 weeks of age. In this study, besides Avil-Ank3$^{wt/wt}$ and Avil-Ank3$^{fl/fl}$ mice, adult C57BL/6J mice (The Jackson Laboratory) were used. For the determination of conduction velocity in dorsal roots, animals of either sex were used. For the other experiments, male mice were considered. The CCI rat model[19] was adapted for use in mice, with the placement of three silk ligatures around the sciatic nerve. In addition to the animals mentioned, Wistar rat and C57BL/6J embryos were also used at E16 and E15.5, respectively.

Culture of DRG neurons

DRG were isolated from E16 Wistar rat embryos. Briefly, dissected ganglia were digested in 0.04% trypsin-EDTA (Gibco) for 1 hr at 37°C. Digestion was stopped with 5% fetal bovine serum (FBS) in Neurobasal (Gibco) and the DRG were centrifuged. The medium was removed and the ganglia were resuspended in final medium (Neurobasal medium

containing 2% B27 (Gibco), 2 mM L-glutamine (Gibco), 1% penicillin–streptomycin (Gibco), and 50 ng/ml of nerve growth factor (Millipore)). A single cell suspension was obtained by pipetting up and down 30 times. Cells were seeded in 24-well plates with glass coverslips coated with poly-L-lysine (20 µg/mL, Sigma-Aldrich) and laminin (5 µg/mL, Sigma-Aldrich), at a density of 25,000 cells per well. Cells were maintained at 37°C in a 95% air / 5% CO2 incubator in final medium, which was partially changed two times a week. To obtain monocultures growing in the near-absence of glial cells, 1 day after cell seeding cells were exposed for 48 hr to the cytostatic agents uridine and 5-fluoro-2′-deoxyuridine (40 µM each, Sigma–Aldrich).

Immunocytochemistry

At 7, 14, 21 or 28 days *in vitro*, DRG neurons were fixed for 10 min with 2% paraformaldehyde (PFA) (Sigma-Aldrich) and washed for 15 min with phosphate-buffered saline (PBS, pH 7.4). Immunocytochemistry was done immediately after. Cells were incubated with 0.1% Triton-X100 in PBS for 5 min, followed by incubation with 200 mM NH_4Cl for 10 min. Cells were washed three times for 5 min with PBS after each step. Non-specific antibody-binding sites were blocked with 5% FBS in PBS for 1 hr at room temperature and then incubated with primary antibodies diluted in blocking solution overnight at 4°C. Primary antibodies were mouse anti-AnkG (1:100, sc-12719 Santa Cruz Biotechnology), rabbit anti-AnkG (1:1,000, 386 003 Synaptic Systems), rabbit anti-βIV-spectrin SD (1:250, kind gift from Prof. M. N. Rasband)[20], mouse anti-PanNa_v channels (1:100, S8809 Sigma-Aldrich), goat anti-TRIM46 (1:100, sc-104716 Santa Cruz Biotechnology) and rabbit anti-βIII-tubulin (1:500, 302 302 Synaptic Systems). After three washes with PBS, cells were incubated for 1 hr at room temperature with the appropriate secondary antibodies: donkey anti-mouse Alexa Fluor 488 (1:500), donkey anti-goat Alexa Fluor 488 (1:500) and/or donkey anti-rabbit Alexa Fluor 647 (1:350) (all from Jackson ImmunoResearch Laboratories). Cells were washed with PBS, and the coverslips were mounted with mounting medium (ibidi). Pseudounipolar neurons with a stem axon shorter than 70 µm were classified as short-stem pseudounipolar, since they had an axonal $AnkG^+$ domain that extended beyond the bifurcation to each of the axon branches (third panel of Fig. 1C). In contrast, all pseudounipolar neurons with a long stem axon (>70 µm) had an AIS-like segment that ended before the bifurcation (fourth panel of Fig. 1C).

Immunohistochemistry

Mouse L3 and L4 DRG of each animal (and in some cases, also the corresponding dorsal roots) were pooled and fixed in ice-cold 2% PFA. All tissues were fixed for 2 hr, except for DRG samples immunolabeled for βIV-spectrin and $Na_v1.1$ and embryonic ganglia that were

fixed for 1 hr. After being washed three times with PBS, tissues were embedded in 3% agar (Sigma-Aldrich) and serial cross sections of 70 µm thickness were prepared with a tissue slicer (VT 1000S, Leica). The slices were placed in PBS into 24-well multiwell plates (Corning Falcon) for processing through free-floating immunochemistry in the next day. First, endogenous autofluorescence was blocked with 0.1% sodium borohydride in Tris-EDTA buffer at pH 9.0 for 15 min. Then, the tissues were washed with desionized water (3x 5 min). Subsequently, the samples were permeabilized with 100% methanol for 20 min at -20°C and washed with PBS (3x 5 min). Endogenous IgGs were blocked with the Mouse on Mouse (M.O.M.®) Blocking Reagent (Vector Laboratories) according to the manufacturer instructions (1 drop of the stock solution in 0.05% Triton-X100 diluted in PBS) for 45 min. After being washed with PBS (3x 5 min), tissues were incubated with the blocking solution (0.5% fish gelatin in PBS) for 1 hr at RT. Subsequently, the samples were incubated with primary antibody diluted in the blocking buffer overnight at 4°C. Mouse primary antibodies used were: anti-AnkG (1:200, 75-146 Neuromab), anti-PanNa_v channels (1:100, S8809 Sigma-Aldrich), anti-Na_v1.1 (1:100, 75-023 Neuromab), anti-Na_v1.7 (1:100, 75-103 Neuromab), anti-Na_v1.8 (1:100, 75-166 Neuromab), anti-K_v1.1 (1:500, 75-105 Neuromab) and anti-K_v1.2 (1:500, ab192758 abcam). The following rabbit primary antibodies were used: anti-AnkG (1:1500, 386 003 Synaptic Systems), anti-βIV-spectrin (1:100, kind gift from Prof Maren Engelhardt, Heidelberg University, Germany)[21], anti-MBP (1:500, 10458-1-AP Proteintech), anti-Nav1.6 (1:100, ASC-009 Alomone), and anti-Caspr[22] (1:500, kind gift from Prof Elior Peles, Weizmann Institute of Science, Rehovot, Israel). The following goat antibodies were used: anti-TRIM46 (1:100, sc-104716 Santa Cruz Biotechnology), anti-TrkA, anti-TrkB and anti-TrkC (1:700, R&D Systems, AF1056-SP, AF1494-SP and AF1404-SP, respectively). After incubation with primary antibodies, the tissues were washed in PBS (3x 10 min) and then incubated for 1 hr at room temperature with donkey secondary antibodies conjugated with Alexa Fluor 488 (1:500), 568 (1:500) or 647 (1:350), all from Jackson ImmunoResearch Laboratories. Lastly, samples were washed with PBS (3x 10 min), mounted with mounting medium (ibidi), coverslipped, and placed in 4°C until further confocal imaging, which occurred up to one week later.

Image acquisition and analysis of fixed samples

Cultured cells were visualized under a fluorescence microscope (Leica DMI6000 B) with a 40x / 0.60 NA objective coupled to a camera (Hamamatsu C11440-22c). Images of fixed tissue were acquired with a laser scanning confocal microscope Leica TCS SP5 II, a 63x / 1.30 NA glycerol immersion objective, 1 AU pinhole, 1.7x zoom and 1024 x 1024 pixels in z stacks with 0.46-µm steps. All image analysis was performed using ImageJ/Fiji. In the case of cultured cells, AIS analysis was done drawing a line profile along the proximal axon,

starting at the soma and past the AIS. Each fluorescence profile was normalized, and the AIS start and end positions were considered to be the proximal and distal axonal positions where the fluorescence surpassed or declined to 33%, respectively. AIS length was calculated as the axonal distance between start and end positions. In confocal tissue images, variations in fluorescence intensity in the z-axis required that AIS start and end positions be determined by an intensity over 30% comparing to the average cell body membrane intensity in the respective z-stack layer. The normalized AIS $Na_v1.7$ fluorescence was obtained by dividing the average AIS membrane intensity by the average cell body membrane intensity in the z-stack layer where the $Na_v1.7$ fluorescence had its maximum value. The AIS fluorescence profile along the axon was obtained by applying a Fiji script[23] on axonal paths created with the Simple Neurite Tracer plugin. 3D axonal distances (e.g., from the axon start position to the AIS start position, or AIS length) were determined using the "3D Distance Tool", which uses a triangulation method to calculate the linear distance between user-defined consecutive points. Several points were defined along the axon and the sum of the linear distances between consecutive points was used to determine the AIS start position and length.

Behavioral tests

Acetone and von Frey thresholds were performed with the left (ipsilateral) paw at baseline (3 days before sham or CCI surgery) and at determined timepoints after surgery. Behavioral accommodation was allowed for approximately 15 min before the tests were initiated. Mechanical thresholds were measured using the up-down method for obtaining the 50% threshold using von Frey hairs.[24] Sensitivity to cold was tested using the acetone test as previously described.[25]

Calcium Imaging

Mice were injected with AAV.PHP.S.CMV.dTomato.P2a.GCaMP6s.WPRE (titers: 1.14-14.2x10^{13} genome copies/ml, VectorBuilder), an adeno-associated virus encoding the calcium probe GCaMP6s and cell marker dtomato. The virus was diluted in PBS so that a total of 50 µl containing ~3x10^{12} genome copies were injected per animal. Intravenous administration of viral vectors was performed by injection into the retro-orbital sinus of adult C57BL/6J and Avil-Ank3 mice at 5 and 7 weeks of age, respectively. After allowing time for expression (3 weeks), calcium imaging was performed. Dissection of DRG was done in naïve or CCI mice under anesthesia via intraperitoneal injection of pentobarbital (50 mg/kg, i.p.). Briefly, the vertebral column was quickly cut out and immersed in oxygenated artificial cerebrospinal fluid (aCSF) at room temperature, containing: 115 mM NaCl, 3 mM KCl, 2 mM $CaCl_2$, 1 mM $MgCl_2$, 1mM NaH_2PO_4, 25 mM $NaHCO_3$ and 11 mM glucose (bubbled

with 95% O_2 / 5% CO_2). The L3 and L4 ganglia were dissected with the spinal nerve and dorsal root attached, and the epineurium that covers the DRG was carefully removed. Ganglia were allowed to recover for at least 15 min in aCSF at room temperature. A piece of stretched fiber mesh attached to a metal ring was used for the DRG fixation. The DRG was placed on a drop of dried varnish nail on the mesh, and the spinal nerve and dorsal root were stretched in opposite directions and glued to the mesh with cyanoacrylate adhesive (Supplementary Fig. 2B). For calcium imaging in the dorsal roots, the preparation was fixed in a similar way but with the dorsal root centered on the drop of dried varnish nail. The preparation was then transferred to a glass-bottomed imaging chamber positioned on the microscope stage. The DRG faced the bottom of the chamber without touching it to allow continuous perfusion of the cells by aCSF at 37 °C at a rate of 0.72 ml/s (Fig. 2A). The DRG was allowed to habituate for 15 min in the chamber before imaging, which lasted 45 min. A Leica SP8 inverted confocal microscope (Leica) with a 10x dry objective (working distance, 2.2 mm) was used for imaging. For GCaMP6s excitation, a laser wavelength at 488 nm (1% laser power) was used, and the images were acquired at a unidirectional scan speed of 700 Hz. Frames were acquired with a line average of 2 at each 1.48 seconds, with an in-plane resolution of 1024 x 512 pixels and 5 AU pinhole. A zoom of 2× or 2.5× was used for imaging in the DRG and dorsal root, respectively.

All image processing was done using Fiji/ImageJ. To generate traces of calcium signals in the DRG from time lapse images, regions of interest surrounding visually identifiable cell bodies were chosen using a free hand selection tool in the z-stack projection of the video (Supplementary Video 1 and respective stack projections in Supplementary Fig. 2C). The fluorescence time course in each soma was measured by averaging all pixels within the ROI. Analysis of traces was done as previously described.[26] For each neuron, the calcium transient rate was determined by dividing the total number of measurable transients by the total recording time. Neurons were classified as having periodic, sporadic or no calcium transients (Supplementary Fig. 2D). Only neurons with periodic transients were considered to have SA, since sparse or irregular transients could be caused by processes other than spontaneous discharge. Neurons were classified as having periodic transients if their minimum rate corresponded to 1.2 per 10 minutes and no intervals between consecutive transients exceeded 15 min. Neurons were classified as small or medium/large according to their soma cross-sectional area, assuming that 70% of the smallest neurons in the lumbar DRG are unmyelinated.[27] Our measurements of 2203 DRG neurons from 4 naïve animals indicated that neurons with the soma area exceeding 500 μm^2 (corresponding diameter, 25 µm) could be considered as medium/large. In the dorsal roots, the number of calcium transients detected was normalized by the time frame and total analyzed tissue area. Several longitudinal non-overlapping regions of interest (35

µm x 5 µm) were defined in the imaging field of the video. For each region of interest, the plugin KymoResliceWide was used to obtain a kymograph describing the fluorescence profile over time. Calcium transients were identified in each trace as described for the DRG.

In the experiments in which calcium imaging was followed by immunolabeling, the DRG was fixed while being attached to the mesh (to keep orientation). After embedding in agar, serial sections of 150 µm thickness were prepared. The immunofluorescence was performed as described above for the slice containing the DRG surface. Neurons with recorded SA were found according to their position in relation to the dtomato$^+$ neurons identified in the imaging field.

Recordings from DRG neurons and dorsal roots

Whole-cell patch-clamp recordings were performed in *ex vivo* preparations of L3 and L4 DRG from adult C57BL/6J mice 4 dpi (3 animals). The ganglia were dissected in oxygenated aCSF as for calcium imaging experiments. The spinal nerve and dorsal root were stretched in opposite directions and glued with cyanoacrylate adhesive to a glass coverslip. Before recording, each DRG was incubated in aCSF containing 5-10 mg/ml of collagenase A (Sigma Aldrich) for 1-2 hr at 32°C. Digestion with collagenase was necessary for loosening the tissue surrounding the DRG cell body, cleaning the cell membrane. Each DRG was then allowed to recover for 30 min in aCSF at room temperature before recording. All recordings were performed at 22−24 °C. The DRG neurons were visualized using the oblique infrared light-emitting diode illumination technique[28]. Whole-cell recordings were obtained after separation of satellite glial cells from the neuronal surface by applying a positive pressure through the patch pipette. The pipettes were pulled from thick-walled glass (BioMedical Instruments, Germany) and fire-polished (resistance, 4−5 MΩ). The pipette solution contained: 3 mM KCl, 150 mM K-gluconate, 1 mM $MgCl_2$, 1 mM BAPTA, 10 mM HEPES (pH 7.3 adjusted with KOH, final K^+ concentration of 160 mM). We used an EPC10-Double amplifier (HEKA, Lambrecht, Germany) with a signal low-pass filtered at 2.9 kHz and sampled at 10 kHz. Offset potentials were compensated before seal formation. Liquid junction potentials were calculated and corrected for in all experiments. Passive and active membrane properties were studied by injecting a series of 100-ms-long current steps of increasing amplitudes. We analyzed the APs evoked by the smallest suprathreshold current injection (Supplementary Fig. 3A).

Compound action potentials were recorded in 5–10 mm long L3 and L4 dorsal roots. Suction electrodes used for both stimulation and recording were fabricated from thick-walled glass and fire-polished to fit the diameter of the root. We used the differential AC amplifier (1700, A–M Systems) with a low-pass filter set to 10 kHz. A 50 µs pulse (10−150 µA) was applied to recruit Aβ- and Aδ-fibers. Conduction velocity was calculated by dividing

conduction distance, the root length between the openings of suction electrodes, by conduction time.

Computer Simulations

A multicompartment model of a mouse Aδ-fiber DRG neuron was created. Morphological parameters in this model were based on our immunofluorescence data from adult mouse DRG and dorsal roots and on studies of others (Supplementary Table 1). The dimensions of the soma, AIS, unmyelinated region of the stem axon adjacent to the AIS, heminode, first internode and first node of Ranvier were obtained from our confocal images of a CCI DRG neuron exhibiting SA revealed by calcium imaging (shown in Fig. 2E). The stem axon contained four internodes. According to our observations, each internode is 2.1 times longer than the previous one, but the nodes of Ranvier have the same length. The stem axon diameter increases with a distance from the soma (immunofluorescence data) and the nodes of Ranvier were not constricted[29] (except the last one connected to the bifurcation). For the first three internodes, myelin thickness was extrapolated based on the ratios of axon to fiber diameter.[29] This ratio was 0.95, 0.87 and 0.7 for the first, second and third internodes, respectively. In the fourth internode, fiber diameter was obtained from the axon diameter using linear regression[30]. Diameter and length of the three nodes that form the bifurcation were extrapolated based on ratios of the diameter of these compartments to the most distal stem axon internode, obtained from confocal images of the bifurcation. The same applies to the diameters of the first internode of the central and peripheral axonal branches (counting from the bifurcation). The length of the first internode of central and peripheral axons were extrapolated from.[31] Since the fourth internode of the central and peripheral branches has “normal” dimensions,[31] it and the following 29 internodes in each axonal branch were created with “normal” properties. In the central axon, diameter and length of “normal” internodes and nodes were set in agreement with average values from our immunofluorescence data of weakly myelinated fibers in the dorsal root. In the peripheral axon, diameter of “normal” internodes was obtained by multiplying the “normal” central internode diameter by 1.4.[32] Length of “normal” peripheral internodes was taken from Koszowski *et al.*[33]. The diameter of “normal” peripheral nodes was obtained using the average linear regression associating node and internode diameters.[34] In both axonal branches, length and diameter of the second and third internodes and second to fourth nodes was derived from that of the first and “normal” ones by linear interpolation. In both axonal branches, fiber diameters were obtained from axon diameters.[30] We did electrophysiological recordings to set passive and active membrane properties in the model. Recorded DRG neurons were separated based on cell body size in medium and large neurons (soma cross-section area of 500-700 μm^2 and >700 μm^2 respectively). Averaged

parameters from the most excitable medium-sized DRG neurons were considered (Supplementary Fig. 3A). The integration step was 25 μs. The spatial grid was set to 0.1 of the characteristic length (λ) for all compartments, with the exception of the AIS and the unmyelinated stem axon portion just distal to the AIS, where these values were multiplied by 11. A uniform membrane capacitance of 1 μF/cm^2 (in unmyelinated regions) and axial resistance of 100 Ωcm were assumed. The leak conductance was set to 300 μS/cm,^{2} to give the neuron an input resistance of 93 MΩ, matching the mean value for the most excitable medium-sized DRG neurons in our sample (Supplementary Fig. 3A). Leak conductance of all internodes in the peripheral and central branches was extrapolated taking into consideration myelin thickness,[31] and capacitance was determined using myelin thickness,[30] with a dielectric constant for myelin of 13.[35] We used models of Na_v and delayed-rectifier K_v channels created for the spinal sensory neurons.[36] The only modification done was the 4 mV left-shift of all activation and inactivation parameters of Na_v channels to adjust the beginning of their activation (Supplementary Fig. 3B) to that reported for dissociated large DRG neurons.[37] Na_v channels were inserted in all compartments except internodes (Table S1). In nodes of Ranvier, their conductance was adjusted to 10 nS/μm^2 to give a conduction velocity of 3.2 m/s, in agreement with our Aδ-fiber CAP recordings. The same Na_v conductance was inserted in the AIS and heminode. In the soma and the stem axon adjacent to the AIS, the Na_v conductance was adjusted to 0.6 nS/μm^2 to obtain a maximum AP depolarization rate of 281 V/s corresponding to the mean value in the cluster 2 DRG neurons (Supplementary Fig. 3A). Assuming the single Na_v channel current of 0.85 pA (at -20 mV),[38] our Na_v conductances corresponded to 9.2 channels/μm^2 in the cell body and 168 channels/μm^2 in the AIS and Aδ-fiber nodes of Ranvier, with 40% of them available at the resting potential of −75 mV. This Na_v channel density in the AIS is in agreement with experimental data for the spinal sensory neurons.[38] Delayed-rectifier K_v channels were inserted in all compartments with a density of 0.35 nS/μm^2, to obtain the Na_v to K_v channel ratio in the soma of our model as previously described.[28] Moreover, since we did not observe any AIS-specific K_v channels and this model was built for investigating the specific role of the AIS channels on SA threshold, K_v channels were introduced with a threshold higher than that of Na_v channels, so that they did not affect the threshold of SA.

Results

DRG neurons assemble an AIS *in vivo*

Although DRG neurons in culture assemble AIS-like domains,[39] they generally fail to recapitulate pseudounipolarization, the process of DRG neuron maturation from a bipolar to a pseudounipolar morphology.[12] To explore how the AIS-like domain assembly occurs during morphological maturation, DRG neurons were cultured in the absence (monoculture) or presence (mixed culture) of glial cells. In monoculture, most neurons stayed at the most immature morphological stage, the spindle-shaped bipolar, with both proximal axons containing a high density of AnkG (Fig. 1A-B). In mixed culture, most neurons acquired a pseudounipolar morphology with a stem axon containing an AnkG-enriched segment at 28 days *in vitro* (Fig. 1A- B). In mixed cultures, DRG neurons went through all the morphological stages of pseudounipolarization possessing AIS-like segments (Fig. 1C). These results implicate that pseudounipolarization depends on glia, whereas AIS assembly is a cell-intrinsic process that occurs before pseudounipolarization. In bell-shaped bipolar neurons, this domain had a more proximal start and end positions and a shorter length, compared to pseudounipolar neurons (Supplementary Fig. 1A-B), supporting that the structural properties of the AIS-like compartment depend on DRG morphology. Moreover, TRIM46 and βIV-spectrin were also enriched in the proximal stem axon in DRG neuron mixed cultures (Supplementary Fig. 1C).

We then investigated whether adult mouse DRG neurons *in vivo* possess an AIS. Since DRG neurons are heterogeneous, the AIS existence was examined in different populations expressing TrkA, TrkB or TrkC. Our data revealed that *in vivo* medium to large DRG neurons (soma cross-sectional area > 400 μm^2) have an AIS in the glomerulus of Cajal. All neurons with AIS were myelinated, as evidenced by myelin immunolabeling and/or by the presence of a heminode and nodes of Ranvier in the stem axon (Fig. 1D). The AIS was detected in the proximal stem axon of most medium/large neurons (68.1±2.6% of medium/large DRG neurons marked by βIII-tubulin; mean±SEM; n = 4 mice; >60 neurons per animal), belonging to $TrkA^+$, $TrkB^+$ and $TrkC^+$ populations (Supplementary Fig. 1D). AnkG enrichment was also revealed in the proximal stem axon of small neurons, but given the absence of a glomerulus of Cajal and the long length of the stem axon, its end position and spatial restriction could not be unequivocally determined (Supplementary Fig. 1D). Different types of neurons had an AIS with a comparable start position, but the AIS length

and predominance were significantly higher in $TrkA^+$ neurons comparing to $TrkB^+$ or $TrkC^+$ neurons (Supplementary Fig. 1E-G).

To determine the morphological stage at which AnkG starts to be accumulated in the proximal axon, mouse DRG at embryonic day 15.5 were immunolabeled. At this timepoint, bipolar DRG neurons could have up to two $AnkG^+$ proximal axons, whereas most pseudounipolar neurons had a $AnkG^+$ stem axon (Supplementary Fig. 1H). This showed that AIS assembly, as defined by AnkG clustering, is already occurring at the bipolar morphological stage, in agreement with our *in vitro* data. To characterize the DRG neuron AIS, we tested whether it contains conventional AIS proteins, such as TRIM46, βIV-spectrin and Na_v channels ($PanNa_v$), and have found that all were present in this domain (Fig. 1E-F). Moreover, we examined the specific Na_v channel isoforms present in the AIS of CNS neurons ($Na_v1.1$, $Na_v1.2$ and $Na_v1.6$)[40] or expressed by adult myelinated DRG neurons ($Na_v1.7$ and $Na_v1.8$).[41] Of these, $Na_v1.1$ and $Na_v1.7$ were enriched in the AIS (Fig. 1E-F and Supplementary Fig. 1I-K). Of note, the lower predominance of βIV-spectrin and $Na_v1.1$ in AISs is likely due to the lower sensitivity of the antibodies used since their staining was fainter (Fig. 1F). These Na_v channels and βIV-spectrin, which is typically localized to the AIS actin/spectrin cystoskeleton,[39] were co-localized with AnkG in the AIS (Fig. 1 G-H). In contrast, TRIM46 was localized in the AIS axoplasm, where it typically interacts with AIS microtubules (Fig. 1H).[42] We also examined the distribution of K_v channels found in the AIS of CNS neurons ($K_v1.1$, $K_v1.2$, $K_v7.2$ and $K_v7.3$),[40] but none of these was AIS-specific (Supplementary Fig. 1I-K).

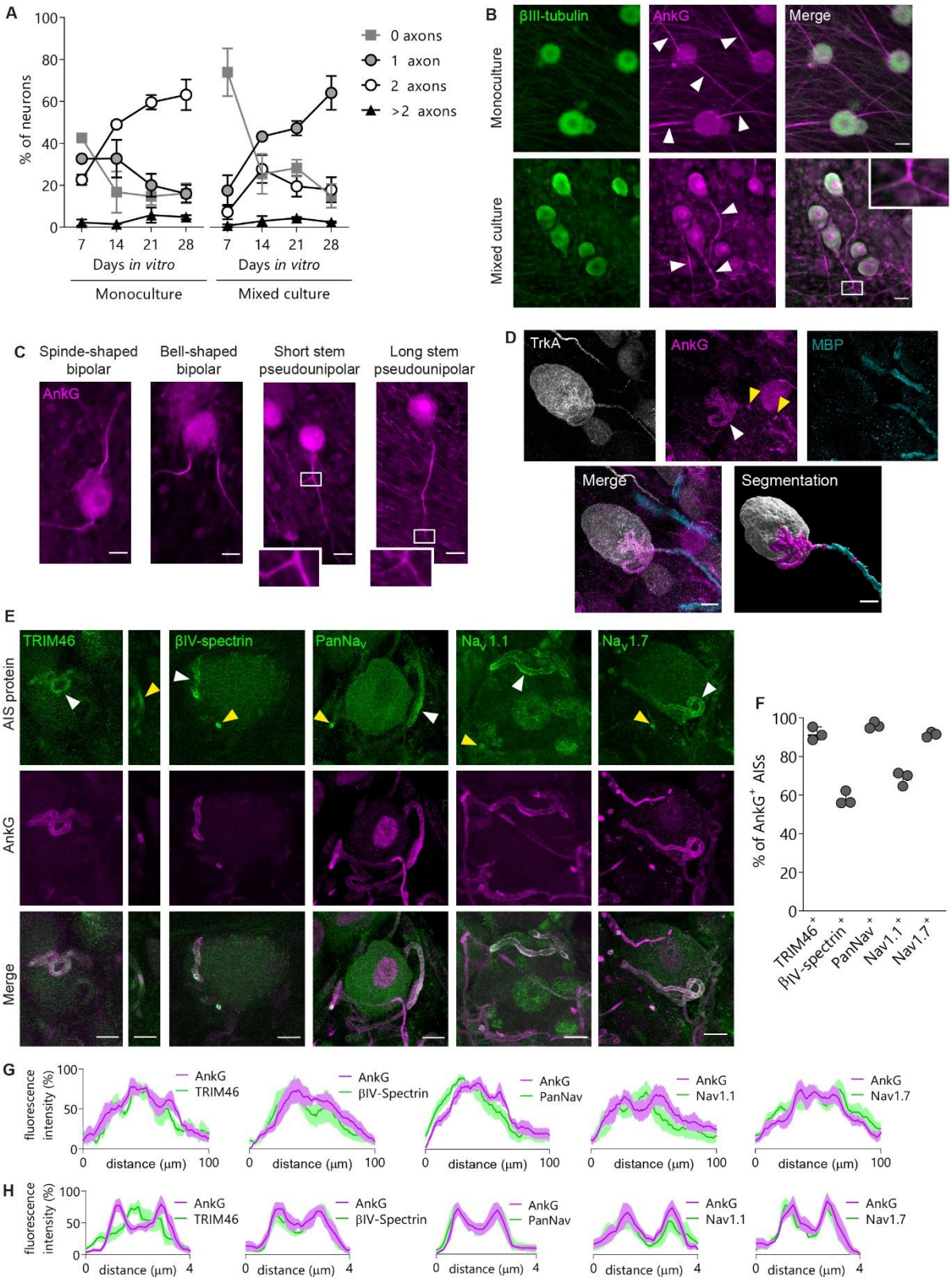

Figure 1 DRG neurons possess an AIS *in vivo*. (**A**) Fraction of cultured DRG neurons with none, one, two or more AnkG$^+$ proximal axons over time (mean±SEM, n=3 independent cultures, >60 neurons per culture and timepoint). (**B**) Representative images of cultured

DRG neurons at 28 days *in vitro* immunolabeled with βIII-tubulin and AnkG. In monoculture (top) most neurons have a spindle-shaped bipolar morphology. In mixed cultures (bottom), DRG neurons become pseudounipolar (a bifurcation is shown in the inset). Proximal axons containing high densities of AnkG (white arrowheads) are observed in both cultures. (**C**) Immunolabeling in mixed culture with AnkG, showing AIS-like structures in the proximal axons at all stages of pseudounipolarization (bifurcations shown in the insets). (**D**) Compressed confocal z-stack of an adult mouse $TrkA^+$ DRG neuron with AIS (white arrowhead) in the glomerulus of Cajal and myelin in the stem axon, labeled by AnkG and myelin basic protein (MBP), respectively. The heminode and node of Ranvier are indicated by yellow arrowheads. The Imaris-segmentation of the neuron is shown. (**E**) Z-stack projections of adult mouse DRG neurons showing the co-localization of AnkG with TRIM46, βIV-Spectrin, $PanNa_v$, $Na_v1.1$ and $Na_v1.7$ in the AIS (white arrowheads), heminodes and nodes of Ranvier (yellow arrowheads). (**F**) Percentage of $AnkG^+$ AISs that are also enriched in other AIS markers (mean ± SEM, $n = 3$ animals, >50 AISs per animal). (**G**) Mean (± SEM) normalized fluorescence intensity profile along the proximal axon is shown for AnkG and other AIS proteins, as indicated ($n = 5$ AISs). (**H**) Mean (± SEM) normalized fluorescence intensity profile along the cross section of the axon, in the portion of the AIS with the highest AnkG intensity ($n = 5$ AISs). Scale bars, 20 µm (B-C) and 10 µm (D-E).

DRG neurons with SA have Nav1.7 upregulation at the AIS

In the following experiments, we used the chronic constriction injury (CCI) model of painful neuropathy which is characterized by SA of several types (tonic, irregular and bursting) in DRG neurons.[43] Behavioral tests validated our mouse model showing that CCI produced early robust neuropathic pain-like behaviors that lasted for weeks (Supplementary Fig. 2A). To observe SA in DRG neurons, we did calcium imaging in isolated ganglia (Supplementary Fig. 2B-D and Supplementary Video 1). For that, an adeno-associated virus encoding the calcium probe GCaMP6s and the cell marker dtomato was injected into control (naïve) and CCI (4 days post-injury, dpi) mice. In DRG neurons, single APs produce small changes in fluorescence intensity and non-measurable GCaMP6s calcium transients,[44] and therefore, all detectable calcium transients are evoked by repetitive discharges.[45] Of note, our experiment may detect only a fraction of neurons with SA, since not all are transduced and those with low-frequency firing may not produce measurable transients. Periodic calcium transients revealed SA in both small and medium/large DRG neurons after CCI, but not in naïve animals (Fig. 2A). Application of 4 mM lidocaine completely abolished CCI-induced calcium transients indicating that they were evoked by SA (Fig. 2A). Thus, calcium imaging revealed CCI-induced SA in DRG neurons.

To examine whether CCI causes alterations in the AIS, DRG neurons were immunolabeled for Nav1.7 in naïve and CCI (4 dpi) mice. CCI did not change the percentage of neurons with AIS (not shown). The comparison of naïve vs CCI neurons does not account for the fact that within CCI neurons, only a fraction exhibits SA. As such, in animals with CCI, we did correlative immunolabeling for Nav1.7 in neurons generating SA to compare them with CCI neurons where SA was not detected by calcium imaging (Fig. 2B). The percentage of neurons with AIS was significantly higher in the population with SA, supporting that the presence of the AIS on its own is not sufficient but might facilitate SA initiation (Fig 2C). In comparison with neurons without SA, the AIS of neurons with SA had a similar length and start position, but higher normalized Nav1.7 fluorescence intensity (Fig. 2D-F). Accordingly, in neurons with SA the calcium transient rate did not correlate with the AIS length or position, but it significantly correlated with the AIS Nav1.7 fluorescence intensity (Fig. 2G-I). This suggests that the accumulation of Nav1.7 channels at the AIS facilitates this pathological activity.

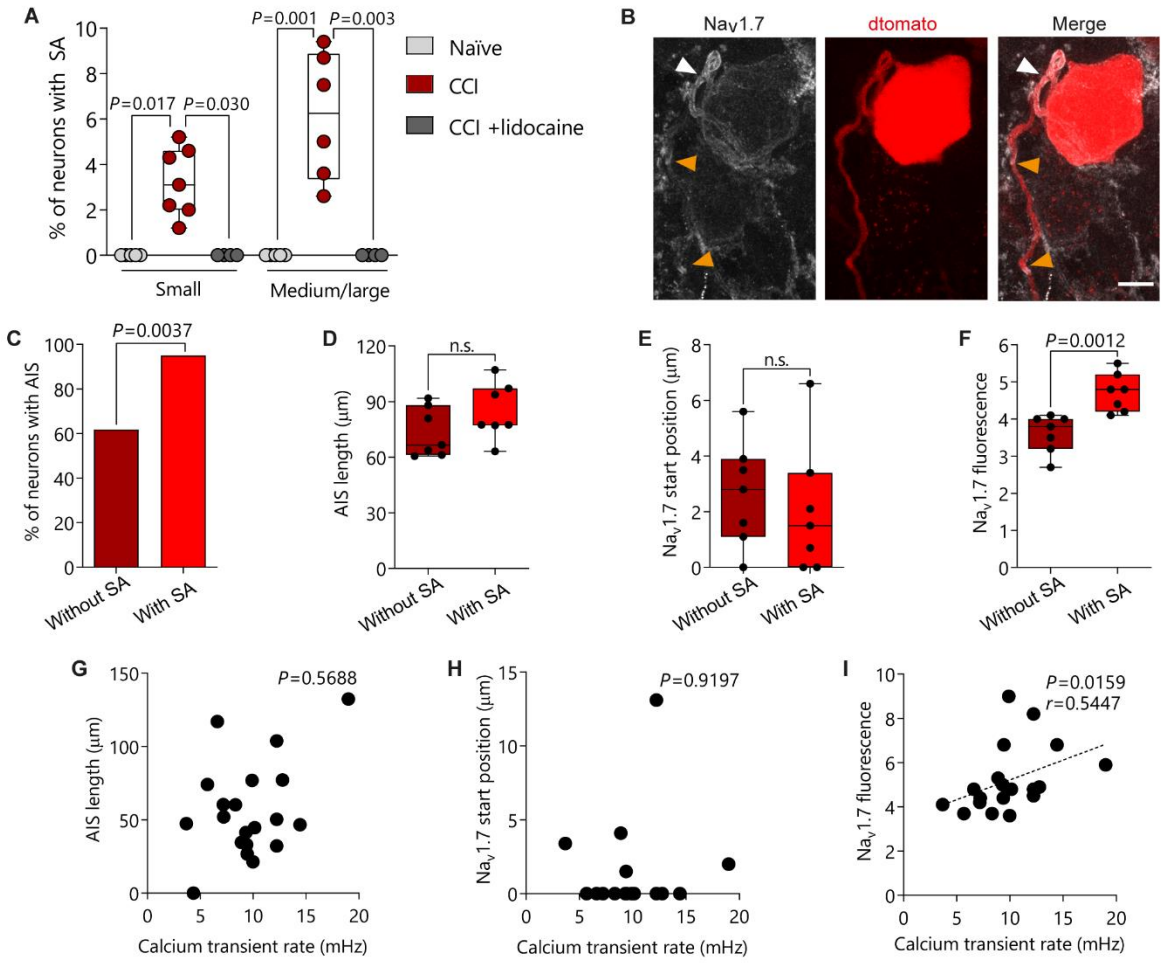

Figure 2 CCI-induced alterations in the AIS of DRG neurons. (**A**) Percentage of DRG neurons with SA from naïve and CCI animals without or with 4 mM lidocaine (*n* = 4-6 animals, >50 neurons per animal and category; Kruskal–Wallis with Dunn's multiple comparisons test; H = 28.1). (**B**) Z-stack projection of a dtomato$^+$ DRG neuron, in which SA was revealed by calcium imaging, possessing a Nav1.7$^+$ AIS (white arrowhead), heminode and node of Ranvier (orange arrowheads). Scale bar, 10 µm. (**C**) Percentage of neurons with $Na_v1.7^+$ AIS (without SA: *n* = 110 neurons, with SA: *n* = 20 neurons; Chi-square test; Chi-square statistic = 8.417; df = 1). (**D**) Length of the $Na_v1.7^+$ AIS, (**E**) start position of $Na_v1.7$ in the axon, and (**F**) $Na_v1.7$ fluorescence in the AIS, normalized to that in the soma, for CCI neurons without or with SA (*n* = 7 animals; a total of 68 neurons without SA and 19 neurons with SA were analyzed; Mann-Whitney test; U = 14.0, 18.0 and 0.5 for (D), (E) and (F), respectively; non-statistically significant p-values: 0.1946 and 0.4534 in (D) and (E), respectively; df = 12). Scatter plots showing the lack of significant correlations between calcium transient rate and the length of the $Na_v1.7^+$ AIS (**G**) and $Na_v1.7$ start position in the axon (**H**). (**I**) There is a correlation between calcium transient rate and the normalized $Na_v1.7$ fluorescence at the AIS (*n* = 19 neurons; Spearman's correlations).

The AIS facilitates SA by lowering its threshold

To study the role of the AIS in SA initiation, we created a computational model of an Aδ-DRG neuron (Fig. 3A and Supplementary Fig. 3). Although DRG neurons are known to express several Na_v channel isoforms, we modelled a generic Na_v current with activation properties resembling those of naïve tetrodotoxin-sensitive currents recorded in sensory neurons. Tetrodotoxin-resistant Na_v channels have substantially higher activation thresholds,[37] and therefore, are unlikely to initiate SA; for this reason, their contribution was not considered.

In our model, SA appeared when membrane potential reached -66.7 mV and was maintained for as long as the depolarization persisted. The APs were initiated in the distal AIS (70 µm from the soma) as evidenced by the earliest appearance of depolarization at that point (Fig. 3B, inset). Reduction of the AIS Na_v conductance to the somatic level (0.6 nS/µm2), to model a neuron without AIS, resulted in AP initiation in the soma (Fig. 3C, inset). In the model with AIS, the APs were still initiated in the distal AIS when its Na_v conductance was reduced by 75% (from 10 to 2.5 nS/µm^2) (Fig. 3D). Besides, the threshold of SA increased with a reduction in AIS Na_v conductance, being highest in the neuron without AIS (-59.8 mV, Fig. 3E). In accordance with our experimental data, our modeling results indicate that although the AIS is not sufficient for the initiation of SA, when the membrane potential in a DRG neuron is depolarized, the AIS becomes the most favorable compartment for AP initiation. Furthermore, an increase in AIS Na_v conductance in the model facilitates SA by lowering its threshold, in agreement with our correlative immunofluorescence data on the $Na_v1.7$ channel expression and SA.

Since AIS morphology may affect the excitability of CNS neurons,[9] we also simulated the impact of AIS morphological alterations on the SA threshold. AIS position and length were changed within the unmyelinated portion of the stem axon whose total length remained constant. Changes of up to 20 µm in the AIS position or length had a minor effect on the SA threshold (<0.1 mV and <0.8 mV, respectively), in accordance with previous studies.[46] These results further support our correlative immunofluorescence data on the AIS morphological properties and SA.

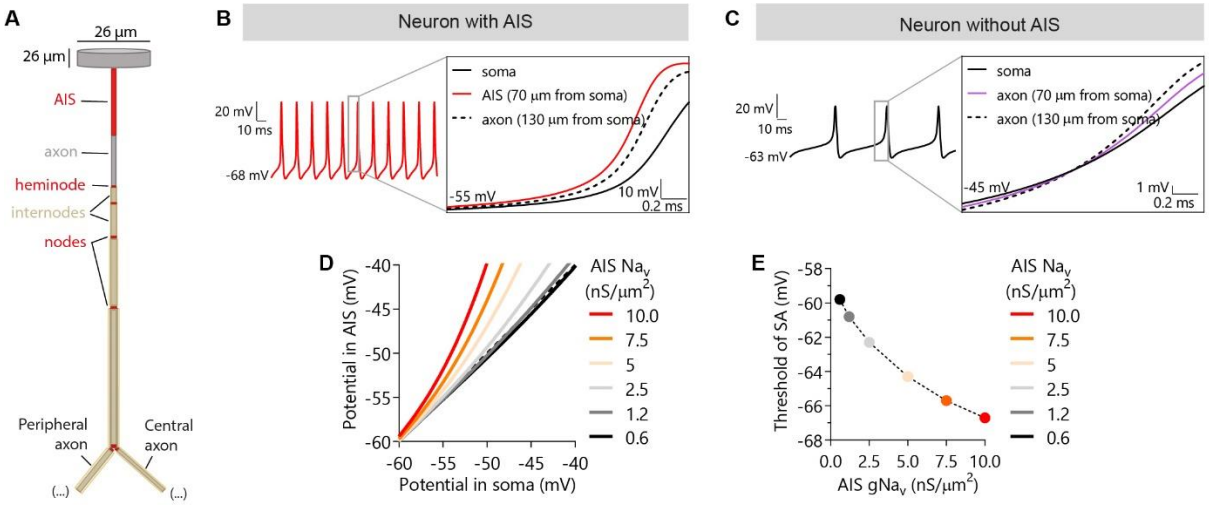

Figure 3 The AIS of DRG neurons is the most favorable site for SA initiation and lowers the threshold of SA. (**A**) Model of an Aδ-neuron based on our physiological and morphological data. The central and peripheral axons have 33 internodes each (not depicted). (**B**) Simulations of SA showing that spikes are initiated in the distal part of the AIS if its Na_v conductance is equal to that in the nodes of Ranvier (10.0 nS/µm2, left panel), (**C**) or in the soma and proximal stem axon if the neuron does not have an AIS (conductance of 0.6 nS/µm2, right panel). (**D**) Membrane potentials in the soma and distal AIS (at 70 µm from the soma) during the AP onset plotted against each other. (**E**) Threshold of SA plotted against Na_v conductance (gNa_v) in the AIS.

AIS disassembly attenuates SA and mechanical allodynia

To confirm the simulation results predicting the SA origin in the AIS, we used a genetic mouse model - Advillin-CreERT2 crossed with Ank3-floxed - allowing AIS disassembly in adult DRG neurons. Immunolabeling showed that from 3 to 6 weeks after the first tamoxifen injection (wpt), the percentage of small Avil-Ank3$^{fl/fl}$ neurons with an AnkG^{+} stem axon was the same as in control neurons (Fig. 4A-B). This AnkG stability and the fact that most small neurons had a stem axon without PanNa$_v$ enrichment indicate that small DRG neurons do not have AIS (Fig. 4A-B). In contrast, from 3 to 6 wpt, the percentage of medium/large Avil-Ank3$^{fl/fl}$ neurons with AnkG^{+} or PanNav^{+} AIS progressively decreased (Fig. 4A and C), in agreement with previous observations that AnkG is needed for Na$_v$ channel clustering at the AIS in CNS neurons.[18]

Since AnkG loss in adult neurons causes a slow and progressive destabilization of nodes of Ranvier in the sciatic nerve,[47] we examined whether this was the case for sensory axons in our model. In dorsal roots, the percentage of nodes with AnkG immunolabeling decreased from 5 wpt on in Avil-Ank3$^{fl/fl}$ axons (Supplementary Fig. 4A-B), but the percentage of nodes with Na$_v$ channels only decreased from 6 wpt (Supplementary Fig. 4A-B). To examine the time course of Na$_v$ channel loss in sensory axons, we determined the conduction velocity of myelinated fibers by recording compound APs in dorsal roots. In comparison with the control group, the conduction velocity of Avil-Ank3$^{fl/fl}$ Aβ-fibers decreased at 6 wpt, but no difference was found for Aδ-fibers at all timepoints (Supplementary Fig. 4C). Together, these data show that at 5 wpt, Avil-Ank3$^{fl/fl}$ DRG neurons have already undergone AIS disassembly with loss of Na$_v$ channels, but not in the nodes.

Next, we tested whether AIS disassembly at this timepoint (5 wpt) leads to alterations in SA in the CCI model. Calcium imaging done 4 dpi (Fig. 4D) showed that the levels of SA in small DRG neurons were the same between Avil-Ank3$^{wt/wt}$ and Avil-Ank3$^{fl/fl}$ animals, but the percentage of medium/large neurons with SA in Avil-Ank3$^{fl/fl}$ mice was significantly lower than in the control group (Fig. 4E). Similarly, the rate of calcium transients was the same between small Avil-Ank3$^{wt/wt}$ and Avil-Ank3$^{fl/fl}$ neurons with SA, but it was lower in medium/large Avil-Ank3$^{fl/fl}$ neurons with SA comparing to the respective control group (Fig. 4F). These results show that the AIS of myelinated DRG neurons is a major source of SA in the CCI model. The remaining SA observed in Avil-Ank3$^{fl/fl}$ neurons most probably was originated in the AISs that persisted at this timepoint (approximately 20% of neurons still have AIS; Fig. 4C). Additionally, according to the literature[7, 8] and to our model, the remaining SA may also be originated in the DRG neuron cell body. Next, we analyzed SA transmitted to the CNS through the dorsal roots. The frequency of calcium

transients in Avil-Ank3$^{wt/wt}$ dorsal roots was significantly higher than in Avil-Ank3$^{fl/fl}$ roots (Fig. 4G). Thus, SA initiated in the AIS of the DRG neurons is transmitted to the CNS.

To examine the contribution of the AIS to pain-like behavior, we did von Frey hair and acetone tests (Fig. 4H). Avil-Ank3$^{wt/wt}$ and Avil-Ank3$^{fl/fl}$ mice had similar baseline sensitivity to mechanical and cold stimuli (Fig. 4I-J). After CCI, mechanical allodynia was significantly attenuated in Avil-Ank3$^{fl/fl}$ mice (Fig. 4I), whereas acetone-induced cold allodynia was similar in both groups (Fig. 4J). Given our finding that the AIS is present in medium/large DRG neurons, this is consistent with previous observations that mechanical and cold allodynia are mostly mediated by large and small neurons, respectively.[48, 49] Longer effects (>5wpt) of the AIS disassembly on pain-like behavior could not be studied due to the slow and progressive tamoxifen-induced Na_v channel loss at nodes of Ranvier (Supplementary Fig. 4A-C).

To confirm that the robust attenuation of both SA and mechanical allodynia at 5 wpt was caused by disassembly of the AIS, rather than by perturbing the nodes of Ranvier, we analyzed the dorsal root, spinal nerve and CCI site at 7 dpi. We did not find any abnormal Na_v channel accumulation (Supplementary Fig. 4D) nor differences in the length of nodes and paranodes between Avil-Ank3$^{wt/wt}$ and Avil-Ank3$^{fl/fl}$ in all tissues analyzed (Supplementary Fig. 4E-F). In the injury site, where a partial destruction of paranodes and nodes was observed, the percentage of single paranodes and of absent nodes was also the same between control and Avil-Ank3$^{fl/fl}$ mice (Supplementary Fig. 4G-H). These results show that the differences in SA and pain between Avil-Ank3$^{wt/wt}$ and Avil-Ank3$^{fl/fl}$ mice were caused by AIS disassembly, rather than indirect effects on the nodes of Ranvier. Altogether, these data demonstrate that the AIS is a major source of CCI-induced SA causing mechanical allodynia, hence providing a new insight in the cellular mechanisms that cause this type of pathological pain.

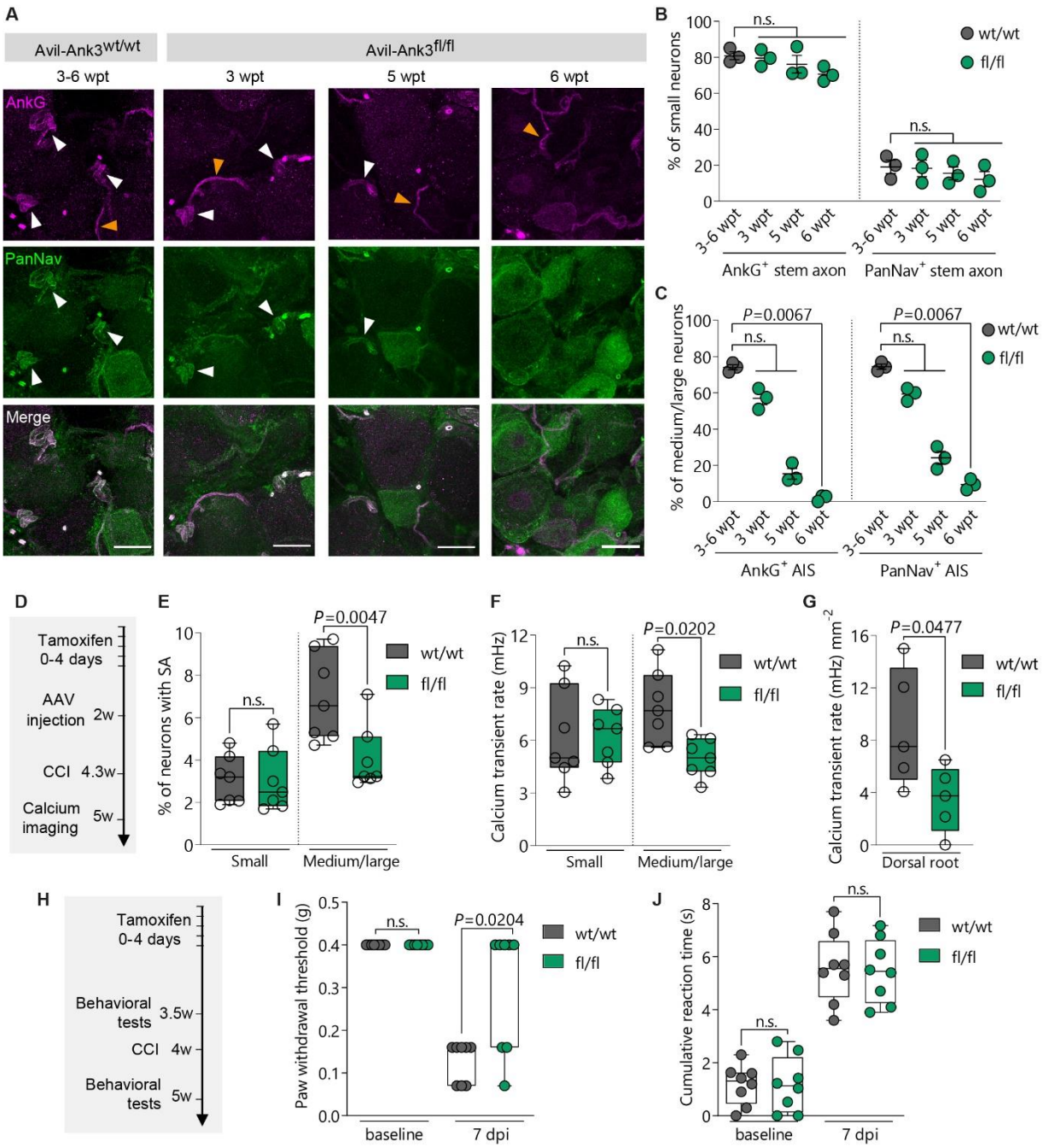

Figure 4 Abolition of AnkG expression in adult DRG neurons leads to AIS disassembly and decrease in CCI-induced SA and mechanical allodynia. (**A**) Z-stack projection of the DRG of Avil-Ank3$^{wt/wt}$ and Avil-Ank3$^{fl/fl}$ mice at 3, 5 and 6 wpt. In Avil-Ank3$^{fl/fl}$ animals, AnkG^{+} and PanNav^{+} AISs progressively disappear (white arrowheads), but the stem axons of small neurons continue to have AnkG enrichment (orange arrowheads). Scale bars, 20 µm. (**B**) Fraction of small DRG neurons with AnkG^{+} or PanNav^{+} stem axons (mean ± SEM; *n* = 3 animals; Kruskal-Wallis with Dunn's multiple comparisons test; H = 4.98 and 1.79 for AnkG and PanNav, respectively; non-statistically significant p-values: 0.1768 and 0.6588 for AnkG and PanNav, respectively; total df = 11). (**C**) Fraction of

medium/large DRG neurons with AnkG$^+$ or PanNav$^+$ AIS (mean±SEM; *n* = 3 animals; Kruskal-Wallis with Dunn's multiple comparisons test; H = 10.4; non-statistically significant p-values: 0.9245 (wt *versus* flox 3 wpt) and 0.1246 (wt *versus* flox 5wpt), for both AnkG$^+$ and PanNav$^+$ AISs; total df = 11). (**D**) Experimental design for SA analysis in Avil-Ank3$^{wt/wt}$ and Avil-Ank3$^{fl/fl}$ mice, at 5 wpt, 4 dpi. (**E**) Percentage of neurons with SA in the DRG and (**F**) their frequency of calcium transients (*n* = 7 animals; one-way ANOVA with Holm-Sidak's multiple comparisons test; F = 9.47 and 2.62 for (E) and (F), respectively; non-statistically significant p-values: 0.9511 and 0.9957 for small neurons, for (E) and (F), respectively; total df = 27). (**G**) Frequency of calcium transients in the dorsal root (*n* = 5 animals; unpaired t-test; t = 2.336; df = 8). (**H**) Experimental design for the evaluation of pain-like behaviors in Avil-Ank3$^{wt/wt}$ and Avil-Ank3$^{fl/fl}$ mice, at 5 wpt, 7 dpi. Behavioral responses of adult mice to the von Frey (**I**) and acetone (**J**) tests for analysis of mechanical and cold allodynia, respectively (*n* = 8 animals; Kruskal-Wallis with Dunn's multiple comparisons test; H = 22.2 and 23.3 for (I) and (J), respectively; non-statistically significant p-values: > 0.9999, for both (I) and (J); total df = 31).

Discussion

The hypothesis that DRG neurons might have an AIS has intrigued the scientific community for decades.[12, 14, 15] Here, we show that myelinated DRG neurons possess an AIS that initiates spontaneous discharges leading to mechanical allodynia in a neuropathic pain model.

The insufficient knowledge about the subcellular location of specific channels inducing pain has hampered the development of powerful analgesics.[50] Our observation that the AIS contributes to CCI-induced mechanical allodynia is consistent with previous findings that $Na_v1.1$ is associated with mechanical hypersensitivity,[41] and $Na_v1.7$ is needed for mechanical allodynia in this pain model.[51] Thus, the identification of a new cellular compartment where these channels contribute to SA initiation and pathological pain extends the possibilities for their therapeutic targeting.

The AIS was observed in myelinated medium to large DRG neurons, but not in small, presumably unmyelinated, neurons. Hence, the contribution of the AIS to mechanical pain is in line with previous evidence that large myelinated neurons are major mediators of mechanical hypersensitivity.[49] Since the AIS was present mostly in $TrkA^+$ neurons, which are nociceptors,[52] the AIS of these neurons in particular is likely to represent a major source of SA leading to mechanical allodynia in the CCI model. SA could also originate in the AIS of $TrkB^+$ and $TrkC^+$ neurons, which function as mechanoreceptors and/or proprioceptors.[53] As such, these neurons, that normally convey innocuous sensation, could evoke central sensitization and activate spinal nociceptive processing pathways.[54]

Our finding that DRG neurons possess an AIS is crucial for understanding the physiology of this unique type of neuron. Maintenance of the AIS requires significant metabolic costs, and therefore it is reasonable to assume that this compartment has important physiological function(s) that remain to be elucidated. Its presence in different DRG neuron populations suggests that its physiological role is not constrained by sensory modality. The AIS might be purpose-built for AP initiation inside the ganglion, to optimize the detection and response to stimuli such as cross-excitation of neighboring cells.[55] Besides, since the blood DRG barrier is highly permeable, the AIS might facilitate spike initiation in response to chemical stimuli coming from the systemic circulation and hence contribute to a putative chemosensory role. Another possible role of the AIS is to increase the fidelity of somatic invasion by spikes passing through the bifurcation point on their way from the periphery to the CNS. This might serve as a feedback mechanism giving information to the cell body about the intensity of peripheral stimuli.[31] Finally, the AIS might contribute to DRG neuron polarity by functioning as a cargo-filtering zone that

separates the stem axon proximal and distal portions, which have different ultrastructural features.[12]

In conclusion, we show that DRG neurons have an AIS which is a major source of SA causing mechanical allodynia in neuropathic pain. These findings are important for better understanding the DRG neuron function in health and chronic pain conditions.

Supplementary figures

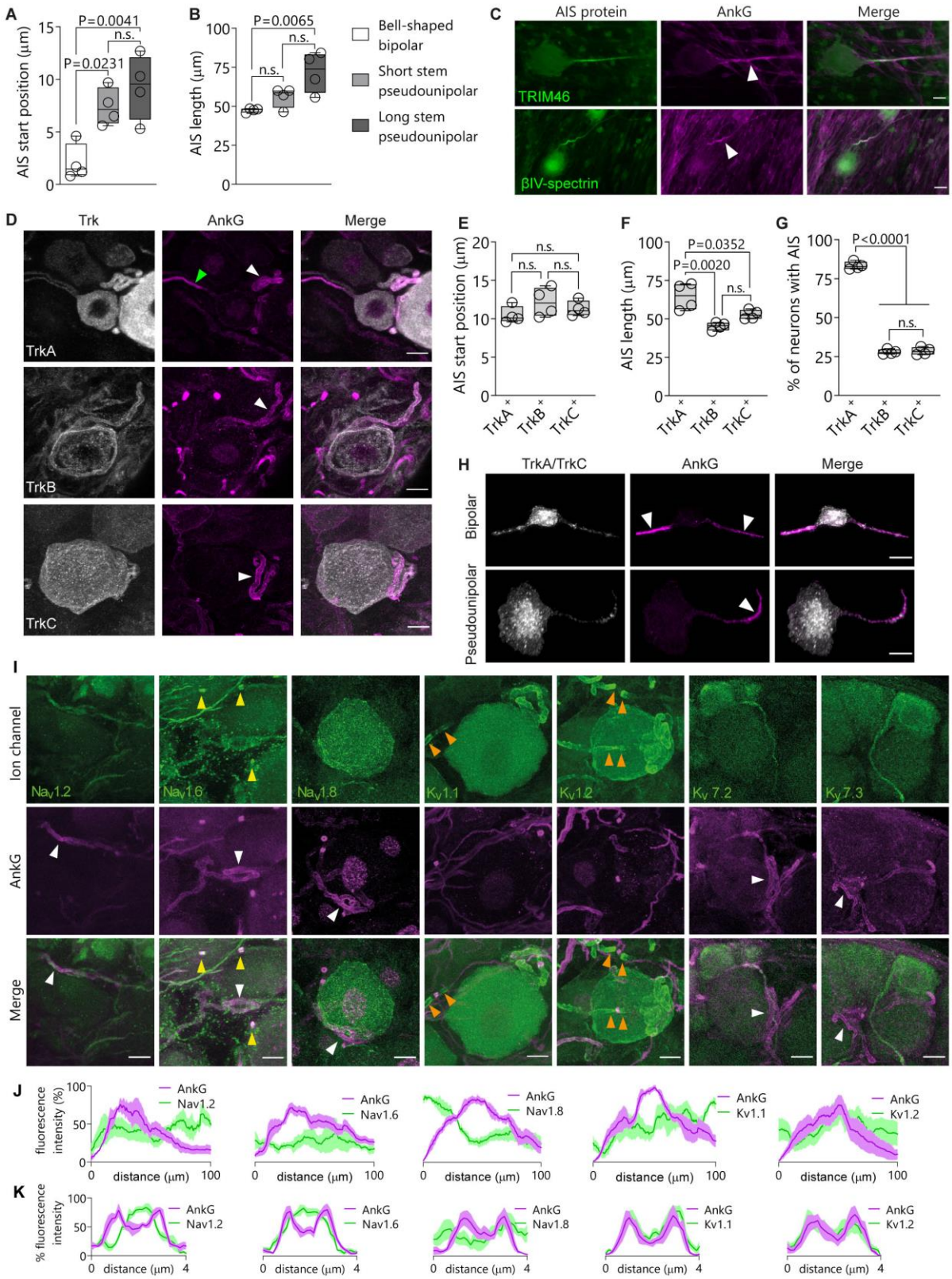

Figure S1. Characterization of the AIS of DRG neurons *in vivo*. (**A**) AIS start position and (**B**) AIS length in bell-shaped bipolar, short stem pseudounipolar and long stem

pseudounipolar neurons in mixed culture at DIV 28 (*n* = 4 independent cultures, one-way ANOVA with Tukey's correction for multiple comparisons, F = 10.6 and 8.78 for AIS start position and AIS length, respectively; non-statistically significant p-values: 0.5054 (for AIS start position, short *versus* long stem pseudounipolar), 0.3677 (for AIS length, bell-shaped *versus* short stem pseudounipolar) and 0.0580 (for AIS length, short *versus* long stem pseudounipolar); total df = 11). Color code in (A) and (B) is the same. (**C**) Immunolabeling of pseudounipolar DRG neurons in mixed cultures with AnkG and either TRIM46 or βIV-spectrin. (**D**) Compressed confocal z-stacks of adult mouse DRG neurons immunolabeled with AnkG and either TrkA (top), TrkB (middle) or TrkC (bottom). The AIS is present in neurons belonging to all subpopulations (white arrowheads). Small TrkA+ neurons contain AnkG in the stem axon (top, green arrowhead). (**E**) AIS start position, (**F**) AIS length and (**G**) fraction of medium/large neurons with AIS in $TrkA^+$, $TrkB^+$ and $TrkC^+$ neuron populations (*n* = 4 animals, >30 neurons per animal; one-way ANOVA with Tukey's correction for multiple comparisons; F = 1.45, 12.5 and 855 for (E), (F) and (G), respectively: non-statistically significant p-values: 0.2556, 0.6892, 0.6743 (for $TrkA^+$ *versus* $TrkB^+$, $TrkA^+$ *versus* $TrkC^+$, and $TrkB^+$ *versus* $TrkC^+$, respectively, in (E)), 0.1841 (in (F)), and 0.9266 (in (G)); total df = 11). (**H**) Z-stack 3D views of mouse DRG neurons at E15.5, immunolabeled for AnkG and TrkA together with TrkC. Fluorescence from neighboring neurons was eliminated by image thresholding to facilitate the visualization of the cell of interest. White arrowheads indicate clustering of AnkG in the proximal axons of neurons at the bipolar (top) and pseudounipolar (bottom) morphological stages. (**I**) Confocal images showing the expression of voltage-gated channels that are not AIS-specific. $Na_v1.2$ channels were present in the stem axon axoplasm, $Na_v1.6$ channels in nodes of Ranvier (yellow arrowheads) and $Na_v1.8$ channels in cell bodies. $K_v1.1$ and $K_v1.2$ channels were detected in juxtaparanodes (orange arrowheads) and in the proximal stem axon even in the absence of an AIS. $K_v7.2$ and $K_v7.3$ channels were present in small unmyelinated DRG neurons. The AIS is indicated by white arrowheads. (**J**) Mean (± SEM) normalized fluorescence intensity profile along the proximal axon is shown for AnkG and the other voltage-gated ions channels (*n* = 5 AISs). (**K**) Mean (± SEM) normalized fluorescence intensity profile along the cross section of the axon, in the portion of the AIS with the highest AnkG intensity (*n* = 5 AISs). Scale bars, 20 µm (C) and 10 µm (D, H and I).

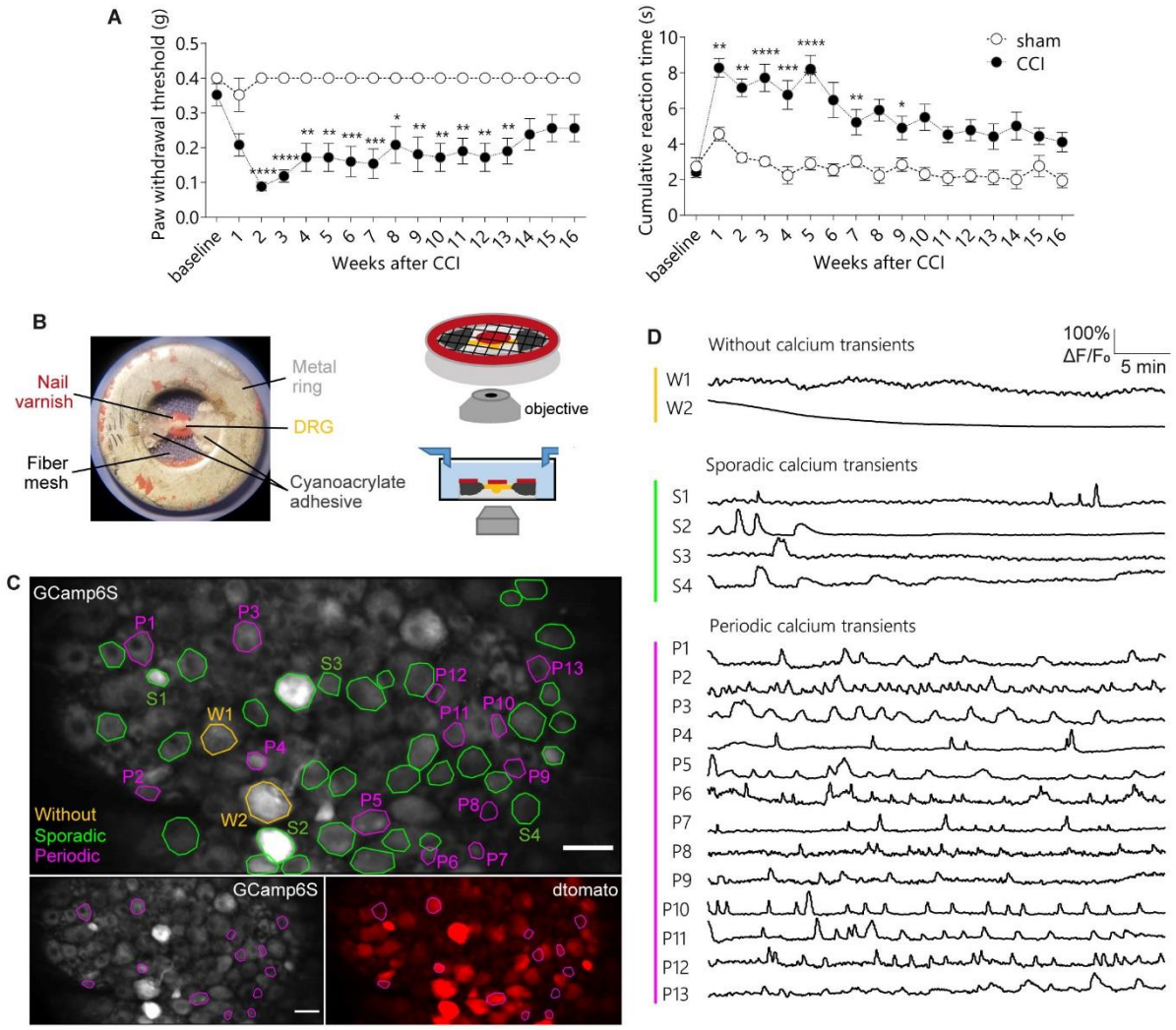

Figure S2 Chronic constriction injury (CCI) induces neuropathic pain-like behaviors and spontaneous activity (SA). (**A**) Behavioral responses of adult mice to the von Frey (left) and acetone (right) tests following CCI in comparison with sham-operated mice (mean ±SEM; sham: n = 5 animals, CCI: n = 10 animals; *P < 0.05, **P < 0.01, ***P < 0.001, ****P < 0.0001; one-way ANOVA with Sidak's multiple comparisons test; F = 8.275 and 8.931 for von Frey and acetone tests, respectively; total df = 254). Color code in both graphs is the same. (**B**) Photograph of the bottom view of a DRG preparation glued to a piece of stretched mesh fixed to a metal ring. Schematics of the top view of the metal ring (rigth, top) and lateral view of the imaging chamber (right, bottom) are shown. (**C**) Calcium imaging fields showing GCaMP6s and dtomato-expressing neurons in a DRG from a CCI animal (4 days post-injury). In the top image, neurons with no or orange contour do not have calcium transients, while neurons with sporadic or periodic calcium transients are indicated by green and magenta contours, respectively. In the bottom images, the expression of GCaMP6s and dtomato is shown and only neurons with periodic calcium transients, which indicate SA,

have contours. Scale bars, 50 µm. (**D**) Calcium traces of the neurons W1-2, S1-4 and P1-13 from (C).

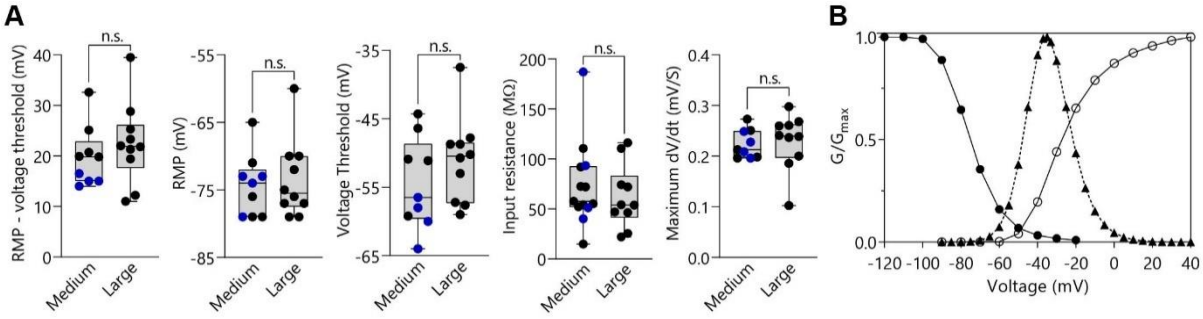

Figure S3 Patch-clamp recording data used in the Aδ-DRG neuron model. (**A**) Electrophysiological properties of adult mouse DRG neurons in intact ganglia 4 days after CCI (19 neurons from 3 animals). DRG neurons were separated based on cell body size in medium and large neurons (diameter of 25-30 μm and 31-38 μm, respectively). The difference between resting membrane potential (RMP) and AP voltage threshold, the RMP, the AP voltage threshold, the input resistance, and the maximum depolarization rate (dV/dt) are shown for each cluster (unpaired t-test; t = 0.7955, 0.3440, 1.164, 0.6927 and 0.2732, from the first to the last graph, respectively; p-values: 0.4373, 0.7350, 0.2604, 0.4961 and 0.7880, from the first to the last graph, respectively; df = 17). For computer modeling, only the most excitable medium-sized DRG neurons, whose values are represented as blue dots, were considered. (**B**) Normalized characteristics for the modelled Na_v channel activation (open circles), steady-state inactivation (closed circles) and window current (triangles). Data points were measured using simulated currents.

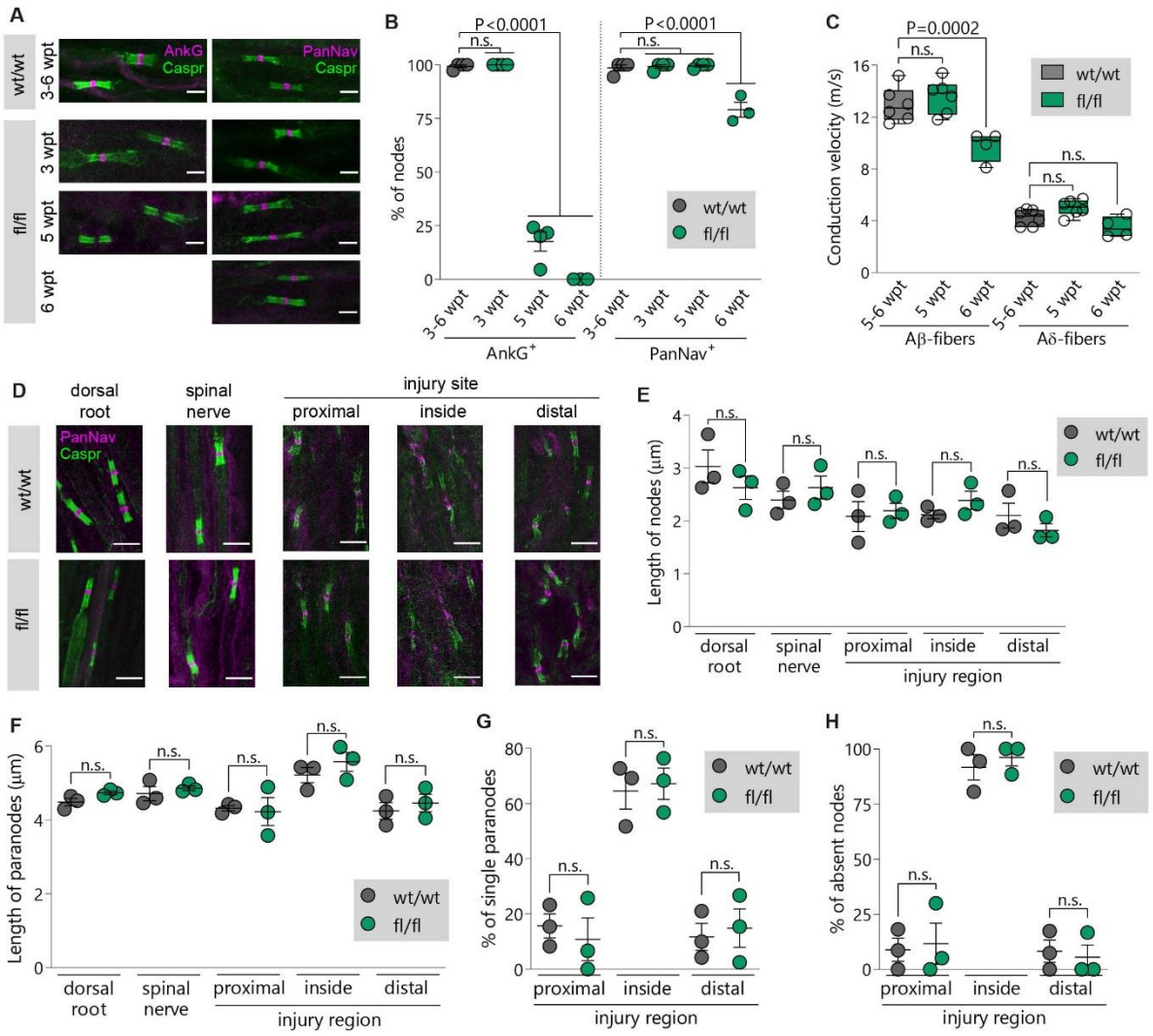

Figure S4 Characterization of the nodes of Ranvier of Avil-Ank3$^{wt/wt}$ and Avil-Ank3$^{fl/fl}$ mice after CCI. (**A**) Z-stack projections showing the nodes of Ranvier of the dorsal roots of Avil-Ank3$^{wt/wt}$ and Avil-Ank3$^{fl/fl}$ mice at 3, 5 and 6 wpt immunolabeled for Caspr and AnkG or PanNa$_v$. (**B**) Percentage of AnkG$^+$ and PanNa$_v^+$ nodes at different timepoints (mean ± SEM; n = 3-4 animals; one-way ANOVA with Sidak's multiple comparisons test; F = 374; all non-statistically significant p-values: > 0.9999; total df = 29). (**C**) Conduction velocity of Aβ- and Aδ-fibers in dorsal roots (4-6 animals, one way ANOVA with Holm-Sidak's multiple comparisons test; F = 105.5; all non-statistically significant p-values: 0.5058; total df = 31). (**D**) Z-stack projections of nodes of Ranvier in the dorsal root, spinal nerve and at the injury site (in the sciatic nerve) of Avil-Ank3$^{wt/wt}$ and Avil-Ank3$^{fl/fl}$ mice at 5 wpt, 7 days post-injury. Length of nodes of Ranvier (**E**) and paranodes (**F**) in the dorsal root, spinal nerve and injury site (mean ± SEM; 3 animals; Kruskal-Wallis with Dunn's multiple comparisons test; H = 17.2 and 18.8 for nodes and paranodes, respectively; all non-statistically significant p-values: > 0.9999; total df = 29). Percentage of nodes of Ranvier that have a single paranode (**G**) and PanNav immunolabeling partially or completely absent between the paranodes (**H**)

(mean ± SEM; 3 animals; Kruskal-Wallis with Dunn's multiple comparisons test; H = 11.7 and 12.1 for (G) and (H), respectively; all non-statistically significant p-values: > 0.9999; total df = 17). Scale bars, 5 µm.

References

1. van Hecke, O., et al. (2014). Neuropathic pain in the general population: a systematic review of epidemiological studies. *Pain*, 155(4), 654-62.
2. North, R.Y., T.T. Lazaro, and P.M. Dougherty. (2018). Ectopic Spontaneous Afferent Activity and Neuropathic Pain. *Neurosurgery*, 65(CN_suppl_1), 49-54.
3. Liu, C.N., et al. (2000). Tactile allodynia in the absence of C-fiber activation: altered firing properties of DRG neurons following spinal nerve injury. *Pain*, 85(3), 503-21.
4. Babbedge, R.C., et al. (1996). In vitro characterization of a peripheral afferent pathway of the rat after chronic sciatic nerve section. *Journal of Neurophysiology*, 76(5), 3169-77.
5. Kajander, K.C., S. Wakisaka, and G.J. Bennett. (1992). Spontaneous discharge originates in the dorsal root ganglion at the onset of a painful peripheral neuropathy in the rat. *Neuroscience letters*, 138(2), 225-8.
6. Vaso, A., et al. (2014). Peripheral nervous system origin of phantom limb pain. *Pain*, 155(7), 1384-91.
7. Amir, R., J.D. Kocsis, and M. Devor. (2005). Multiple interacting sites of ectopic spike electrogenesis in primary sensory neurons. *The Journal of neuroscience : the official journal of the Society for Neuroscience*, 25(10), 2576-85.
8. Ma, C. and R.H. LaMotte. (2007). Multiple sites for generation of ectopic spontaneous activity in neurons of the chronically compressed dorsal root ganglion. *The Journal of neuroscience : the official journal of the Society for Neuroscience*, 27(51), 14059-14068.
9. Leterrier, C. (2018). The Axon Initial Segment: An Updated Viewpoint. *The Journal of neuroscience : the official journal of the Society for Neuroscience*, 38(9), 2135-2145.
10. Palmer, L.M. and G.J. Stuart. (2006). Site of action potential initiation in layer 5 pyramidal neurons. *The Journal of neuroscience : the official journal of the Society for Neuroscience*, 26(6), 1854-63.
11. Sobotzik, J.M., et al. (2009). AnkyrinG is required to maintain axo-dendritic polarity in vivo. *Proceedings of the National Academy of Sciences of the United States of America*, 106(41), 17564-9.
12. Nascimento, A.I., F.M. Mar, and M.M. Sousa. (2018). The intriguing nature of dorsal root ganglion neurons: Linking structure with polarity and function. *Progress in Neurobiology*, 168, 86-103.

13. Matsumoto, E. and J. Rosenbluth. (1985). Plasma membrane structure at the axon hillock, initial segment and cell body of frog dorsal root ganglion cells. *Journal of neurocytology*, 14(5), 731-47.
14. Devor, M. and M. Obermayer. (1984). Membrane differentiation in rat dorsal root ganglia and possible consequences for back pain. *Neuroscience Letters*, 51(3), 341-346.
15. Gumy, L.F., et al. (2017). MAP2 Defines a Pre-axonal Filtering Zone to Regulate KIF1- versus KIF5-Dependent Cargo Transport in Sensory Neurons. *Neuron*, 94(2), 347-362.
16. Jenkins, P.M., et al. (2013). E-cadherin polarity is determined by a multifunction motif mediating lateral membrane retention through ankyrin-G and apical-lateral transcytosis through clathrin. *The Journal of biological chemistry*, 288(20), 14018-31.
17. Lau, J., et al. (2011). Temporal control of gene deletion in sensory ganglia using a tamoxifen-inducible Advillin-Cre-ERT2 recombinase mouse. *Molecular pain*, 7, 100-100.
18. Zhou, D., et al. (1998). AnkyrinG is required for clustering of voltage-gated Na channels at axon initial segments and for normal action potential firing. *The Journal of cell biology*, 143(5), 1295-304.
19. Bennett, G.J. and Y.K. Xie. (1988). A peripheral mononeuropathy in rat that produces disorders of pain sensation like those seen in man. *Pain*, 33(1), 87-107.
20. Berghs, S., et al. (2000). betaIV spectrin, a new spectrin localized at axon initial segments and nodes of ranvier in the central and peripheral nervous system. *The Journal of cell biology*, 151(5), 985-1002.
21. Höfflin, F., et al. (2017). Heterogeneity of the Axon Initial Segment in Interneurons and Pyramidal Cells of Rodent Visual Cortex. *Frontiers in cellular neuroscience*, 11, 332.
22. Peles, E., et al. (1997). Identification of a novel contactin-associated transmembrane receptor with multiple domains implicated in protein-protein interactions. *The EMBO journal*, 16(5), 978-988.
23. Conde-Sousa, E., *Extended Plot Profile (2.1.1)*. 2021.
24. Chaplan, S.R., et al. (1994). Quantitative assessment of tactile allodynia in the rat paw. *Journal of neuroscience methods*, 53(1), 55-63.
25. Bautista, D.M., et al. (2006). TRPA1 mediates the inflammatory actions of environmental irritants and proalgesic agents. *Cell*, 124(6), 1269-82.

26. Emery, E.C., et al. (2016). In vivo characterization of distinct modality-specific subsets of somatosensory neurons using GCaMP. *Science Advances*, 2(11), e1600990.
27. Tandrup, T. (1993). A method for unbiased and efficient estimation of number and mean volume of specified neuron subtypes in rat dorsal root ganglion. *The Journal of comparative neurology*, 329(2), 269-76.
28. Safronov, B.V., V. Pinto, and V.A. Derkach. (2007). High-resolution single-cell imaging for functional studies in the whole brain and spinal cord and thick tissue blocks using light-emitting diode illumination. *Journal of neuroscience methods*, 164(2), 292-8.
29. Spencer, P.S., C.S. Raine, and H. WiśNiewski. (1973). Axon diameter and myelin thickness—unusual relationships in dorsal root ganglia. *The Anatomical Record*, 176(2), 225-243.
30. Johnson, C., et al. (2015). Minimizing the caliber of myelinated axons by means of nodal constrictions. *Journal of neurophysiology*, 114(3), 1874-1884.
31. Amir, R. and M. Devor. (2003). Electrical excitability of the soma of sensory neurons is required for spike invasion of the soma, but not for through-conduction. *Biophysical journal*, 84(4), 2181-91.
32. Suh, Y.S., K. Chung, and R.E. Coggeshall. (1984). A study of axonal diameters and areas in lumbosacral roots and nerves in the rat. *The Journal of comparative neurology*, 222(4), 473-81.
33. Koszowski, A.G., G.C. Owens, and S.R. Levinson. (1998). The effect of the mouse mutation claw paw on myelination and nodal frequency in sciatic nerves. *The Journal of neuroscience : the official journal of the Society for Neuroscience*, 18(15), 5859-5868.
34. Rydmark, M. (1981). Nodal axon diameter correlates linearly with internodal axon diameter in spinal roots of the cat. *Neuroscience Letters*, 24(3), 247-250.
35. Min, Y., et al. (2009). Interaction forces and adhesion of supported myelin lipid bilayers modulated by myelin basic protein. *Proceedings of the National Academy of Sciences of the United States of America*, 106(9), 3154-3159.
36. Melnick, I.V., et al. (2004). Ionic basis of tonic firing in spinal substantia gelatinosa neurons of rat. *Journal of neurophysiology*, 91(2), 646-55.
37. Ho, C. and M.E. O'Leary. (2011). Single-cell analysis of sodium channel expression in dorsal root ganglion neurons. *Molecular and cellular neurosciences*, 46(1), 159-166.

38. Safronov, B.V. (1999). Spatial distribution of NA+ and K+ channels in spinal dorsal horn neurones: role of the soma, axon and dendrites in spike generation. *Progress in Neurobiology*, 59(3), 217-41.
39. Dzhashiashvili, Y., et al. (2007). Nodes of Ranvier and axon initial segments are ankyrin G-dependent domains that assemble by distinct mechanisms. *The Journal of cell biology*, 177(5), 857-870.
40. Huang, C.Y.-M. and M.N. Rasband. (2018). Axon initial segments: structure, function, and disease. *Annals of the New York Academy of Sciences*, 1420(1), 46-61.
41. Bennett, D.L., et al. (2019). The Role of Voltage-Gated Sodium Channels in Pain Signaling. *Physiological reviews*, 99(2), 1079-1151.
42. van Beuningen, S.F.B., et al. (2015). TRIM46 Controls Neuronal Polarity and Axon Specification by Driving the Formation of Parallel Microtubule Arrays. *Neuron*, 88(6), 1208-1226.
43. Xie, W., et al. (2005). Neuropathic pain: early spontaneous afferent activity is the trigger. *Pain*, 116(3), 243-56.
44. Chisholm, K.I., et al. (2018). Large Scale In Vivo Recording of Sensory Neuron Activity with GCaMP6. *eNeuro*, 5(1), ENEURO.0417-17.2018.
45. Walters, M.C., et al. (2019). Calcium Imaging of Parvalbumin Neurons in the Dorsal Root Ganglia. *eNeuro*, 6(4), ENEURO.0349-18.2019.
46. Goethals, S. and R. Brette. (2020). Theoretical relation between axon initial segment geometry and excitability. *Elife*, 9.
47. Saifetiarova, J., A.M. Taylor, and M.A. Bhat. (2017). Early and Late Loss of the Cytoskeletal Scaffolding Protein, Ankyrin G Reveals Its Role in Maturation and Maintenance of Nodes of Ranvier in Myelinated Axons. *The Journal of neuroscience : the official journal of the Society for Neuroscience*, 37(10), 2524-2538.
48. MacDonald, D.I., J.N. Wood, and E.C. Emery. (2020). Molecular mechanisms of cold pain. *Neurobiology of Pain*, 7, 100044.
49. Xu, Z.Z., et al. (2015). Inhibition of mechanical allodynia in neuropathic pain by TLR5-mediated A-fiber blockade. *Nature Medi*, 21(11), 1326-31.
50. Kingwell, K. (2019). Nav1.7 withholds its pain potential. *Nat Rev Drug Discov*.
51. Minett, M.S., et al. (2014). Pain without nociceptors? Nav1.7-independent pain mechanisms. *Cell reports*, 6(2), 301-12.
52. Fang, X., et al. (2005). trkA is expressed in nociceptive neurons and influences electrophysiological properties via Nav1.8 expression in rapidly conducting nociceptors. *The Journal of neuroscience : the official journal of the Society for Neuroscience*, 25(19), 4868-4878.

53. Crawford, L.K. and M.J. Caterina. (2020). Functional Anatomy of the Sensory Nervous System: Updates From the Neuroscience Bench. *Toxicologic pathology*, 48(1), 174-189.
54. Devor, M. (2009). Ectopic discharge in Abeta afferents as a source of neuropathic pain. *Experimental brain research*, 196(1), 115-28.
55. Devor, M. (1999). Unexplained peculiarities of the dorsal root ganglion. *Pain*, Suppl 6, 27-35.

GENERAL CONCLUSIONS AND FUTURE PERSPECTIVES

General conclusions and future perspectives

The hypothesis that DRG neurons might have an AIS has intrigued the scientific community for decades [1, 2], but even recent studies have failed to detect an AIS in these neurons [3], so these neurons have been regarded as lacking this compartment [4]. In this study, we optimized fixation and immunolabeling protocols, and provide functional evidence, to prove that most myelinated DRG neurons possess an AIS *in vivo*.

Comparing to CNS neurons, DRG neurons seem to have a longer AIS [5-7] and so far, they are the only neuron type for which the $Na_v1.7$ channel expression in the AIS was shown [8]. In future studies, further characterization of the DRG neuron AIS is needed to better understand its molecular organization and how it is assembled and maintained. For that, it should be determined whether it possesses an enrichment in canonical AIS molecules such as MAPs (for instance EB1/EB3), actin-associated proteins (for instance phosphorylated myosin light chain) and CAMs (for instance NF186).

Assembly and maintenance of the AIS in most myelinated DRG neurons require significant metabolic costs, and therefore, it is reasonable to assume that this compartment may have important physiological functions that remain to be elucidated. However, the physiological roles of the AIS of DRG neurons pose an enigma. Why do these neurons need an AIS in their proximal stem axon, if action potentials are initiated in their peripheral terminals and conducted directly towards the central axon without even passing through the stem axon? Further investigations are crucial for answering this intriguing question and determining the role(s) of the AIS in DRG neuron physiology. Overall, the AIS seems to be purpose-built for AP initiation inside the ganglion in response to physiological stimuli. In fact, not only the AIS, but also the cell body of DRG neurons seem to be designed to generate impulses in response to physiological stimuli, since the latter is excitable and bears a wide variety of receptors for neurotransmitters. But unfortunately the functional benefits of soma and proximal axon excitability remain unknown, despite many hypothesis have been put forward [9]. Other possible function of the AIS might be to contribute to DRG neuron polarity. Early observations suggest that the proximal and distal regions of the stem axon comprise two structurally different compartments that might be separated by a cargo-filtering zone [2]. Given that the AIS of CNS neurons is a region of sorting of intracellular traffic, it is likely that the AIS of DRG neurons is serving a similar filtering function in the stem axon [4]. Finally, an additional enigma remains to be unraveled regarding the AIS heterogeneity that was observed among DRG neurons. Why is the AIS absent in some myelinated DRG neurons? And why is the AIS longer and more predominant in $TrkA^+$ neurons than in $TrkB^+$

and TrkC$^+$ neurons? AIS heterogeneity has also been observed in subpopulations of several CNS neuron types, including interneurons, pyramidal [5] and motor neurons [2]. It could reflect a functional neuronal specialization, but such putative function remains a mystery.

Neuropathic pain is a common unmet clinical problem that urgently requires more effective analgesic drugs with minimal side effects. In this study, we demonstrate that the AIS of DRG neurons plays a key role in this type of pathological pain, by initiating SA and causing mechanical allodynia. These findings reveal the AIS as a potential therapeutic target for chronic pain management. As so, future studies are important to further validate and extend these observations. Since pain-like behaviors could not be assessed beyond the first week after injury, it is crucial to establish the contribution of the AIS for mechanical allodynia in the long-term. This requires the development of new methods relying on drugs or genetics that provide AIS disassembly without disrupting the nodes of Ranvier. Moreover, the contribution of the AIS to other pathological pain symptoms, such as heat allodynia and spontaneous pain, needs to be established. The latter is of particular clinical relevance, but the evaluation of spontaneous pain in rodent models still lacks consensual behavioral readouts [10]. Finally, it is crucial to determine the importance of the AIS in other surgical neuropathic pain models, in particular the CCD model, in which the DRG itself is chronically compressed; or the sciatic nerve or spinal nerve transection models, which in contrast to CCI lack a local inflammatory component. Even non-surgical neuropathic pain models ought to be investigated, such as those of diabetes- or chemotherapy-induced peripheral neuropathy. There is a possibility that the AIS might be less relevant for animal models in which small unmyelinated DRG neurons are predominantly injured, given the absence of an AIS in these cells. However, this is not certain, since in many models the uninjured DRG neurons present altered neurophysiology and SA [11]. Overall, the importance of the AIS should be established in a variety of neuropathic pain animal models with seemingly different cellular mechanisms.

Our work shows that, under pathological conditions, the AIS accounts for most of the SA originated within the ganglia. These results are in agreement with previous studies demonstrating that the soma and a previously unidentified axonal site within the ganglion initiate ectopic SA in neuropathic pain [12]. In future investigations, it would be interesting to characterize the SA originated in the AIS using electrophysiological measurements and determine how its frequency and pattern compares with the SA originated in the soma and in the peripheral axon. Besides, it would be useful to understand how the SA originated within the DRG interacts with the physiological and pathological activity coming from the peripheral neuron branch, since it is unknown whether it adds to and/or blocks these peripheral inputs. Even though much is still unknown, ectopic SA has been proven to cause pathological pain, likely by functioning as a spontaneous raw pain signal and triggering

central sensitization [13]. In agreement with our findings, animal and human studies have demonstrated that the SA originated within the DRG triggers mechanical allodynia [14, 15]. These authors attenuated this neuropathic pain symptom by local application of lidocaine to the DRG at concentrations that block the DRG SA but are too low to block axonal impulse propagation. As so, they proposed the direct delivery of diluted lidocaine to the DRG as a possible therapeutic strategy to attenuate chronic pain symptoms without perturbing peripheral axon inputs. The finding that the AIS is the main source of SA within the DRG provides a clearer perspective of the cellular compartments that should be therapeutically targeted for pain management.

The observation that the AIS of DRG neurons contains $Na_v1.1$ and $Na_v1.7$ is significant since these channel subtypes, especially the $Na_v1.7$, have been implicated in pain. However, it should be noted that, given the unavailability of antibodies providing a specific signal, our results do not exclude the possibility that the AIS of DRG neurons also contains $Na_v1.3$ and $Na_v1.9$ channels, which have also been implicated in neuropathic pain [16]. Future research should determine whether these and other ion channels, such as K_v or Ca_v channels, are enriched in the AIS of DRG neurons. For more than 15 years, there has been a huge effort to develop inhibitors of Na_v channels for producing potent analgesics. In particular the $Na_v1.7$ channel has been a promising therapeutic target, due to the discovery of gene mutations associated with pain insensitivity and hypersensitivity in patients. This human genetic validation led to the development of many $Na_v1.7$ blockers in the form of low molecular weight compounds, peptidic blockers and monoclonal antibodies, both by academia and pharmaceutical companies. Nevertheless, despite the excellent *in vitro* pharmacology of $Na_v1.7$ channel inhibitors and some compelling results using rodent pain models, these blockers have not yielded robust analgesia in human clinical trials [17]. The failure of these inhibitors has been attributed to many causes, including the fact that complete inhibition of $Na_v1.7$ channels might be needed for pain relief, but it is difficult to achieve *in vivo* and may lead to unwanted side effects, such as blockade of protective nociception. In addition, it is still unknown where, anatomically, $Na_v1.7$ inhibition is needed for chronic pain relief [18]. This is particularly relevant, since this channel subtype is present in many DRG neuron compartments, such as the soma, unmyelinated axons, nodes of Ranvier of some Aδ-fibers, peripheral and central terminals [19] and at the ends of transected peripheral axons [20]. In this context, our finding that the $Na_v1.7$ channel is highly enriched at the AIS might be important for its therapeutic targeting, since targeting specifically the AIS $Na_v1.7$ channels could potentially reduce side effects and simultaneously increase the efficacy of channel inhibition.

Our computer simulations indicate that most spontaneous discharges within the DRG originate in the AIS because this is the most favorable compartment for AP initiation,

due to its lower AP threshold. This implies that any cell-intrinsic or -extrinsic pathological mechanism that causes DRG neuron depolarization could potentially lead to the initiation of SA in the AIS. This goes in line with $Na_v1.7$ channel being considered as having an important role in impulse initiation and pacemaking, due to its ability to amplify subthreshold depolarizations [16]. However, in physiological conditions, SA is virtually inexistent, which implies that the AIS must undergo injury-induced pathological changes leading to hyperexcitability. So, what aberrant alterations occur at the AIS that allow it to behave as a pacemaker in neuropathic pain conditions? Our correlative immunofluorescence shows that $Na_v1.7$ channel accumulation at the AIS is associated with SA levels. This is in agreement with previous studies indicating that abnormal increases in sodium conductance lead to repetitive firing [21]. Therefore, it can be hypothesized that after injury, $Na_v1.7$ channel accumulation might occur at the AIS of some DRG neurons, resulting in the facilitation of SA initiation in this compartment. Determining if this is in fact the case, and how this occurs would be extremely valuable. Na_v channel density at the AIS could be altered by dysregulation of channel expression, but it is not consensual whether $Na_v1.7$ upregulation occurs in NP models of nerve ligation [22, 23]. In addition, Na_v channel density could also be affected by abnormal channel trafficking and anchoring in the AIS membrane. In this context, AnkG and NF are likely involved in the recruitment of $Na_v1.7$ to the AIS, since it was recently reported that this channel interacts with these AIS proteins [24]. Finally, SA initiation in the AIS could be triggered by alterations in the intrinsic properties of channels leading to hyperexcitability [25]. Upon injury, the properties of AIS Na_v channels could potentially be affected by changes in the splice variants being expressed, associated auxiliary β-subunits or post-translational modifications. Unfortunately, such putative pathological alterations in DRG neurons remain to be established.

In conclusion, this work proved the existence of the AIS in myelinated DRG neurons and determined its contribution to SA and mechanical allodynia in neuropathic pain. These findings signify an advance in the understanding of the DRG neuron function, both in physiological and pathological conditions, and therefore potentially pave the way for new therapeutic developments. Hopefully, they will ultimately contribute to address the medical needs of patients with chronic pain.

References

1. Devor, M. and M. Obermayer. (1984). Membrane differentiation in rat dorsal root ganglia and possible consequences for back pain. *Neuroscience Letters*, 51(3), 341-346.
2. Nascimento, A.I., F.M. Mar, and M.M. Sousa. (2018). The intriguing nature of dorsal root ganglion neurons: Linking structure with polarity and function. *Progress in Neurobiology*, 168, 86-103.
3. Gumy, L.F., et al. (2017). MAP2 Defines a Pre-axonal Filtering Zone to Regulate KIF1- versus KIF5-Dependent Cargo Transport in Sensory Neurons. *Neuron*, 94(2), 347-362.e7.
4. Leterrier, C. (2018). The Axon Initial Segment: An Updated Viewpoint. *The Journal of neuroscience : the official journal of the Society for Neuroscience*, 38(9), 2135-2145.
5. Höfflin, F., et al. (2017). Heterogeneity of the Axon Initial Segment in Interneurons and Pyramidal Cells of Rodent Visual Cortex. *Frontiers in cellular neuroscience*, 11, 332.
6. Duflocq, A., et al. (2011). Characterization of the axon initial segment (AIS) of motor neurons and identification of a para-AIS and a juxtapara-AIS, organized by protein 4.1B. *BMC biology*, 9, 66-66.
7. Meza, R.C., et al. (2018). Role of the Axon Initial Segment in the Control of Spontaneous Frequency of Nigral Dopaminergic Neurons In Vivo. *The Journal of neuroscience : the official journal of the Society for Neuroscience*, 38(3), 733-744.
8. Berger, S.L., et al. (2018). Localized Myosin II Activity Regulates Assembly and Plasticity of the Axon Initial Segment. *Neuron*, 97(3), 555-570.e6.
9. Devor, M. (1999). Unexplained peculiarities of the dorsal root ganglion. *Pain*, Suppl 6, 27-35.
10. Tappe-Theodor, A. and R. Kuner. (2014). Studying ongoing and spontaneous pain in rodents--challenges and opportunities. *The European journal of neuroscience*, 39(11), 1881-90.
11. Tran, E.L. and L.K. Crawford. (2020). Revisiting PNS Plasticity: How Uninjured Sensory Afferents Promote Neuropathic Pain. *Frontiers in cellular neuroscience*, 14, 612982.
12. Ma, C. and R.H. LaMotte. (2007). Multiple sites for generation of ectopic spontaneous activity in neurons of the chronically compressed dorsal root ganglion. *The Journal of neuroscience : the official journal of the Society for Neuroscience*, 27(51), 14059-14068.
13. Devor, M. (2009). Ectopic discharge in Abeta afferents as a source of neuropathic pain. *Experimental brain research*, 196(1), 115-28.
14. Vaso, A., et al. (2014). Peripheral nervous system origin of phantom limb pain. *Pain*, 155(7), 1384-91.
15. Yatziv, S.L. and M. Devor. (2019). Suppression of neuropathic pain by selective silencing of dorsal root ganglion ectopia using nonblocking concentrations of lidocaine. *Pain*, 160(9), 2105-2114.
16. Bennett, D.L., et al. (2019). The Role of Voltage-Gated Sodium Channels in Pain Signaling. *Physiological reviews*, 99(2), 1079-1151.

17. Eagles, D.A., C.Y. Chow, and G.F. King. (2020). Fifteen years of Na(V) 1.7 channels as an analgesic target: Why has excellent in vitro pharmacology not translated into in vivo analgesic efficacy? *British journal of pharmacology*.
18. Kingwell, K. (2019). Nav1.7 withholds its pain potential. *nature reviews. Drug discovery*.
19. Black, J.A., et al. (2012). Expression of Nav1.7 in DRG neurons extends from peripheral terminals in the skin to central preterminal branches and terminals in the dorsal horn. *Molecular pain*, 8, 82-82.
20. Persson, A.K., et al. (2011). Nav1.7 accumulates and co-localizes with phosphorylated ERK1/2 within transected axons in early experimental neuromas. *Experimental neurology*, 230(2), 273-9.
21. Waxman, S.G., et al. (1999). Sodium channels and pain. *Proceedings of the National Academy of Sciences of the United States of America*, 96(14), 7635-7639.
22. Tian, J.J., et al. (2020). Upregulation of Nav1.7 by endogenous hydrogen sulfide contributes to maintenance of neuropathic pain. *International journal of molecular medicine*, 46(2), 782-794.
23. Kim, C.H., et al. (2002). Changes in three subtypes of tetrodotoxin sensitive sodium channel expression in the axotomized dorsal root ganglion in the rat. *Neuroscience Letters*, 323(2), 125-8.
24. Kanellopoulos, A.H., et al. (2018). Mapping protein interactions of sodium channel Na(V)1.7 using epitope-tagged gene-targeted mice. *The EMBO journal*, 37(3), 427-445.
25. Huang, Z.-J. and X.-J. Song. (2008). Differing alterations of sodium currents in small dorsal root ganglion neurons after ganglion compression and peripheral nerve injury. *Molecular pain*, 4, 20-20.

APPENDIX

This Appendix contains the manuscript

Nascimento, A.I., F.M. Mar, and M.M. Sousa. (2018). The intriguing nature of dorsal root ganglion neurons: Linking structure with polarity and function. *Progress in Neurobiology*, 168, 86-103. doi: 10.1016/j.pneurobio.2018.05.002.

Progress in Neurobiology 168 (2018) 86–103

Contents lists available at ScienceDirect

Progress in Neurobiology

journal homepage: www.elsevier.com/locate/pneurobio

Review article

The intriguing nature of dorsal root ganglion neurons: Linking structure with polarity and function

Ana Isabel Nascimento[a,b], Fernando Milhazes Mar[a,1], Mónica Mendes Sousa[a,*,1]

[a] Nerve Regeneration Group, Instituto de Biologia Molecular e Celular—IBMC and Instituto de Inovação e Investigação em Saúde, University of Porto, Rua Alfredo Allen, 208, 4200-135 Porto, Portugal

[b] Instituto de Ciências Biomédicas Abel Salazar-ICBAS, Rua Jorge Viterbo Ferreira 228, 4050-313 Porto, Portugal

ARTICLE INFO

Keywords:
Dorsal root ganglia
Neuronal polarity
Axonal cytoskeleton
Axon regeneration
Axonal transport
Axon initial segment

ABSTRACT

Dorsal root ganglion (DRG) neurons are the first neurons of the sensory pathway. They are activated by a variety of sensory stimuli that are then transmitted to the central nervous system. An important feature of DRG neurons is their unique morphology where a single process -the stem axon- bifurcates into a peripheral and a central axonal branch, with different functions and cellular properties. Distinctive structural aspects of the two DRG neuron branches may have important implications for their function in health and disease. However, the link between DRG axonal branch structure, polarity and function has been largely neglected in the field, and relevant information is rather scattered across the literature. In particular, ultrastructural differences between the two axonal branches are likely to account for the higher transport and regenerative ability of the peripheral DRG neuron axon when compared to the central one. Nevertheless, the cell intrinsic factors contributing to this central-peripheral asymmetry are still unknown. Here we critically review the factors that may underlie the functional asymmetry between the peripheral and central DRG axonal branches. Also, we discuss the hypothesis that DRG neurons may assemble a structure resembling the axon initial segment that may be responsible, at least in part, for their polarity and electrophysiological features. Ultimately, we suggest that the clarification of the axonal ultrastructure of DRG neurons using state-of-the-art techniques will be crucial to understand the physiology of this peculiar cell type.

1. Introduction

In vertebrates, all somatosensory pathways (with the exception of those coming from the head) begin with the activation of DRG neurons. These neurons are responsible for thermoception (sensing temperature), nociception (feeling pain), mechanoreception (sensing pressure) and proprioception (sensing body spatial position). Their cell body is inside DRGs, which are ganglia located alongside the spinal cord (Fig. 1). Interestingly, DRG neurons have a single process -the stem axon- that bifurcates within the ganglion into a peripheral and a central axonal branch. This is known as pseudo-unipolar morphology. The two DRG neuron branches have axonal hallmarks, such as being, in the case of some DRG neurons, myelinated. Additionally, the peripheral branch is the site of axon potential generation and the central branch synapses with second order neurons, which are both axonal features. However, *in vivo,* the peripheral DRG neuron branch is positive for the somatodendritic marker microtubule-associated protein 2 (MAP2) (Papasozomenos et al., 1985), raising the hypothesis that at the molecular level it might have some dendritic-like features. Despite this peculiarity, both DRG neuron branches are generally considered axons.

Sensory stimuli lead to the generation of action potentials in the terminal of the peripheral branch that are conducted toward the stem axon bifurcation. From this point, action potentials are conducted along the central axon towards the CNS. The central axon enters the spinal cord *via* the dorsal root and then bifurcates into an ascending and a descending branch that grow longitudinally along the lateral margin of the spinal cord over several segments. In the case of some neurons, the ascending central branches synapse in the gracile or cuneate nuclei of the brainstem (Giuffrida and Rustioni, 1992). From the ascending and descending central branches, collaterals are generated in the spinal cord that penetrate the gray matter and synapse in specific laminae of the spinal grey matter (Mense, 1990). In contrast to the central branch, the

Abbreviations: ankG, ankyrinG; AIS, axon initial segment; DRG, dorsal root ganglion; EM, electron microscopy; NGF, nerve growth factor; MAP2, microtubule-associated protein 2; SGC, satellite glial cell; Trk, tyrosine receptor kinase

* Corresponding author.
E-mail address: msousa@ibmc.up.pt (M.M. Sousa).

[1] Equal contribution.

https://doi.org/10.1016/j.pneurobio.2018.05.002
Received 6 December 2017; Received in revised form 26 April 2018; Accepted 1 May 2018
Available online 02 May 2018

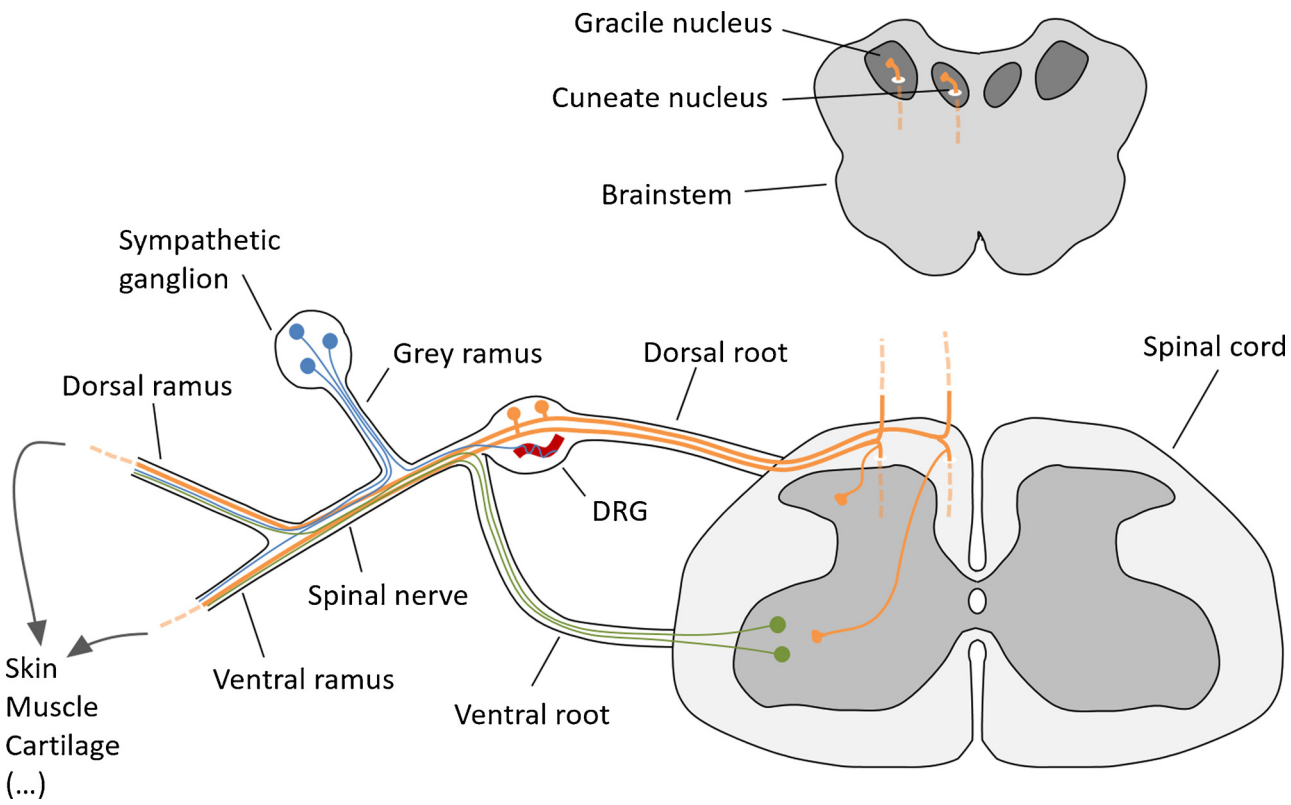

Fig. 1. Schematic drawing showing DRG neurons (orange) with an axonal branch going to the periphery, and a central axon bifurcating and synapsing in the spinal cord laminae and in the brainstem nuclei. The spinal nerve contains not only the processes of DRG neurons but also of motor (green) and sympathetic (blue) neurons. Sympathetic fibers are depicted entering in the DRG, where they associate mainly with blood vessels (red). Adapted from (Xie et al., 2010).

peripheral DRG neuron axon rarely branches proximally to its terminal arbor (Devor et al., 1984).

DRG neurons represent a remarkably diverse and complex population. Thus, several attempts have been made to classify them. Initially DRG neurons were categorized according to several physiological properties: conduction velocity (Aα, Aβ, Aδ and C fibers), sensory modality (nociceptors, mechanoreceptors, proprioceptors and thermoreceptors), peripheral targets, and intensity of stimulus necessary to activate them, among others (reviewed in Perl (1992)). More recently, attempts to classify DRG neurons mainly based on molecular markers have been made. Although several traditional markers are widely used, there is still not a definite and consensual classification of DRG neurons based on neurochemical phenotype (Li et al., 2015). Despite this heterogeneity, in this review we focus on features of the DRG neuron that are probably common to all subtypes.

For a long time, the peculiar morphology of DRG neurons has raised many questions regarding their physiology (Devor, 1999). However, the heterogeneity among DRG neurons has hindered a complete understanding of the behavior of these cells in health and disease. The overall goal of this review is to integrate early ultrastructural findings with current understanding of the function and polarity of DRG neurons. We start with an overview of the maturation of these neurons, followed by a critical analysis of the most interesting structural features of their cell body, stem axon and axonal branches. Then we provide an in-depth discussion of the functional differences between the central and peripheral axons of DRG neurons. Also, we present the possibility of the existence of an axon initial segment (AIS)-like structure in DRG neurons and discuss its possible functions in this cell type. We end with an analysis of the available *in vitro*, *ex vivo* and *in vivo* models that can be used to study DRG neuron biology, and on how these could be possibly improved.

2. The origin and maturation of DRG neurons

2.1. Embryonic development of the DRG

During development, neural crest cells originate DRG, autonomic and enteric ganglia neurons, and all the PNS glial cells (Douarin et al., 1991). In contrast, in the CNS, neurons and glia are originated in the neural tube (Rowitch, 2004). Neural crest cells are located dorsally to the neural tube and migrate ventrally in chain-like structures to the DRG between E8.5 and E10 in the mouse (Kasemeier-Kulesa et al., 2005; Serbedzija et al., 1990). After migrating to the DRG, neural crest cells may originate neurons directly or divide *in situ*. Interestingly, live-imaging in chick embryo slices revealed that bipolar neural crest cells within the DRG become non-polarized before dividing, and then originate two DRG neurons that acquire their bipolar shape by inheriting their site of neurite initiation from the progenitor (Boubakar et al., 2017).

DRG neurons are specified from the cell progeny of neural crest cells in two broad and overlapping successive waves controlled by the activity of the transcription factors neurogenin 1 and 2 (Ma et al., 1999) (Fig. 2). In the lumbar mouse DRG, the first wave of neurogenesis occurs from E10.5 to E12.5, whereas the second wave begins at E11.5 and lasts until E13.5 (Lawson and Biscoe, 1979). The first neurogenin 2-dependent wave of neurogenesis originates mostly, but not exclusively, large-diameter proprioceptors that express tyrosine receptor kinase C (TrkC) and mechanoreceptors that express TrkB or Ret. The second neurogenin 1-dependent wave gives rise mostly to $TrkA^+$ small-diameter neurons that may become mechanoreceptors, nociceptors or thermoceptors (reviewed in Liu and Ma (2011)). A third wave of neurogenesis occurs later from the progeny of boundary cap cells. This is a neural crest-derived cell population that transiently occupies the

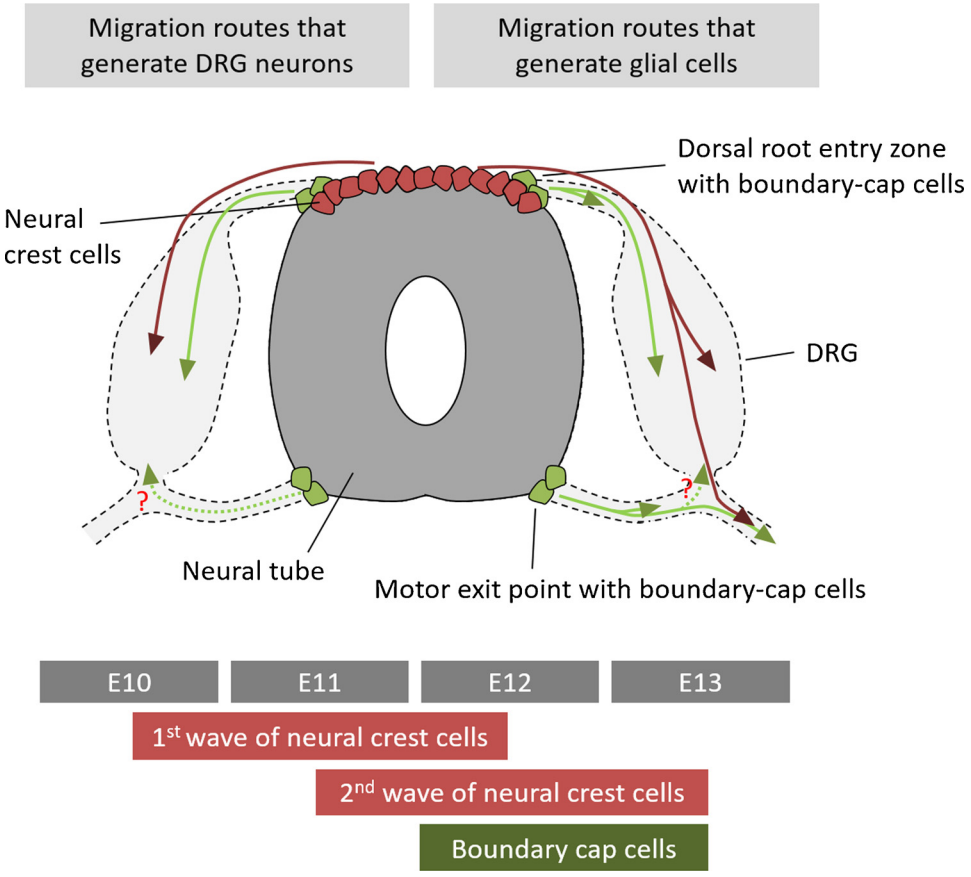

Fig. 2. Migration pathways of neural crest cells (red) and boundary cap cells (green) originating DRG neurons (left) and glial cells (right). Neural crest cells delaminate from the dorsal neural tube and specify DRG neurons in two overlapping waves. A third wave of neurogenesis is specified from boundary cap cells, which are intermediate progenitors that appear transiently at dorsal root entry zones and prospective motor exit points. Both progenitor types give rise to DRG neurons and peripheral glia. The timeline of neurogenesis in mouse lumbar DRGs is presented. The question marks refer to the possibility that boundary-cap cells from motor exit points might also invade the DRG (Maro et al., 2004).

surface of the neural tube at the dorsal root entry zones and the prospective motor exit points. This third wave of neurogenesis starts after E12 and in contrast to what was initially thought, it originates not only TrkA$^+$ nociceptors (Maro et al., 2004) but also TrkB$^+$ and TrkC$^+$ neurons (Gresset et al., 2015). Of note, DRG neurons are specified long before they innervate their peripheral or central targets, which may not occur simultaneously (Jackman and Fitzgerald, 2000).

DRG neurons are supported by two types of glial cells: the satellite glial cells (SGCs) and the Schwann cells. These glial cells arise around E11 in mouse lumbar DRGs (Britsch et al., 2001; Kurtz et al., 1994) and similarly to DRG neurons, they are specified from neural crest cells (Jacob et al., 2014) and from boundary-cap cells (Maro et al., 2004). SGCs are only present in DRGs and interact with the cell bodies and initial part of the stem axon of DRG neurons. In contrast, Schwann cells envelop the distal part of the stem axon and both peripheral and central axons. Myelinating Schwann cells form a myelin sheath around a single axon, while non-myelinating Schwann cells ensheath multiple axons in a Remak bundle. Of note, outside the DRG, virtually all Schwann cells from the dorsal and ventral roots, and many Schwann cells from the skin distal peripheral nerves, are derived from boundary-cap cells (Gresset et al., 2015) (Fig. 2). Despite associating with different compartments of DRG neurons, Schwann cells and SGCs have a similar morphology, consisting of a laminar shape, lack of processes and a very extended surface area (Pannese, 1981). Recently, using rat DRGs, SGCs were shown to develop postnatally and express several markers associated specifically with Schwann cell precursors (George et al., 2018). Purified SGCs were further shown to be transcriptionally and morphologically very similar to adult rat Schwann cells, capable of myelinating axons *in vitro*. Given these observations it was hypothesized that SGCs are a population of cells of the Schwann cell lineage that have their differentiation arrested through contact with the DRG neuronal soma (George et al., 2018).

2.2. Pseudo-unipolarization: cell body elongation or fusion of two opposing axons?

During embryonic development, DRG neurons are bipolar and undergo a unique morphological change, termed pseudo-unipolarization, to assume their mature form (Fig. 3A). Pseudo-unipolarization was first mentioned by His (1886) and described in detail by Ramón y Cajal (1904). This phenomenon was examined *ex vivo* using classical silver impregnation methods (His, 1886; Ramón y Cajal, 1890) and later confirmed using scanning electron microscopy (EM) (Matsuda et al., 1996; Matsuda and Uehara, 1984), transmission EM (Tennyson, 1965), retrograde tracing techniques (Barber and Vaughn, 1986), and immunohistochemistry for cytoskeletal markers (Riederer and Barakat-Walter, 1992). Rámon y Cajal (1955) summarized the sequence of events leading to the formation of the two branches in developing DRG neurons as follows (Fig. 3A) (Rámon y Cajal, 1955). In early stages, most DRG neurons are spindle-shaped bipolar. As the cell body bulges more in a direction (eccentric bulged bipolar morphology), the two processes approach each other forming an angle of less than 90 degrees (bell-shaped bipolar conformation). Then the cell body elongates and constricts between the initial segments of the two processes to form the stem axon from which the two axonal processes protrude (Matsuda et al., 2000). Several observations suggest that the stem axon derives from cell body bulging instead of fusion of both branches. First, no sign of close apposition of the central and peripheral axon was ever noted (Matsuda et al., 1996; Takahashi and Ninomiya, 1987), and the primitive stem axons are thicker than the sum of the diameters of the two individual processes (Matsuda et al., 1996). In addition, the proximal part of the stem axon has many ultrastructural features similar to the cell body of DRG neurons. For instance, the proximal portion of the stem axon has a moderate amount of endoplasmic reticulum (ER) in developing neurons (Tennyson, 1965) and membrane folds that

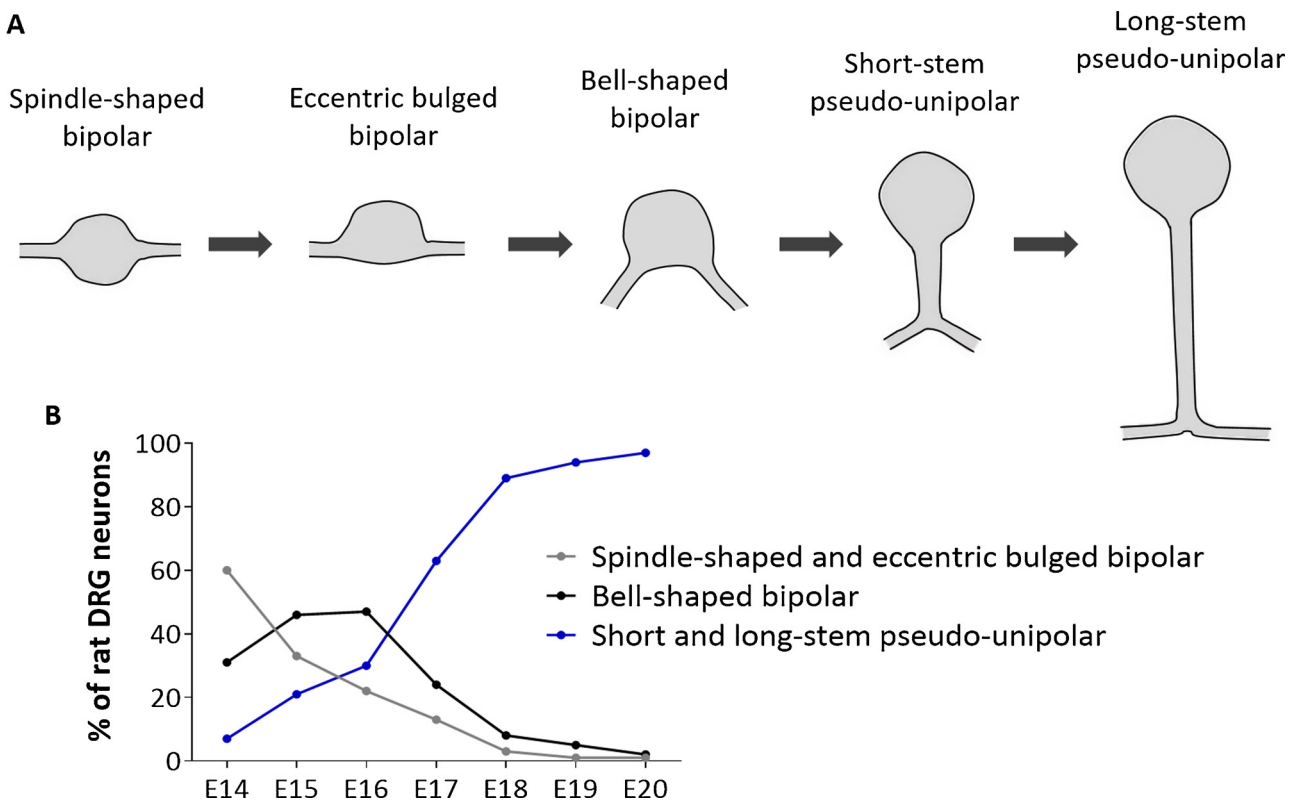

Fig. 3. Morphological stages of DRG neurons during pseudo-unipolarization (A). Schematic drawing adapted from (Ribeiro et al., 2012). (B). Percentage of DRG neurons with spindle-shaped bipolar, eccentric bulged bipolar, bell-shaped bipolar or pseudo-unipolar morphology during embryonic development in thoracic rat DRGs; graph constructed using data from (Matsuda et al., 1996).

interdigitate with SGCs in adult neurons (Zenker and Högl, 1976). Furthermore, in adult (Gumy et al., 2017; Papasozomenos et al., 1985) and embryonic (Riederer and Barakat-Walter, 1992) DRGs, the proximal region of the stem axon is labeled by the somatodendritic marker MAP2. Despite these evidences, in several reports, pseudo-unipolarization is described as deriving from the fusion of two opposing processes (Boubakar et al., 2017; Kiernan and Barr, 2009; Pomp et al., 2005; Singh, 2014), a phenomenon which was never supported by clear observations. To confirm either of the above hypotheses, it would be interesting to take advantage of recent techniques such as live imaging of DRG neurons expressing a fluorescent marker, to enable the clear observation of the sequence of events taking place during pseudo-unipolarization.

The onset of pseudo-unipolarization may vary with the species, but the process is apparently only concluded in late embryonic development and early post-natal stages. In rats, at E14, only 7% of neurons are pseudo-unipolar, while at E19 this percentage abruptly increases to 94% (Matsuda et al., 1996) (Fig. 3B). In mice, at E12, all DRG neurons are bipolar whereas the bell-shaped bipolar and pseudo-unipolar neurons are predominant at E15 (Barber and Vaughn, 1986). On the other hand, in the chick embryo, pseudo-unipolar neurons are detected after E6 and increase in number to 53% at E14 and to 82% at 2 days after hatching (Matsuda et al., 1996). So far it is not clear whether pseudo-unipolarization of DRG neurons is concluded before or after central and peripheral target innervation. It is however possible that pseudo-unipolarization ends after target innervation as mouse undifferentiated bipolar DRG neurons already have the central axons within their central synaptic target fields in the spinal cord (Barber and Vaughn, 1986).

The knowledge on the cellular and molecular mechanisms leading to pseudo-unipolarization may enable us to understand how DRG neuron polarity is established and maintained. However, the factors inducing pseudo-unipolarization have been neglected in the field and remain unknown. Although there are several studies characterizing mutants where DRG neuron specification or projection pattern are impaired (reviewed in Lallemend and Ernfors (2012)), none of these mutants affect specifically the DRG pseudo-unipolar morphology or central-peripheral polarity. *In vitro* studies support that pseudo-unipolarization is not cell-autonomous but instead depends on glial cells (Takahashi and Ninomiya, 1987). Further supporting this observation, DRG neurons from newborn rats are bipolar in purified cultures, but are pseudo-unipolar when co-cultured with Schwann cells (Mudge, 1984). Moreover, DRG neurons from chick embryos have multiple MAP2-positive neurites in the absence of glial cells, but have a single axon when in co-culture with glial cells (De Koninck et al., 1993). One should now clarify the contribution to pseudo-unipolarization of cellular contact and of molecules secreted by glial cells. This could be achieved using *in vitro* co-cultures either providing contact or performed in transwell systems.

3. Dissecting the peculiar structure of DRG neurons

3.1. The cell body: functional implications of its unique features

The cell body of DRG neurons is typically circular to oval and of variable size ranging from 20 to 100 μm in diameter in rats (Lee et al., 1986). The cell bodies of DRG neurons are completely wrapped by sheaths that may have one or several layers of SGCs. Morphologically, these glial cells are characterized by a laminar and irregular shape, often with lamellar expansions and microvilli that increase their surface area. The perineural sheaths are generally continuous and have the outer surface covered by basal lamina. Importantly, each neuron and its surrounding SGC sheath constitute a morphological unit that is separated from other units by connective tissue (Fig. 4A). Occasionally, there are two or three neuron cell bodies, in direct mutual contact or separated from each other by a single SGC sheath, sharing a common connective envelope (Pannese, 2010). Similarly, perineural SGC sheaths

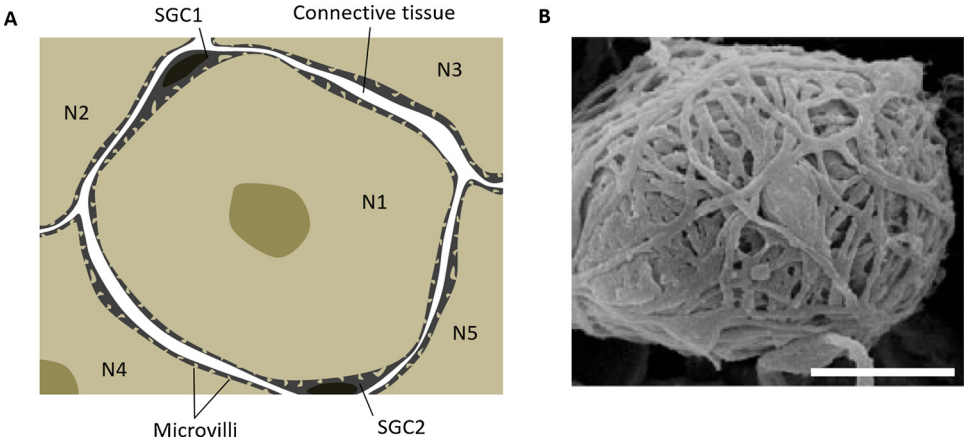

Fig. 4. Peculiar features of the cell body of DRG neurons. (A) Schematic drawing of a DRG neuron cell body (N1) enveloped by a sheath of satellite glial cells (SGC1 and SGC2, black). Each neuron and its surrounding SGC sheath constitute a morphological unit that is separated from the sheaths encircling the adjacent DRG neuron cell bodies (N2–N5) by connective tissue. Microvilli are observed on the surface of DRG neuron cell bodies. (B) Scanning electron micrograph showing an intricate meshwork of sympathetic fibers forming a terminal Dogiel's nest around the cell body of a rat DRG neuron. Image from (Matsuda et al., 2005). Scale bar, 10 µm.

are also found around parasympathetic and sympathetic neurons (Hanani, 2010). In contrast, structural neuron-glia units similar to these do not exist in the CNS.

Vertebrate DRG neurons have many fine processes (microvilli) arising from the cell body (Fig. 4A). These projections increase the cell body surface considerably and, in rabbits, they are more abundant in areas of contact with SGCs. Therefore they may allow an extensive molecular exchange between neurons and SGCs (Pannese et al., 1999). In fact, in the last few years several studies have demonstrated that there is bidirectional communication between the soma of DRG neurons and the surrounding SGCs that affects the afferent input into the spinal cord. This is the case during electrical stimulation of DRG neurons that elicits vesicular ATP release from their soma, and activation of receptors in SGCs (Zhang et al., 2007). Importantly, changes in this SGC-DRG neuron communication under pathological conditions often lead to chronic pain (reviewed in Huang et al. (2013)). Examples of neuromodulators and neurotransmitters implicated in this reciprocal communication are ATP, as referred to above, tumor necrosis factor-α (Zhang et al., 2007) and glutamate (Kung et al., 2013). Nonetheless, it is unknown if receptors in the DRG neuron soma are located preferentially on microvilli or are also present on the surface between these projections.

An additional interesting feature of the DRG neuron soma is the classically denominated terminal Dogiel's nest (Fig. 4B) which was first described in the late nineteenth century (Garcia-Poblete et al., 2003). Terminal Dogiel's nests are endings of sympathetic axons that present the shape of a nest or of a plexus enveloping individual DRG neurons. The axons comprising these nests are positive for tyrosine hydroxylase, which is a commonly used marker for sympathetic fibers that also labels a subset of small DRG neurons (Brumovsky et al., 2006). Sprouting can occur from sympathetic fibers coming from the spinal nerve that innervate the DRG blood vessels, or as newly ingrowing collateral axons from the grey and dorsal rami of the spinal nerve (Chung and Chung, 2001; Xie et al., 2010) (Fig. 1). The functional consequences of this sympathetic sprouting have been controversial as studies using animal models have yielded contradictory results (Garcia-Poblete et al., 2003). Many reports support that sympathetic sprouting in the DRG is an important underlying mechanism for neuropathic pain, for instance after peripheral nerve injury (McLachlan et al., 1993) or in the chronically compressed DRG (Chien et al., 2005). According to this view, sympathetic fibers only form nests around DRG neurons in conditions of neuropathic pain (Cheng et al., 2015; Xie et al., 2011). Interestingly, after spinal nerve injury, DRG neurons surrounded by sympathetic axons are more likely to be spontaneously active, which is a hallmark of neuropathic pain (Xie et al., 2011). Sympathetic fibers seem to enhance excitability and drive spontaneous activity in sensory neurons *via* the release of sympathetic neurotransmitters (Xie et al., 2010). Conversely, there is some evidence suggesting that spontaneously active DRG neurons attract sympathetic fibers, which may happen *via* the release of neurotrophic factors by these neurons or by their surrounding SGCs (reviewed in Zhang and Strong (2008)). So far there is no evidence showing classical synaptic contacts between the DRG neuron cell body and sympathetic fibers in conditions of neuropathic pain. Nevertheless, while in healthy adult DRGs there are no detectable synapses at all (Zenker and Högl, 1976), in a model of neuropathic pain, tyrosine hydroxylase-positive synapse-like structures were observed by EM near DRG neuron cell bodies (Chung et al., 1997). In a recent study, spinal nerve injury elicited sprouting of axons from nociceptors and tyrosine hydroxylase-positive neurons (Cheng et al., 2015). These sprouted axons established synapse-like structures with each other that were positive for the synaptic proteins PSD95 and synaptophysin. These putative synapses were simultaneously located around large DRG neurons and near activated SGCs, which release excess levels of NGF. By using intrathecal injection of NGF antibodies to injured rats and injection of exogenous NGF to naïve rats, it was demonstrated that elevated levels of NGF are both required and sufficient for the formation of this intra-DRG neurite sprouting and formation of synapse-like structures (Cheng et al., 2015). These observations suggest that not only sympathetic neuron axons form Dogiel's nests, but also axons from nociceptors are capable of making these peculiar structures around DRG neuron cell bodies.

In contrast to the above line of thought, some studies show that sympathetic-sensory coupling is not a key factor in the development of neuropathic pain, as sympathetic sprouting does not often correlate with the presence or degree of this pathology (reviewed in Garcia-Poblete et al. (2003)). In fact, some studies show that sympathetic axons also form nests around DRG neurons in healthy animals. The number of nests increases with increasing phylogenetic complexity (Matsuda et al., 2005) and in rats their number increases with age (Ramer and Bisby, 1998). To date, the functional meaning of sympathetic sprouting in physiological conditions remains obscure.

3.2. *The stem axon: a proximal and a distal compartment?*

The stem axon is the portion of the DRG neuron axon that goes from the cell body to the bifurcation into the central and peripheral axonal branches. Although most DRG neurons are unmyelinated (Tandrup, 1995), so far the characterization of the stem axon of unmyelinated DRG neurons has been neglected when compared to that of myelinated ones. As so, most of the information provided here concerns the stem axon of myelinated DRG neurons.

The stem axon can be impressively long, ranging from 100 to 600 µm in length in cats (Hoheisel and Mense, 1986) and its diameter is considerably large going up to 4.2 µm in adult rats (Zenker and Högl, 1976) and 15 µm in adult cats (Spencer et al., 1973). The proximal region of the stem axon is always unmyelinated and ensheathed by a

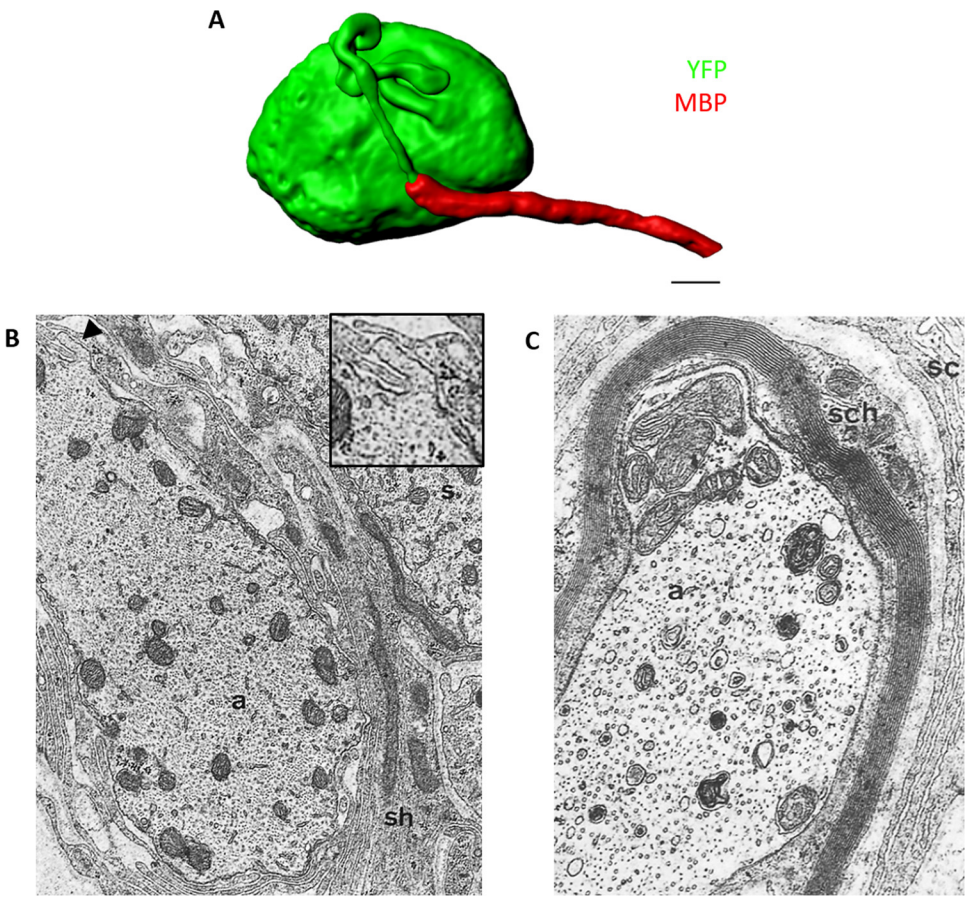

Fig. 5. The morphology and ultrastructure of the stem axon. (A) Segmented confocal z-stack of a myelinated YFP$^+$ DRG neuron (green) from adult Thy1-YFP-16 mice immunostained for myelin basic protein (MBP, red) to label myelin. Intensity-based segmentation was performed using the Bitplane Imaris software (v8.1.2). Scale bar, 10 µm. (B,C) Transmission electron micrograph showing the ultrastructure of the stem axon (a) of a rat DRG neuron. In the unmyelinated region (B), the stem axon is surrounded by a multilayered sheath of satellite glial cells *(sh)* and its membrane has folds (arrowhead, showed with higher magnification in the inset). The soma (*s*) of the respective DRG neuron can be seen. In contrast, in the distal myelinated part of the stem axon (C), the membrane is smooth and surrounded by a myelin sheath and Schwann cells (*sch*) that are surrounded by cytoplasmic leaflets of satellite cells (*sc*) (Zenker and Högl, 1976).

multilayered coat of SGCs that is continuous with that enveloping the cell body. In contrast, the distal part of the stem axon is ensheathed by Schwann cells and can be myelinated (Spencer et al., 1973; Zenker and Högl, 1976). Interestingly, the first internodes of the stem axon are, in proportion to the axon diameter, unusually short and thinly myelinated (Spencer et al., 1973; Zenker and Högl, 1976).

Studies using scanning EM showed that in some higher vertebrates (in rats and rabbits, but not in adult frogs or chicks) the proximal portion of the stem axon that is ensheathed by SGCs may form a structure known as the glomerulus of Cajal (Matsumoto and Rosenbluth, 1985). This glomerulus consists of the stem axon making a tortuous coiled path (Fig. 5A) and eventually spiraling around the SGCs sheath (Matsuda et al., 2005; Matsuda and Uehara, 1981). The glomerulus of Cajal is not present in all DRG neurons and larger diameter neurons are more likely to have this structure (Matsuda and Uehara, 1981). This glomerulus may allow the DRG neuron to accommodate a longer stem axon. As suggested by Devor (1999), the length of the stem axon may overcome the shunting effect that occurs during spike propagation from the peripheral to the central axon, when the signal passes through the bifurcation. In DRG neurons with a large cell body, spike conduction from the peripheral to the central axon may be compromised due to a high membrane capacitance and low membrane resistance of the soma. To compensate for this effect, a longer and thinner stem axon may be needed, as it will generate a higher internal resistance to the dissipation of the spike into it, thus increasing the current available for forward spike propagation to the central axon. Therefore, a long stem axon may allow to electronically isolate large cell bodies, and reduce the risk of spike propagation failure. Such electrical compensation may explain the preferential presence of glomerulus of Cajal in large diameter DRG neurons.

The characterization of the stem axon by EM shows that it is not uniform along its length, since its unmyelinated and myelinated parts have different ultrastructural features. In the proximal unmyelinated region, the stem axon has many membrane folds that interdigitate with folds of adjacent SGCs (Fig. 5B), whereas the distal region of the stem axon, ensheathed by Schwann cells, is smooth (Fig. 5C) (Zenker and Högl, 1976). Regarding organelle content, the stem axon contains striking larger numbers of mitochondria (Spencer et al., 1973; Zenker and Högl, 1976) and ribosomes (Spencer et al., 1973; Zelená, 1972; Zenker and Högl, 1976), and a higher density of microtubules and ER (Zenker and Högl, 1976) in its proximal unmyelinated region than in the distal myelinated portion (Zenker and Högl, 1976). Also, in the unmyelinated part of the stem axon, microtubules are closely packed in fascicles and connected with lateral cross bridges (Bird and Lieberman, 1976; Nakazawa and Ishikawa, 1995; Zenker and Högl, 1976). This ultrastructural feature is consistent with the enrichment of Trim46 in this region (Gumy et al., 2017), as this microtubule-associated protein induces the formation of microtubule fascicles (van Beuningen et al., 2015). Overall, these observations raise the question of whether the stem axon may comprise two different and possibly compartmentalized regions. Supporting this notion, recently, in cultured DRG neurons, MAP2 was shown to define a cargo-filtering region in the proximal axon by coordinating the activities of molecular motors (Gumy et al., 2017). Enrichment of MAP2 was also shown in the proximal stem axon and in the peripheral branch of DRG neurons *in vivo* (Papasozomenos et al., 1985). Such a cargo-filtering zone within the stem axon may underlie the ultrastructural differences between its proximal and distal regions. Another possibility is that myelination in the distal part of the stem axon may induce ultrastructural alterations. In fact, it was proposed that myelinating Schwann cells down-regulate the microtubule content of the axoplasm (Bustos et al., 1991). For this reason, it would be interesting to analyze the ultrastructure of completely unmyelinated stem axons to determine if these also present proximal-distal differences.

At the bifurcation, neurofilaments and microtubules divide into two

Table 1
Structural differences between peripheral (P) and central (C) DRG neuron axons in adult animals. All data was collected using EM; central and peripheral DRG neuron axons were analyzed at the level of the dorsal root and near the DRG respectively, unless indicated otherwise. Particular procedures performed to eliminate motor or sympathetic axons from the peripheral nerve are mentioned.

Structural Feature	Species	Unmyelinated axons	Myelinated axons	Reference and specific technical details (if any)
Axonal diameter	cat	P ≈ 1.3-fold C	P ≈ 2.2-fold C	(Lee et al., 1986) analysis inside the DRG using intracellular labeling
		P ≈ 1.7-fold C	P ≈ C	(Fadic et al., 1985)
		P ≈ 1.6-fold C	P ≈ C	(Fadic et al., 1985) peripheral axons at the level of the sural nerve
		–	P ≈ C	(Ochs et al., 1978) with and without ventral rhizotomy
	rat	P ≈ 2.0-fold C	P ≈ 1.4-fold C	(Suh et al., 1984) with ventral rhizotomy and sympathectomy
	monkey	–	P ≈ C	(Ochs et al., 1978) with ventral rhizotomy
Microtubule density	cat	P ≈ 3-fold C	P ≈ 2-fold C	(Fadic et al., 1985)
		P ≈ 3-fold C	P ≈ 1.8-fold C	(Fadic et al., 1985) peripheral axons at the level of the sural nerve
		P ≈ 3-fold C	P ≈ C	(Ochs et al., 1978) with ventral rhizotomy
	lizard	P ≈ 2-fold C	P ≈ 3-fold C	(Pannese et al., 1984)
	rat	–	P ≈ 1.4-fold C	(Zenker et al., 1975)
	monkey	–	P ≈ C	(Ochs et al., 1978) with ventral rhizotomy
	frog	–	P ≈ 9-fold C	(Smith, 1973)
Neurofilament Density	cat	P ≈ 0.4-fold C	P ≈ C	(Ochs et al., 1978) with ventral rhizotomy
	frog	–	P ≈ C	(Smith, 1973)

streams, one going to the peripheral process and the other to the central one (Hongchien, 1970). The possible functional consequences of these features, illustrated in a single report, are discussed in detail in Section 4.2. In addition, the bifurcation has fasciculated microtubules (Nakazawa and Ishikawa, 1995), and a triangular area which is occupied by clusters of mitochondria (Hongchien, 1970). In myelinated fibers, the bifurcation is constricted and has a node of Ranvier, while unmyelinated fibers show a triangular expansion at this region (Hongchien, 1970). Of note, in addition to the bifurcation of the stem axon, the DRG central axon undergoes a second bifurcation once it enters the spinal cord in the dorsal root entry zone. Although signaling events that regulate this central bifurcation have been disclosed (Schmidt and Rathjen, 2010; Schmidt et al., 2018), whether an asymmetric axonal transport or cytoskeleton organization occur in the two central branches is not known.

3.3. The peripheral and central DRG neuron axons: structural differences

In the following paragraphs, we will discuss the structural differences between the central and peripheral DRG neuron axons. The main differences are summarized in Table 1.

3.3.1. Asymmetries in diameter and cytoskeleton organization in the central and peripheral axon of DRG neurons

The axonal diameter of the two DRG neuron axons has been extensively studied by intracellular labeling with horseradish peroxidase (Hoheisel and Mense, 1986; Lee et al., 1986) and by EM analysis of cross-sections of the dorsal root, and of spinal and peripheral nerves (Fadic et al., 1985; Ochs et al., 1978; Suh et al., 1984). In unmyelinated DRG neurons, central axons have a smaller diameter than the peripheral ones (Hoheisel and Mense, 1986; Lee et al., 1986; Suh et al., 1984). However, in myelinated DRG neurons, there is not a consensus as to whether such a difference exists (Lee et al., 1986; Suh et al., 1984). In cats, by EM analysis, central and peripheral myelinated axons were shown to have similar diameters (Fadic et al., 1985; Ochs et al., 1978), whereas by intracellular labeling, myelinated central axons were shown to have a smaller diameter (Lee et al., 1986), similarly to myelinated rat axons assessed by EM (Suh et al., 1984). An increased diameter on both myelinated and unmyelinated peripheral axons is consistent with their higher nerve conduction velocity (Waddell et al., 1989). The mechanisms underlying the central-peripheral differences in DRG axon diameter are still obscure.

In both DRG neuron axons, the density of microtubules decreases as axon diameter increases (Fadic et al., 1985; Ochs et al., 1978; Pannese et al., 1984), as is generally the case in the nervous system (Peters et al., 1991). Some microtubules are arranged in fascicles at nodes of Ranvier and the density of fasciculated microtubules is higher in nodes proximal to the cell body (Nakazawa and Ishikawa, 1995). Differences in microtubule density have been observed between peripheral and central DRG neuron axons. In several species, microtubule density is significantly higher in peripheral DRG neuron axons than in central ones of a similar diameter, both in myelinated (Fadic et al., 1985; Pannese et al., 1984; Smith, 1973; Zenker et al., 1975) and unmyelinated (Fadic et al., 1985; Pannese et al., 1984) fibers. However, there are contradicting results showing that in cats and monkeys microtubule density in myelinated axons is the same in central and peripheral axons of similar diameter (Ochs et al., 1978).

Concerning neurofilaments, both DRG neuron axons possess axially oriented neurofilaments that increase in number as a function of axon diameter (Ochs et al., 1978; Smith, 1973), as expected. In unmyelinated axons, a single study shows that the peripheral branch has a smaller density of neurofilaments than the central branch (Ochs et al., 1978). In contrast, in myelinated axons, no differences were observed in neurofilament density between both axons (Ochs et al., 1978; Smith, 1973). The degree of phosphorylation of neurofilaments is higher in central than in peripheral DRG neuron axons and inversely correlates with the transport of neurofilaments (Watson et al., 1989). This asymmetry may contribute to central-peripheral differences in axon diameter, as the phosphorylation status of neurofilaments may control axon caliber by regulating neurofilament transport and content (Hoffman et al., 1984; Shea and Lee, 2011).

In relation to the actin cytoskeleton, little is known on a putative differential arrangement in the two DRG neuron axons. This is a subject to be explored in the future.

3.3.2. Smooth endoplasmic reticulum, ribosomes and local protein translation asymmetry in DRG neuron axons

Smooth ER-like structures have been observed by EM analysis in the central (Berthold et al., 1993; Smith, 1973) and peripheral (Pannese and Ledda, 1991; Smith, 1973) DRG neuron axons, including peripheral nerves (Tsukita and Ishikawa, 1976). In the myelinated fibers of peripheral nerves, the smooth ER forms a continuous tridimensional network which was suggested to extend from the cell body to the axon terminals (Tsukita and Ishikawa, 1976), with most ER tubules running parallel to the axon (Berthold et al., 1993; Tsukita and Ishikawa, 1976). During the bell-shaped bipolar stage of rabbit neuroblasts, one process contains a small amount of ER resembling an axon, while the other contains a considerable amount of granular ER, typical of dendrites (Tennyson, 1965). However, in this study, the process that originates the central and peripheral DRG neuron axon was not determined. In

adult amphibians, myelinated DRG neurons seem to possess slightly more ER in central axons (Smith, 1973). A possible difference in smooth ER content in central and peripheral DRG neuron axons should be revisited as it may result in the differential synthesis of lipids, including cholesterol and phospholipids used to produce new cellular membrane. Such a disparity could be relevant, among others, to the different cell autonomous ability of the two DRG neuron axons to grow and regenerate, as discussed in Section 4.3.1.

Axons possess mechanisms for local protein translation that are beginning to be unraveled (reviewed in Jung et al. (2012)). The traditional view is that the ability of PNS axons to locally synthesize proteins is much higher than that of CNS axons (Twiss and Fainzilber, 2009), which may be related to their different ribosome content. Ribosomes have been observed in DRG neuron axons (Koenig et al., 2000; Pannese and Ledda, 1991; Zelená, 1972), where they are organized into plaque-like structures near the axolemma (Koenig et al., 2000; Pannese and Ledda, 1991; Zelená, 1972) and only occasionally in close attachment to the ER (Pannese and Ledda, 1991). A systematic analysis of serial sections of myelinated axons of rabbit DRG neurons showed that ribosomes are only exceptionally located in central dorsal root axons, but are abundant in a few peripheral processes (Pannese and Ledda, 1991). Similarly, only a few mouse sciatic nerve axons have ribosomes (Court et al., 2008). Of interest, ribosomes were shown to be transferred from adjacent Schwann cells to peripheral axons in the mouse sciatic nerve after peripheral nerve injury (Court et al., 2008; Muller et al., 2018). In this case, an asymmetric transference of ribosomes from adjacent glial cells may contribute to differences in ribosome content between the two DRG neuron axons under pathological conditions.

4. Factors underlying functional central-peripheral polarity in DRG neurons

The central and peripheral DRG neuron axons present different functional characteristics. An intriguing question is how two axons linked to the same cell body can display such different properties. In fact, the structural and molecular differences that may underlie this central-peripheral asymmetry have been largely neglected, as discussed below.

4.1. Peculiarities in axon conduction velocity

DRG neurons have an important central-peripheral polarity regarding electrophysiological properties. Although both axons conduct action potentials, the peripheral process functions as dendrite-like, since the action potential is generated at its peripheral terminal and then propagates towards the bifurcation of the stem process; in contrast the central process is axon-like, since it conducts the signal from the bifurcation to the CNS (Du et al., 2014). In addition, in cats and rats, signal conduction velocity is higher in the peripheral process than in the central process, both in unmyelinated (Lee et al., 1986; Waddell et al., 1989) and myelinated sensory neurons (Loeb, 1976; Waddell et al., 1989). As discussed in Section 3.3.1, these data are consistent with the peripheral axons being larger than central ones, since conduction velocity positively correlates with axon diameter (Lee et al., 1986).

4.2. Axonal transport in central and peripheral DRG neuron axons: differences in velocity, amount of protein transported and sorting

Early pulse-chase radiolabeling studies have established that axonal transport occurs *via* fast and slow components. Fast transport carries vesicles and organelles that move rapidly at average speeds of ~50–400 mm/d. In contrast, the slow component of axonal transport moves at an average speed of ~0.2–10 mm/day and can be further categorized into slow component a and b. Whereas slow component a moves the slowest and includes cytoskeletal proteins such as tubulin and neurofilament, slow component b is highly heterogeneous as it includes cytosolic/soluble molecules such as synaptic proteins, metabolic enzymes, chaperones, motors, actin and cytoskeleton-associated proteins (spectrin, tau, cofilin) (reviewed in Roy (2018)). Although slow axonal transport conveys proteins that are critical for neuronal function, it has remained much more enigmatic than fast axonal transport. So far, a handful of examples of slow axonal transport have been studied that have elucidated some of its mechanisms. It is known that neurofilaments are transported by dynein and kinesin with velocities similar to vesicles, but as they often pause, this results in an overall slow movement of the entire population (Uchida et al., 2009; Wang and Brown, 2001). Recently, a new model for the slow axonal transport of cytosolic cargos was proposed, based on short-lived direct interactions with kinesin-1 (Twelvetrees et al., 2016). In contrast, synapsin appears to form complexes which bind to fast moving vesicles instead of binding directly to motors and move intermittently along axonal microtubules (Tang et al., 2013). Overall, a substantial amount of evidence suggests that slow axonal transport shares its mechanism with fast axonal transport, which is dependent on microtubule-based motors (Tang et al., 2013; Terada et al., 2000; Wang and Brown, 2002).

Axonal transport in the central and peripheral DRG neuron branches was compared in early studies using injection of radioactive aminoacids in the DRG. Various reports show that, in several species, the velocity of fast axonal transport in the central and peripheral branches of sensory neurons is the same, between 350 and 450 mm/day depending on the species (Anderson and McClure, 1973; Komiya and Kurokawa, 1978; Ochs, 1972). In contrast, the average velocity of slow axonal transport is much higher in peripheral DRG neuron axons than in central ones (Komiya and Kurokawa, 1978; Mori et al., 1979; Wujek and Lasek, 1983). In the case of fast axonal transport, despite similar velocities, less radioactive protein is found in the central branch when compared to the peripheral one, suggesting that the amount of protein transported to the peripheral axon is higher (Anderson and McClure, 1973; Komiya and Kurokawa, 1978; Lasek, 1968; Ochs, 1972). In the case of the slow component of axonal transport, it is not consensual whether the amount of protein transported to the peripheral axon is higher than that transported to the central branch (Komiya and Kurokawa, 1978; Mori et al., 1979). One should note that differences in the net amount of protein transport may be correlated with variations in the total volume of axoplasm present in the central and in the peripheral DRG neuron branch. The different features of axonal transport in central and peripheral DRG neuron axons are summarized in Table 2.

Given that axonal transport relies on microtubule-based motors, microtubule organization in DRG neuron axons is likely a key determinant in transport dynamics. Recently, Wortman et al. (2014) suggested that closely spaced parallel microtubules may enable a cargo to simultaneously engage motors on more than one microtubule, thus dramatically enhancing motor activity and increasing the velocity of transport (Wortman et al., 2014). In addition, cargo pause at polymer ends, and cargo run length, are related to the average microtubule length whereas cargo pause time is inversely correlated with the abundance of microtubules (Yogev et al., 2016). Overall, these recent studies show that the density and length of microtubules is extremely important for axonal transport dynamics. The possible contribution of the microtubule cytoskeleton to DRG neuron asymmetry in axonal transport remains unexplored. In view of the above recent data (Wortman et al., 2014; Yogev et al., 2016), the increased density of microtubules in the peripheral branch of DRG neurons (as discussed in Section 3.3.1.) could support an increased transport velocity. It would also be interesting to compare microtubule length in both axons of DRG neurons. In summary, a better knowledge on microtubule organization in both branches may shed light on the mechanisms leading to the asymmetry in velocity and amount of protein transported along both DRG neuron axons.

Taking into account their different functions, each of the DRG neuron branches should have specific requirements regarding protein

Table 2
Comparison of axonal transport in central (C) and peripheral (P) DRG neuron axons (dorsal root or sciatic nerve respectively, unless indicated otherwise). All experiments were made by injection of a radioactive aminoacid in DRGs and subsequent collection of the DRG, sciatic nerve and its branches, dorsal root and in some cases spinal cord.

Type of Axonal Transport	Species	Velocity	Relative amount of protein transported	Component and specific technical details (if any)
Slow	rat	P (1.0 mm/day) > C (0.5 mm/day)	P ≈ C	(Komiya and Kurokawa, 1978)
		P (3.5 mm/day) > C (2.0 mm/day)		(Wujek and Lasek, 1983) SCa
		P (1.0 mm/day) > C (0.4 mm/day)		(Wujek and Lasek, 1983) SCb
		P (2–3 mm/day) > C (1–2 mm/day)	P ≈ 1.9 -fold C	(Mori et al., 1979) neurofilament triplet proteins, identified by electrophoresis
		P (9–13 mm/day) > C (3–4 mm/day)	P ≈ 3-fold C	(Mori et al., 1979) tubulins, identified by electrophoresis
		P (19 mm/day) > C (4 mm/day)	P ≥ 2-fold C	(Mori et al., 1979) actin, identified by electrophoresis
Fast	rat	P ≈ C (350 mm/day)	P ≈ 3-fold C	(Komiya and Kurokawa, 1978)
	cat	P (38 mm/day) ≈ C (376 mm/day)	P ≈ 1.8-fold C	(Anderson and McClure, 1973) central axon analyzed in the dorsal column
		P (409 mm/day) ≈ C (391 mm/day)	–	(Ochs, 1972) central axon analyzed in the dorsal column
		–	P > C	(Lasek, 1968)
	monkey	P (420 mm/day) ≈ C (428 mm/day)	P ≈ 3-5-fold C	(Ochs, 1972)
		P (416 mm/day) ≈ C (397 mm/day)	–	(Ochs, 1972) central axon analyzed in the dorsal column

content. Early radiolabeling data mostly suggested that similar proteins are transported to both axons, not only in naïve conditions but also after peripheral or central DRG neuron axon lesion (Bisby, 1981; Perry et al., 1983; Perry and Wilson, 1981; Stone and Wilson, 1979). Different patterns of radioactivity of transported proteins were however observed in the two DRG neuron branches in one study (Anderson and McClure, 1973). The lack of sensitivity of these initial studies certainly precluded the identification of a high number of proteins. Hence, the possibility that DRG neurons possess the ability to differentially sort proteins to their two axons is still open. Supporting this hypothesis, an isoform of collapsin response mediator protein-2 was identified in the peripheral DRG neuron axon but not in the central one using 2-dimension electrophoresis followed by MALDI-TOF mass spectrometry (Katano et al., 2006). An asymmetrical distribution of MAP2 was also observed using immunohistochemistry, with peripheral DRG neuron axons showing a more intense staining (Papasozomenos et al., 1985). Additionally, an isoform of the mammalian brain sodium channel (BNaC1α) was found to be transported exclusively to the peripheral DRG neuron axon and localized at specialized mechanosensory terminal endings (García-Añoveros et al., 2001). Also, upon inflammation, selective transport to the peripheral axonal branch was shown for TRPV1, a receptor expressed in nociceptors that acts as a transducer of peripheral noxious heat stimuli (Ji et al., 2002). Despite of the above scattered reports in the literature, a bone-fide marker of the peripheral or central DRG neuron axon remains to be identified. Additionally, although cargo filtering in the DRG neuron stem axon has been recently described (Gumy et al., 2017), there is no available data showing cargo filtering in the two DRG neuron axonal branches. State-of-the-art proteomic data showing asymmetric protein distribution and supporting differential transport in DRG neuron axons is lacking and should be the subject of further research.

The question of how proteins and organelles might be selectively transported from the cell body to one of the DRG axons is of considerable interest. As referred to above in Section 3.2., at the stem axon bifurcation, there are two separate sets of microtubule networks that go down into each of the two DRG neuron axons (Hongchien, 1970). As such, one should consider that once cargoes enter into one of the microtubule networks (either directed to the peripheral or to the central DRG neuron axon) it would be challenging to redirect them to the other branch. It would be interesting to analyse whether the microtubules entering into each DRG neuron axon have a different organization and/or post-translational modifications as these could account, at least partially, for selective cargo transport.

4.3. Why does the peripheral DRG neuron axon regenerate more robustly?

One of the most striking differences between the two DRG neuron axons is their ability to regenerate. Peripheral branches, which are located entirely in the PNS, are capable of effectively growing long distances after injury and reinnervate their peripheral targets (Lisney, 1987) (Fig. 6A). In contrast, DRG central axons injured in the dorsal root present a lower rate of regeneration (Komiya, 1981; Wujek and Lasek, 1983) and are not capable of regrowing across the dorsal root entry zone (transitional zone between the CNS and PNS) (Di Maio et al., 2011) (Fig. 6B). If the injury is performed in the dorsal column tract of the spinal cord, DRG neuron central axons are not capable of regenerating beyond the lesion site (Neumann and Woolf, 1999) (Fig. 6B). The possible reasons underlying these striking differences in regenerative potential are discussed below.

4.3.1. Cell extrinsic versus intrinsic factors

Environmental factors may at least partially account for the differences in regeneration between both DRG neuron axons. The environment created by Schwann cells in the PNS contributes to its successful regeneration, while in the injured CNS there is the accumulation of inhibitory molecules that prevent axonal regrowth (reviewed in Gaudet et al. (2011)). In fact, when peripheral nerve grafts are provided to injured central DRG neuron axons, their regrowth capacity is enhanced, supporting an important role of cell extrinsic factors in the regeneration outcome (Zelená and Jirmanova, 1988). Nevertheless, central DRG neuron axons within the PNS dorsal root (i.e, in the presence of Schwann cells) fail to regenerate with the same rate as peripheral DRG neuron axons (Komiya, 1981; Wujek and Lasek, 1983), supporting the existence of intrinsic differences between both branches. In contrast, motor neuron axons regenerate at similar rates in the ventral root and in the peripheral nerve (Wujek and Lasek, 1983). Of note, Schwann cells express motor and sensory phenotypes (Höke et al., 2006; Jesuraj et al., 2012) and growth factor expression by denervated Schwann cells varies between dorsal roots, ventral roots and peripheral nerves (Brushart et al., 2013). Thus, variations in the support by Schwann cells with different phenotypes may account, to some extent, for the regeneration dissimilarity between the central and peripheral DRG neuron axons.

Injury to the peripheral DRG neuron axon triggers important changes in gene expression that lead to increased intrinsic regenerative ability. In contrast, when a dorsal root or a dorsal column tract spinal cord injury occurs, DRG neurons are not able to establish a robust regenerative program (Mar et al., 2016; Schreyer and Skene, 1993). In particular, regeneration-associated genes, such as GAP-43 (Chong et al., 1994; Schreyer and Skene, 1993) and CAP-23 (Mason et al., 2002), and transcription factors such as ATF-3 (Seijffers et al., 2006) and Smad1 (Zou et al., 2009) are upregulated after peripheral axon injury comparing to central axon injury. Accordingly, *in vitro*, DRG neurons cultured some days after a peripheral nerve injury show a higher growth

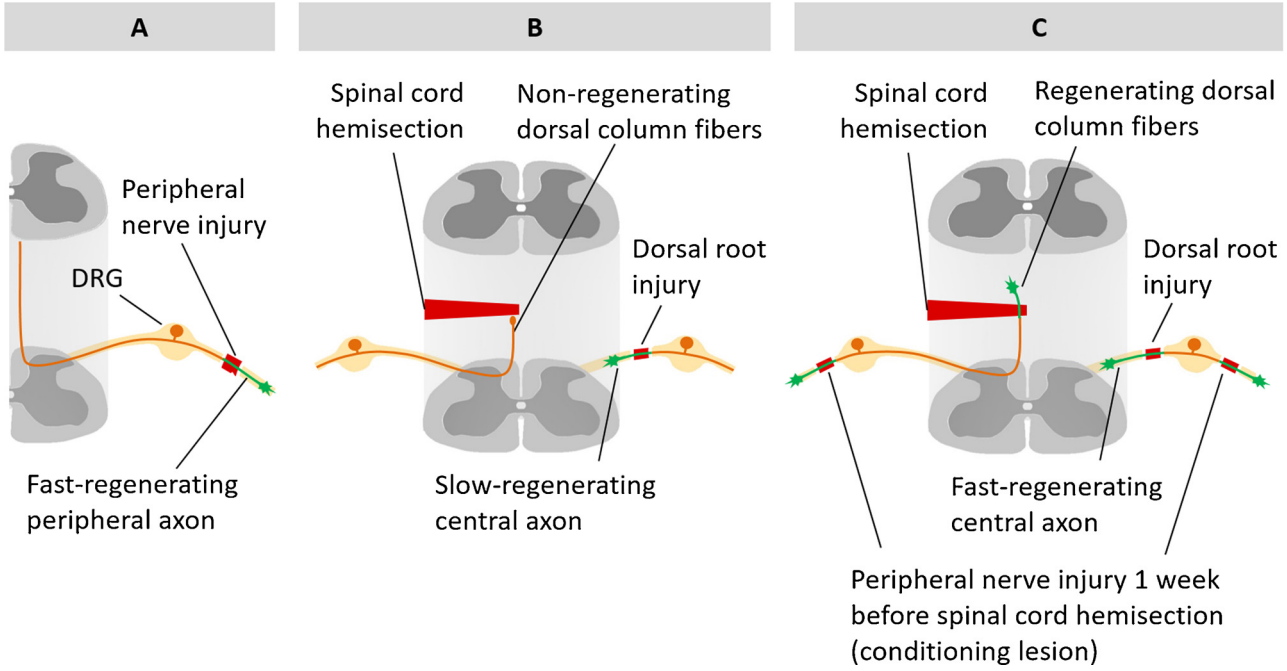

Fig. 6. Differences in regenerative ability between the central and peripheral DRG neuron axons. (A) The peripheral DRG neuron axon (orange) is capable of growing long distances beyond the lesion site (green), possibly reinnervating its targets. (B) After injury to the dorsal column tract (left), central DRG neuron axons (orange) are not capable of regenerating beyond the lesion site. In contrast, if the dorsal root is injured (right) the central axons can slowly grow beyond the lesion site (green) but they are not capable of regenerating across the dorsal root entry zone. (C) Schematic drawing of the conditioning lesion effect. If an injury to peripheral DRG neuron axons is performed some days before the central lesion (conditioning lesion), the regeneration ability of the central axons increases (green axon): dorsal column tract fibers are able to regenerate beyond the lesion site and dorsal root axons grow faster.

competence than after a dorsal root (Smith and Skene, 1997) or a dorsal column tract spinal cord injury (Seijffers et al., 2006). Interestingly, injury to the peripheral DRG neuron axon increases regeneration of central DRG neuron axons, when the central injury is done some days later in the dorsal root (Richardson and Verge, 1987) or in the spinal cord (Neumann and Woolf, 1999) (Fig. 6C). This phenomenon is known as conditioning lesion effect (Hoffman, 2010). Furthermore, the alterations produced by a peripheral conditioning injury occur even when this injury is performed after a central DRG neuron axon injury (Ylera et al., 2009).

Crucial intrinsic differences have been identified between CNS and PNS axons, contributing to their different regenerative capacities, such as their ability to transport integrins into axons (Eva et al., 2012, 2017). However, a key question that remains to be fully understood is why the intrinsic regenerative capacity of DRG neurons increases after injury to the peripheral axon but not after central axon injury? One of the most obvious cues is that a peripheral lesion deprives neurons of sensory-evoked activity, while a central injury does not. In fact, DRG neurons remain electrically active after a central dorsal column tract injury but not after a peripheral lesion, which influences the ability of these neurons to regenerate (Enes et al., 2010). On a different note, a peripheral DRG neuron axon lesion triggers the activation of "positive" injury signals that are retrogradely transported from the lesion site to the cell body. Some important examples of positive injury signals are the extracellular-signal-regulated kinase (ERK) (Perlson et al., 2005), c-Jun N-terminal kinase (JNK) (Cavalli et al., 2005), signal transducer and activator of transcription 3 (STAT-3) (Ben-Yaakov et al., 2012) and a back-propagating calcium wave (Cho et al., 2013). These positive injury signals contribute to regeneration by promoting a transcriptional switch leading to the upregulation of regeneration-associated genes (reviewed in Mar et al. (2014a)). Many of these signaling pathways are commonly thought to lack activation after central axon injury. However, it has been recently shown for a restricted number of positive injury signals that their activation and retrograde transport is similar after either peripheral axon or dorsal root injury (Mar et al., 2016). In this report, the levels of "negative" injury signals were increased after dorsal root injury when compared to peripheral axon injury, not only in axons but also in DRG neuron cell bodies (Mar et al., 2016). In fact, the absence of a regenerative response following central DRG neuron axon injury may be due to the failure in repressing regeneration inhibitors (Cho et al., 2015; Mar et al., 2016). Recently, DNA methylation temporal profiling of DRG after either dorsal column tract or sciatic nerve axotomy was performed (Lindner et al., 2014). The dataset generated will allow further experimental characterization of the role of this specific epigenetic regulation following peripheral *versus* central injury. Also, to better understand the differences in regenerative capacity between both DRG neuron axons, it would be pertinent to compare the proteomic content of their axoplasms after peripheral and central axon injuries.

On a different note, the activation of some injury signals requires local protein synthesis. For instance, vimentin and importin-β mRNAs are locally translated at the site of axonal injury, leading to the formation of multi-protein signaling complexes that are retrogradely transported by dynein acting as positive injury signals that increase regeneration (Hanz et al., 2003; Perlson et al., 2005; Yudin et al., 2008). One can also consider the hypothesis that in central DRG neuron axons, positive injury signals are not as activated as in the peripheral axon due to an eventual smaller protein synthesis ability in the former (Pannese and Ledda, 1991).

In summary, following the identification of several signaling pathways that are activated by injury, the picture that is emerging is that injury signaling, and the reasons underlying the different regenerative capacities of the central and peripheral DRG neuron axons, may be more complex than initially anticipated.

4.3.2. Axonal transport as a central mediator of successful axon regeneration

Axonal transport is extremely important for successful axon

regeneration. First, as mentioned above, many positive injury signals activated at the peripheral injury site need to be retrogradely transported to the cell body to promote regeneration. In addition, axonal regrowth is dependent on the *de novo* assembly of the axonal components, and on the delivery of these building blocks to the axon tip. Most of these components are synthesized in the neuronal cell body and are then anterogradely transported through the axon (Liu et al., 2011). Indeed, radiolabeling studies revealed that the rate of axon regeneration correlates with the rate of anterograde slow axonal transport in each of the DRG neuron axons (Wujek and Lasek, 1983).

A number of reports further support the importance of axonal transport regulation in the outcome of axon regeneration. Several early radiolabeling studies show collectively that injury to the peripheral DRG neuron axon increases the amount of protein being transported to both DRG neuron axons, while an injury to the central DRG neuron axon does not produce a similar effect (Bisby, 1981; Perry et al., 1983; Perry and Wilson, 1981). Recently, similar findings were reported using transgenic mice that allow tracking neuronal mitochondria (Mar et al., 2014b). In this system, injury to the peripheral DRG neuron axon increased axonal transport of mitochondria in both axonal branches, whereas injury to the central DRG neuron axon failed to yield a similar effect (Mar et al., 2014b). This increase in axonal transport elicited by a peripheral DRG neuron axon injury was not restricted to mitochondria but extended to lysosomes and synaptic vesicles. The reasons for the differences in regeneration capacity between both DRG neuron axons are still not fully understood. Identifying why and how axonal transport is promoted by peripheral DRG neuron axon injury would be of great interest for the axon regeneration field.

4.3.3. Lessons from invertebrate sensory neurons

Non-mammalian experimental models including *Drosophila* and *C. elegans* are very amenable to genetic manipulations and precise laser surgeries, allowing the induction of controlled and reproducible injuries. For this reason, such models are very useful to study regeneration. In a specific type of *Drosophila* sensory neuron, when the axon is injured some hours before dendrite severing, dendrites are more resistant to degeneration (Chen et al., 2012). In these neurons, *in vivo* axotomy but not dendrite severing cause the upregulation of growing microtubules and microtubule polarity switching in the dendritic arbor (Stone et al., 2010). These results show that axon injury but not dendrite injury activates a global cellular response that causes changes in the microtubule cytoskeleton. Similarly, it would be interesting to investigate whether injury to the DRG neuron peripheral axon but not to the central axon promotes global changes in the microtubule cytoskeleton. Conditioning effects were also observed in bipolar sensory neurons of *C. elegans* that have a single dendrite and axon. In a mutant where conventional DLK-1–mediated axon regeneration is eliminated, the axon does not regenerate after axotomy, except if the dendrite and axon are severed concomitantly. These results suggest that severing the dendrite triggers a nonconventional regeneration pathway that is not activated by axotomy alone. The authors further demonstrate that this non-conventional regeneration pathway shares numerous similarities with the conditioning lesion effect of DRG neurons (Chung et al., 2016). Overall, non-mammalian animal models with a relatively simple nervous system should be powerful in unraveling the mechanisms that underlie the conditioning effect and consequently the DRG neuron central-peripheral asymmetry in regeneration ability.

5. Evidence supporting the existence of an axon initial segment-like region in DRG neurons

The AIS is a specialized ~20–40-μm-long structure located in the proximal axon of multipolar neurons (Fig. 7A left) (Yang et al., 2007). It is the region where action potentials are generated and it is crucial for fine-tuning neuronal excitability and maintaining neuronal polarity (reviewed in Jones and Svitkina (2016)). *In vitro*, cultured embryonic DRG neurons assemble a distinctive region that has a positioning and molecular composition similar to the AIS (Fig. 7A right) (Dzhashiashvili et al., 2007). In cultured DRG neurons the AIS-like region is enriched in ankyrin G (ankG) (Zhang and Bennett, 1998), βIV-spectrin (Hedstrom et al., 2007; Yang et al., 2007), voltage-gated sodium channels (Dzhashiashvili et al., 2007) and neurofascin186 (Dzhashiashvili et al., 2007; Zhang and Bennett, 1998). In DRG neuron cultures, when cells present multiple neurites, the AIS is located in the initial portion of some of these neurites (Dzhashiashvili et al., 2007); when DRG neurons present a pseudo-unipolar morphology, the AIS is located within the stem axon (Fig. 7B) (Hedstrom et al., 2007; Yang et al., 2007).

In vitro, the AIS-like region and the nodes of Ranvier assemble by very different mechanisms in DRG neurons (Dzhashiashvili et al., 2007). In rats, the formation of nodes of Ranvier depends on interactions with adjacent glia that lead to the establishment of clusters containing neurofascin along the length of the axon (Eshed et al., 2005). Neurofascin then recruits ankG which in turn is responsible for the subsequent localization and assembly of the nodes of Ranvier (Dzhashiashvili et al., 2007). In contrast, the assembly of the AIS appears to be intrinsically specified as DRG neurons cultured in the absence of glial cells assemble this structure (Zhang and Bennett, 1998). In addition, neurofascin186 is not necessary for clustering ankG at the AIS of cultured rat DRG neurons (Dzhashiashvili et al., 2007). Similarly, the AIS is intrinsically assembled by multipolar neurons (Ogawa and Rasband, 2008). Recently, Gumy et al. (2017) did not detect this ankG-rich region in cultured DRG neurons. Of note, this study used adult DRG neurons whereas in previous *in vitro* studies where the AIS was detected, embryonic DRG neurons were used (Dzhashiashvili et al., 2007; Hedstrom et al., 2007; Yang et al., 2007). It is possible that adult DRG neurons do not recapitulate *in vitro* the AIS assembly.

In rat embryos (E16), immunostaining for ankG revealed that this protein is homogeneously distributed along the length of both DRG neuron axons (Lambert et al., 1997), supporting that at this developmental stage the AIS has still not been assembled. Later, ankG disappears from unmyelinated processes whereas in myelinating axons, ankG redistributes at clusters which later form the nodes of Ranvier (Lambert et al., 1997). The *in vivo* existence of the AIS in adult DRG neurons as defined by the enrichment in one of its components lacks strong experimental support. A single report suggests that the proximal region of the stem axon in adult mouse and rat DRG contains ankG (Brandao et al., 2012). However, the specific enrichment of ankG in this region is unclear. Thereby, additional data is needed to unequivocally support the existence of the AIS *in vivo* in DRG neurons. Recently, ankG-enriched stem axon regions were only detected in less than 2% of adult rat DRG neuron sections (Gumy et al., 2017). Therefore, so far, there is no compelling evidence that the AIS is an ubiquitous feature of DRG neurons *in vivo*. One should however note that the AIS may be technically challenging to detect in DRG sections as it is difficult to uniformly orient DRG neuron axons. More importantly, the stem axon can have up to 600 μm in length and the AIS may be located in a distal position. Finally, since DRG neurons are highly heterogeneous, it is possible that only some subtypes assemble an AIS. The existence of the AIS in DRG neurons should be investigated using techniques allowing the visualization of the entire stem axon until the first internode (in myelinated neurons) or until the bifurcation (in unmyelinated neurons). Given that the AIS is of utmost importance for neuronal physiology, it is of considerable importance to definitely determine if DRG neurons, or a subpopulation of DRG neurons, have an AIS *in vivo*.

5.1. The axon initial segment as a possible key structure for DRG neuron polarity

Although in multipolar neurons the AIS is assembled after axon specification (Galiano et al., 2012), it is essential for the maintenance of neuronal polarity. Indeed, upon AIS dismantlement the axon loses its identity and acquires many of the molecular and structural features of

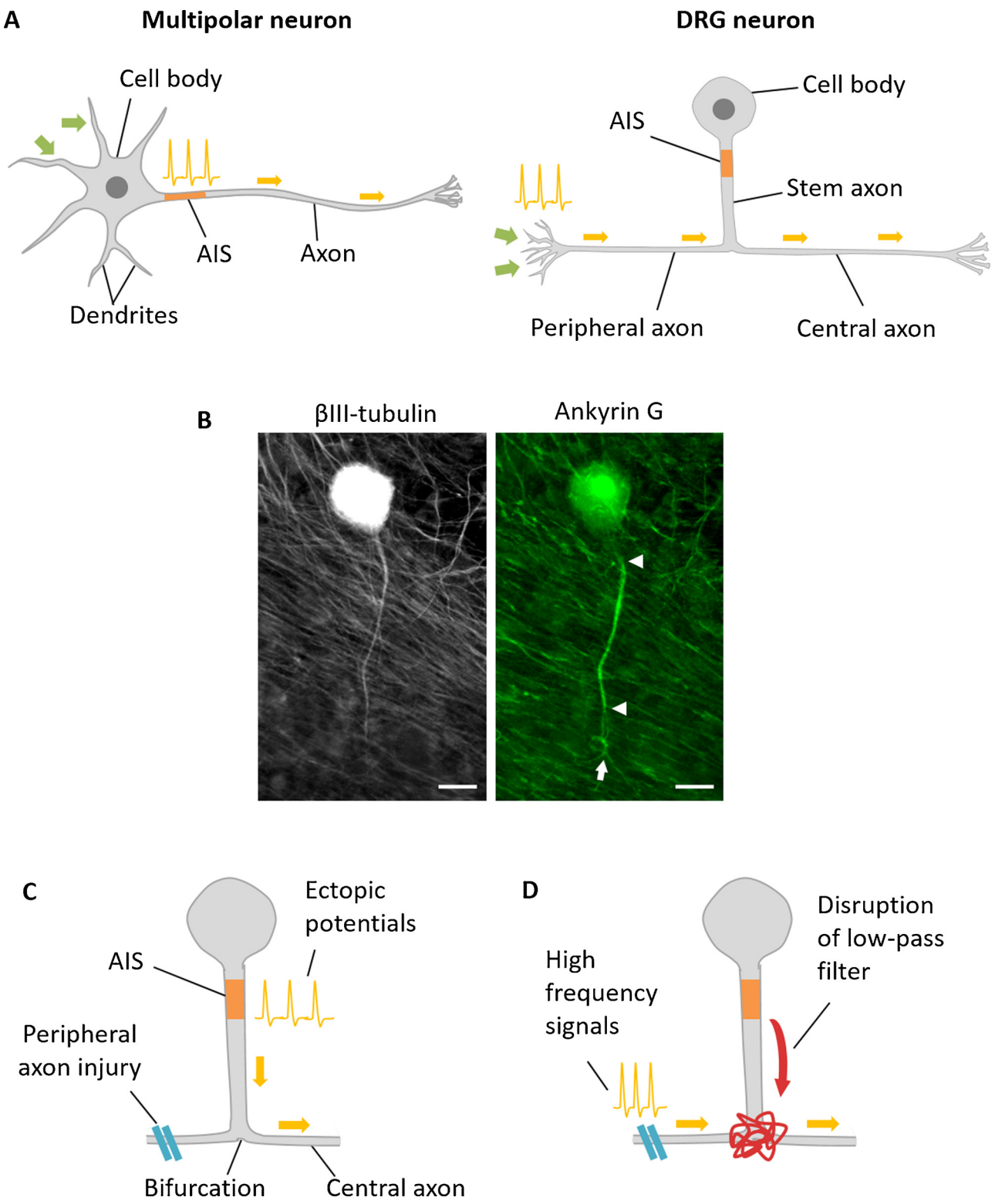

Fig. 7. The axon initial segment of pseudo-unipolar DRG neurons. (A) Schematic drawing showing the location of the axon initial segment in multipolar neurons and hypothetically in DRG neurons. (B) Cultured DRG neuron immunostained for βIII-tubulin (left, white) and ankyrin G (green, right) to label the neuron and the axon initial segment, respectively. The arrow points to the stem axon bifurcation while the arrowheads mark the beginning and end of the axon initial segment. Scale bar, 20 μm. (C, D) Peripheral insults such as axon injury could cause site-specific changes in the AIS of DRG neurons that could contribute to neuropathic pain. After peripheral nerve injury, the AIS of DRG neurons could become sufficiently hyperexcitable to generate ectopic action potentials (C) or to decrease the low-pass filtering at the T-junction, thereby allowing the transmission of high-frequency signals to higher order neurons in the somatic afferent pathway (D).

dendrites, both *in vitro* (Hedstrom et al., 2008) and *in vivo* (Sobotzik et al., 2009). The AIS maintains neuronal polarity as it establishes membrane (Kobayashi et al., 2018; Winckler et al., 1999) and cytosolic (Song et al., 2009) barriers that restrict the diffusion of molecules to somatodendritic or axonal domains.

If an AIS-like structure exists in DRG neurons, it could contribute to the polarity and asymmetry of this cell type (Fig. 7A). If the AIS of the DRG neuron is located in the stem axon it would not be positioned to function as a barrier between the central and peripheral processes, but rather between the cell body and both axons. As previously discussed, the stem axon has a higher number/density of organelles in its proximal non-myelinated region than in its distal myelinated portion (Spencer et al., 1973; Zelená, 1972; Zenker and Högl, 1976). In mature DRG neurons an AIS-like structure could be responsible for these differences by functioning as an intracellular filter between these two domains. If the AIS would assemble prior to pseudo-unipolarization in one of the neurites of the DRG neuron in the bipolar stage, it could contribute to the establishment of polarity between the central and peripheral axons. As such, the AIS would not contribute to the maintenance of polarity between both axons but it could contribute to its establishment.

5.2. Could an axon initial segment-like structure regulate sensory signal transmission?

The AIS is the region of multipolar neurons where action potentials are generated (Kole and Stuart, 2012). In contrast, in DRG neurons, action potentials are generated at the peripheral nerve terminal. In sensory neurons, there is an initial transduction of the stimulus into a receptor current that is converted into an action potential discharge by voltage-gated sodium channels (Carr et al., 2009). The classical view is that the site of sensory signal transduction and the site of action potential generation are spatially separated. In myelinated nerve endings, namely in the Pacinian corpuscle, the action potential is thought to initiate at the first node of Ranvier (Carr et al., 2009). However, the site of action potential initiation is not so well resolved in the case of unmyelinated nerve endings, where sodium channels are distributed more evenly (Black and Waxman, 2018). One study suggests that a single unmyelinated nerve terminal can have several spatially discrete sites of action potential generation that can move towards the nerve terminal during hyperpolarization. Moreover, these sites seem to reside in parallel with transduction channels (Carr et al., 2009). Overall, the distribution of voltage-gated sodium channels in the peripheral endings of DRG neurons does not support the existence of a stereotypical AIS-like structure in the peripheral nerve terminal.

Although under physiological conditions action potentials are initiated only in the peripheral terminal of DRG neurons, this is not the case in some pathological conditions. After inflammation (Weng et al., 2012), partial nerve injury (Devor, 2009) or direct compression of the DRG (Ma and LaMotte, 2007), a portion of the axon and/or cell body of DRG neurons becomes sufficiently hyperexcitable to generate ectopic action potentials. Ectopic firing alters the sensory information delivered to higher order neurons in the somatic afferent pathway (Ma and LaMotte, 2007). In fact, ectopic discharges are considered to be a key driver of neuropathic pain (Djouhri et al., 2006). However, little is known about where or how ectopic activity is generated in the sensory neuron (Ma and LaMotte, 2007). Ectopic activity is caused by an abnormal hyperexcitability of the membrane, namely an enhancement of subthreshold oscillations (Liu et al., 2000). This abnormal excitability results from alterations in the function, distribution and density of molecules of excitability such as voltage-gated sodium channels, which have been widely implicated in inflammatory and neuropathic pain (reviewed in Levinson et al. (2012)). If the AIS of DRG neurons contains a high density of these molecules, it might be one key subcellular region where site-specific changes lead to ectopic firing (Fig. 7C). In the sciatic-nerve axotomy model, ectopic spikes may arise alternatively in the soma, in the injured axon end (neuroma), in the bifurcation or in the stem axon (Amir et al., 2005). In a chronically compressed rat DRG, ectopic firing is generated at the cell body, and in the axon at a site within or close to the DRG, which includes the hypothetic location of the AIS (Ma and LaMotte, 2007).

Sensory transmission in DRG neurons is commonly conceptualized as an uninterrupted conduction of action potentials along peripheral and central axons towards the CNS. However due to the pseudo-unipolar morphology, there is impedance mismatch at the bifurcation that is responsible for an increased probability of spike propagation failure at this point. As a consequence of a local lower safety factor for spike propagation, there may be low-pass filtering of action potentials (filter that passes low frequencies and suppresses high frequencies) at the stem axon bifurcation. Experimentally, it has been observed that high-frequency signals fail during their passage through the bifurcation both *in vitro* (Luscher et al., 1994; Stoney, 1990) and *in vivo* in adult rat C-fiber neurons (Gemes et al., 2013). Interestingly, this filtering capacity decreases in C-fiber neurons after peripheral nerve injury, which may contribute to neuropathic pain (Gemes et al., 2013). As discussed in Section 3.2., several morphological parameters including a longer and thinner stem axon increase the probability of spike conduction through the bifurcation to the central axon and thus inhibit low-pass filtering. Additionally, other factors could play a role in this filtering, such as variations of membrane potential and membrane conductance in the vicinity of the bifurcation (Sundt et al., 2018). More specifically, increasing the excitability of the DRG neuron cell body or stem axon, for instance by enrichment of these regions in voltage-gated sodium channels, could promote spike through-conduction and therefore inhibit low-pass filtering (Devor and Obermayer, 1984). For large diameter DRG neurons, excitability of these two domains appears to have little functional consequence on spike propagation, because they are electrotonically distant from the bifurcation (Amir and Devor, 2003). However, if the soma and proximal stem axon are electrotonically close enough to the bifurcation, which is the case in small diameter DRG neurons, they can have significant influence over the low-pass filtering. In fact, in small-diameter unmyelinated DRG neurons, increased membrane conductance and hyperpolarization of the somatic/perisomatic resting membrane potential have been suggested to contribute to low-pass filtering at the bifurcation (Du et al., 2014; Sundt et al., 2018). Nevertheless, little is known about how changes in membrane potential and membrane conductance affect peripheral sensory transmission. It is possible that these two parameters might be regulated locally if an AIS-like structure exists in the stem axon, as a way to control low-pass filtering (Fig. 7D). As so, one of the possible functions of an AIS in DRG neurons, especially in the small diameter ones, could be to control the selective elimination of high-frequency signals therefore “gating” peripheral signaling.

6. How to study DRG neurons?

6.1. The need for physiologically-relevant in vitro models

To investigate any cellular and molecular mechanism underlying the physiology of DRG neurons it is important to use a primary cell culture system that can invoke a physiological cellular behavior. When DRG neurons either from developing or adult rodents are cultured *in vitro*, a wide variety of cell morphologies is observed, but mostly these cultures do not recapitulate the *in vivo* cell biology of DRG neurons. When embryonic DRGs are used, a reduced number of long neurites per neuron with low branching is generally obtained, whereas adult DRG neurons mostly grow multiple highly ramified neurites. The number, length and dendritic *versus* axonal nature of these neurites varies according to the culture conditions. For instance in DRG neuron monocultures, supplementing the medium with NGF promotes the formation of neurites that are positive for the somatodendritic marker MAP2. In contrast, in the presence of both NGF and SGCs, virtually no DRG neuron extends MAP2-positive neurites (De Koninck et al., 1993).

Ideally, DRG neuron cultures should recapitulate the pseudo-unipolarization morphogenic process and a central-peripheral axonal asymmetry should also be obtained. In this regard, a better knowledge on the roles of mechanical, cell-contact and soluble cues that participate in pseudo-unipolarization would be useful to develop physiologically-relevant culture systems. The dimensionality of the culture system seems to be important for the development of a pseudo-unipolar morphology, as the percentage of DRG neurons with a single primary neurite is higher in three-dimensional collagen gels than in two-dimensional ones, where most DRG neurons extend more than one neurite (Ribeiro et al., 2012). In addition, as mentioned in Section 2.2., some *in vitro* studies have shown that pseudo-unipolarization is not cell-autonomous but instead requires the presence of glial cells (De Koninck et al., 1993; Mudge, 1984; Takahashi and Ninomiya, 1987). In terms of trophic cues, the effect of semaphorin3A on pseudo-unipolarization of DRG neurons would be interesting to explore as this molecule seems to instruct neuronal polarity by driving the asymmetric subcellular distribution of molecules in bipolar DRG neurons (Lerman et al., 2007). To investigate the existence of central-peripheral asymmetry in cultured DRG neurons, immunofluorescence for proteins that have been described to be asymmetrically distributed *in vivo* (an isoform of collapsin response mediator protein-2, MAP2, BNaC1α and Trpv1) or EM analysis could be performed. Using EM analysis, it has been shown that in DRG explants, DRG neurons can have ultrastructural central-peripheral asymmetry in spite of not having central nor peripheral connections. More specifically, spindle-shaped bipolar DRG neurons have one process that is thicker than the other and has more free ribosomes in its proximal region, thus resembling the peripheral process *in vivo* (Takahashi and Ninomiya, 1987). These results suggest that to obtain central-peripheral asymmetry it may not be needed to provide central nor peripheral cellular targets in the culture system.

The development of suitable *in vitro* models should also take into account the heterogeneity of DRG neurons *in vivo*. The culture system conditions may induce a DRG neuron phenotype typical of one or more specific subpopulations and hence bias the results. For instance, in the presence of NGF, cultured DRG neurons acquire a peptidergic phenotype which is typical of a specific DRG neuron subpopulation (Hall et al., 1997), but in the absence of NGF this does not happen (Patel et al., 2000). In addition, neurotrophic factors such as neurotrophin 3 are needed for the survival of other DRG neuron subpopulations (Hory-Lee et al., 1993). As most DRG neuron cultures are performed in the presence of NGF alone, some DRG neuron subpopulations may be underrepresented in most *in vitro* assays. Thus, the neurochemical phenotype of cultured DRG neurons should be taken into consideration when interpreting results from such assays.

6.2. Solutions to technical challenges of ex vivo and in vivo approaches

The structural organization of the DRG makes it difficult to depict single DRG neuron cell bodies with the respective stem axon and axonal branches. Also, DRG neurons represent a highly heterogeneous group, which creates the need for validating identified features as present in all DRG neurons or restricted to only some subtypes. As so, experimental designs and model selections are particularly relevant to study these neurons.

There is a number of different techniques to achieve single DRG neuron labeling. Transgenic mice expressing a fluorescent marker in a small percentage of DRG neurons may be used. As an example, there are several transgenic mouse lines expressing GFP under the control of the neuronal promoter thy1 (Feng et al., 2000). However, depending on the aim of the analysis, such animal models may have a major drawback, as DRG neurons from different subtypes are labeled. For labeling specific subpopulations of DRG neurons, immunostaining for molecular markers or *in situ* hybridization may be performed. Nevertheless, these techniques have major limitations as their use is limited to *ex vivo* analyses. As an alternative, several reporter mouse models that express fluorescent reporter genes in specific DRG neuron subpopulations may be used (reviewed in Le Pichon and Chesler et al. (2014)). In addition, genetic labeling of specific DRG neuron subtypes can be obtained by using mice in which the Cre-lox site specific recombination system induces the expression of reporter genes. There are already several Cre-driver mouse lines available that express the recombinase in specific subsets of DRG neurons (reviewed in Le Pichon and Chesler et al. (2014)). Nevertheless, these traditional transgenic models have some technical limitations that in the future can be overcome by the use of more powerful tools for genomic engineering such as the CRISPR/Cas9 (Sun et al., 2016).

It is important to highlight that the analysis of DRG neuron axons *ex vivo* and *in vivo* encompasses major technical challenges. Since the dorsal roots contain only the central axons of DRG neurons, there is no risk of contamination with axons from other cell types. In contrast, the spinal (Xie et al., 2010) and many peripheral nerves (for instance the sciatic nerve) contain not only peripheral DRG neuron axons but also myelinated motor fibers and unmyelinated sympathetic axons which are widely ignored (Chad et al., 1983; Schmalbruch, 1986). Because of that, in some studies where mixed nerves are used, ventral rhizotomy and/or sympathectomy are performed to eliminate motor and sympathetic fibers respectively (Ochs et al., 1978; Suh et al., 1984). However, both surgical procedures affect the phenotype of DRG neurons (Bolden et al., 1997; Li et al., 2009), and so they are not ideal to study the peripheral axon in its physiological state. To distinguish axons from different neuron types, histochemical staining for carbonic anhydrase, cholinesterase and tyrosine hydroxylase were commonly used to label DRG, motor or sympathetic axons respectively (Riley et al., 1988; Roth and Kummer, 1994). Nevertheless, there are exceptions to this staining pattern as for instance unmyelinated DRG neuron axons do not stain for carbonic anhydrase (Riley et al., 1984) and some of them stain for tyrosine hydroxylase (Li et al., 2011). Other techniques may be performed for the exclusive labeling of DRG axons in mixed nerves, such as intraganglionic injection of tracers (Lee et al., 1986), transduction with adeno-associated viruses of specific serotypes (Mason et al., 2010), or *in vivo* electroporation of the adult DRG (Saijilafu et al., 2011). An alternative approach relies on the usage of specific peripheral nerves that contain only DRG neuron axons. That is the case of the saphenous nerve which is a branch of the rat femoral nerve that is typically used in research as a purely sensory nerve (Hu et al., 2010). In addition, recently, a transgenic mouse line was developed that allows the selective labeling of DRG neuron axons in mixed nerves- the tamoxifen-inducible Advillin-Cre-ERT2 (Lau et al., 2011). Advillin is an actin binding protein expressed almost exclusively by sensory neurons throughout development and adulthood (Akopian and Wood, 1995; Hasegawa et al., 2007).

The animal models and labeling approaches mentioned in the previous paragraphs may be combined with other experimental designs to study DRG neurons and their subpopulations in a selective way. For instance, selective labeling could be used for the ultrastructural analysis of specific DRG neurons *in vivo* by correlative light-electron microscopy (Bishop et al., 2011). Moreover, an approach for specific labeling of a given population could be combined with transgenic mouse models or injection of fluorescent probes to allow *ex vivo* or *in vivo* live-imaging of that specific DRG neuron population. Such combinatorial approaches could be useful to study for instance axonal transport (Gibbs et al., 2016; Mar et al., 2014b) and actin (Schachtner et al., 2012) or microtubule (Kleele et al., 2014) dynamics in specific DRG neurons, without the contamination of other cell types or DRG neuron subpopulations. Selective labeling could also be useful in studies of live imaging of embryo slices to monitor the polarity program of DRG sensory neurons from cell division to neurite extension (Boubakar et al., 2017).

In addition to the challenge of labeling specifically DRG neurons and their subpopulations, there is also the challenge of determining their precise function. Since the expression of certain genes can be associated with specific sensory modalities, efforts have been made to

determine the transcriptional profiles of DRG neurons, both at whole population and single cell levels (Chiu et al., 2014). At the single cell level, parallel quantitative real-time PCR (Chiu et al., 2014), and low coverage (Usoskin et al., 2014) and high coverage (Li et al., 2016) RNA-sequencing have been used. Such methodologies have allowed the identification of a greater number of DRG neuron subtypes whose cellular functions can be studied in detail using several experimental approaches. Genetic ablation has been the most widely used strategy for functionally analyzing DRG neuron subtypes (reviewed in Le Pichon and Chesler et al. (2014)). Also, pharmacological manipulations have proved valuable in activating specific DRG neuron subsets (Han et al., 2013). For activating subpopulations that lack defined pharmacology, several groups have performed chemical genetics (Vrontou et al., 2013). Similarly, optogenetic approaches can be used to target channelrhodopsin to specific DRG neuron subsets and optically activate them, thus eliciting the stimulation of peripheral sensory pathways in freely moving animals (Daou et al., 2013). Using these animal models, *in vivo* electrophysiological recordings have been the gold standard technique for the functional analysis of DRG neurons challenged with specific stimuli (Han et al., 2013). However, since electrophysiology is technically demanding, in recent years *in vivo* calcium imaging approaches have been used to visualize the activity of DRG neurons in live animals, either using calcium-sensitive dyes (Han et al., 2013) or genetically encoded calcium indicators (Emery et al., 2016). Overall, several sophisticated techniques have been developed that can be used for subsequent studies to define the functional role of DRG neurons with a high degree of cell-type specificity.

7. Conclusion

Sensory DRG neurons have a single axon that bifurcates into a central and a peripheral branch. This unique morphology raises many questions regarding the maintenance of asymmetric functions and properties. Early studies have shown that the stem axon and its branches have peculiar ultrastructural features that may have important implications for the physiology of DRG neurons. Both axonal branches have differences in diameter, microtubule density and ribosome numbers, among others. However, these asymmetries were still not causally related to the functional differences observed between the central and peripheral DRG neuron axons, namely their differential transport or regeneration capacities. Moreover, it is unknown how proteins and organelles can be selectively transported from the cell body to one of the axonal branches. In addition, various reports suggest that DRG neurons may have an AIS-like structure, but its functions and existence *in vivo* are still enigmatic. These observations further sustain the importance of linking structure with function and polarity in DRG neurons, but this subject has been largely neglected in the field. Thus, here we discussed the current knowledge on the biology of DRG neurons in light of early structural findings. Further characterization, making use of state-of–the-art techniques will certainly improve our understanding of DRG neuron biology and function under physiological conditions, with possible important consequences in pathological states.

Acknowledgments

Work from the authors' group was supported by Fundação Grunenthal, Bolsa Jovens Investigadores em Dor 2016 (to F.M.M); Prémio Melo e Castro - Santa Casa da Misericórdia de Lisboa (to M.M.S); and Norte-01-0145-FEDER-000008 - Porto Neurosciences and Neurologic Disease Research Initiative at i3S, funded by Norte Portugal Regional Operational Programme (NORTE 2020), under the PORTUGAL 2020 Partnership Agreement, through the European Regional Development Fund (ERDF). A.I.N is funded by a FCT fellowship (SFRH/BD/130014/2017).

References

Akopian, A.N., Wood, J.N., 1995. Peripheral nervous system-specific genes identified by subtractive cDNA cloning. J. Biol. Chem. 270, 21264–21270.
Amir, R., Devor, M., 2003. Electrical excitability of the soma of sensory neurons is required for spike invasion of the soma, but not for through-conduction. Biophys. J. 84, 2181–2191.
Amir, R., Kocsis, J.D., Devor, M., 2005. Multiple interacting sites of ectopic spike electrogenesis in primary sensory neurons. J. Neurosci. 25, 2576–2585.
Anderson, L.E., McClure, W.O., 1973. Differential transport of protein in axons: comparison between the sciatic nerve and dorsal columns of cats. Proc. Natl. Acad. Sci. U. S. A 70, 1521–1525.
Barber, R.P., Vaughn, J.E., 1986. Differentiation of dorsal root ganglion cells with processes in their synaptic target zone of embryonic mouse spinal cord: a retrograde tracer study. J. Neurocytol. 15, 207–218.
Ben-Yaakov, K., Dagan, S.Y., Segal-Ruder, Y., Shalem, O., Vuppalanchi, D., Willis, D.E., Yudin, D., Rishal, I., Rother, F., Bader, M., Blesch, A., Pilpel, Y., Twiss, J.L., Fainzilber, M., 2012. Axonal transcription factors signal retrogradely in lesioned peripheral nerve. EMBO J. 31, 1350–1363.
Berthold, C.H., Fabricius, C., Rydmark, M., Andersen, B., 1993. Axoplasmic organelles at nodes of Ranvier. I. Occurrence and distribution in large myelinated spinal root axons of the adult cat. J. Neurocytol. 22, 925–940.
Bird, M.M., Lieberman, A.R., 1976. Microtubule fascicles in the stem processes of cultured sensory ganglion cells. Cell Tissue Res. 169, 41–47.
Bisby, M.A., 1981. Axonal transport in the central axon of sensory neurons during regeneration of their peripheral axon. Neurosci. Lett. 21, 7–11.
Bishop, D., Nikic, I., Brinkoetter, M., Knecht, S., Potz, S., Kerschensteiner, M., Misgeld, T., 2011. Near-infrared branding efficiently correlates light and electron microscopy. Nat. Methods 8, 568–570.
Black, J.A., Waxman, S.G., 2002. Molecular identities of two tetrodotoxin-resistant sodium channels in corneal axons. Exp. Eye Res. 75, 193–199.
Bolden, D.A., Sternini, C., Kruger, L., 1997. GAP-43 mRNA and calcitonin gene-related peptide mRNA expression in sensory neurons are increased following sympathectomy. Brain Res. Bull. 42, 39–50.
Boubakar, L., Falk, J., Ducuing, H., Thoinet, K., Reynaud, F., Derrington, E., Castellani, V., 2017. Molecular memory of morphologies by septins during neuron generation allows early polarity inheritance. Neuron 95, 834–851 e835.
Brandao, K.E., Dell'Acqua, M.L., Levinson, S.R., 2012. AKAP localizes in a specific subset of TRPV1 and Ca(V)1.2 positive nociceptive rat DRG neurons. J. Comp. Neurol. 520, 81–99.
Britsch, S., Goerich, D.E., Riethmacher, D., Peirano, R.I., Rossner, M., Nave, K.-A., Birchmeier, C., Wegner, M., 2001. The transcription factor Sox10 is a key regulator of peripheral glial development. Genes Dev. 15, 66–78.
Brumovsky, P., Villar, M.J., Hokfelt, T., 2006. Tyrosine hydroxylase is expressed in a subpopulation of small dorsal root ganglion neurons in the adult mouse. Exp. Neurol. 200.
Brushart, T.M., Aspalter, M., Griffin, J.W., Redett, R., Hameed, H., Zhou, C., Wright, M., Vyas, A., Höke, A., 2013. Schwann cell phenotype is regulated by axon modality and central-peripheral location, and persists in vitro. Exp. Neurol. 247, 272–281.
Bustos, J., Vial, J.D., Faundez, V., Alvarez, J., 1991. Axons sprout and microtubules increase after local inhibition of RNA synthesis, and microtubules decrease after inhibition of protein synthesis: a morphometric study of rat sural nerves. Eur. J. Neurosci. 3, 1123–1133.
Carr, R.W., Pianova, S., McKemy, D.D., Brock, J.A., 2009. Action potential initiation in the peripheral terminals of cold-sensitive neurones innervating the guinea-pig cornea. J. Physiol. 587, 1249–1264.
Cavalli, V., Kujala, P., Klumperman, J., Goldstein, L.S., 2005. Sunday driver links axonal transport to damage signaling. J. Cell Biol. 168, 775–787.
Chad, D., Rasool, C., Bradley, W.G., Good, P., Reichlin, S., 1983. Unmyelinated axon subpopulations in the rat peripheral nervous system. Neurology 33, 848–852.
Chen, L., Stone, M.C., Tao, J., Rolls, M.M., 2012. Axon injury and stress trigger a microtubule-based neuroprotective pathway. Proc. Natl. Acad. Sci. U. S. A. 109, 11842–11847.
Cheng, C.F., Cheng, J.K., Chen, C.Y., Rau, R.H., Chang, Y.C., Tsaur, M.L., 2015. Nerve growth factor-induced synapse-like structures in contralateral sensory ganglia contribute to chronic mirror-image pain. Pain 156, 2295–2309.
Chien, S.Q., Li, C., Li, H., Xie, W., Pablo, C.S., Zhang, J.-M., 2005. Sympathetic fiber sprouting in chronically compressed dorsal root ganglia without peripheral axotomy. J. Neuropathic Pain Symptom Palliation 1, 19–23.
Chiu, I.M., Barrett, L.B., Williams, E.K., Strochlic, D.E., Lee, S., Weyer, A.D., Lou, S., Bryman, G.S., Roberson, D.P., Ghasemlou, N., Piccoli, C., Ahat, E., Wang, V., Cobos, E.J., Stucky, C.L., Ma, Q., Liberles, S.D., Woolf, C.J., 2014. Transcriptional profiling at whole population and single cell levels reveals somatosensory neuron molecular diversity. eLife 3, e04660.
Cho, Y., Shin, J.E., Ewan, E.E., Oh, Y.M., Pita-Thomas, W., Cavalli, V., 2015. Activating injury-responsive genes with hypoxia enhances axon regeneration through neuronal HIF-1alpha. Neuron 88, 720–734.
Cho, Y., Sloutsky, R., Naegle, K.M., Cavalli, V., 2013. Injury-induced HDAC5 nuclear export is essential for axon regeneration. Cell 155, 894–908.
Chong, M., Reynolds, M., Irwin, N., Coggeshall, R., Emson, P., Benowitz, L., Woolf, C., 1994. GAP-43 expression in primary sensory neurons following central axotomy. J. Neurosci. 14, 4375–4384.
Chung, K., Chung, J.M., 2001. Sympathetic sprouting in the dorsal root ganglion after spinal nerve ligation: evidence of regenerative collateral sprouting. Brain Res. 895, 204–212.

Chung, K., Yoon, Y.W., Chung, J.M., 1997. Sprouting sympathetic fibers form synaptic varicosities in the dorsal root ganglion of the rat with neuropathic injury. Brain Res. 751, 275–280.
Chung, S.H., Awal, M.R., Shay, J., McLoed, M.M., Mazur, E., Gabel, C.V., 2016. Novel DLK-independent neuronal regeneration in Caenorhabditis elegans shares links with activity-dependent ectopic outgrowth. Proc. Natl. Acad. Sci. U. S. A. 113, E2852–E2860.
Court, F.A., Hendriks, W.T., MacGillavry, H.D., Alvarez, J., van Minnen, J., 2008. Schwann cell to axon transfer of ribosomes: toward a novel understanding of the role of glia in the nervous system. J. Neurosci. 28, 11024–11029.
Daou, I., Tuttle, A.H., Longo, G., Wieskopf, J.S., Bonin, R.P., Ase, A.R., Wood, J.N., De Koninck, Y., Ribeiro-da-Silva, A., Mogil, J.S., Seguela, P., 2013. Remote optogenetic activation and sensitization of pain pathways in freely moving mice. J. Neurosci. 33, 18631–18640.
De Koninck, P., Carbonetto, S., Cooper, E., 1993. NGF induces neonatal rat sensory neurons to extend dendrites in culture after removal of satellite cells. J. Neurosci. 13, 577–585.
Devor, M., 1999. Unexplained peculiarities of the dorsal root ganglion. Pain (Suppl. 6), S27–35.
Devor, M., 2009. Ectopic discharge in Abeta afferents as a source of neuropathic pain. Exp. Brain Res. 196, 115–128.
Devor, M., Obermayer, M., 1984. Membrane differentiation in rat dorsal root ganglia and possible consequences for back pain. Neurosci. Lett. 51, 341–346.
Devor, M., Wall, P.D., McMahon, S.B., 1984. Dichotomizing somatic nerve fibers exist in rats but they are rare. Neurosci. Lett. 49, 187–192.
Di Maio, A., Skuba, A., Himes, B.T., Bhagat, S.L., Hyun, K., Tessler, A., Bishop, D., Son, Y.-J., 2011. In vivo imaging of dorsal root regeneration: rapid immobilization and presynaptic differentiation at the CNS/PNS border. J. Neurosci. 31, 4569–4582.
Djouhri, L., Koutsikou, S., Fang, X., McMullan, S., Lawson, S.N., 2006. Spontaneous pain, both neuropathic and inflammatory, is related to frequency of spontaneous firing in intact C-fiber nociceptors. J. Neurosci. 26, 1281–1292.
Douarin, N.L., Dulac, C., Dupin, E., Cameron-Curry, P., 1991. Glial cell lineages in the neural crest. Glia 4, 175–184.
Du, X., Hao, H., Gigout, S., Huang, D., Yang, Y., Li, L., Wang, C., Sundt, D., Jaffe, D.B., Zhang, H., Gamper, N., 2014. Control of somatic membrane potential in nociceptive neurons and its implications for peripheral nociceptive transmission. Pain 155, 2306–2322.
Dzhashiashvili, Y., Zhang, Y., Galinska, J., Lam, I., Grumet, M., Salzer, J.L., 2007. Nodes of Ranvier and axon initial segments are ankyrin G–dependent domains that assemble by distinct mechanisms. J. Cell Biol. 177, 857–870.
Emery, E.C., Luiz, A.P., Sikandar, S., Magnusdottir, R., Dong, X., Wood, J.N., 2016. In vivo characterization of distinct modality-specific subsets of somatosensory neurons using GCaMP. Sci. Adv. 2, e1600990.
Enes, J., Langwieser, N., Ruschel, J., Carballosa-Gonzalez, M.M., Klug, A., Traut, M.H., Ylera, B., Tahirovic, S., Hofmann, F., Stein, V., Moosmang, S., Hentall, I.D., Bradke, F., 2010. Electrical activity suppresses axon growth through Ca(v)1.2 channels in adult primary sensory neurons. Curr. Biol. 20, 1154–1164.
Eshed, Y., Feinberg, K., Poliak, S., Sabanay, H., Sarig-Nadir, O., Spiegel, I., Bermingham Jr, J.R., Peles, E., 2005. Gliomedin mediates Schwann cell-axon interaction and the molecular assembly of the nodes of Ranvier. Neuron 47, 215–229.
Eva, R., Crisp, S., Marland, J.R., Norman, J.C., Kanamarlapudi, V., ffrench-Constant, C., Fawcett, J.W., 2012. ARF6 directs axon transport and traffic of integrins and regulates axon growth in adult DRG neurons. J. Neurosci. 32, 10352–10364.
Eva, R., Koseki, H., Kanamarlapudi, V., Fawcett, J.W., 2017. EFA6 regulates selective polarised transport and axon regeneration from the axon initial segment. J. Cell Sci. 130, 3663–3675.
Fadic, R., Vergara, J., Alvarez, J., 1985. Microtubules and caliber of central and peripheral processes of sensory axons. J. Comp. Neurol. 236, 258–264.
Feng, G., Mellor, R.H., Bernstein, M., Keller-Peck, C., Nguyen, Q.T., Wallace, M., Nerbonne, J.M., Lichtman, J.W., Sanes, J.R., 2000. Imaging neuronal subsets in transgenic mice expressing multiple spectral variants of GFP. Neuron 28, 41–51.
Galiano, M.R., Jha, S., Ho, T.S., Zhang, C., Ogawa, Y., Chang, K.J., Stankewich, M.C., Mohler, P.J., Rasband, M.N., 2012. A distal axonal cytoskeleton forms an intra-axonal boundary that controls axon initial segment assembly. Cell 149, 1125–1139.
García-Añoveros, J., Samad, T.A., Žuvela-Jelaska, L., Woolf, C.J., Corey, D.P., 2001. Transport and localization of the DEG/ENaC ion channel BNaC1α to peripheral mechanosensory terminals of dorsal root ganglia neurons. J. Neurosci. 21, 2678–2686.
Garcia-Poblete, E., Fernandez-Garcia, H., Moro-Rodriguez, E., Catala-Rodriguez, M., Rico-Morales, M.L., Garcia-Gomez-de-las-Heras, S., Palomar-Gallego, M.A., 2003. Sympathetic sprouting in dorsal root ganglia (DRG): a recent histological finding? Histol. Histopathol. 18, 575–586.
Gaudet, A.D., Popovich, P.G., Ramer, M.S., 2011. Wallerian degeneration: gaining perspective on inflammatory events after peripheral nerve injury. J. Neuroinflammation 8 110-110.
Gemes, G., Koopmeiners, A., Rigaud, M., Lirk, P., Sapunar, D., Bangaru, M.L., Vilceanu, D., Garrison, S.R., Ljubkovic, M., Mueller, S.J., Stucky, C.L., Hogan, Q.H., 2013. Failure of action potential propagation in sensory neurons: mechanisms and loss of afferent filtering in C-type units after painful nerve injury. J. Physiol. 591, 1111–1131.
George, D., Ahrens, P., Lambert, S., 2018. Satellite glial cells represent a population of developmentally arrested Schwann cells. Glia 0, 1–11.
Gibbs, K.L., Kalmar, B., Sleigh, J.N., Greensmith, L., Schiavo, G., 2016. In vivo imaging of axonal transport in murine motor and sensory neurons. J. Neurosci. Methods 257, 26–33.
Giuffrida, R., Rustioni, A., 1992. Dorsal root ganglion neurons projecting to the dorsal column nuclei of rats. J. Comp. Neurol. 316, 206–220.
Gresset, A., Coulpier, F., Gerschenfeld, G., Jourdon, A., Matesic, G., Richard, L., Vallat, J.-M., Charnay, P., Topilko, P., 2015. Boundary caps give rise to neurogenic stem cells and terminal glia in the skin. Stem Cell Rep. 5, 278–290.
Gumy, L.F., Katrukha, E.A., Grigoriev, I., Jaarsma, D., Kapitein, L.C., Akhmanova, A., Hoogenraad, C.C., 2017. MAP2 defines a pre-axonal filtering zone to regulate KIF1- versus KIF5-dependent cargo transport in sensory neurons. Neuron 94, 347–362 e347.
Hall, A.K., Ai, X., Hickman, G.E., MacPhedran, S.E., Nduaguba, C.O., Robertson, C.P., 1997. The generation of neuronal heterogeneity in a rat sensory ganglion. J. Neurosci. 17, 2775–2784.
Han, L., Ma, C., Liu, Q., Weng, H.J., Cui, Y., Tang, Z., Kim, Y., Nie, H., Qu, L., Patel, K.N., Li, Z., McNeil, B., He, S., Guan, Y., Xiao, B., Lamotte, R.H., Dong, X., 2013. A subpopulation of nociceptors specifically linked to itch. Nat. Neurosci. 16, 174–182.
Hanani, M., 2010. Satellite glial cells in sympathetic and parasympathetic ganglia: in search of function. Brain Res. Rev. 64, 304–327.
Hanz, S., Perlson, E., Willis, D., Zheng, J.Q., Massarwa, R., Huerta, J.J., Koltzenburg, M., Kohler, M., van-Minnen, J., Twiss, J.L., Fainzilber, M., 2003. Axoplasmic importins enable retrograde injury signaling in lesioned nerve. Neuron 40, 1095–1104.
Hasegawa, H., Abbott, S., Han, B.X., Qi, Y., Wang, F., 2007. Analyzing somatosensory axon projections with the sensory neuron-specific Advillin gene. J. Neurosci. 27, 14404–14414.
Hedstrom, K.L., Ogawa, Y., Rasband, M.N., 2008. AnkyrinG is required for maintenance of the axon initial segment and neuronal polarity. J. Cell Biol. 183, 635–640.
Hedstrom, K.L., Xu, X., Ogawa, Y., Frischknecht, R., Seidenbecher, C.I., Shrager, P., Rasband, M.N., 2007. Neurofascin assembles a specialized extracellular matrix at the axon initial segment. J. Cell Biol. 178, 875–886.
His, W., 1886. Zur Geschichte des menschlichen Rückenmarkes und der Nervenwurzeln. S. Hirzel, Leipzig.
Hoffman, P.N., 2010. A conditioning lesion induces changes in gene expression and axonal transport that enhance regeneration by increasing the intrinsic growth state of axons. Exp. Neurol. 223, 11–18.
Hoffman, P.N., Griffin, J.W., Price, D.L., 1984. Control of axonal caliber by neurofilament transport. J. Cell Biol. 99, 705–714.
Hoheisel, U., Mense, S., 1986. Non-myelinated afferent fibres do not originate exclusively from the smallest dorsal root ganglion cells in the cat. Neurosci. Lett. 72, 153–157.
Höke, A., Redett, R., Hameed, H., Jari, R., Zhou, C., Li, Z.B., Griffin, J.W., Brushart, T.M., 2006. Schwann cells express motor and sensory phenotypes that regulate axon regeneration. J. Neurosci. 26, 9646–9655.
Hongchien, H., 1970. Axonal bifurcation in the dorsal root ganglion of the cat: a light and electron microscopic study. J. Comp. Neurol. 140, 227–240.
Hory-Lee, F., Russell, M., Lindsay, R.M., Frank, E., 1993. Neurotrophin 3 supports the survival of developing muscle sensory neurons in culture. Proc. Natl. Acad. Sci. U. S. A. 90, 2613–2617.
Hu, X., Cai, J., Yang, J., Smith, G.M., 2010. Sensory axon targeting is increased by NGF gene therapy within the lesioned adult femoral nerve. Exp. Neurol. 223, 153–165.
Huang, L.-Y.M., Gu, Y., Chen, Y., 2013. Communication between neuronal somata and satellite glial cells in sensory ganglia. Glia 61, 1571–1581.
Jackman, A., Fitzgerald, M., 2000. Development of peripheral hindlimb and central spinal cord innervation by subpopulations of dorsal root ganglion cells in the embryonic rat. J. Comp. Neurol. 418, 281–298.
Jacob, C., Lötscher, P., Engler, S., Baggiolini, A., Varum Tavares, S., Brügger, V., John, N., Büchmann-Møller, S., Snider, P.L., Conway, S.J., Yamaguchi, T., Matthias, P., Sommer, L., Mantei, N., Suter, U., 2014. HDAC1 and HDAC2 control the specification of neural crest cells into peripheral glia. J. Neurosci. 34, 6112–6122.
Jesuraj, N.J., Nguyen, P.K., Wood, M.D., Moore, A.M., Borschel, G.H., Mackinnon, S.E., Sakiyama-Elbert, S.E., 2012. Differential gene expression in motor and sensory Schwann cells in the rat femoral nerve. J. Neurosci. Res. 90, 96–104.
Ji, R.-R., Samad, T.A., Jin, S.-X., Schmoll, R., Woolf, C.J., 2002. p38 MAPK activation by NGF in primary sensory neurons after inflammation increases TRPV1 levels and maintains heat hyperalgesia. Neuron 36, 57–68.
Jones, S.L., Svitkina, T.M., 2016. Axon initial segment cytoskeleton: architecture, development, and role in neuron polarity. Neural Plast. 2016, 6808293.
Jung, H., Yoon, B.C., Holt, C.E., 2012. Axonal mRNA localization and local protein synthesis in nervous system assembly, maintenance and repair. Nat. Rev. Neurosci. 13, 308–324.
Kasemeier-Kulesa, J.C., Kulesa, P.M., Lefcort, F., 2005. Imaging neural crest cell dynamics during formation of dorsal root ganglia and sympathetic ganglia. Development 132, 235–245.
Katano, T., Mabuchi, T., Okuda-Ashitaka, E., Inagaki, N., Kinumi, T., Ito, S., 2006. Proteomic identification of a novel isoform of collapsin response mediator protein-2 in spinal nerves peripheral to dorsal root ganglia. Proteomics 6, 6085–6094.
Kiernan, J.A., Barr, M.L., 2009. Barr's the Human Nervous System: An Anatomical Viewpoint. Wolters Kluwer Health/Lippincott Williams & Wilkins.
Kleele, T., Marinkovic, P., Williams, P.R., Stern, S., Weigand, E.E., Engerer, P., Naumann, R., Hartmann, J., Karl, R.M., Bradke, F., Bishop, D., Herms, J., Konnerth, A., Kerschensteiner, M., Godinho, L., Misgeld, T., 2014. An assay to image neuronal microtubule dynamics in mice. Nat. Commun. 5, 4827.
Kobayashi, T., Storrie, B., Simons, K., Dotti, C.G., 1992. A functional barrier to movement of lipids in polarized neurons. Nature 359, 647–650.
Koenig, E., Martin, R., Titmus, M., Sotelo-Silveira, J.R., 2000. Cryptic peripheral ribosomal domains distributed intermittently along mammalian myelinated axons. J. Neurosci. 20, 8390–8400.
Kole, Maarten H.P., Stuart, Greg J., 2012. Signal processing in the axon initial segment. Neuron 73, 235–247.
Komiya, Y., 1981. Axonal regeneration in bifurcating axons of rat dorsal root ganglion

cells. Exp. Neurol. 73, 824–826.
Komiya, Y., Kurokawa, M., 1978. Asymmetry of protein transport in two branches of bifurcating axons. Brain Res. 139, 354–358.
Kung, L.H., Gong, K., Adedoyin, M., Ng, J., Bhargava, A., Ohara, P.T., Jasmin, L., 2013. Evidence for glutamate as a neuroglial transmitter within sensory ganglia. PLoS One 8, e68312.
Kurtz, A., Zimmer, A., Schnutgen, F., Bruning, G., Spener, F., Muller, T., 1994. The expression pattern of a novel gene encoding brain-fatty acid binding protein correlates with neuronal and glial cell development. Development 120, 2637–2649.
Lallemend, F., Ernfors, P., 2012. Molecular interactions underlying the specification of sensory neurons. Trends Neurosci. 35, 373–381.
Lambert, S., Davis, J.Q., Bennett, V., 1997. Morphogenesis of the node of Ranvier: co-clusters of ankyrin and ankyrin-binding integral proteins define early developmental intermediates. J. Neurosci. 17, 7025–7036.
Lasek, R., 1968. Axoplasmic transport in cat dorsal root ganglion cells: as studied with [3-H]-L-leucine. Brain Res. 7, 360–377.
Lau, J., Minett, M.S., Zhao, J., Dennehy, U., Wang, F., Wood, J.N., Bogdanov, Y.D., 2011. Temporal control of gene deletion in sensory ganglia using a tamoxifen-inducible Advillin-Cre-ERT2 recombinase mouse. Mol. Pain 7 100-100.
Lawson, S.N., Biscoe, T.J., 1979. Development of mouse dorsal root ganglia: an autoradiographic and quantitative study. J. Neurocytol. 8, 265–274.
Le Pichon, C.E., Chesler, A.T., 2014. The functional and anatomical dissection of somatosensory subpopulations using mouse genetics. Front. Neuroanat. 8.
Lee, K.H., Chung, K., Chung, J.M., Coggeshall, R.E., 1986. Correlation of cell body size, axon size, and signal conduction velocity for individually labelled dorsal root ganglion cells in the cat. J. Comp. Neurol. 243, 335–346.
Lerman, O., Ben-Zvi, A., Yagil, Z., Behar, O., 2007. Semaphorin3A accelerates neuronal polarity in vitro and in its absence the orientation of DRG neuronal polarity in vivo is distorted. Mol. Cell. Neurosci. 36, 222–234.
Levinson, S.R., Luo, S., Henry, M.A., 2012. The role of sodium channels in chronic pain. Muscle Nerve 46, 155–165.
Li, C.L., Li, K.C., Wu, D., Chen, Y., Luo, H., Zhao, J.R., Wang, S.S., Sun, M.M., Lu, Y.J., Zhong, Y.Q., Hu, X.Y., Hou, R., Zhou, B.B., Bao, L., Xiao, H.S., Zhang, X., 2015. Somatosensory neuron types identified by high-coverage single-cell RNA-sequencing and functional heterogeneity. Cell Res. 26, 83–102.
Li, C.L., Li, K.C., Wu, D., Chen, Y., Luo, H., Zhao, J.R., Wang, S.S., Sun, M.M., Lu, Y.J., Zhong, Y.Q., Hu, X.Y., Hou, R., Zhou, B.B., Bao, L., Xiao, H.S., Zhang, X., 2016. Somatosensory neuron types identified by high-coverage single-cell RNA-sequencing and functional heterogeneity. Cell Res. 26, 83–102.
Li, F., Li, L., Song, X.Y., Zhong, J.H., Luo, X.G., Xian, C.J., Zhou, X.F., 2009. Preconditioning selective ventral root injury promotes plasticity of ascending sensory neurons in the injured spinal cord of adult rats—possible roles of brain-derived neurotrophic factor, TrkB and p75 neurotrophin receptor. Eur. J. Neurosci. 30, 1280–1296.
Li, L., Rutlin, M., Abraira, V.E., Cassidy, C., Kus, L., Gong, S., Jankowski, M.P., Luo, W., Heintz, N., Koerber, H.R., Woodbury, C.J., Ginty, D.D., 2011. The functional organization of cutaneous low-threshold mechanosensory neurons. Cell 147, 1615–1627.
Lindner, R., Puttagunta, R., Nguyen, T., Di Giovanni, S., 2014. DNA methylation temporal profiling following peripheral versus central nervous system axotomy. Sci. Data 1, 140038.
Lisney, S.J., 1987. Functional aspects of the regeneration of unmyelinated axons in the rat saphenous nerve. J. Neurol. Sci. 80, 289–298.
Liu, C.N., Michaelis, M., Amir, R., Devor, M., 2000. Spinal nerve injury enhances subthreshold membrane potential oscillations in DRG neurons: relation to neuropathic pain. J. Neurophysiol. 84, 205–215.
Liu, K., Tedeschi, A., Park, K.K., He, Z., 2011. Neuronal intrinsic mechanisms of axon regeneration. Annu. Rev. Neurosci. 34, 131–152.
Liu, Y., Ma, Q., 2011. Generation of somatic sensory neuron diversity and implications on sensory coding. Curr. Opin. Neurobiol. 21, 52–60.
Loeb, G.E., 1976. Decreased conduction velocity in the proximal projections of myelinated dorsal root ganglion cells in the cat. Brain Res. 103, 381–385.
Luscher, C., Streit, J., Quadroni, R., Luscher, H.R., 1994. Action potential propagation through embryonic dorsal root ganglion cells in culture. I. Influence of the cell morphology on propagation properties. J. Neurophysiol. 72, 622–633.
Ma, C., LaMotte, R.H., 2007. Multiple sites for generation of ectopic spontaneous activity in neurons of the chronically compressed dorsal root ganglion. J. Neurosci. 27, 14059–14068.
Ma, Q., Fode, C., Guillemot, F., Anderson, D.J., 1999. Neurogenin1 and neurogenin2 control two distinct waves of neurogenesis in developing dorsal root ganglia. Genes Dev. 13, 1717–1728.
Mar, F.M., Bonni, A., Sousa, M.M., 2014a. Cell intrinsic control of axon regeneration. EMBO Rep. 15, 254–263.
Mar, F.M., Simoes, A.R., Leite, S., Morgado, M.M., Santos, T.E., Rodrigo, I.S., Teixeira, C.A., Misgeld, T., Sousa, M.M., 2014b. CNS axons globally increase axonal transport after peripheral conditioning. J. Neurosci. 34, 5965–5970.
Mar, F.M., Simoes, A.R., Rodrigo, I.S., Sousa, M.M., 2016. Inhibitory injury signaling represses axon regeneration after dorsal root injury. Mol. Neurobiol. 53, 4596–4605.
Maro, G.S., Vermeren, M., Voiculescu, O., Melton, L., Cohen, J., Charnay, P., Topilko, P., 2004. Neural crest boundary cap cells constitute a source of neuronal and glial cells of the PNS. Nat. Neurosci. 7, 930–938.
Mason, M.R., Lieberman, A.R., Grenningloh, G., Anderson, P.N., 2002. Transcriptional upregulation of SCG10 and CAP-23 is correlated with regeneration of the axons of peripheral and central neurons in vivo. Mol. Cell. Neurosci. 20, 595–615.
Mason, M.R.J., Ehlert, E.M.E., Eggers, R., Pool, C.W., Hermening, S., Huseinovic, A., Timmermans, E., Blits, B., Verhaagen, J., 2010. Comparison of AAV serotypes for gene delivery to dorsal root ganglion neurons. Mol. Ther. 18, 715–724.
Matsuda, S., Baluk, P., Shimizu, D., Fujiwara, T., 1996. Dorsal root ganglion neuron development in chick and rat. Anat. Embryol. 193, 475–480.
Matsuda, S., Kobayashi, N., Mominoki, K., Wakisaka, H., Mori, M., Murakami, S., 2000. Morphological transformation of sensory ganglion neurons and satellite cells. Kaibogaku Zasshi 73, 603–613.
Matsuda, S., Kobayashi, N., Terashita, T., Shimokawa, T., Shigemoto, K., Mominoki, K., Wakisaka, H., Saito, S., Miyawaki, K., Saito, K., Kushihata, F., Chen, J., Gao, S.-Y., Li, C.-Y., Wang, M., Fujiwara, T., 2005. Phylogenetic investigation of Dogiel's pericellular nests and Cajal's initial glomeruli in the dorsal root ganglion. J. Comp. Neurol. 491, 234–245.
Matsuda, S., Uehara, Y., 1981. Cytoarchitecture of the rat dorsal root ganglia as revealed by scanning electron microscopy. J. Electron Microsc. (Tokyo) 30, 136–140.
Matsuda, S., Uehara, Y., 1984. Prenatal development of the rat dorsal root ganglia. A scanning electron-microscopic study. Cell Tissue Res. 235, 13–18.
Matsumoto, E., Rosenbluth, J., 1985. Plasma membrane structure at the axon hillock, initial segment and cell body of frog dorsal root ganglion cells. J. Neurocytol. 14, 731–747.
McLachlan, E.M., Janig, W., Devor, M., Michaelis, M., 1993. Peripheral nerve injury triggers noradrenergic sprouting within dorsal root ganglia. Nature 363, 543–546.
Mense, S., 1990. Structure-function relationships in identified afferent neurones. Anat. Embryol. 181, 1–17.
Mori, H., Komiya, Y., Kurokawa, M., 1979. Slowly migrating axonal polypeptides. Inequalities in their rate and amount of transport between two branches of bifurcating axons. J. Cell Biol. 82, 174–184.
Mudge, A.W., 1984. Schwann cells induce morphological transformation of sensory neurones in vitro. Nature 309, 367–369.
Muller, K., Schnatz, A., Schillner, M., Woertge, S., Muller, C., von Graevenitz, I., Waisman, A., van Minnen, J., Vogelaar, C.F., 2018. A predominantly glial origin of axonal ribosomes after nerve injury. Glia 0, 1–20.
Nakazawa, E., Ishikawa, H., 1995. Occurrence of fasciculated microtubules at nodes of Ranvier in rat spinal roots. J. Neurocytol. 24, 399–407.
Neumann, S., Woolf, C.J., 1999. Regeneration of dorsal column fibers into and beyond the lesion site following adult spinal cord injury. Neuron 23, 83–91.
Ochs, S., 1972. Rate of fast axoplasmic transport in mammalian nerve fibres. J. Physiol. 227, 627–645.
Ochs, S., Erdman, J., Jersild Jr, R.A., McAdoo, V., 1978. Routing of transported materials in the dorsal root and nerve fiber branches of the dorsal root ganglion. J. Neurobiol. 9, 465–481.
Ogawa, Y., Rasband, M.N., 2008. The functional organization and assembly of the axon initial segment. Curr. Opin. Neurobiol. 18, 307–313.
Pannese, E., 1981. The satellite cells of the sensory ganglia. Adv. Anat. Embryol. Cell Biol. 65, 1–111.
Pannese, E., 2010. The structure of the perineuronal sheath of satellite glial cells (SGCs) in sensory ganglia. Neuron Glia Biol. 6, 3–10.
Pannese, E., Ledda, M., 1991. Ribosomes in myelinated axons of the rabbit spinal ganglion neurons. J. Submicrosc. Cytol. Pathol. 23, 33–38.
Pannese, E., Ledda, M., Arcidiacono, G., Rigamonti, L., Procacci, P., 1984. A comparison of the density of microtubules in the central and peripheral axonal branches of the pseudounipolar neurons of lizard spinal ganglia. Anat. Rec. 208, 595–605.
Pannese, E., Procacci, P., Berti, E., Ledda, M., 1999. The perikaryal surface of spinal ganglion neurons: differences between domains in contact with satellite cells and in contact with the extracellular matrix. Anat. Embryol. 199, 199–206.
Papasozomenos, S.C., Binder, L.I., Bender, P.K., Payne, M.R., 1985. Microtubule-associated protein 2 within axons of spinal motor neurons: associations with microtubules and neurofilaments in normal and beta, beta'-iminodipropionitrile-treated axons. J. Cell Biol. 100, 74–85.
Patel, T.D., Jackman, A., Rice, F.L., Kucera, J., Snider, W.D., 2000. Development of sensory neurons in the absence of NGF/TrkA signaling in vivo. Neuron 25, 345–357.
Perl, E.R., 1992. Function of dorsal root ganglion neurons: an overview. In: Scott, S.A. (Ed.), Sensory Neurons: Diversity, Development, and Plasticity. Oxford University Press, pp. 3–23.
Perlson, E., Hanz, S., Ben-Yaakov, K., Segal-Ruder, Y., Seger, R., Fainzilber, M., 2005. Vimentin-dependent spatial translocation of an activated MAP kinase in injured nerve. Neuron 45, 715–726.
Perry, G.W., Krayanek, S.R., Wilson, D.L., 1983. Protein synthesis and rapid axonal transport during regrowth of dorsal root axons. J. Neurochem. 40, 1590–1598.
Perry, G.W., Wilson, D.L., 1981. Protein synthesis and axonal transport during nerve regeneration. J. Neurochem. 37, 1203–1217.
Peters, A., Palay, S.L., Webster, H.F., 1991. The fine structure of the nervous system: neurons and their supporting cells. Oxford University Press.
Pomp, O., Brokhman, I., Ben-Dor, I., Reubinoff, B., Goldstein, R.S., 2005. Generation of peripheral sensory and sympathetic neurons and neural crest cells from human embryonic stem cells. Stem Cells 23, 923–930.
Ramer, M.S., Bisby, M.A., 1998. Normal and injury-induced sympathetic innervation of rat dorsal root ganglia increases with age. J. Comp. Neurol. 394, 38–47.
Ramón y Cajal, S., 1890. Sur l'origin et les ramification des fibres nerveuses de la molle embryonnaire. Anat. Anz. 5, 85–95.
Ramón y Cajal, S., 1904. Asociación del método del nitrato de plata con el embrionario para el estudio de los focos motores y sensitivos. Trab. Lab. Invest. Biol. Univ. Madrid 3, 65–96.
Rámon y Cajal, S., 1955. Histologie du système nerveux de l'homme et des Vertèbres. Maloine, Paris.
Ribeiro, A., Vargo, S., Powell, E.M., Leach, J.B., 2012. Substrate three-dimensionality induces elemental morphological transformation of sensory neurons on a physiologic timescale. Tissue Eng. Part A 18, 93–102.
Richardson, P.M., Verge, V.M.K., 1987. Axonal regeneration in dorsal spinal roots is

accelerated by peripheral axonal transection. Brain Res. 411, 406–408.
Riederer, B.M., Barakat-Walter, I., 1992. Differential distribution of two microtubule-associated proteins, MAP2 and MAP5, during chick dorsal root ganglion development in situ and in culture. Brain Res. Dev. Brain Res. 68, 111–123.
Riley, D.A., Ellis, S., Bain, J.L.W., 1984. Ultrastructural cytochemical localization of carbonic anhydrase activity in rat peripheral sensory and motor nerves, dorsal root ganglia and dorsal column nuclei. Neuroscience 13, 189–206.
Riley, D.A., Sanger, J.R., Matloub, H.S., Yousif, N.J., Bain, J.L.W., Moore, G.H., 1988. Identifying motor and sensory myelinated axons in rabbit peripheral nerves by histochemical staining for carbonic anhydrase and cholinesterase activities. Brain Res. 453, 79–88.
Roth, S., Kummer, W., 1994. A quantitative ultrastructural investigation of tyrosine hydroxylase-immunoreactive axons in the hairy skin of the guinea pig. Anat. Embryol. 190, 155–162.
Rowitch, D.H., 2004. Glial specification in the vertebrate neural tube. Nat. Rev. Neurosci. 5, 409–419.
Roy, S., 2014. Seeing the unseen: the hidden world of slow axonal transport. Neuroscientist 20, 71–81.
Saijilafu, Hur, E.-M., Zhou, F.-Q., 2011. Genetic dissection of axon regeneration via in vivo electroporation of adult mouse sensory neurons. Nat. Commun. 2 543-543.
Schachtner, H., Li, A., Stevenson, D., Calaminus, S.D.J., Thomas, S., Watson, S.P., Sixt, M., Wedlich-Soldner, R., Strathdee, D., Machesky, L.M., 2012. Tissue inducible Lifeact expression allows visualization of actin dynamics in vivo and ex vivo. Eur. J. Cell Biol. 91, 923–929.
Schmalbruch, H., 1986. Fiber composition of the rat sciatic nerve. Anat. Rec. 215, 71–81.
Schmidt, H., Rathjen, F.G., 2010. Signalling mechanisms regulating axonal branching in vivo. BioEssays 32, 977–985.
Schmidt, H., Stonkute, A., Juttner, R., Koesling, D., Friebe, A., Rathjen, F.G., 2009. C-Type natriuretic peptide (CNP) is a bifurcation factor for sensory neurons. Proc. Natl. Acad. Sci. U. S. A. 106, 16847–16852.
Schreyer, D.J., Skene, J.H., 1993. Injury-associated induction of GAP-43 expression displays axon branch specificity in rat dorsal root ganglion neurons. J. Neurobiol. 24, 959–970.
Seijffers, R., Allchorne, A.J., Woolf, C.J., 2006. The transcription factor ATF-3 promotes neurite outgrowth. Mol. Cell. Neurosci. 32, 143–154.
Serbedzija, G.N., Fraser, S.E., Bronner-Fraser, M., 1990. Pathways of trunk neural crest cell migration in the mouse embryo as revealed by vital dye labelling. Development 108, 605–612.
Shea, T.B., Lee, S., 2011. Neurofilament phosphorylation regulates axonal transport by an indirect mechanism: a merging of opposing hypotheses. Cytoskeleton (Hoboken) 68, 589–595.
Singh, V., 2014. Textbook of Clinical Neuroanatomy. Elsevier Health Sciences.
Smith, D.S., Skene, J.H., 1997. A transcription-dependent switch controls competence of adult neurons for distinct modes of axon growth. J. Neurosci. 17, 646–658.
Smith, R.S., 1973. Microtubule and neurofilament densities in amphibian spinal root nerve fibers: relationship to axoplasmic transport. Can. J. Physiol. Pharmacol. 51, 798–806.
Sobotzik, J.-M., Sie, J.M., Politi, C., Del Turco, D., Bennett, V., Deller, T., Schultz, C., 2009. AnkyrinG is required to maintain axo-dendritic polarity in vivo. Proc. Natl. Acad. Sci. U. S. A. 106, 17564–17569.
Song, A.-h., Wang, D., Chen, G., Li, Y., Luo, J., Duan, S., Poo, M.-m., 2009. A selective filter for cytoplasmic transport at the axon initial segment. Cell 136, 1148–1160.
Spencer, P.S., Raine, C.S., Wisniewski, H., 1973. Axon diameter and myelin thickness. Unusual relationships in dorsal root ganglia. Anat. Rec. 176, 225–243.
Stone, G.C., Wilson, D.L., 1979. Qualitative analysis of proteins rapidly transported in ventral horn motoneurons and bidirectionally from dorsal root ganglia. J. Neurobiol. 10, 1–12.
Stone, M.C., Nguyen, M.M., Tao, J., Allender, D.L., Rolls, M.M., 2010. Global up-regulation of microtubule dynamics and polarity reversal during regeneration of an axon from a dendrite. Mol. Biol. Cell 21, 767–777.
Stoney Jr, S.D., 1990. Limitations on impulse conduction at the branch point of afferent axons in frog dorsal root ganglion. Exp. Brain Res. 80, 512–524.
Suh, Y.S., Chung, K., Coggeshall, R.E., 1984. A study of axonal diameters and areas in lumbosacral roots and nerves in the rat. J. Comp. Neurol. 222, 473–481.
Sun, L., Lutz, B.M., Tao, Y.-X., 2016. The CRISPR/Cas9 system for gene editing and its potential application in pain research. Transl. Perioper. Pain Med. 1, 22–33.
Sundt, D., Gamper, N., Jaffe, D.B., 2015. Spike propagation through the dorsal root ganglia in an unmyelinated sensory neuron: a modeling study. J. Neurophysiol. 114, 3140–3153.
Takahashi, K., Ninomiya, T., 1987. Morphological changes of dorsal root ganglion cells in the process-forming period. Prog. Neurobiol. 29, 393–410.
Tandrup, T., 1995. Are the neurons in the dorsal root ganglion pseudounipolar? A comparison of the number of neurons and number of myelinated and unmyelinated fibres in the dorsal root. J. Comp. Neurol. 357, 341–347.
Tang, Y., Scott, D., Das, U., Gitler, D., Ganguly, A., Roy, S., 2013. Fast vesicle transport is required for the slow axonal transport of synapsin. J. Neurosci. 33, 15362–15375.
Tennyson, V.M., 1965. Electron microscopic study of the developing neuroblast of the dorsal root ganglion of the rabbit embryo. J. Comp. Neurol. 124, 267–317.
Terada, S., Kinjo, M., Hirokawa, N., 2000. Oligomeric tubulin in large transporting complex is transported via kinesin in squid giant axons. Cell 103, 141–155.
Tsukita, S., Ishikawa, H., 1976. Three-dimensional distribution of smooth endoplasmic reticulum in myelinated axons. J. Electron Microsc. (Tokyo) 25, 141–149.
Twelvetrees, Alison E., Pernigo, S., Sanger, A., Guedes-Dias, P., Schiavo, G., Steiner, Roberto A., Dodding, MarkP., Holzbaur, Erika L.F., 2016. The dynamic localization of cytoplasmic dynein in neurons is driven by kinesin-1. Neuron 90, 1000–1015.
Twiss, J.L., Fainzilber, M., 2009. Ribosomes in axons—scrounging from the neighbors? Trends Cell Biol. 19, 236–243.
Uchida, A., Alami, N.H., Brown, A., 2009. Tight functional coupling of kinesin-1A and dynein motors in the bidirectional transport of neurofilaments. Mol. Biol. Cell 20, 4997–5006.
Usoskin, D., Furlan, A., Islam, S., Abdo, H., Lonnerberg, P., Lou, D., Hjerling-Leffler, J., Haeggstrom, J., Kharchenko, O., Kharchenko, P.V., Linnarsson, S., Ernfors, P., 2014. Unbiased classification of sensory neuron types by large-scale single-cell RNA sequencing. Nat. Neurosci. 18, 145–153.
van Beuningen, S.F., Will, L., Harterink, M., Chazeau, A., van Battum, E.Y., Frias, C.P., Franker, M.A., Katrukha, E.A., Stucchi, R., Vocking, K., Antunes, A.T., Slenders, L., Doulkeridou, S., Sillevis Smitt, P., Altelaar, A.F., Post, J.A., Akhmanova, A., Pasterkamp, R.J., Kapitein, L.C., de Graaff, E., Hoogenraad, C.C., 2015. TRIM46 controls neuronal polarity and axon specification by driving the formation of parallel microtubule arrays. Neuron 88, 1208–1226.
Vrontou, S., Wong, A.M., Rau, K.K., Koerber, H.R., Anderson, D.J., 2013. Genetic identification of C-fibers that detect massage-like stroking of hairy skin in vivo. Nature 493, 669–673.
Waddell, P.J., Lawson, S.N., McCarthy, P.W., 1989. Conduction velocity changes along the processes of rat primary sensory neurons. Neuroscience 30, 577–584.
Wang, L., Brown, A., 2001. Rapid intermittent movement of axonal neurofilaments observed by fluorescence photobleaching. Mol. Biol. Cell 12, 3257–3267.
Wang, L., Brown, A., 2002. Rapid movement of microtubules in axons. Curr. Biol. 12, 1496–1501.
Watson, D.F., Griffin, J.W., Fittro, K.P., Hoffman, P.N., 1989. Phosphorylation-dependent immunoreactivity of neurofilaments increases during axonal maturation and β,β′-iminodipropionitrile intoxication. J. Neurochem. 53, 1818–1829.
Weng, X., Smith, T., Sathish, J., Djouhri, L., 2012. Chronic inflammatory pain is associated with increased excitability and hyperpolarization-activated current (Ih) in C- but not Adelta-nociceptors. Pain 153, 900–914.
Winckler, B., Forscher, P., Mellman, I., 1999. A diffusion barrier maintains distribution of membrane proteins in polarized neurons. Nature 397, 698–701.
Wortman, Juliana C., Shrestha, Uttam M., Barry, Devin M., Garcia, Michael L., Gross, Steven P., Yu, Clare C., 2014. Axonal transport: how high microtubule density can compensate for boundary effects in small-caliber axons. Biophys. J. 106, 813–823.
Wujek, J.R., Lasek, R.J., 1983. Correlation of axonal regeneration and slow component B in two branches of a single axon. J. Neurosci. 3, 243–251.
Xie, W., Strong, J.A., Mao, J., Zhang, J.-M., 2011. Highly localized interactions between sensory neurons and sprouting sympathetic fibers observed in a transgenic tyrosine hydroxylase reporter mouse. Mol. Pain 7, 53.
Xie, W., Strong, J.A., Zhang, J.-M., 2010. Increased excitability and spontaneous activity of rat sensory neurons following in vitro stimulation of sympathetic fiber sprouts in the isolated dorsal root ganglion. Pain 151, 447–459.
Yang, Y., Ogawa, Y., Hedstrom, K.L., Rasband, M.N., 2007. βIV spectrin is recruited to axon initial segments and nodes of Ranvier by ankyrinG. J. Cell Biol. 176, 509–519.
Ylera, B., Erturk, A., Hellal, F., Nadrigny, F., Hurtado, A., Tahirovic, S., Oudega, M., Kirchhoff, F., Bradke, F., 2009. Chronically CNS-injured adult sensory neurons gain regenerative competence upon a lesion of their peripheral axon. Curr. Biol. 19, 930–936.
Yogev, S., Cooper, R., Fetter, R., Horowitz, M., Shen, K., 2016. Microtubule organization determines axonal transport dynamics. Neuron 92, 449–460.
Yudin, D., Hanz, S., Yoo, S., Iavnilovitch, E., Willis, D., Gradus, T., Vuppalanchi, D., Segal-Ruder, Y., Ben-Yaakov, K., Hieda, M., Yoneda, Y., Twiss, J.L., Fainzilber, M., 2008. Localized regulation of axonal RanGTPase controls retrograde injury signaling in peripheral nerve. Neuron 59, 241–252.
Zelená, J., 1972. Ribosomes in myelinated axons of dorsal root ganglia. Z. Zellforsch. Mikrosk. Anat. 124, 217–229.
Zelená, J., Jirmanova, I., 1988. Grafts of pacinian corpuscles reinnervated by dorsal root axons. Brain Res. 438, 165–174.
Zenker, W., Högl, E., 1976. The prebifurcation section of the axon of the rat spinal ganglion cell. Cell Tissue Res. 165, 345–363.
Zenker, W., Mayr, R., Gruber, H., 1975. Neurotubules: different densities in peripheral motor and sensory nerve fibres. Experientia 31, 318–320.
Zhang, J.M., Strong, J.A., 2008. Recent evidence for activity-dependent initiation of sympathetic sprouting and neuropathic pain. Sheng Li Xue Bao 60.
Zhang, X., Bennett, V., 1998. Restriction of 480/270-kD ankyrin (G) to axon proximal segments requires multiple ankyrin (G)-specific domains. J. Cell Biol. 142, 1571–1581.
Zhang, X., Chen, Y., Wang, C., Huang, L.Y., 2007. Neuronal somatic ATP release triggers neuron-satellite glial cell communication in dorsal root ganglia. Proc. Natl. Acad. Sci. U. S. A. 104.
Zou, H., Ho, C., Wong, K., Tessier-Lavigne, M., 2009. Axotomy-induced Smad1 activation promotes axonal growth in adult sensory neurons. J. Neurosci. 29, 7116–7123.